

TOOLS FOR HIGHER-ORDER NETWORK ANALYSIS

A DISSERTATION
SUBMITTED TO THE INSTITUTE FOR COMPUTATIONAL AND
MATHEMATICAL ENGINEERING
AND THE COMMITTEE ON GRADUATE STUDIES
OF STANFORD UNIVERSITY
IN PARTIAL FULFILLMENT OF THE REQUIREMENTS
FOR THE DEGREE OF
DOCTOR OF PHILOSOPHY

Austin Reilley Benson
June 6, 2017

Abstract

Networks are a fundamental model of complex systems throughout the sciences, and network datasets are typically analyzed through lower-order connectivity patterns described at the level of individual nodes and edges. However, higher-order connectivity patterns captured by small subgraphs, also called network motifs, describe the fundamental structures that control and mediate the behavior of many complex systems. We develop three tools for network analysis that use higher-order connectivity patterns to gain new insights into network datasets: (1) a framework to cluster nodes into modules based on joint participation in network motifs; (2) a generalization of the clustering coefficient measurement to investigate higher-order closure patterns; and (3) a definition of network motifs for temporal networks and fast algorithms for counting them. Using these tools, we analyze data from biology, ecology, economics, neuroscience, online social networks, scientific collaborations, telecommunications, transportation, and the World Wide Web.

Acknowledgments

I owe a great debt of gratitude to many folks for my ability to finally complete this dissertation. First, the content of this dissertation is comprised of collaborative research. Thank you to my co-authors Ashwin Paranjape, David Gleich, Hao Yin, and Jure Leskovec. Second, the research would not have been possible without generous funding from an Office of Technology Licensing Stanford Graduate Fellowship and from DARPA SIMPLEX. The SGF program was especially beneficial during my scientific wayfinding in the early years at Stanford.

Throughout my time at Stanford, I was fortunate to receive guidance from a number of more senior folks. Thanks especially to Andrew Tomkins, David Gleich, Grey Ballard, Johan Ugander, Jack Poulson, Jure Leskovec, Lexing Ying, Margot Gerritsen, Michael Saunders, Moses Charikar, Ravi Kumar, and Rob Schreiber. Additional thanks to Johan for reading and signing off on this thesis, to Moses for serving on my defense committee, to Lexing for chairing my defense committee, and to Margot for making ICME such a great place.

Jure has been an amazingly supportive and dedicated advisor. He is always pushing me to turn algorithmic ideas into meaningful applications, which has shaped the way that I think about research. I value his ability to provide guidance while simultaneously letting me pursue my own interests and ideas.

David also deserves special recognition. He has been an incredible collaborator and even better mentor ever since I started working with him while I was an undergraduate at Berkeley. My career and this thesis would not have been possible without his support and guidance.

Next, thank you to all of the ICME and SNAP students for all of the wonderful interactions. Special thanks to Anil, Brad, David, Eileen, Hima, Jason, Milinda, Nolan, Rikel, Ron, Ryan, Sven, Tim, Victor, Will, Xiaotong, Yingzhou, and Yuekai.

My family has been a tremendous support network. Thank you to my parents—Karen and Craig Benson—and to my Davis family—Marianne, Brian, Oak, and Bob Hallet—for all of your help.

Finally, thank you to the amazing Catherine Hallet Benson for her continued support, which keeps me going.

Contents

Abstract	v
Acknowledgments	vii
1 Higher-order thinking in network analysis	1
1.1 Contributions	6
1.1.1 Chapter 2 – Higher-order network clustering	7
1.1.2 Chapter 3 – Higher-order clustering coefficients	8
1.1.3 Chapter 4 – Motifs in temporal networks	9
1.1.4 Additional artifacts and impact	9
2 Higher-order network clustering	13
2.1 Organization via higher-order structures	13
2.2 The motif-based spectral clustering algorithm	17
2.2.1 Review of cuts, volumes, conductance and the graph Laplacian for weighted, undirected graphs	17
2.2.2 Definition of network motifs	18
2.2.3 Motif conductance	21
2.2.4 The motif adjacency matrix and the motif Laplacian	21
2.2.5 The spectral algorithm for finding a single cluster	22
2.2.6 Interlude for matrix computations	24
2.2.7 Motif Cheeger inequality for network motifs with three nodes	26
2.2.8 Motif Cheeger inequality for network motifs with four or more nodes	29
2.2.9 Analysis of computational complexity	32
2.2.10 Methods for simultaneously finding multiple clusters	34
2.2.11 Extensions for multiple motifs, weighted motifs, and weighted, signed, and colored networks	35
2.3 Case studies	37
2.3.1 Alternative clustering algorithms for evaluation	37

2.3.2	Comparing motif conductance and edge conductance	38
2.3.3	Motif M_6 in the Florida Bay food web	39
2.3.4	Coherent feedforward loops in the <i>S. cerevisiae</i> transcriptional regulation network	48
2.3.5	Bi-directed length-2 paths in a transportation reachability network	53
2.3.6	The bi-fan motif in the <i>C. elegans</i> neuronal network	58
2.3.7	Motif M_6 in the English Wikipedia article network	63
2.3.8	Motif M_6 in the Twitter follower network	65
2.3.9	Motif M_7 in the Stanford web graph	68
2.3.10	Semi-cliques in collaboration networks	70
2.4	Scalability experiments	72
2.4.1	Triangular motifs	72
2.4.2	Larger k -clique motifs	78
2.5	An extension to local higher-order clustering	80
2.5.1	Overview	80
2.5.2	Motif-based personalized PageRank	81
2.5.3	Experiments on synthetic networks	85
2.5.4	Experiments on real-world networks	89
2.6	Related work and discussion	94
3	Higher-order clustering coefficients	99
3.1	The clustering coefficient and closure probabilities	99
3.2	Definitions of higher-order clustering coefficients	100
3.3	Theoretical Analysis	103
3.3.1	A method to compute higher-order clustering coefficients	103
3.3.2	Probabilistic interpretations	103
3.3.3	Bounds on higher-order clustering coefficients	105
3.3.4	Analysis for the $G_{n,p}$ model	106
3.3.5	Analysis for the small-world model	109
3.4	Empirical Analysis	112
3.5	Relating higher-order clustering coefficients to motif conductance through 1-hop neighborhoods	118
3.5.1	A formal relationship between 1-hop neighborhoods and motif conductance	118
3.5.2	Experiments	122
3.6	Related work and discussion	128

4	Motifs in temporal networks	129
4.1	Analyzing network data with timestamped edges	129
4.2	Definitions of temporal networks and temporal motifs	132
4.3	Counting algorithms	135
4.3.1	General counting framework	135
4.3.2	Faster algorithms	142
4.4	Experiments	151
4.4.1	Data	152
4.4.2	Empirical observations of motif counts	153
4.4.3	Algorithm scalability	159
4.5	Prior definitions of temporal motifs and other related work	160
4.6	Discussion	162

List of Tables

1.1	Tools for higher-order network analysis developed in this thesis . . .	6
2.1	Matrix computations for the weighted motif adjacency matrix	24
2.2	Connected components of the Florida Bay food web motif adjacency matrix for motif M_6	41
2.3	Ecological classification of nodes in the Florida Bay foodweb	46
2.4	Evaluation of clustering algorithms in the Florida Bay food web . . .	47
2.5	Non-trivial connected components of the motif adjacency matrix of the <i>S. cerevisiae</i> network for the coherent feedforward loop	49
2.6	Clustering of coherent feedforward loops	52
2.7	Correlations between principal eigenvectors and city metadata . . .	56
2.8	Networks for scalability experiments	73
2.9	Performance of motif-based clustering	76
2.10	Linear models for computation time	77
2.11	Time to compute W_M for k -clique motifs	79
2.12	Recovery of ground truth community structure in undirected graphs	90
2.13	Recovery of ground truth communities in directed graphs	92
3.1	Higher-order clustering coefficients for several networks	114
3.2	Summary statistics of datasets	123
3.3	Fiedler and 1-hop neighborhood clusters	125
3.4	Testing neighborhood centers as seeds	126
4.1	Notation for Chapter 4	134
4.2	Example execution of Algorithm 5 for counting instances of the δ -temporal motif M and network in Figure 4.1	137
4.3	Summary statistics of temporal network datasets	152
4.4	Time to count the eight 3-edge δ -temporal triangle motifs	159

List of Figures

1.1	Example higher-order network structure (network motif) appearing in different domains	3
2.1	Higher-order network structures and the higher-order network clustering framework	14
2.2	Formal motif definition	20
2.3	Julia implementation of the motif-based spectral clustering algorithm	25
2.4	Quadratic forms on indicator functions for set assignment	31
2.5	Edge conductance and motif conductance	38
2.6	Sweep profile plot on the Florida Bay food web	42
2.7	Higher-order organization of the Florida Bay food web	44
2.8	Higher-order clusters in the Florida Bay food web	45
2.9	Higher-order organization of the <i>S. cerevisiae</i> transcriptional regulation network	51
2.10	Higher-order spectral analysis of a network of airports in Canada and the United States	54
2.11	Loess regressions of city metadata against principal eigenvectors . .	57
2.12	Transportation reachability network matrix	58
2.13	Higher-order cluster in the <i>C. elegans</i> neuronal network	60
2.14	Sweep profile plots for <i>C. elegans</i>	61
2.15	Clusters in <i>C. elegans</i>	62
2.16	Clusters in the English Wikipedia hyperlink network	64
2.17	Clusters in the 2010 Twitter follower network	66
2.18	@photobali and @photomadrid Twitter accounts	67
2.19	Clusters in the Stanford web graph	69
2.20	Clusters in co-authorship networks	71
2.21	Recovery in the planted partition model	86
2.22	Recovery in the LFR model	88
2.23	Three directed motif groups	91
2.24	Distribution of set size and conductance for seeded APPR in EMAIL-EU-CORE	93
2.25	Sweep profile for a single seed in EMAIL-EU-CORE	94

3.1	Overview of higher-order clustering coefficients as clique expansion probabilities	102
3.2	Families of 1-hop neighborhoods of a node u with degree d_u	105
3.3	Higher-order clustering in the small-world model	110
3.4	Joint distributions of $(C_2(u), C_3(u))$	116
3.5	Average higher-order clustering coefficients as a function of degree .	118
3.6	NCP plots for two networks with two different clique sizes	127
4.1	Temporal graphs and δ -temporal motifs	130
4.2	All 2-node and 3-node, 3-edge δ -temporal motifs	140
4.3	Worst-case example for counting triangular motifs with Algorithm 5	141
4.4	The three classes of 3-node, 3-edge star temporal motifs	142
4.5	Graph structure of worst-case instance for Algorithm 9	151
4.6	Counts of instances of all 2- and 3-node, 3-edge δ -temporal motifs with $\delta = 1$ hour	154
4.7	Blocking and non-blocking behavior	155
4.8	Switching behavior in non-blocking motifs	156
4.9	Cyclic temporal triangles	157
4.10	Counts for all 2- and 3-node, 3-edge δ -temporal motifs in four time intervals for the STACKOVERFLOW dataset	157
4.11	Motif counts over various time scales in the COLLEGE MSG dataset . .	158
4.12	Scalability of temporal motif counting in	160

List of Algorithms

1	Motif-based clustering algorithm for finding a single cluster	23
2	Motif-based clustering algorithm for finding several clusters	35
3	Motif-PageRank-Nibble	83
4	Approximate-Weighted-PPR	83
5	General counting method for temporal motifs	136
6	Framework for fast counting of 3-node, 3-edge star and triangle temporal motifs	145
7	Fast counting of 3-node, 3-edge temporal star motifs	146
8	Fast temporal triangle motif counting subroutine	148
9	Fast temporal triangle motif counting	149

Chapter 1

Higher-order thinking in network analysis

A network is a model for a system of connections between things. The core of a network model is a graph, a mathematical object consisting of nodes (modeling the things) and edges (modeling the connections between things). This thesis provides new graph theoretic methods to analyze datasets associated with network models. Such network datasets show up in a wide variety of scientific disciplines, and this thesis alone analyzes networks from the following domains.

- *Ecological systems* – Nodes are species and edges are who-eats-whom relationships in food web models. (Here, the edges are *directed* to represent asymmetry—sharks regularly consume sardines, but sharks are not a part of a sardine’s diet!) We examine the graph structure behind aquatic layers in a food web of Florida Bay.
- *Human communication systems* – Nodes are people and edges are messages between people. Again, there is a natural direction to the edges. Our network datasets also have temporal information associated with the graph to denote when messages are sent. We analyze the differences between communication behaviors in e-mail, SMS texting, and phone call networks.
- *Neural systems* – Nodes are neurons and edges are synapses. We examine the patterns of connections in the complete neural network of the nematode worm *C. elegans*.
- *Payment systems* – Nodes are people, businesses, or accounts and edges are payments between them. We analyze transactions between addresses on Bitcoin. We again have temporal information corresponding to when payments are made.
- *Transcription regulation networks* – Nodes are groups of genes and edges represent which groups of genes regulate genetic transcription in which

other groups of genes. The edges in the network data also carry information about whether the regulation type is activation or suppression (in this case, we say that the edges are *signed*). We analyze the transcription regulation network of the yeast *S. cerevisiae*.

- *Transportation systems* – Nodes are locations and edges represent connectivity. We analyze an air travel reachability network, where nodes are cities and edges represent how long it takes to travel from one city to another using commercial airline flights. Our analysis also incorporates additional geographical data available for the nodes.
- *Scientific collaborations* – Nodes are scientists and there is an edge between two scientists if they have co-authored a paper. We look at collaboration patterns between physicists.
- *Social networks* – Nodes are people and edges are social relationships. We examine Facebook friendships, Twitter followers, and Stack Overflow question-and-answer interactions.
- *The World Wide Web* – Nodes are web pages and edges are hyperlinks. We analyze the structure of the Stanford web graph and Wikipedia.

The above descriptions illustrate how graphs, which consist of nodes and edges, are a natural mathematical structure for network models. The graph is the backbone of the network datasets, even though we may have additional information such as timestamps, signed edges, geographical data, etc. Consequently, we often frame our analysis of and questions about networks in terms of nodes and edges. For example, we might be interested in the number of edges that a node is in (how many different species does the shark consume in the food web?), the number of edges between subsets of the nodes (how many Facebook friendships are there between Stanford students?), or whether or not there exists a sequence of edges to traverse to go from one node to another (can I get from Palo Alto to Berkeley on public transit?).

While analysis in terms of nodes and edges is natural, there is substantial evidence that *higher-order structures*, or small subgraph patterns between a few nodes (Figure 1.1), are essential to the behavior of many complex systems modeled by networks [Milo et al., 2002; Yaveroglu et al., 2014]. This idea has a long history in sociology. In the early 1900s, Simmel theorized that triangles (a complete graph on three nodes) form in social networks because two friends of the same individual get opportunities to meet and become friends themselves [Simmel, 1908], an idea later popularized by Granovetter [1973] as *triadic closure*. Bavelas [1950] surveyed several studies that examined how small communication patterns used between individuals in a group affects their ability to jointly perform tasks, and Davis and Leinhardt [1971] found that certain directed triads were less common than predicted by a null model, providing numerical evidence for the ranked groups

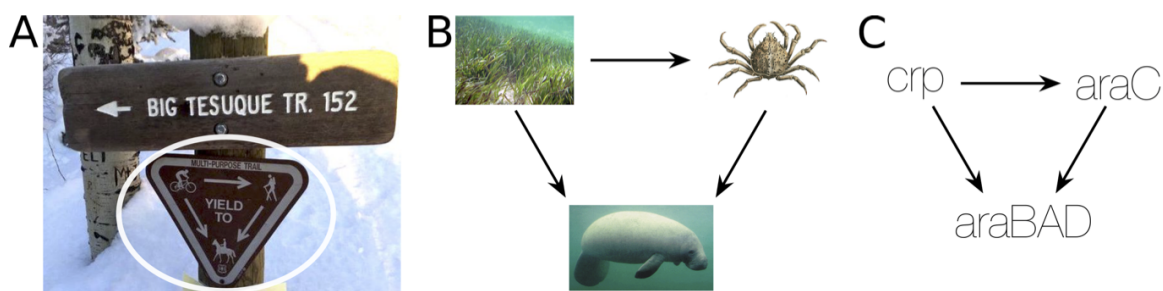


Figure 1.1 – Example higher-order network structure (*network motif*) appearing in different domains. **A:** Traffic yielding pattern on the Big Tesuque Trail—bikers yield to hikers and equestrians, and hikers also yield to equestrians (photo taken by the author after presenting the research in Chapter 2 at the Santa Fe Institute in December, 2015). **B:** The same pattern is called an omnivory chain in ecology [Bascompte, 2009; Camacho et al., 2007]. Here we show an example in the Florida Bay food web, where the seagrass producer (thalassia) is a food source for crabs and manatees, and crabs are also a food source for the manatees [Ulanowicz et al., 1998]. **C:** In transcription regulation networks, the pattern is called a feedforward loop (figure reproduced from [Shen-Orr et al., 2002]). In *E. coli*, the operon *crp* encodes transcription factors that regulate operons *araC* and *araBAD*, and *araC* also encodes a transcription factor that regulates *araBAD*. Feedforward loops occur more frequently than one would expect by chance in the *E. coli* and *S. cerevisiae* transcription networks [Milo et al., 2002] and function as delay units in transcription [Mangan and Alon, 2003; Mangan et al., 2003].

social network theory of Homans [1950]. In more recent work, Ugander et al. [2013] use small subgraph frequencies within induced Facebook friendship subgraphs to identify social processes.

In network analysis more broadly, higher-order structure is often described through the idea of a *network motif*. Shen-Orr et al. [2002] introduced the term when they analyzed the frequency of higher-order interactions through subgraph patterns, which they called network motifs, in the transcription regulation network of *E. coli*.¹ This style of analysis was popularized in a landmark paper of Milo et al. [2002] (published in *Science* the same year), where they dubbed network motifs the “building blocks of complex networks” and identified motifs common in gene regulation networks, food webs, and electronic circuits. In follow-up work, Milo et al. [2004] showed that the profile of z-scores (with respect to samples of a

¹Shen-Orr et al. [2002] borrowed the phrase motif from gene sequence analysis, where motifs are “short, recurring patterns in DNA that are presumed to have a biological function” [D’haeseleer, 2006].

configuration model with the same degree distribution) for the frequencies of the 13 connected, 3-node directed subgraphs were sufficient to distinguish biological, neurological, social, and linguistic networks. In subsequent research, important motifs have been identified in a variety of domains, including brain science [Sporns and Kötter, 2004], ecology [Camacho et al., 2007], biology [Wuchty et al., 2003], and social network analysis [Leskovec et al., 2010a].

Milo et al. [2002] defined network motifs as “patterns of interconnections occurring in complex networks at numbers that are significantly higher than those in randomized networks.” The “significant” qualifier in this definition has caused some confusion around the terminology. Some take the qualifier to heart and use the term *graphlet* to specify any small network pattern and reserve the motif designation for graphlets that occur significantly more frequently with respect to some null model and some measure of statistical significance [Pržulj et al., 2004].² However, one could just as well call a graphlet a small subgraph, and indeed, many do [Demeyer et al., 2013; Lahiri and Berger-Wolf, 2007; Pinar et al., 2017; Ugander et al., 2013]. Usually, there is an implicit assumption that motifs and graphlets are *connected* patterns, whereas general subgraphs do not carry this assumption. In this thesis, we just use “motifs” to specify patterns in networks and sometimes use the term subgraph when discussing the more mathematical points. In Chapter 2, we also add to the vernacular by defining an “anchored motif”, which provides a formalism for specifying a subset of the nodes in a motif relevant to certain computations. We also use “higher-order structures” as a catch-all phrase.

Operating under the assumption that higher-order structures are important to networks, the algorithmic data mining community has developed a litany of methods for efficiently finding and counting them. These include, to name a few, algorithms for enumerating triangles that perform especially well given the power-law degree distributions typical of many real-world networks [Berry et al., 2014; Latapy, 2008; Schank and Wagner, 2005], fast algorithms for enumerating general motifs via principled heuristics [Ahmed et al., 2015; Demeyer et al., 2013; Houbraken et al., 2014; Wernicke and Rasche, 2006], algorithms that approximate the total number of triangles [De Stefani et al., 2016; Lim and Kang, 2015; Seshadhri et al., 2014; Tsourakakis et al., 2009], and algorithms that approximate the total number of motifs composed of 4 or more nodes [Bressan et al., 2017; Jha et al., 2015; Słota and Madduri, 2013; Wang et al., 2014]. For the computations in this thesis, we only need the method of Schank and Wagner [2005, Algorithm 1] for enumerating triangles and the method of Chiba and Nishizeki [1985] for enumerating cliques. We use these algorithms because they are straightforward to implement and are fast for the datasets that we analyze.

²Presumably, the term graphlets is a play on wavelets, which are used in signal processing to localize time and frequency, but I have not found this explicitly mentioned in the literature.

We summarize the setup—networks consisting of nodes and edges model a broad range of systems, higher-order interactions (patterns between a small number of nodes) are important to many networks, and we have algorithms adept at finding and counting these higher-order structures. However, higher-order structures have not been well integrated into the analyses, models, and algorithms that we actually use to study the structure of complex networks. This thesis develops new methods, or *tools*, for analyzing network data based on higher-order structures, i.e., *for higher-order network analysis*. Consequently, the network analyst is able to examine data in terms of the higher-order interactions that are important to him or her.

We demonstrate how our tools use higher-order interactions as a primitive in order to gain new insights into complex systems. For example, our analysis of the neural network for the nematode worm *C. elegans* in Section 2.3.6 finds a cluster of 20 neurons in the frontal section of the worm that is a plausible control of nictation, a type of worm movement. We discover this group through a new algorithm that looks for subsets of the graph in which a certain 4-node “bi-fan” motif is contained. The higher-order structure is key to the discovery—we need to optimize an objective function for sets of nodes that models the bi-fan motif—and *not* simply edges, as is typically done—in order to find this group. Later, in Section 3.4, we find that under a generalized “closure” model for the presence of edges in the network, 3-cliques (triangles) in *C. elegans* are more common than expected, while 4-cliques are less common than expected, which challenges a longstanding view of how edges tend to cluster together in network models of complex systems [Watts and Strogatz, 1998]. In this case, the consideration of higher-order structure at the level of 4-cliques was necessary for the finding.

Higher-order analysis is a small part of network science, but higher-order thinking has still shown up in several contexts. For example, motifs have been used to generate features for both prediction problems [Bonato et al., 2014; Chakraborty et al., 2014; Milenkovic and Przulj, 2008; Ugander et al., 2013] and unsupervised learning tasks [Henderson et al., 2012; Yaveroglu et al., 2014], motif frequencies are used to fit parameters of random graph models [Benson et al., 2014; Bickel et al., 2011; Gleich and Owen, 2012; Wasserman and Pattison, 1996], and motif modeling is used to improve network alignment algorithms [Milenkovic et al., 2010; Mohammadi et al., 2016]. In addition, there are several higher-order approaches that do not necessarily use motif structure but are similar in spirit. Examples include “meta paths” to represent multi-relational networked data [Sun et al., 2011; Zhang et al., 2014a], higher-order and variable-order Markov chain models [Benson et al., 2017; Chierichetti et al., 2012; Rosvall et al., 2014; Wu et al., 2016], and “higher-order network” models for aggregating temporal paths in networks where edges have timestamps [Scholtes, 2017; Scholtes et al., 2016, 2014].

The new ideas in Chapters 2 and 3 also align with recent higher-order network analyses that directly generalize classical ideas to account for higher-order structures in the network. For example, Tsourakakis [2015] generalized the (edge) densest subgraph problem to the k -clique densest subgraph problem, Zhang and Parthasarathy [2012] generalized (edge-based) k -cores to triangle-based k -cores, and Sariyuce et al. [2015] generalized k -core and k -truss decompositions to account for clique containment with the nucleus decomposition. We describe our contributions in more detail in the following section.

1.1 Contributions

The core contributions of this thesis are three new tools for higher-order network analysis. We contextualize and summarize them in Table 1.1.

Table 1.1 – Tools for higher-order network analysis developed in this thesis.

Concept	Classical tools	New tool
Discover modules (clusters of nodes) in a network using only the network topology.	Algorithms for optimizing edge-based objective functions such as modularity, conductance, and normalized cut. [Andersen et al., 2006; Leskovec et al., 2009; Newman and Girvan, 2004; Von Luxburg, 2007]	Algorithms for optimizing higher-order , motif-based objective functions. Chapter 2; [Benson et al., 2016; Yin et al., 2017b]
Measure the tendency of edges in a network to cluster.	The clustering coefficient based on relative triangle frequencies. [Barrat and Weigt, 2000; Watts and Strogatz, 1998]	Higher-order clustering coefficients based on relative clique frequencies. Chapter 3; [Yin et al., 2017a,b]
Count the frequency of higher-order structures in a network.	Motifs in static networks. [Milo et al., 2002; Pržulj et al., 2004]	Motifs in temporal networks. Chapter 4; [Paranjape et al., 2017]

In addition to developing the tools, we make a concerted effort to use the tools to gain new insights into a variety of network datasets. Thus, there is a considerable data mining component to the chapters ahead, which are also meaningful contributions. The next few subsections provide additional details on the tools and the insights that they provide.

1.1.1 Chapter 2 – Higher-order network clustering

The first tool is a framework for graph clustering based on motifs. Graph clustering is a broad research problem that assigns nodes in a graph to clusters, where the clusters are meant to represent some module in the network. Typically, the objective function modeling what it means to have good clusters involves a combination of the number of *edges* contained within the clusters and the number of *edges* that go between clusters. We re-define what it means to be a good cluster with an objective function that considers the number of *motifs* contained within the clusters and the number of *motifs* that go between clusters. Thus, if a particular motif is important for some domain, we can run an algorithm to optimize an objective function that accounts for that motif.

Our main theoretical contributions include (i) defining the new objective function, *motif conductance*, which is a generalization of the classical conductance measure of cluster quality; and (ii) a spectral algorithm for finding sets with small motif conductance. The algorithm is accompanied by an approximation guarantee on the quality of the output clusters in terms of motif conductance. The algorithm and quality guarantee are generalizations of the Fiedler partition or sweep cut procedure and the Cheeger inequality.

Using this framework we show that

- a particular directed triangular motif reveals aquatic layers in a food web;
- in the *C. elegans* neural system, a cluster we find based on a previously studied 4-node motif (the “bi-fan”) is a plausible control mechanism for nictation, a type of movement in the worm;
- clustering with length-2 paths automatically reveals the hub structure and geography of an air travel transportation reachability network;
- clustering with the feedforward loop (Figure 1.1C) reveals known modules in transcription regulation networks with higher accuracy than edge-based methods; and
- clustering with particular directed triangular motifs reveal anomalous clusters in the English Wikipedia web graph and the Twitter follower network.

We then extend the algorithm to handle the problem of *localized clustering* or *targeted clustering*, where the goal is to find a (small) cluster of nodes containing a given seed node. Again, existing approaches optimize the classical conductance, and we instead optimize motif conductance. Our approach is a generalization of the approximate Personalized PageRank method [Andersen et al., 2006].

The algorithmic framework and applications appeared as a publication in *Science* [Benson et al., 2016],³ which was joint work with David Gleich and Jure

³See the accompanying perspective piece by Pržulj and Malod-Dognin [2016] for a broader context for this work.

Leskovec. The extension to localized clustering will appear in a paper in the proceedings of the 2017 KDD conference [Yin et al., 2017b], which was joint work with Hao Yin, David, and Jure. Hao implemented the localized algorithm, ran the experiments for the results in Section 2.5, and came up with the idea to look at recovery in the planted partition model (Section 2.5.3).

1.1.2 Chapter 3 – Higher-order clustering coefficients

The second tool is a measurement for the extent to which nodes in a network cluster together. This is a generalization of the classical clustering coefficient that measures the fraction of length-2 paths that induce a triangle. We reinterpret the clustering coefficient as a clique expansion and closure process—a 2-clique (an edge) *expands* with an adjacent edge and we check if this structure *closes* by forming a 3-clique (a triangle). We generalize this by considering an ℓ -clique that expands with an adjacent edge and checking if this structure closes by forming an $(\ell + 1)$ -clique. We call the fraction of (ℓ -clique, adjacent edge) pairs that induce an $(\ell + 1)$ -clique the ℓ th-order clustering coefficient.

We theoretically analyze the higher-order clustering coefficient in the Erdős-Rényi and small-world random graph models and empirically analyze the higher-order clustering coefficient on three real-world networks. We find that although the *C. elegans* neural network has high clustering in the traditional sense, it does not have high third-order clustering (3-cliques tend not to expand into 4-cliques). This could arise from the fact that 4-cliques represent redundant processing units and their absence leads to a more efficient neural architecture.

We also make a connection between higher-order clustering coefficients and motif conductance. We show that if a network has a large ℓ th-order clustering coefficient, then there is a node whose 1-hop neighborhood subgraph has small motif conductance for the ℓ -clique motif. This is a generalization of the $\ell = 2$ case studied by Gleich and Seshadhri [2012]. In fact, I came up with the definition for the higher-order clustering coefficient when I was trying to generalize a lemma from Gleich and Seshadhri [2012] to the $\ell = 3$ case (for triangle conductance).

The definitions and analysis of the higher-order clustering coefficient is based on a paper with Hao Yin and Jure Leskovec that has been submitted for publication and is currently on arXiv [Yin et al., 2017a]. The connection to motif conductance is based on part of a paper with Hao, Jure, and David Gleich that will appear in the proceedings of the 2017 KDD conference [Yin et al., 2017b]. Hao helped a substantial amount on the proofs of Propositions 14 and 15 and Theorem 16.

1.1.3 Chapter 4 – Motifs in temporal networks

The third tool is a definition of motifs in temporal networks along with algorithms for efficiently counting them. The goal of the research in Chapter 4 is to provide the foundations of higher-order network analysis—a definition for higher-order structures and efficient algorithms for finding them—for a broader class of network datasets, i.e., those that contain temporal information. We consider a temporal network to be a collection of (u, v, t) tuples (temporal edges), where u and v are elements of a node set V and $t \in \mathbb{R}_+$ is a timestamp. We define a temporal motif by a multigraph, an ordering on the edges in the multigraph, and a time window δ , and we define an instance of the temporal motif in a temporal network to be a subset of the temporal edges that match the edge pattern of the multigraph, appear in the specified order, and all occur within δ time units of each other. We provide a general algorithm for efficiently counting the number of instances of temporal motifs in a given temporal network along with specialized fast algorithms for certain classes of motifs. We also show some basic higher-order analyses on several temporal network datasets.

Chapter 4 is based on a paper with Ashwin Paranjape and Jure Leskovec that appeared in the proceedings of the 2017 WSDM conference [Paranjape et al., 2017]. Ashwin helped with the design, implementation, and analysis of the algorithms and executed the experiments in Section 4.4.2.

1.1.4 Additional artifacts and impact

In addition to the content of this thesis and the associated publications, other artifacts of this research include the following.

- Implementations of the motif-based spectral clustering algorithm
 - for the SNAP software library, which is available at <https://github.com/snap-stanford/snap>;
 - in Julia, which is available at <https://github.com/arbenson/higher-order-organization-julia>; and
 - in MATLAB, which is available at <https://github.com/arbenson/higher-order-organization-matlab>.
- Implementations of the temporal motif counting algorithms for the SNAP software library, which is available at <https://github.com/snap-stanford/snap>.
- Julia notebooks to reproduce the results in the main text of Benson et al. [2016], which are available at <https://github.com/arbenson/higher-order-organization-julia>.
- Metadata for the nodes in the transportation reachability network of Frey

and Dueck [2007] (city latitudes, longitudes, and metropolitan populations), which is available at

<http://snap.stanford.edu/data/reachability.html>.

- Metadata for the nodes in the Florida Bay food web Frey and Dueck [2007] (group classification), which is available at <http://snap.stanford.edu/data/Florida-bay.html>.
- The EMAIL-EU-CORE network dataset with department labels for all of the nodes, which is available at <http://snap.stanford.edu/data/email-Eu-core.html>.
- The WIKI-CATS network dataset with article names and category classifications for all of the nodes, which is available at <http://snap.stanford.edu/data/wiki-topcats.html>.
- The STACKOVERFLOW temporal network dataset, which is available at <http://snap.stanford.edu/data/sx-stackoverflow.html>.
- The MATHOVERFLOW temporal network dataset, which is available at <http://snap.stanford.edu/data/sx-mathoverflow.html>.
- The SUPERUSER temporal network dataset, which is available at <http://snap.stanford.edu/data/sx-superuser.html>.
- The ASKUBUNTU temporal network dataset, which is available at <http://snap.stanford.edu/data/sx-askubuntu.html>.
- The EMAIL-EU temporal network dataset and 4 department-level subnetworks, which are available at <http://snap.stanford.edu/data/email-Eu-core-temporal.html>.
- The WIKITALK temporal network dataset, which is available at <http://snap.stanford.edu/data/wiki-talk-temporal.html>.

Furthermore, the ideas of this thesis have already had impact on the broader research community. As an example, Meier et al. [2016] used the motif-based clustering algorithm in functional connectivity networks of brains and found symmetry patterns between the hemispheres of the brain. In their article “Network analytics in the age of big data” published in *Science*, Pržulj and Malod-Dognin [2016] contextualize the framework of Chapter 2 as an important step towards understanding the large-scale datasets coming from a “complex world of interconnected entities.” As discussed at the beginning of this introduction, network models and analysis are fundamental because of their wide applicability, and Pržulj and Malod-Dognin [2016] emphasize this point when (generously) discussing our work: “The importance of this result lies in its applicability to a broad range of networked data that we must understand to answer fundamental questions facing humanity today, from climate change and impacts of genetically modified organisms, to the environment, to food security, human migrations, economic and societal crises, understanding diseases, aging, and personalizing medical treatments.” Indeed, I

hope that the ideas that follow are a step towards tackling these problems.

Chapter 2

Higher-order network clustering

2.1 Organization via higher-order structures

Networks are a standard representation of data throughout the sciences, and higher-order connectivity patterns are essential to understanding the fundamental structures that control and mediate the behavior of many complex systems [Holland and Leinhardt, 1970; Mangan et al., 2003; Milo et al., 2002; Pržulj et al., 2004; Rosvall et al., 2014; Yang and Leskovec, 2014]. The most common higher-order structures are small network subgraphs, which we refer to as network motifs (Figure 2.1A). Network motifs are considered building blocks for complex networks [Milo et al., 2002; Yaveroglu et al., 2014]. For example, feedforward loops (Figure 2.1A, M_5) have proven fundamental to understanding transcriptional regulation networks [Mangan and Alon, 2003], triangular motifs (Figure 2.1A, M_1 – M_7) are crucial for social networks [Davis and Leinhardt, 1971; Holland and Leinhardt, 1970], open bidirectional wedges (Figure 2.1A, M_{13}) are key to structural hubs in the brain [Honey et al., 2007], and two-hop paths (Figure 2.1A, M_8 – M_{13}) are essential to understanding air traffic patterns [Rosvall et al., 2014]. While network motifs have been recognized as fundamental units of networks, the higher-order *organization* of networks at the level of network motifs has largely remained an open question.

In this chapter, we use higher-order network structures to gain new insights into the organization of complex systems. We develop a framework that identifies clusters of network motifs. For each network motif (Figure 2.1A), a different higher-order clustering may be revealed (Figure 2.1B), which means that different organizational patterns are exposed depending on the chosen motif.

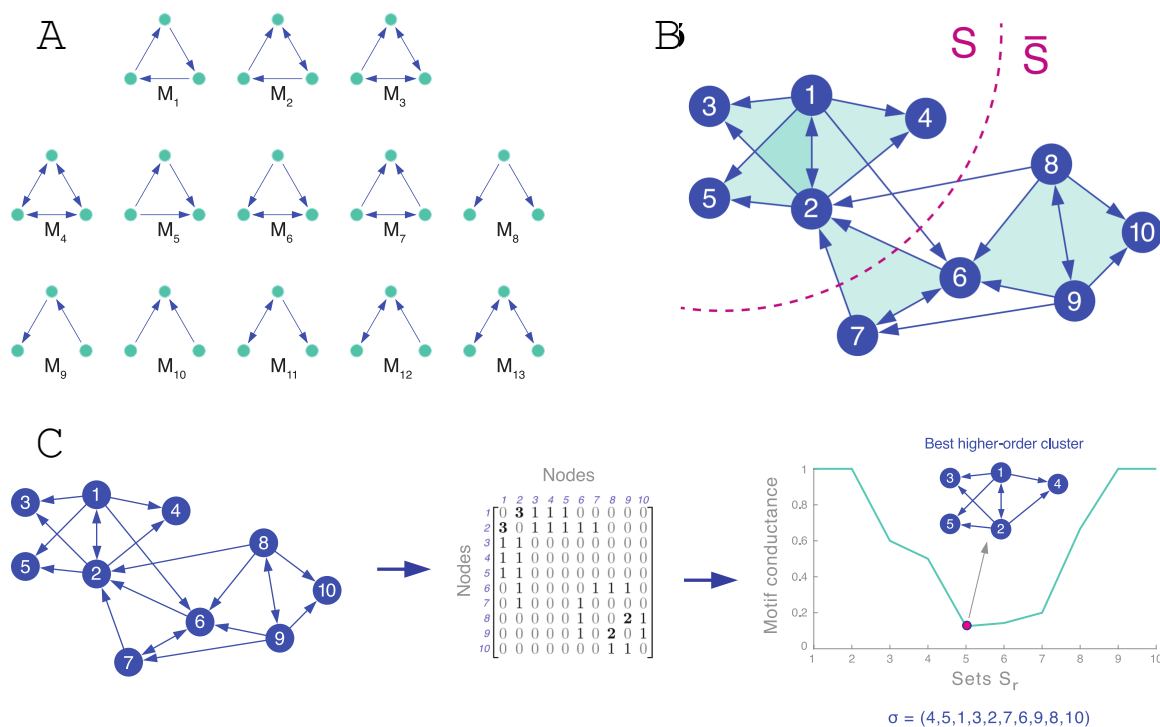


Figure 2.1 – Higher-order network structures and the higher-order network clustering framework. A: Higher-order structures are captured by network motifs. For example, all 13 connected three-node directed motifs are shown here. *B:* Clustering of a network based on motif M_7 . For a given motif M , our framework aims to find a set of nodes S that minimizes motif conductance, $\phi_M(S)$, which we define as the ratio of the number of motifs cut (filled triangles cut) to the minimum number of nodes in instances of the motif in either S or \bar{S} (Section 2.2 provides the formalities). In this case, there is one motif cut. *C:* The higher-order network clustering framework. Given a graph and a motif of interest (in this case, M_7), the framework forms a motif adjacency matrix (W_M) by counting the number of times two nodes co-occur in an instance of the motif. An eigenvector of a Laplacian transformation of the motif adjacency matrix is then computed. The ordering σ of the nodes provided by the components of the eigenvector produces nested sets $S_r = \{\sigma_1, \dots, \sigma_r\}$ of increasing size r . We prove in Section 2.2.7 that the set S_r with the smallest motif-based conductance, $\phi_M(S_r)$, is a near-optimal higher-order cluster.

Conceptually, given a network motif M , our framework searches for a cluster of nodes S with two goals. First, the nodes in S should participate in many instances of M . Second, the set S should avoid cutting instances of M , which occurs when only a subset of the nodes from a motif are in the set S (Figure 2.1B). More precisely, given a motif M , the higher-order clustering framework aims to find a cluster (defined by a set of nodes S) that minimizes the following ratio:

$$(2.1) \quad \phi_M(S) = \text{cut}_M(S, \bar{S}) / \min(\text{vol}_M(S), \text{vol}_M(\bar{S})),$$

where \bar{S} denotes the remainder of the nodes (the complement of S), $\text{cut}_M(S, \bar{S})$ is the number of instances of motif M with at least one node in S and one in \bar{S} , and $\text{vol}_M(S)$ is the number of nodes in instances of M that reside in S . Equation (2.1) is a generalization of the conductance metric in spectral graph theory, one of the most useful graph partitioning scores [Schaeffer, 2007]. We refer to $\phi_M(S)$ as the motif conductance of S with respect to M . (The formal mathematics of these definitions are discussed later in Sections 2.2.2 and 2.2.3).

Finding the exact set of nodes S that minimizes the motif conductance is NP-hard [Wagner and Wagner, 1993]. To approximately minimize Equation (2.1) and hence identify higher-order clusters, we develop an optimization framework that provably finds near-optimal clusters (Section 2.2). We extend the spectral graph clustering methodology, which is based on the eigenvalues and eigenvectors of matrices associated with the graph [Schaeffer, 2007], to account for higher-order structures in networks. The resulting method maintains the properties of traditional spectral graph clustering: computational efficiency, ease of implementation, and mathematical guarantees on the near-optimality of obtained clusters. Specifically, a cluster S identified by our higher-order clustering framework satisfies a motif Cheeger inequality:

$$(2.2) \quad \phi_M(S) \leq 2\sqrt{\phi_M^*},$$

where $\phi_M^* = \min_{T \subset V} \phi_M(T)$ is the optimal motif conductance over all possible sets T . In other words, our optimization framework can find a cluster that is at most a quadratic factor away from optimal. We prove this inequality in Section 2.2.7.

The algorithm (illustrated in Figure 2.1C) efficiently identifies a cluster of nodes S as follows:

- i. Given a network and a motif M of interest, form the motif adjacency matrix W_M whose entries (i, j) are the co-occurrence counts of nodes i and j in the motif M

$$(2.3) \quad (W_M)_{ij} = \text{number of instances of } M \text{ that contain nodes } i \text{ and } j.$$

- ii. Compute the spectral ordering σ of the nodes from the normalized motif Laplacian matrix constructed via W_M . The normalized motif Laplacian matrix is $N_M = D^{-1/2}(D - W_M)D^{-1/2}$, where D is a diagonal matrix with the row-sums of W_M on the diagonal ($D_{ii} = \sum_j (W_M)_{ij}$), and $D^{-1/2}$ is the same matrix with the inverse square-roots on the diagonal ($D_{ii}^{-1/2} = 1/\sqrt{\sum_j (W_M)_{ij}}$). The spectral ordering σ is the by-value ordering of $D^{-1/2}z$, where z is the eigenvector corresponding to the second smallest eigenvalue of N_M , i.e., σ_i is the index of $D^{-1/2}z$ with the i th smallest value.
- iii. Find the prefix set of σ with the smallest motif conductance, formally: $S := \arg \min_r \phi_M(S_r)$, where $S_r = \{\sigma_1, \dots, \sigma_r\}$.

For triangular motifs, the algorithm scales to networks with billions of edges and typically only takes several hours to process graphs of such size (Section 2.4). On smaller networks with hundreds of thousands of edges, the algorithm can process some motifs up to size 9 (specifically, we look at cliques up to size 9). While the worst-case computational complexity of the algorithm for triangular motifs scales as $m^{1.5}$, where m is the number of edges in the network, in practice the algorithm is much faster. Analyzing 16 real-world networks where the number of edges m ranges from 159,000 to 2 billion we found the computational complexity to scale as $m^{1.2}$. Moreover, the algorithm can easily be parallelized and sampling techniques can be used to further improve performance [Seshadhri et al., 2014].

The framework can be applied to directed, undirected, and weighted networks as well as motifs. Moreover, it can also be applied to networks with positive and negative signs on the edges, which are common in social networks (friend vs. foe or trust vs. distrust edges) and metabolic networks (edges signifying activation vs. inhibition). For example, in Section 2.3.4, we analyze a transcriptional regulation network with signed edges where the sign corresponds to activation or suppression of genetic transcription. The framework can be used to identify higher-order structure in networks where domain knowledge suggests the motif of interest. This is the case for our analysis of a transcriptional regulation network (Section 2.3.4), a network of neural connections in the nematode worm *C. elegans* (Section 2.3.6), and a transportation reachability network (Section 2.3.5). We also show that when a domain-specific higher-order pattern is not known in advance, the framework can also serve to identify which motifs are important for the modular organization of a given network; for example, in Section 2.3.3, we identify a motif that organizes a food web.

Such a general framework allows for a study of complex higher-order organizational structures in a number of different networks using individual motifs and sets of motifs. The framework and mathematical theory immediately extend to other spectral methods such as algorithms for finding overlapping clusters [Whang et al.,

2015] and localized algorithms that find clusters around a seed node [Andersen et al., 2006] (we develop the localized clustering extension in Section 2.5). To find several clusters, one can use embeddings from multiple eigenvectors and k -means clustering [Ng et al., 2001] or apply recursive bi-partitioning [Boley, 1998] (see Section 2.2.10 for details).

Our higher-order network clustering framework unifies motif analysis and network partitioning—two fundamental tools in network science—and reveals new organizational patterns and modules in complex systems. Prior efforts along these lines do not provide worst-case performance guarantees on the obtained clustering [Serrouf et al., 2011], do not reveal which motifs organize the network [Michoel et al., 2011], or rely on expanding the size of the network [Benson et al., 2015; Krzakala et al., 2013]. Our theoretical results in Section 2.2.7 also explain why classes of hypergraph partitioning methods are more general than previously assumed and how motif-based clustering provides a rigorous framework for the special case of partitioning directed graphs (Section 2.6).

2.2 The motif-based spectral clustering algorithm

We now cover the background and theory for deriving and understanding our method. We start by reviewing the graph Laplacian and cut, volume, and conductance measures for sets of vertices in a graph. We then define network motifs in and generalize the notions of cut, volume, and conductance to motifs. From this, we present the spectral algorithm for finding sets with small motif conductance and the associated theory (motif Cheeger inequality). We then analyze the complexity of the algorithm and discuss some extensions of the framework.

2.2.1 Review of cuts, volumes, conductance and the graph Laplacian for weighted, undirected graphs

Consider a weighted, undirected graph $G = (V, E)$, with $|V| = n$. Further assume that G has no isolated nodes. Let W encode the weights of the graph:

$$(2.4) \quad W_{ij} = W_{ji} = \text{weight of edge } (i, j).$$

The diagonal degree matrix D is defined by $D_{ii} = \sum_{j=1}^n W_{ij}$, and the graph Laplacian is defined as $L = D - W$. We now relate these matrices to the conductance

$\phi(S)$ of a subset $S \subset V$ of nodes in G .

$$(2.5) \quad \phi(S) = \text{cut}(S, \bar{S}) / \min(\text{vol}(S), \text{vol}(\bar{S})),$$

$$(2.6) \quad \text{cut}(S, \bar{S}) = \sum_{i \in S, j \in \bar{S}} W_{ij},$$

$$(2.7) \quad \text{vol}(S) = \sum_{i \in S} D_{ii}$$

Here, $\bar{S} = V \setminus S$ is the complement of the set S . (Note that conductance is a symmetric measure in S and \bar{S} , i.e., $\phi(S) = \phi(\bar{S})$.) Conceptually, the cut and volume measures are defined as follows:

$$(2.8) \quad \text{cut}(S, \bar{S}) = \text{weighted sum of edges that are cut}$$

$$(2.9) \quad \text{vol}(S) = \text{weighted number of edge end points in } S.$$

In general, sets with low conductance are considered good clusters [Schaeffer, 2007]. They model the conceptual definition that good clusters are isolated from the rest of the network (there are few edges leaving S when the cut is small) and not too small (there is enough volume in S).

Since we have assumed G has no isolated nodes, $\text{vol}(S) > 0$. If G is disconnected, it is easy to see that $\phi(C) = 0$ for any connected component C . Thus, we usually consider breaking G into connected components as a pre-processing step for algorithms that try to find low-conductance sets.

We now relate the cut metric to a quadratic form on L . Later, we will derive a similar form for a motif cut measure. For any vector $y \in \mathbb{R}^n$,

$$(2.10) \quad y^T L y = \sum_{(i,j) \in E} w_{ij} (y_i - y_j)^2.$$

Now, define x to be an indicator vector for a set of nodes S i.e., $x_i = 1$ if node i is in S and $x_i = -1$ if node i is in \bar{S} . If an edge (i, j) is cut, then x_i and x_j take different values and $(x_i - x_j)^2 = 4$; otherwise, $(x_i - x_j)^2 = 0$. Thus,

$$(2.11) \quad x^T L x = 4 \cdot \text{cut}(S, \bar{S}).$$

Over the next few sections, we generalize these ideas for motifs.

2.2.2 Definition of network motifs

We now define network motifs as used in this chapter. We consider motifs to be a pattern of edges on a small number of nodes. Formally, we define a motif on

k nodes by a tuple (B, \mathcal{A}) , where B is a $k \times k$ binary matrix and $\mathcal{A} \subset \{1, 2, \dots, k\}$ is a set of anchor nodes. The matrix B encodes the edge pattern between the k nodes, and \mathcal{A} labels a relevant subset of nodes for defining motif conductance. (More specifically, the anchored nodes are the ones that contribute to the cut and volume counts; we make this formal later.) In many cases, \mathcal{A} is just the entire set of nodes. As an example, motif M_4 (the directed triangle with all bidirectional links; Figure 2.1A), where all nodes are anchors is denoted by

$$(B, \mathcal{A}) = \left(\begin{bmatrix} 0 & 1 & 1 \\ 1 & 0 & 1 \\ 1 & 1 & 0 \end{bmatrix}, \{1, 2, 3\} \right)$$

Let $\chi_{\mathcal{A}}$ be a selection function that takes the subset of a k -tuple indexed by \mathcal{A} , and let $\text{set}(\cdot)$ be the operator that takes an (ordered) tuple to an (unordered) set. Specifically,

$$\text{set}((v_1, v_2, \dots, v_k)) = \{v_1, v_2, \dots, v_k\}.$$

The set of all motifs in an unweighted (possibly directed) graph with node set V and adjacency matrix A , denoted $\mathcal{M}(B, \mathcal{A})$, is defined by

$$(2.12) \quad \mathcal{M}(B, \mathcal{A}) = \{(\text{set}(v), \text{set}(\chi_{\mathcal{A}}(v))) \mid v \in V^k, v_1, \dots, v_k \text{ distinct}, A_{v,v} = B\},$$

where $A_{v,v}$ is the $k \times k$ adjacency matrix on the subgraph induced by the k nodes of the *ordered* vector v . Sometimes, a distinction is made between a *functional* and a *structural* motif [Sporns and Kötter, 2004] (or a subgraph and an induced subgraph [Inokuchi et al., 2000]) to distinguish whether a motif specifies simply the existence of a set of edges (functional motif or subgraph) or the existence and non-existence of edges (structural motif or induced subgraph). By asserting the equivalency $A_{v,v} = B$, we refer to structural motifs in this work. However, a function motif is just a union of structural motifs. Our clustering framework allows for the simultaneous consideration of several motifs (see Section 2.2.11), so we have not lost any generality and can cluster based on structural motifs.

Figure 2.2 illustrates these definitions. The set operator is a convenient way to avoid duplicates when defining $\mathcal{M}(B, \mathcal{A})$ for motifs exhibiting symmetries. Henceforth, we will just use $(v, \chi_{\mathcal{A}}(v))$ to denote $(\text{set}(v), \text{set}(\chi_{\mathcal{A}}(v)))$ when discussing elements of $\mathcal{M}(B, \mathcal{A})$. Furthermore, we call any $(v, \chi_{\mathcal{A}}(v)) \in \mathcal{M}(B, \mathcal{A})$ a *motif instance*. When B and \mathcal{A} are arbitrary or clear from context, we will simply denote the motif set by \mathcal{M} .

We call motifs where $\chi_{\mathcal{A}}(v) = v$ *simple motifs* (Figure 2.2B) and motifs where $\chi_{\mathcal{A}}(v) \neq v$ *anchored motifs* (Figure 2.2C). Existing motif analysis has only analyzed

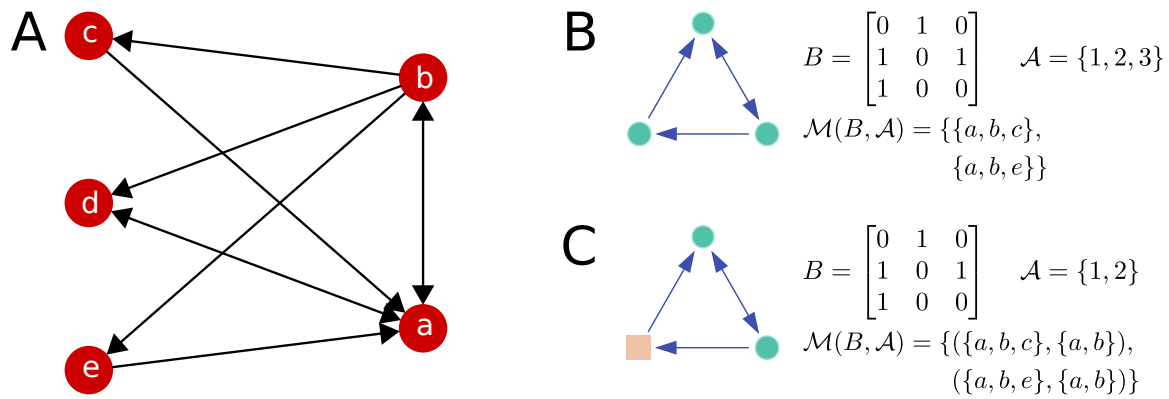


Figure 2.2 – Formal motif definition. A motif consists of a $k \times k$ binary matrix B and a set of anchor nodes $\mathcal{A} \subseteq \{1, \dots, k\}$. **A:** Example network. **B:** Example simple motif, where the anchor nodes are the entire index set. In this case, we can think of motifs as just subsets of nodes. The set $\mathcal{M}(B, \mathcal{A})$ lists all of the subsets of nodes where the induced subgraph is isomorphic to the graph defined by the matrix B . **C:** Example anchored motif, where the green nodes are the anchor nodes. There are two instances of the anchored motif in the graph in A. The tuple $(\{a, b, d\}, \{a, b\})$ is not included in the set of motif instances because the induced subgraph on the nodes a, b , and d is not isomorphic to the graph defined by the matrix B .

simple motifs. However, the anchored motif provides us with a more general framework, and we use an anchored motif for the analysis of the transportation reachability network in Section 2.3.5.

2.2.3 Motif conductance

Recall that the key definitions for defining conductance are the notions of cut and volume. For an unweighted graph, these are

$$(2.13) \quad \phi(S, \bar{S}) = \text{cut}(S, \bar{S}) / \min(\text{vol}(S), \text{vol}(\bar{S})),$$

$$(2.14) \quad \text{cut}(S, \bar{S}) = \text{number of edges cut},$$

$$(2.15) \quad \text{vol}(S) = \text{number of edge end points in } S.$$

Our syntactic definition of motif conductance simply replaces an edge with a motif instance of type M :

$$(2.16) \quad \phi_M(S) = \text{cut}_M(S, \bar{S}) / \min(\text{vol}_M(S), \text{vol}_M(\bar{S})),$$

$$(2.17) \quad \text{cut}_M(S, \bar{S}) = \text{number of motif instances cut},$$

$$(2.18) \quad \text{vol}_M(S) = \text{number of motif instance end points in } S.$$

We say that a motif instance is cut if there is at least one anchor node in S and at least one anchor node in \bar{S} and we say that an “end point in S ” is any anchor node of a motif instance in S . We can formalize this when given a motif set \mathcal{M} as in Equation (2.12):

$$(2.19) \quad \text{cut}_M(S, \bar{S}) = \sum_{(v, \chi_{\mathcal{A}}(v)) \in \mathcal{M}} \text{Ind}[\exists i, j \in \chi_{\mathcal{A}}(v) \mid i \in S, j \in \bar{S}],$$

$$(2.20) \quad \text{vol}_M(S) = \sum_{(v, \chi_{\mathcal{A}}(v)) \in \mathcal{M}} \sum_{i \in \chi_{\mathcal{A}}(v)} \text{Ind}[i \in S],$$

where $\text{Ind}[s]$ is the truth-value indicator function on s , i.e., $\text{Ind}[s]$ takes the value 1 if the statement s is true and 0 otherwise. The motif cut measure only counts an instance of a motif as cut if the anchor nodes are separated, and the motif volume counts the number of anchored nodes in the set. However, two nodes in an anchor set may be a part of several motif instances. Specifically, following the definition in Equation (2.12), there may be many different v with the same $\chi_{\mathcal{A}}(v)$, and the nodes in $\chi_{\mathcal{A}}(v)$ still get counted proportional to the number of motif instances.

2.2.4 The motif adjacency matrix and the motif Laplacian

Given an unweighted, directed graph and a motif set \mathcal{M} , we conceptually define the motif adjacency matrix by

$$(2.21) \quad (W_M)_{ij} = \text{number of motif instances in } \mathcal{M} \text{ where} \\ i \text{ and } j \text{ participate as anchor nodes in the motif.}$$

Or, formally,

$$(2.22) \quad (W_M)_{ij} = \begin{cases} \sum_{(v, \chi_{\mathcal{A}}(v)) \in \mathcal{M}} \text{Ind}[\{i, j\} \subset \chi_{\mathcal{A}}(v)], & i \neq j \\ 0 & \text{otherwise} \end{cases}$$

Note that weight is added to $(W_M)_{ij}$ only if i and j appear in the anchor set. This is important for the transportation reachability network analyzed in Section 2.3.5, where weight is added between cities i and j based on the number of intermediary cities that can be traversed between them.

Next, we define the motif diagonal degree matrix as

$$D_M = \text{diag}(W_M e),$$

where e is the vector of all ones and the motif Laplacian as

$$L_M = D_M - W_M.$$

Finally, we define the normalized motif Laplacian as

$$N_M = D_M^{-1/2} L_M D_M^{-1/2} = I - D_M^{-1/2} W_M D_M^{-1/2}.$$

In the next section, we develop our clustering algorithm based on computing an eigenvector of N_M .

2.2.5 The spectral algorithm for finding a single cluster

We are now ready to describe the algorithm for finding a single cluster in a graph, which we present in Algorithm 1. The algorithm finds a partition of the nodes into S and \bar{S} . The motif conductance is symmetric in the sense that $\phi_M(S) = \phi_M(\bar{S})$, so either set of nodes (S or \bar{S}) could be interpreted as a cluster. However, in practice, it is common that one set is substantially smaller than the other. We consider this smaller set to represent a module in the network.

The algorithm itself is simple. First, the algorithm pre-processes the (possibly) directed graph into the weighted adjacency matrix. Second, it uses a well-known spectral graph partitioning method on the weighted graph graph [Alon, 1986; Alon and Milman, 1985; Chung, 2007; Fiedler, 1973; Mihail, 1989]. The novel insight here is that this process provides theoretical results in terms of motif conductance, as we will show in Section 2.2.7. Specifically, we show that when the motif M has

Algorithm 1 – Motif-based clustering algorithm for finding a single cluster. The algorithm forms a weighted undirected graph and then runs a classical spectral partitioning method on the weighted graph. Our theory in Section 2.2.7 gives bounds on the cluster quality in terms of motif conductance.

Input: Directed, unweighted graph G and motif M
Output: Motif-based cluster (subset of nodes in G)

- 1 $(W_M)_{ij} \leftarrow$ number of instances of M that contain nodes i and j .
- 2 $D_M \leftarrow \text{diag}(W_M e)$.
- 3 $N_M \leftarrow I - D_M^{-1/2} W_M D_M^{-1/2}$.
- 4 $z \leftarrow$ eigenvector of second smallest eigenvalue for N_M
- 5 $\sigma_i \leftarrow$ index of $D_M^{-1/2} z$ with i th smallest value
- 6 /* Sweep procedure */
- 7 $S_l^* \leftarrow \arg \min_{S_l} \phi(S_l)$, where $S_l = \{\sigma_1, \dots, \sigma_l\}$
- 8 **if** $|S_l^*| < |\bar{S}_l^*|$ **then**
- 9 **return** S_l^*
- 10 **else**
- 11 **return** \bar{S}_l^*

three nodes, the output set S satisfies

$$(2.23) \quad \phi_M(S) \leq 2\sqrt{\phi_M^*},$$

where $\phi_M^* = \min_{T \subset V} \phi_M(T)$ is the smallest motif conductance over all possible sets of nodes. This is a generalization of the celebrated Cheeger inequality for graphs [Alon and Milman, 1985; Cheeger, 1970; Mihail, 1989]. Hence, we call this bound a *motif Cheeger inequality*, which we will prove and discuss in Section 2.2.7

Finally, we find that it is often informative to look at all conductance values found from the “sweep” procedure in this algorithm (Line 7), where the algorithm sweeps over several sets and picks out the one with smallest motif conductance. We refer to a plot of $\phi(S_l)$ versus l as a *sweep profile plot*. In the following subsection, we show that when the motif has three nodes, the conductance of any set S in the weighted graph equals the motif conductance in the original graph G . Thus, in this case, the sweep profile shows how motif conductance varies with the size of the sets in Algorithm 1.

2.2.6 Interlude for matrix computations

Before providing the theoretical analysis for Algorithm 1, we use this subsection to show how, for several motifs, the motif adjacency matrix W_M (Equation (2.21)) has a clean formula in terms of simple matrix computations. Let A be the adjacency matrix for the original graph, and let U and B be the adjacency matrix of the unidirectional and bidirectional links of G . Formally, $B = A \circ A^T$ and $U = A - B$, where \circ denotes the Hadamard (entry-wise) product. Table 2.1 lists the formula of W_M for all 7 of the directed triangle motifs in terms of matrix computations involving U and B .

Table 2.1 – Matrix computations for the weighted motif adjacency matrix. For the adjacency matrix A , $B = A \circ A^T$ and $U = A - B$.

Motif	Matrix computations	$W_M =$
M_1	$C = (U \cdot U) \circ U^T$	$C + C^T$
M_2	$C = (B \cdot U) \circ U^T + (U \cdot B) \circ U^T + (U \cdot U) \circ B$	$C + C^T$
M_3	$C = (B \cdot B) \circ U + (B \cdot U) \circ B + (U \cdot B) \circ B$	$C + C^T$
M_4	$C = (B \cdot B) \circ B$	C
M_5	$C = (U \cdot U) \circ U + (U \cdot U^T) \circ U + (U^T \cdot U) \circ U$	$C + C^T$
M_6	$C = (U \cdot B) \circ U + (B \cdot U^T) \circ U^T + (U^T \cdot U) \circ B$	C
M_7	$C = (U^T \cdot B) \circ U^T + (B \cdot U) \circ U + (U \cdot U^T) \circ B$	C

The central computational kernel in these computations is $(X \cdot Y) \circ Z$. Azad et al. [2015] developed and analyzed parallel algorithms for these computations when X , Y , and Z are sparse (and if the graph is sparse, these matrices will be sparse). This matrix-based formulation has worse computational complexity than the fast algorithms discussed later in Section 2.2.9—the computation $X \cdot Y$ counts length-2 paths, which is prohibitively expensive for large, sparse real-world networks. However, the implementation is simple and elegant and works well for small graphs. To demonstrate this, Figure 2.3 contains a complete implementation of Algorithm 1 for motifs M_1 – M_7 in fewer than 50 lines of readable Julia code.

```

1 # Find a motif-based cluster for any directed triangle motif.
2 function MotifSpectralClust(A::SparseMatrixCSC{Int64,Int64}, motif::AbstractString)
3     # Form motif adjacency matrix
4     B = min.(A, A') # bidirectional links
5     U = A - B      # unidirectional links
6     if motif == "M1"
7         C = (U * U) .* U'
8         W = C + C'
9     elseif motif == "M2"
10        C = (B * U) .* U' + (U * B) .* U' + (U * U) .* B
11        W = C + C'
12    elseif motif == "M3"
13        C = (B * B) .* U + (B * U) .* B + (U * B) .* B
14        W = C + C'
15    elseif motif == "M4"
16        W = (B * B) .* B
17    elseif motif == "M5"
18        C = (U * U) .* U + (U * U') .* U + (U' * U) .* U
19        W = C + C'
20    elseif motif == "M6"
21        W = (U * B) .* U + (B * U') .* U' + (U' * U) .* B
22    elseif motif == "M7"
23        W = (U' * B) .* U' + (B * U) .* U + (U * U') .* B
24    else
25        error("Motif must be one of M1, M2, M3, M4, M5, M6, or M7.")
26    end
27
28 # Get Fiedler eigenvector
29 dinvsqrt = spdiagm(1.0 ./ sqrt.(vec(sum(W, 1))))
30 NM = I - dinvsqrt * W * dinvsqrt
31 lambdas, evecs = eigs(NM, nev=2, which=:SM)
32 z = dinvsqrt * real(evecs[:, 2])
33
34 # Sweep cut
35 sigma = sortperm(z)
36 C = W[sigma, sigma]
37 Csums = sum(C, 1)'
38 motifvolS = cumsum(Csums)
39 motifvolSbar = sum(W) * ones(length(sigma)) - motifvolS
40 conductances = cumsum(Csums - 2 * sum(triu(C), 1)') ./ min.(motifvolS, motifvolSbar)
41 split = indmin(conductances)
42 if split <= length(size(A, 1)) / 2
43     return sigma[1:split]
44 else
45     return sigma[(split + 1):end]
46 end
47 end

```

Figure 2.3 – Julia implementation of the motif-based spectral clustering algorithm. Using the matrix computations in Table 2.1, Algorithm 1 for motifs M_1 – M_7 can be implemented in fewer than 50 lines of Julia. This code is available at <https://gist.github.com/arbenson/a7bb06fb74977cddb455e824519a55e>.

Another matrix-based interpretation comes from the inner product of the motif-node incidence matrix. Specifically, let $\mathcal{M}(B, \mathcal{A})$ be a motif set and number the instances of the motif $1, \dots, |\mathcal{M}|$, so that $(v_i, \chi_{\mathcal{A}}(v_i))$ is the i th motif. Define the $|\mathcal{M}| \times n$ motif-node incidence matrix by

$$(A_M)_{ij} = \text{Ind}[j \in \chi_{\mathcal{A}}(v_i)].$$

Then the motif adjacency matrix may be written as

$$W_M = A_M^T A_M - \text{diag}(A_M^T A_M)$$

This provides a convenient algebraic formulation for defining and thinking about the weighted motif adjacency matrix. However, in practice, we do not use this formulation for any computations.

2.2.7 Motif Cheeger inequality for network motifs with three nodes

In spectral graph theory, the Cheeger inequality is a well-known relationship between the second-smallest eigenvalue of the normalized Laplacian and the conductance of a graph. The name of the inequality is attributed to Jeff Cheeger, who actually proved a result about the eigenvalues of Laplacians on manifolds [Cheeger, 1970]. Later on, the bound was generalized to the normalized Laplacian on graphs, which we state here.

Theorem 1 (Cheeger inequality for graphs [Alon, 1986; Alon and Milman, 1985]). *Let λ_2 be the second smallest eigenvalue of the normalized laplacian N for any weighted graph W with node set V . Then*

$$(2.24) \quad \lambda_2/2 \leq \phi^* \leq \sqrt{2\lambda_2},$$

where $\phi^* = \min_{S \subset V} \phi(S)$.

While we cannot expect to find the set with minimum conductance due to the NP-hardness of minimizing conductance [Wagner and Wagner, 1993], we might hope to realize the upper bound of the Cheeger inequality by finding some set S for which $\phi(S) \leq \sqrt{2\lambda_2}$. In other words, if we could construct some S with this property, then we get the upper bound in Theorem 1. By the lower bound of Theorem 1, this set S would then satisfy $\phi(S) \leq \sqrt{4\phi^*} = 2\sqrt{\phi^*}$. The sweep procedure in Algorithm 1 finds such a set S .¹

¹For a clean proof of this result, see Dan Spielman's lecture notes: <http://www.cs.yale.edu/homes/spielman/561/lect06-15.pdf>.

Theorem 2 (Sweep Cheeger inequality [Mihail, 1989]). *The set S output by Algorithm 1 satisfies*

$$(2.25) \quad \phi(S) \leq \sqrt{2\lambda_2} \leq 2\sqrt{\phi^*},$$

where conductance is measured in terms of the weighted graph W .

Algorithm 1 has guarantees on the quality of the output set S , but these guarantees are in terms of the (edge) conductance of sets in the weighted adjacency graph. Instead, we would like guarantees in terms of motif conductance. In the rest of this section, we derive the same guarantees for motif conductance with simple three-node motifs, or in general, motifs with 2 or 3 anchor nodes. The crux of this result is deriving a relationship between the motif conductance function and the weighted motif adjacency matrix, from which the motif Cheeger inequality is essentially a corollary.

For the rest of this section and the next, we use the following notation. Given an unweighted, directed graph G and a motif M , the corresponding weighted graph defined by Equation (2.22) is denoted by G_M . For conductance, cut, and volume, we will also specify the graph in which these measurements are made. Specifically, $\phi_M^{(G)}(S)$, $\text{cut}_M^{(G)}(S)$, and $\text{vol}_M^{(G)}(S)$ denote the motif conductance, motif cut, and motif volume of set S in graph G with respect to motif M .

The following Lemma relates the motif volume to the volume in the weighted graph. This lemma applies to any anchor set \mathcal{A} consisting of at least two nodes. For our main result, we will apply the lemma assuming $|\mathcal{A}| = 3$. However, we will apply the lemma more generally when discussing four-node motifs in Section 2.2.8.

Lemma 3. *Let $G = (V, E)$ be a directed, unweighted graph and let G_M be the corresponding weighted graph for a motif M on k nodes and $|\mathcal{A}|$ anchor nodes, $2 \leq |\mathcal{A}| \leq k$. Then for any subset $S \subset V$,*

$$\text{vol}_M^{(G)}(S) = \frac{1}{|\mathcal{A}| - 1} \text{vol}^{(G_M)}(S)$$

Proof. Consider an instance $(v, \chi_{\mathcal{A}}(v))$ of a motif. Let $(v_1, \dots, v_{|\mathcal{A}|}) = \chi_{\mathcal{A}}(v)$. By Equation (2.22), $(W_M)_{v_1, j}$ is incremented by one for $j = v_2, \dots, v_{|\mathcal{A}|}$. Since $(D_M)_{v_1, v_1} = \sum_j (W_M)_{v_1, j}$, the motif end point v_1 is counted $|\mathcal{A}| - 1$ times. \square

The next lemma states that the truth value for determining whether three binary variables in $\{-1, 1\}$ are not all equal is a quadratic function of the variables. Because this function is quadratic, we will be able to relate motif cuts on three nodes to a quadratic form on the motif Laplacian.

Lemma 4. Let $x_i, x_j, x_k \in \{-1, 1\}$. Then

$$4 \cdot \text{Ind}[x_i, x_j, x_k \text{ not all the same}] = x_i^2 + x_j^2 + x_k^2 - x_i x_j - x_j x_k - x_k x_i.$$

The next lemma contains the essential result that relates motif cuts in the original graph G to weighted edge cuts in G_M . In particular, the lemma shows that the motif cut measure is proportional to the cut on the weighted graph defined in Equation (2.21) when there are three anchor nodes.

Lemma 5. Let $G = (V, E)$ be a directed, unweighted graph and let G_M be the weighted graph for a motif with $|\mathcal{A}| = 3$. Then for any $S \subset V$,

$$\text{cut}_M^{(G)}(S, \bar{S}) = \frac{1}{2} \text{cut}^{(G_M)}(S, \bar{S})$$

Proof. Let $x \in \{-1, 1\}^n$ be an indicator vector of the node set S .

$$\begin{aligned} 4 \cdot \text{cut}_M(S, \bar{S}) &= \sum_{(v, \{i, j, k\}) \in \mathcal{M}} 4 \cdot \text{Ind}[x_i, x_j, x_k \text{ not all the same}] && \text{by definition} \\ &= \sum_{(v, \{i, j, k\}) \in \mathcal{M}} \left(x_i^2 + x_j^2 + x_k^2 \right) - (x_i x_j + x_j x_k + x_k x_i) && \text{by Lemma 4} \\ &= -\frac{1}{2} x^T W_M x + \sum_{(v, \{i, j, k\}) \in \mathcal{M}} x_i^2 + x_j^2 + x_k^2 && \text{by Equation (2.22)} \\ &= -\frac{1}{2} x^T W_M x + \text{vol}_M(V) && \text{since } x_i^2 = x_j^2 = x_k^2 = 1 \\ &= -\frac{1}{2} x^T W_M x + \frac{1}{2} x^T D_M x && \text{by Lemma 3} \\ &= \frac{1}{2} x^T L_M x && \text{by definition} \\ &= 2 \cdot \text{cut}^{(G_M)}(S, \bar{S}) && \text{by Equation (2.11)}. \end{aligned}$$

□

We are now ready to prove our main result, namely that motif conductance on the original graph G is equivalent to (edge) conductance on the weighted graph G_M when there are three anchor nodes. The result is a consequence of the volume and cut relationships provided by Lemmas 3 and 5.

Theorem 6. Let $G = (V, E)$ be a directed, unweighted graph and let G_M be the weighted graph corresponding to the motif adjacency matrix for any motif with $|\mathcal{A}| = 3$. Then for any set $S \subset V$,

$$\phi_M^{(G)}(S) = \phi^{(G_M)}(S)$$

In other words, when there are three anchor nodes, the motif conductance is equal to the conductance on the weighted graph defined by Equation (2.21).

Proof. When $|\mathcal{A}| = 3$, the motif cut and motif volume are both equal to half the motif cut and motif volume measures by Lemmas 3 and 5. \square

For any motif with three anchor nodes, conductance on the weighted graph is equal to the motif conductance. Thus, we can re-interpret the Cheeger inequality on the weighted graph in terms of motif conductance. This leads to our result.

Theorem 7 (Motif Cheeger inequality). *Let G be an unweighted, directed graph and let M be a motif with two or three anchor nodes. Let*

- S be the output of Algorithm 1 with input G and M ,
- λ_2 be the second smallest eigenvalue of N_M , and
- $\phi_M^* = \min_{T \subset V} \phi_M(T)$ be the optimal motif conductance over all sets of nodes T .

Then

- i. $\lambda_2/2 \leq \phi_M^* \leq \sqrt{2\lambda_2}$, and
- ii. $\phi_M(S) \leq 2\sqrt{\phi_M^*}$.

Proof. The result follows from Theorems 1, 2 and 6. \square

The first result provides a lower bound on the optimal motif conductance in terms of the eigenvalue λ_2 . We use this bound in our analysis of a food web (see Section 2.3.3) to show that certain motifs do not provide good clusters, regardless of the procedure used to find a cluster. The second part of the result says that Algorithm 1 outputs a cluster that is within a quadratic factor of optimal. This provides the mathematical guarantees that our procedure finds a good motif-based cluster in a graph, if one exists.

2.2.8 Motif Cheeger inequality for network motifs with four or more nodes

Analogues of the indicator function in Lemma 4 for four or more variables are not quadratic [Ihler et al., 1993]. Subsequently, for motifs with $|\mathcal{A}| > 3$, we no longer get the motif Cheeger inequalities guaranteed by Theorem 7. That being said, solutions found by motif-based partitioning approximate a related value of conductance. We now provide the details.

We begin with a lemma that shows a functional form for four binary variables taking values in $\{-1, 1\}$ to not all be equal. We see that it is quartic, not quadratic.

Lemma 8. Let $x_i, x_j, x_k, x_l \in \{-1, 1\}$. Then the indicator function on all four elements not being equal is

$$(2.26) \quad \begin{aligned} & 8 \cdot \text{Ind}[x_i, x_j, x_k, x_l \text{ not all the same}] \\ & = (7 - x_i x_j - x_i x_k - x_i x_l - x_j x_k - x_j x_l - x_k x_l - x_i x_j x_k x_l). \end{aligned}$$

We *almost* have a quadratic form, if not for the quartic term $x_i x_j x_k x_l$. However, we could use the following related quadratic form:

$$(2.27) \quad \begin{aligned} & 6 - x_i x_j - x_i x_k - x_i x_l - x_j x_k - x_j x_l - x_k x_l \\ & = \begin{cases} 0 & x_i, x_j, x_k, x_l \text{ are all the same} \\ 6 & \text{exactly three of } x_i, x_j, x_k, x_l \text{ are the same} \\ 8 & \text{exactly two of } x_i, x_j, x_k, x_l \text{ are } -1. \end{cases} \end{aligned}$$

The quadratic still takes value 0 if all four entries are the same, and takes a non-zero value otherwise. However, the quadratic takes a larger value if exactly two of the four entries takes the value -1 (see Figure 2.4). From this, we can provide an analogous statement to Lemma 5 for motifs with $|\mathcal{A}| = 4$.

Lemma 9. Let $G = (V, E)$ be a directed, unweighted graph and let G_M be the weighted graph for a motif M with $|\mathcal{A}| = 4$. Then for any $S \subset V$,

$$\text{cut}_M^{(G)}(S, \bar{S}) = \frac{1}{3} \text{cut}^{(G_M)}(S, \bar{S}) - \sum_{(v, \{i,j,k,l\}) \in \mathcal{M}} \frac{1}{3} \cdot \text{Ind}[\text{exactly two of } i, j, k, l \text{ in } S].$$

Proof. Let $x \in \{-1, 1\}^n$ be an indicator vector of the node set S .

$$\begin{aligned} & 6 \cdot \text{cut}_M^{(G)}(S, \bar{S}) + \sum_{(v, \{i,j,k,l\}) \in \mathcal{M}} 2 \cdot \text{Ind}[\text{exactly two of } i, j, k, l \text{ in } S] \\ & = \sum_{(v, \{i,j,k,l\}) \in \mathcal{M}} 6 - x_i x_j - x_i x_k - x_i x_l - x_j x_k - x_j x_l - x_k x_l \\ & = \sum_{(v, \{i,j,k,l\}) \in \mathcal{M}} \frac{3}{2} (x_i^2 + x_j^2 + x_k^2 + x_l^2) - (x_i x_j + x_i x_k + x_i x_l + x_j x_k + x_j x_l + x_k x_l) \\ & = \frac{1}{2} x^T D_M x - \frac{1}{2} x^T W_M x \\ & = \frac{1}{2} x^T L_M x \\ & = 2 \cdot \text{cut}^{(G_M)}(S, \bar{S}). \end{aligned}$$

The first equality follows from Equations (2.19) and (2.27). The third equality

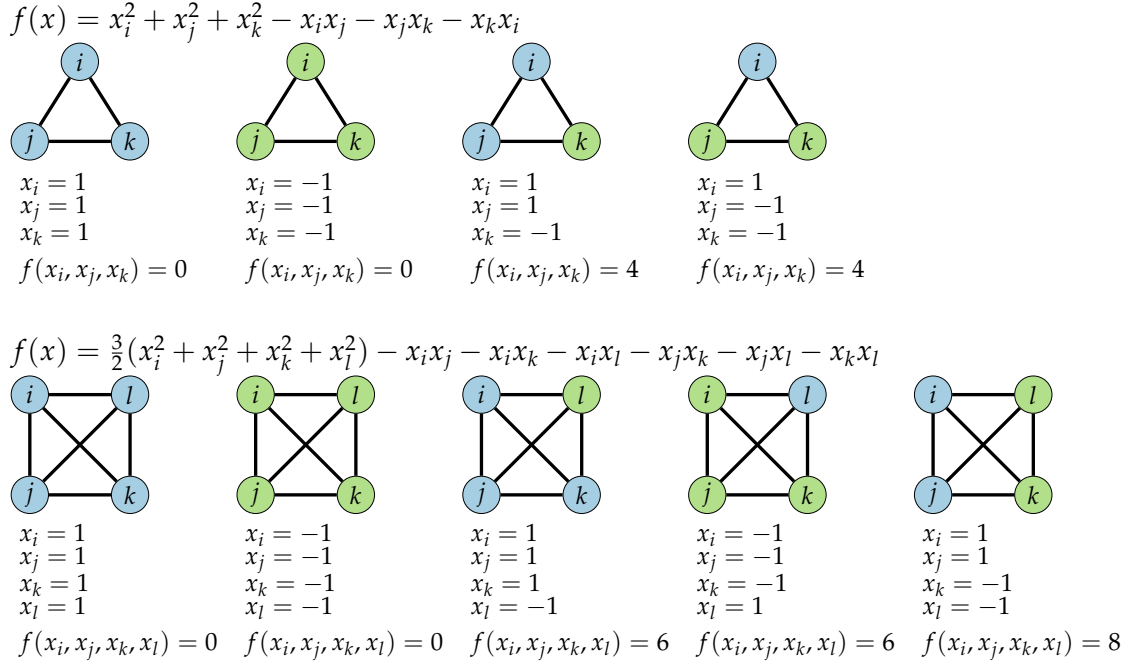


Figure 2.4 – Quadratic forms on indicator functions for set assignment. The blue nodes have assignment to set S and the green nodes have assignment to set \bar{S} . The quadratic function gives the penalty for cutting that motif. **Top:** Illustration of Equation (2.26). The quadratic form is proportional to the indicator on whether or not the motif is cut. **Bottom:** Illustration of Equation (2.27). The quadratic form is equal to zero when all nodes are in the same set. However, the form penalizes 2/2 splits more than 3/1 splits.

follows from Lemma 3. The fourth equality follows from the definition of L_M . The fifth equality follows from Equation (2.11). \square

With four anchor nodes, the motif cut in G is slightly different than the weighted cut in the weighted graph G_M . However, by Lemma 3,

$$\text{vol}_M^{(G)}(S) = \frac{1}{3} \text{vol}^{(G_M)}(S),$$

so the motif volume in G is still proportional to the weighted volume in G_M . We use this to derive the following result.

Theorem 10. *Let $G = (V, E)$ be a directed, unweighted graph and let W_M be the*

weighted adjacency matrix for any motif M with $|\mathcal{A}| = 4$. Then for any $S \subset V$,

$$\phi_M^{(G)}(S) = \phi^{(G_M)}(S) - \frac{\sum_{(v, \{i, j, k, l\}) \in \mathcal{M}} \text{Ind}[\text{exactly two of } i, j, k, l \text{ in } S]}{\text{vol}^{(G_M)}(S)}$$

In other words, when there are four anchor nodes, the weighting scheme in Equation (2.21) models the exact conductance with an additional penalty for splitting the four anchor nodes into two groups of two.

Proof. The result follows from Lemmas 3 and 9. □

To summarize, we still get a motif Cheeger inequality from the weighted graph, but it is in terms of a penalized version of the motif conductance $\phi_M^{(G)}(S)$. However, the penalty makes sense—if the group of four nodes is “more split” (2 and 2 as opposed to 3 and 1), the penalty is larger. When $|\mathcal{A}| > 4$, we can derive similar penalized approximations to $\phi_M^{(G)}(S)$. Developing approximation algorithms for the minimization of motif conductance with motifs consisting of four or more anchor nodes is an open question. Preliminary progress on this problem is presented in Section 3.5. There, we show that if the network has certain measurable clustering structure, then we can find sets with low motif conductance for clique motifs. However, we still desire general theory applicable to any constant-size motif.

2.2.9 Analysis of computational complexity

We now analyze the computational complexity of Algorithm 1. Overall, the complexity of the algorithm is governed by:

- i. forming the motif adjacency matrix W_M
- ii. computing an eigenvector of N_M
- iii. the sweep procedure

We address these in reverse order. Let m and n denote the number of edges in the graph. For the sweep cut, it takes $O(n \log n)$ to sort the indices given the eigenvector using a standard sorting algorithm such as merge sort. Computing motif conductance for each set S_r in the sweep also takes linear time. In practice, the sweep cut step takes a small fraction of the total running time of the algorithm. The time to compute an eigenvector of N_M is not understood as well. In a theoretical sense, there are a number of “fast Laplacian solvers” for solving the system of equations $N_M y = x$ in nearly linear time [Kelner et al., 2013; Koutis et al., 2011; Kyng and Sachdeva, 2016; Spielman and Teng, 2004]. With such a solver, we can run a shifted inverse power method to compute the eigenvector. The recent

algorithm by [Kyng and Sachdeva \[2016\]](#) in this space is specifically designed to be practical and implementable.

For the remainder of the analysis, we consider the issue of the time to compute W_M . We assume that the size of the motif is constant. The time to compute W_M is bounded by the time to find all instances of the motif in the graph, assuming we can update an edge weight in $O(1)$ time (for each instance of the motif, we increment the edge weight of all pairs of nodes in the motif by 1). Naively, for a motif on k nodes, we can compute W_M in $O(n^k)$ time by checking each k -tuple of nodes. Furthermore, there are cases where there are $O(n^k)$ motif instances in the graph, e.g., there are $O(n^3)$ triangles in a complete graph. However, since most real-world networks are sparse, we instead focus on the complexity of algorithms in terms of the number of edges and the maximum degree in the graph. For this case, there are several efficient practical algorithms for real networks with available software [[Aberger et al., 2016](#); [Demeyer et al., 2013](#); [Houbraken et al., 2014](#); [Wernicke, 2006](#); [Wernicke and Rasche, 2006](#)].

Here we will consider three classes of motifs:

- i. triangles and more generally k -cliques,
- ii. wedges (connected, non-triangle three-node motifs), and
- iii. general four-node motifs

[Latapy \[2008\]](#) analyzed a number of algorithms for listing all triangles in an undirected network, including an algorithm that has computational complexity $O(m^{1.5})$. For a directed graph G , we can use the following algorithm:

- i. form a new graph G_{undir} by removing the direction from all edges in G
- ii. find all triangles in G_{undir}
- iii. for every triangle in G_{undir} , check which directed triangle motif it is in G .

The first step takes linear time and the third step is linear assuming we can determine the existence of an edge in $O(1)$ time. Thus, the same $O(m^{1.5})$ complexity holds for directed networks. This analysis holds regardless of the structure of the network. However, additional properties of the network can lead to improved algorithms. For example, in networks with a power law degree sequence with exponent greater than $7/2$, [Berry et al.](#) provide a randomized algorithm with expected running time $O(m)$ [[Berry et al., 2014](#)]. In the case of a bounded degree graph, enumerating over all nodes and checking all pairs of neighbors takes time $O(nd_{\text{max}}^2)$, where d_{max} is the maximum degree in the graph. We note that with triangular motifs, the number of non-zeros in W_M is less than the number of non-zeros in the original adjacency matrix. Thus, we do not have to worry about additional storage requirements. [Chiba and Nishizeki \[1985\]](#) present an algorithm for k -clique enumeration with complexity dependent on the arboricity of the graph. Specifically, their algorithm enumerates all k -cliques in $O(ka^{k-2}m)$ time, where a is the arboricity of the graph. The arboricity of any connected graph is bounded

by $O(m^{1/2})$, so this algorithm runs in time $O(m^{1.5})$ for triangles. Finally, note that the nodes of any connected component of the motif adjacency matrix for k -clique motifs is a k -truss in the original network. Thus, in practice, we can use pruning techniques for k -trusses as a pre-computation to (possibly) reduce the size of the input graph [Cohen, 2008].

Next, we consider wedges (open triads). We can list all wedges by looking at every pair of neighbors of every node. This algorithm has $O(nd_{\max}^2)$ computational complexity, where n is the number of nodes and d_{\max} is again the maximum degree in the graph (a more precise bound is $O(\sum_j d_j^2)$, where d_j is the degree of node j). If the graph is sparse, the motif adjacency matrix will have more non-zeros than the original adjacency matrix, so additional storage is required. Specifically, there is fill-in for all two-hop neighbors, so the motif adjacency matrix has $O(\sum_j d_j^2)$ non-zeros. This is impractical for large real-world networks but manageable for modestly sized networks.

Marcus and Shavitt [2010] present an algorithm for listing all four-node motifs in an undirected graph in $O(m^2)$ time. We can employ the same edge direction check as for triangles to extend this result to directed graphs. Chiba and Nishizeki [1985] develop an algorithm for finding a representation of all quadrangles (motif on four nodes that contains a four-node cycle as a subgraph) in $O(am)$ time and $O(m)$ space, where a is the arboricity of the graph.

Finally, we note that the computation of W_M and the computation of the eigenvector are suitable for parallel computation. There are already distributed algorithms for triangle enumeration [Cohen, 2009], and the parallel computation of eigenvectors of a sparse matrix is a classical problem in scientific computing [Maschhoff and Sorensen, 1996].

2.2.10 Methods for simultaneously finding multiple clusters

For clustering a network into $k > 2$ clusters based on motifs, we could recursively cut the graph using the sweep procedure with some stopping criterion [Boley, 1998; Kannan et al., 2004]. For example, we could continue to cut the largest remaining cluster until the graph is partitioned into some pre-specified number of clusters. We refer to this method as recursive bi-partitioning.

In addition, there are well-known spectral clustering approaches that compute multiple eigenvectors of the (normalized) Laplacian, use the eigenvectors to embed the nodes into Euclidean space, and run a point cloud clustering algorithm (typically k -means) on the embedded nodes [Von Luxburg, 2007]. We can adapt these methods for motif-based clustering by simply running the algorithms on the weighted adjacency matrix. For our work, we use the following adaptation of the

method of Ng et al. [2001].

Algorithm 2 – Motif-based clustering algorithm for finding several clusters.

Input: Directed, unweighted graph G , motif M , number of clusters k

Output: k disjoint motif-based clusters

- 1 $(W_M)_{ij} \leftarrow$ number of instances of M that contain nodes i and j .
 - 2 $D_M \leftarrow \text{diag}(W_M e)$
 - 3 $z_1, \dots, z_k \leftarrow$ eigenvectors of k smallest eigenvalues for
 $N_M = I - D_M^{-1/2} W_M D_M^{-1/2}$
 - 4 $Y_{ij} \leftarrow z_{ij} / \sqrt{\sum_{j=1}^k z_{ij}^2}$ /* row normalize */
 - 5 $E_i \leftarrow Y_{i,:}$ /* Embed node i into \mathbb{R}^k */
 - 6 /* Run k -means clustering on the point cloud $\{E_i\}$ */
-

This method does not have the same Cheeger-like guarantee on quality. However, recent theory shows a cluster quality guarantee when k -means is replaced with a different clustering algorithm [Lee et al., 2014].² We still use k -means for its simplicity and empirical success. Due to our theoretical results equating motif cuts and motif volumes to edge cuts and edge volumes in the weighted graph (Lemmas 3 and 5), we can automatically apply the newly developed theory of Lee et al. [2014] to the case of motifs with three anchor nodes.

2.2.11 Extensions for multiple motifs, weighted motifs, and weighted, signed, and colored networks

We now discuss some easy extensions of the method such as looking for clusters based on several motifs or handling cases where the graph carries additional information such as edge weights or node colors.

Simultaneously clustering based on several motifs. All of our results carry through when considering several motifs simultaneously. In particular, suppose we are interested in clustering based on q different motifs M_1, \dots, M_q . Further suppose that we want to weight the impact of some motifs more than other motifs. Let W_{M_j} be the weighted adjacency matrix for motif M_j and let $\alpha_j \geq 0$ be the weight of motif M_j , $j = 1, \dots, q$. Then we can form the weighted adjacency matrix

$$(2.28) \quad W_M = \sum_{j=1}^q \alpha_j W_{M_j}.$$

²The bounds for multi-way clustering are actually called *higher-order Cheeger inequalities*, where “higher-order” means more than two clusters. We emphasize that we are using the term *higher-order* clustering to mean that our clustering objective is based on higher-order structures.

(We will use this approach in Section 2.3.4 when clustering based on the four “coherent feedforward loops” in the *S. cerevisiae* transcriptional regulation network.)

Now, the cut and volume measures are simply weighted sums by linearity. Suppose that the M_j all have three anchor nodes and let G_M be the weighted graph corresponding to W_M . Then

$$(2.29) \quad \text{cut}^{(G_M)}(S, \bar{S}) = \sum_{j=1}^q \alpha_j \text{cut}_{M_j}(S, \bar{S}),$$

$$(2.30) \quad \text{vol}^{(G_M)}(S) = \sum_{j=1}^q \alpha_j \text{vol}_{M_j}(S),$$

and Theorem 7 applies to a weighted motif conductance equal to

$$\frac{\sum_{j=1}^q \alpha_j \text{cut}_{M_j}(S, \bar{S})}{\min \left(\sum_{j=1}^q \alpha_j \text{vol}_{M_j}(S), \sum_{j=1}^q \alpha_j \text{vol}_{M_j}(\bar{S}) \right)}.$$

Weighted motifs and weighted graphs. We can also generalize the notions of motif cut and motif volume for *weighted motifs*, i.e., each motif instance $(v, \chi_{\mathcal{A}}(v))$ has an associated nonnegative weight $\omega_{(v, \chi_{\mathcal{A}}(v))}$. Our cut and volume metrics are then

$$(2.31) \quad \text{cut}_M(S, \bar{S}) = \sum_{(v, \chi_{\mathcal{A}}(v)) \in \mathcal{M}} \omega_{(v, \chi_{\mathcal{A}}(v))} \text{Ind}[\exists i, j \in \chi_{\mathcal{A}}(v) \mid i \in S, j \in \bar{S}],$$

$$(2.32) \quad \text{vol}_M(S) = \sum_{(v, \chi_{\mathcal{A}}(v)) \in \mathcal{M}} \omega_{(v, \chi_{\mathcal{A}}(v))} \sum_{i \in \chi_{\mathcal{A}}(v)} \text{Ind}[i \in S].$$

Subsequently, we adjust the motif adjacency matrix as follows:

$$(2.33) \quad (W_M)_{ij} = \sum_{(v, \chi_{\mathcal{A}}(v)) \in \mathcal{M}} \omega_{(v, \chi_{\mathcal{A}}(v))} \text{Ind}[\{i, j\} \subset \chi_{\mathcal{A}}(v)]$$

For weighted networks (i.e., the original network is weighted and we want to cluster based on motifs), the algorithm user needs to decide how to weight a motif instance given the weights of the edges in the instance itself. Possibilities include:

- i. the maximum or minimum edge weight;
- ii. the arithmetic or geometric mean of the edge weights; or
- iii. the product of the edge weights.

The weighting scheme would depend on the particular applications and motivations of the user. The important idea is that the motif-based clustering scheme

makes it clear that the weights must be specified *for each motif instance*, and there is no canonical weighting scheme. We note that the general problem of constructing weights for higher-order structures in a weighted graph has been studied in generalizations of the clustering coefficient to weighted networks [Opsahl and Panzarasa, 2009].

Signed and colored networks. Our results easily generalize for signed networks. We only have to generalize Equation (2.12) by allowing the adjacency matrix B to be signed. This allows us to seamlessly analyze the signed *S. cerevisiae* transcriptional regulation network in Section 2.3.4. Extending the method for motifs where the edges or nodes are “colored” or “labeled” is similar. If the edges are colored, then we again just allow the adjacency matrix B to capture this information, where the entries in the matrix are indices for edge colors. If the nodes in the motif are colored, we only count motif instances with the specified pattern.

2.3 Case studies

We now use motif-based clustering to analyze several real-world networks. Our main goal is to show that motif-based clusters find more meaningful and markedly different structures in many real-world networks compared to edge-based clusters. To this end, we first discuss several edge-based clustering algorithms that will be used for comparison.

2.3.1 Alternative clustering algorithms for evaluation

For our experiments, we compare our motif-based spectral clustering to the following methods:

- Standard, edge-based spectral clustering, which is a special case of motif-based clustering. In particular, the motifs

$$(2.34) \quad B_1 = \begin{bmatrix} 0 & 1 \\ 1 & 0 \end{bmatrix}, \quad B_2 = \begin{bmatrix} 0 & 1 \\ 0 & 0 \end{bmatrix}, \quad \mathcal{A} = \{1, 2\}$$

correspond to removing directionality from a directed graph. We refer to the union of these two motifs as M_{edge} (there is a weight of 1 between nodes i and j if there is some edge connecting i and j).

- Infomap, an information-theoretic approach designed to optimally compress network dynamics [Rosvall and Bergstrom, 2008].³

³Software for Infomap was downloaded from <http://mapequation.org/code.html>. We run the “directed” algorithm for directed links when the network under consideration is directed. For all

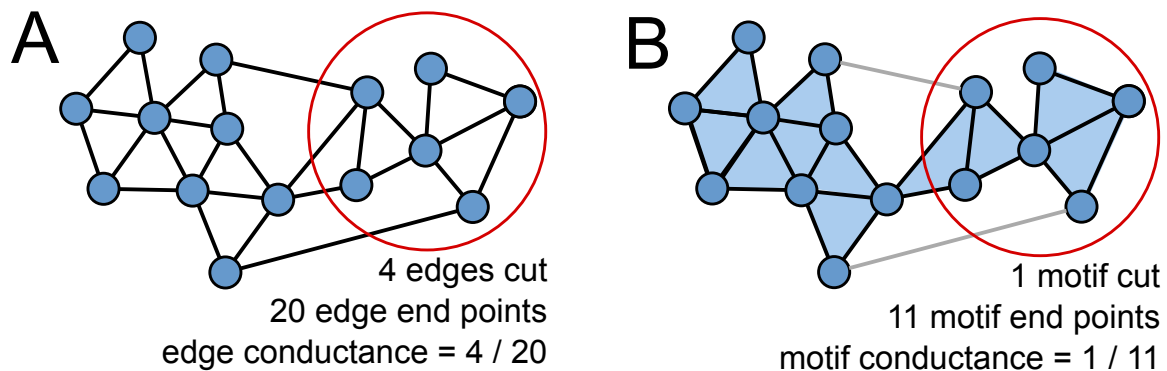


Figure 2.5 – Edge conductance and motif conductance. The edge conductance (A) and the motif conductance (B) is different for the same set of nodes in the same graph, where the motif M is the triangle. Our methods finds clusters of nodes based on the motif conductance, where the user can decide which motif M to use for the clustering. Comparing edge and motif conductance is meaningful because of the probabilistic interpretation of conductance.

- The Louvain method, which is a hierarchical greedy algorithm for modularity maximization [Blondel et al., 2008].⁴

Infomap and the Louvain method are take as input the graph and produce as output a set of labels for the nodes in the graph. In contrast to the spectral methods, we do not have control over the number of clusters. Also, only the spectral methods provide embeddings of the nodes into Euclidean space, which is useful for visualization. Thus, for our analysis of the transportation reachability network in Section 2.3.5, we only compare spectral methods.

2.3.2 Comparing motif conductance and edge conductance

When analyzing data with motif-based clustering, we often compare values of motif conductance to edge conductance (see Figure 2.5). Although these two objective functions measure different (but related) quantities, we argue that comparing them is meaningful because both have a comparable probabilistic interpretation. Let W be a connected, non-bipartite, and (possibly weighted) undirected graph, and let $\{Z_t\}$ be a stochastic process with transition probabilities given by the random

other parameters, we use the default values.

⁴Software for the Louvain method was downloaded from <https://perso.uclouvain.be/vincent.blondel/research/louvain.html>. We use the “oriented” version of the Louvain method for directed graphs.

walk transition matrix $P = WD^{-1}$. Then it is well-known that

$$(2.35) \quad \phi(S) = \max\{\mathbb{P}[Z_1 \in \bar{S} \mid Z_0 \in S], \mathbb{P}[Z_1 \in S \mid Z_0 \in \bar{S}]\},$$

where the initial state Z_0 is chosen randomly from the stationary distribution of the random walk (i.e., from the unique vector π satisfying $P\pi = \pi$) [Meila and Shi, 2001].

When W is a motif-adjacency matrix for a simple motif, then the random walk is equivalent to the following stochastic process $\{Y_t\}$.

- i. when $Y_t = j$, choose a motif instance containing node j as an anchor node uniformly at random, and
- ii. transition to $Y_{t+1} = i$, where i is an anchor node selected uniformly at random from the nodes in the motif instance excluding j .

To see this, let r be the number of anchor nodes in the motif. Then,

$$\begin{aligned} & \mathbb{P}[\text{transition } j \rightarrow i] \\ &= P_{ij} \\ &= \frac{W_{ij}}{\sum_k W_{kj}} \\ &= \frac{\# \text{ motifs containing } i \text{ and } j \text{ as anchors}}{(r-1) \cdot (\# \text{ motifs containing } j \text{ as an anchor})} \quad \text{by Lemma 3} \\ &= \frac{1}{r-1} \mathbb{P}[\text{random motif that contains } j \text{ as an anchor also contains } i \text{ as an anchor}] \end{aligned}$$

Consequently,

$$(2.36) \quad \phi_M(S) = \max\{\mathbb{P}[Y_1 \in \bar{S} \mid Y_0 \in S], \mathbb{P}[Y_1 \in S \mid Y_0 \in \bar{S}]\},$$

where Y_0 is chosen uniformly at random from the stationary distribution (when there are 2 or 3 anchor nodes). Equation (2.36) is comparable between motifs (including the edge motif). Here, small motif conductance of a set S just means that there is a stochastic process that transitions between nodes based on motifs and that this process tends to stay contained in S or \bar{S} .

2.3.3 Motif M_6 in the Florida Bay food web

We now apply the higher-order clustering framework on the Florida Bay food web [Ulanowicz et al., 1998].⁵ In this network, the nodes are compartments

⁵<http://vlado.fmf.uni-lj.si/pub/networks/data/bio/foodweb/Florida.paj>

(roughly, organisms and species) and the edges represent directed carbon exchange—an edge (i, j) means that carbon flows from i to j . Often, this means that species j eats species i . In this domain, motifs model energy flow patterns between several species.

In this case study, we use the framework to identify higher-order modular organization of the network. We focus on three motifs: M_5 corresponds to a hierarchical flow of energy where species i and j are energy sources (prey) for species k , and i is also an energy source for j ; M_6 models two species that prey on each other and then compete to feed on a common third species; and M_8 describes a single species serving as an energy source for two non-interacting species. Prevalence of motif M_5 has been found in food webs [Bascompte, 2009; Bascompte et al., 2005], and motif M_6 is predicted by a niche model [Stouffer et al., 2007].

We first briefly discuss the connectivity of the motif adjacency matrix with respect to these motifs, as we will perform analysis on the largest connected component of these graphs. The original network is weakly connected with 128 nodes and 2,106 edges. The largest connected component of the motif adjacency matrix for motif M_5 contains 127 of the 128 nodes (the compartment of “roots” becomes isolated). The two largest connected components of the motif adjacency matrix for motif M_6 contain 12 and 50 nodes (see Table 2.2; we will also use this connectivity information later in our analysis), and the remaining 66 nodes are isolated. The motif adjacency matrix for M_8 is connected. The original network is weakly connected, so the motif adjacency matrix for M_{edge} is also connected.

Table 2.2 – Connected components of the Florida Bay food web motif adjacency matrix for motif M_6 . There are 50 nodes in component 1, 12 nodes in component 2, and 66 isolated nodes. Component 2 consists of microfauna and detritus (see Table 2.3).

Two largest components Compartment (node)	Component index	Isolated nodes Compartment (node)
Benthic Phytoplankton	1	Barracuda
Thalassia	1	2 μ m Spherical Phytoplankton
Halodule	1	Synedococcus
Syringodium	1	Oscillatoria
Drift Algae	1	Small Diatoms (<20 μ m)
Epiphytes	1	Big Diatoms (>20 μ m)
Predatory Gastropods	1	Dinoflagellates
Detritivorous Polychaetes	1	Other Phytoplankton
Predatory Polychaetes	1	Roots
Suspension Feeding Polychaetes	1	Coral
Macrobenthos	1	Epiphytic Gastropods
Benthic Crustaceans	1	Thor Floridanus
Detritivorous Amphipods	1	Lobster
Herbivorous Amphipods	1	Stone Crab
Isopods	1	Sharks
Herbivorous Shrimp	1	Rays
Predatory Shrimp	1	Tarpon
Pink Shrimp	1	Bonefish
Benthic Flagellates	1	Other Killifish
Benthic Ciliates	1	Snook
Meiofauna	1	Sailfin Molly
Other Cnidaridae	1	Hawksbill Turtle
Silverside	1	Dolphin
Echinoderma	1	Other Horsefish
Bivalves	1	Gulf Pipefish
Detritivorous Gastropods	1	Dwarf Seahorse
Detritivorous Crabs	1	Grouper
Omnivorous Crabs	1	Jacks
Predatory Crabs	1	Pompano
Callinectes sapidus (blue crab)	1	Other Snapper
Mullet	1	Gray Snapper
Blennies	1	Mojarra
Code Goby	1	Grunt
Clown Goby	1	Porgy
Flatfish	1	Pinfish
Sardines	1	Scianids
Anchovy	1	Spotted Seatrout
Bay Anchovy	1	Red Drum
Lizardfish	1	Spadefish
Catfish	1	Parrotfish
Eels	1	Mackerel
Toadfish	1	Filefishes
Brotalus	1	Puffer
Halfbeaks	1	Loon
Needlefish	1	Greeb
Goldspotted killifish	1	Pelican
Rainwater killifish	1	Comorant
Other Pelagic Fishes	1	Big Herons and Egrets
Other Demersal Fishes	1	Small Herons and Egrets
Benthic Particulate Organic Carbon (Benthic POC)	1	Ibis
Free Bacteria	2	Roseate Spoonbill
Water Flagellates	2	Herbivorous Ducks
Water Ciliates	2	Omnivorous Ducks
Acartia Tonsa	2	Predatory Ducks
Oithona nana	2	Raptors
Paracalanus	2	Gruiformes
Other Copepoda	2	Small Shorebirds
Meroplankton	2	Gulls and Terns
Other Zooplankton	2	Kingfisher
Sponges	2	Crocodiles
Water Particulate Organic Carbon (Water POC)	2	Loggerhead Turtle
Input	2	Green Turtle
		Manatee
		Dissolved Organic Carbon (DOC)
		Output
		Respiration

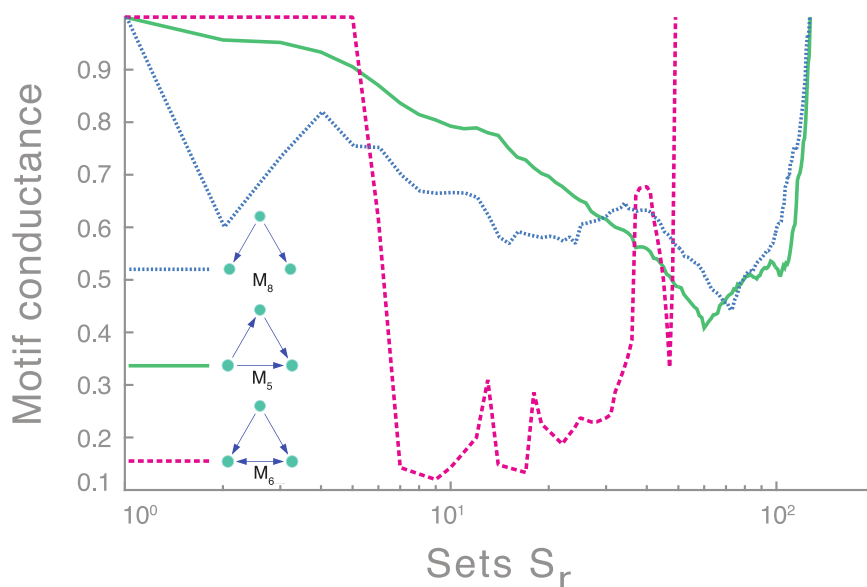


Figure 2.6 – Sweep profile plot on the Florida Bay food web. The sweep profile plot measures $\phi_M(S)$ as S varies in the sweep procedure of Algorithm 1. Here, we look at the sweep profile for three motifs on the Florida Bay ecosystem food web. A priori it is not clear whether the network is organized based on a given motif. For example, motifs M_5 (green) and M_8 (blue) do not reveal any higher-order organization (motif conductance has high values). However, the downward spikes of the red curve show that M_6 reveals rich higher-order clusters [Leskovec et al., 2009]. Ecologically, motif M_6 corresponds to two species mutually feeding on each other and also preying on a common third species. The motif Cheeger inequality guarantees that the motif conductance for the best M_6 found by Algorithm 1 is better than the motif conductance of every set for motifs M_5 and M_8 .

By examining the sweep profile plots of these motifs in Figure 2.6, we see that low motif conductance clusters are only found for motif M_6 , whereas clusters based on motifs M_5 or M_8 have high motif conductance. In fact, the motif Cheeger inequality (Theorem 7) guarantees that clusters based on motif M_5 or M_8 will always have larger motif conductance than clusters based on M_6 . Specifically, Theorem 6 says that the motif conductance of any set is bounded below by $\lambda_2/2$, where λ_2 is the second smallest eigenvalue of the motif normalized Laplacian N_M . The lower bounds ($\lambda_2/2$) on motif conductance for motifs M_5 , M_6 , M_8 are 0.22, 0.03, and 0.22, and the clusters found by Algorithm 1 have motif conductances of 0.44, 0.12, and 0.41. Thus, the cluster S found by the algorithm for M_6 has smaller motif M_6 conductance (0.12) than any possible cluster's M_5 or M_8 conductance. The same conclusions hold for edge-based clustering. For motif

M_{edge} , the lower bound on conductance is 0.2194, and the cluster found by the algorithm has conductance 0.4083.

Subsequently, we use motif M_6 and Algorithm 2 to cluster the food web, revealing four clusters (Figures 2.7 and 2.8). Three represent well-known aquatic layers: (i) the pelagic system; (ii) the benthic predators of eels, toadfish, and crabs; and (iii) the sea-floor ecosystem of macroinvertebrates. The fourth cluster identifies microfauna supported by particulate organic carbon in water and free bacteria (this cluster is the second largest connected component of the motif adjacency matrix—component 2 in Table 2.2). Table 2.3 lists the nodes in each cluster.

We also measure how well the motif-based clusters correlate to known ground truth system subgroup classifications of the nodes [Ulanowicz et al., 1998]. These classes are microbial, zooplankton, and sediment organism microfauna; detritus; pelagic, demersal, and benthic fishes; demersal, seagrass, and algae producers; and macroinvertebrates (Table 2.3, Classification 1). We also consider a set of labels which does not include the subclassification for microfauna and producers. In this case, the labels are microfauna; detritus; pelagic, demersal, and benthic fishes; producers; and macroinvertebrates (Table 2.3, Classification 2).

To quantify how well the clusters found by motif-based clustering reflect the ground truth labels, we use several standard evaluation criteria: adjusted rand index, F1 score, normalized mutual information, and purity [Manning et al., 2008]. We compare these results to the clusters of several methods using the same evaluation criteria. In total, we evaluate six methods:

- i. Motif-based clustering with the embedding + k-means algorithm (Algorithm 2) with 500 iterations of k-means.
- ii. Motif-based clustering with recursive bi-partitioning (repeated application of Algorithm 1 on the largest remaining component). The process continues to cut the largest cluster until there are 4 total.
- iii. Edge-based clustering with the embedding + k-means algorithm, again with 500 iterations of k-means.
- iv. Edge-based clustering with recursive bi-partitioning with the same partitioning process.
- v. The Infomap algorithm.
- vi. The Louvain method.

We control the number of clusters in the first four algorithms, which set to four. We cannot control the number of clusters in the last two algorithms, but both methods happen to find four clusters.

Table 2.4 shows that the motif-based clustering by embedding + k-means has the best performance for each classification criterion on both classifications. We conclude that the organization of compartments in the Florida Bay food web are better described by motif M_6 than by edges.

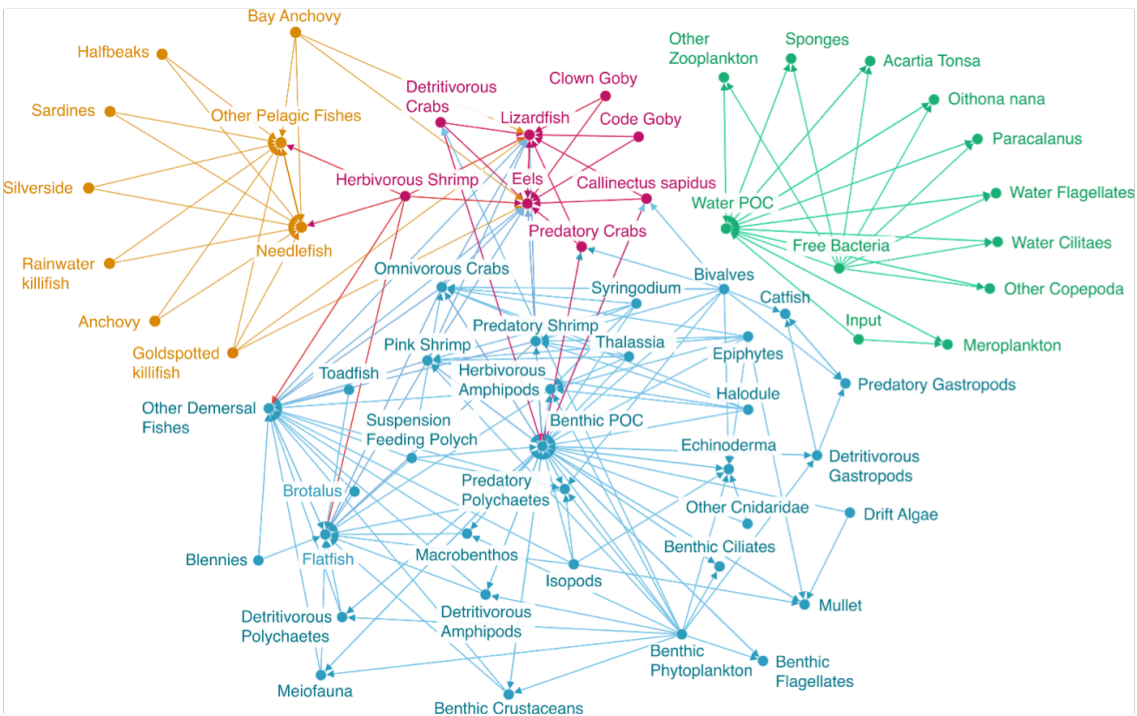
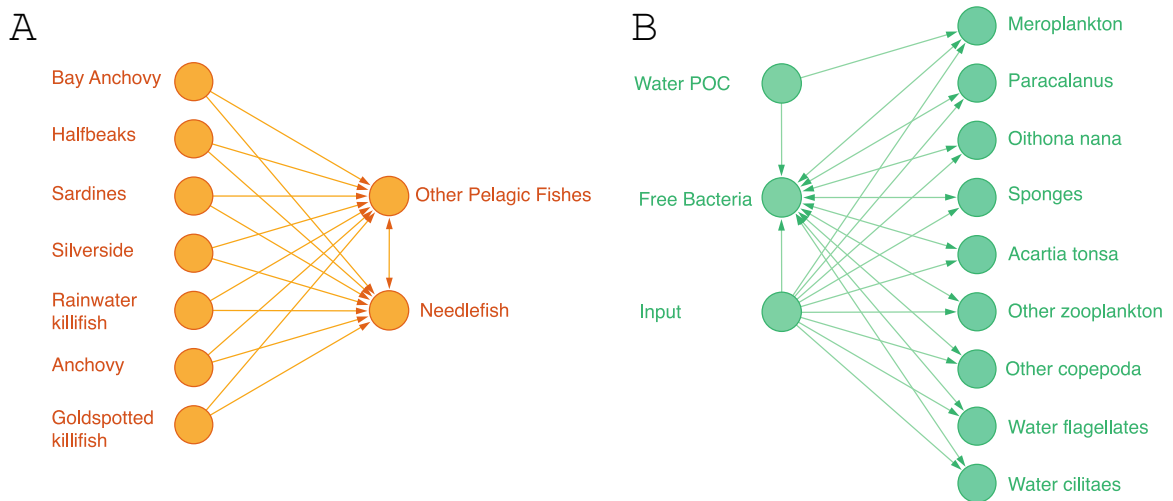


Figure 2.7 – Higher-order organization of the Florida Bay food web. Clustering of the food web based on motif M_6 . (For illustration, edges not participating in at least one instance of the motif are omitted.) The clustering reveals three known aquatic layers: pelagic fishes (yellow), benthic fishes and crabs (red), and sea-floor macroinvertebrates (blue) as well as a cluster of microfauna and detritus (green). Our framework identifies these modules with higher accuracy (61%) than existing methods (48–53%)—see Table 2.4. Figure 2.8 examines the yellow and green higher-order clusters in more detail.



*Figure 2.8 – Higher-order clusters in the Florida Bay food web. A closer look at two of the higher-order clusters from Figure 2.7. **A:** A higher-order cluster (the yellow nodes in Figure 2.7) shows how motif M_6 occurs in the pelagic layer. The needlefish and other pelagic fishes eat each other while several other fishes are prey for these two species. **B:** Another higher-order cluster (the green nodes in Figure 2.7) shows how motif M_6 occurs between microorganisms. Here, several microfauna decompose into Particulate Organic Carbon in the water (water POC) but also consume water POC. Free bacteria serves as an energy source for both the microfauna and water POC.*

Table 2.3 – Ecological classification of nodes in the Florida Bay foodweb. Colors correspond to the visualization in Figure 2.7.

Compartment (node)	Classification 1	Classification 2	Assignment
Free Bacteria	Microbial microfauna	Microfauna	green
Water Flagellates	Microbial microfauna	Microfauna	green
Water Ciliates	Microbial microfauna	Microfauna	green
Acartia Tonsa	Zooplankton microfauna	Microfauna	green
Oithona nana	Zooplankton microfauna	Microfauna	green
Paracalanus	Zooplankton microfauna	Microfauna	green
Other Copepoda	Zooplankton microfauna	Microfauna	green
Meroplankton	Zooplankton microfauna	Microfauna	green
Other Zooplankton	Zooplankton microfauna	Microfauna	green
Sponges	Macroinvertebrates	Macroinvertebrates	green
Water POC	Detritus	Detritus	green
Input	Detritus	Detritus	green
Sardines	Pelagic Fishes	Pelagic Fishes	yellow
Anchovy	Pelagic Fishes	Pelagic Fishes	yellow
Bay Anchovy	Pelagic Fishes	Pelagic Fishes	yellow
Halfbeaks	Pelagic Fishes	Pelagic Fishes	yellow
Needlefish	Pelagic Fishes	Pelagic Fishes	yellow
Goldspotted killifish	Demersal Fishes	Demersal Fishes	yellow
Rainwater killifish	Demersal Fishes	Demersal Fishes	yellow
Silverside	Pelagic Fishes	Pelagic Fishes	yellow
Other Pelagic Fishes	Pelagic Fishes	Pelagic Fishes	yellow
Detritivorous Crabs	Macroinvertebrates	Macroinvertebrates	red
Predatory Crabs	Macroinvertebrates	Macroinvertebrates	red
Callinectes sapidus	Macroinvertebrates	Macroinvertebrates	red
Lizardfish	Benthic Fishes	Benthic Fishes	red
Eels	Demersal Fishes	Demersal Fishes	red
Code Goby	Benthic Fishes	Benthic Fishes	red
Clown Goby	Benthic Fishes	Benthic Fishes	red
Herbivorous Shrimp	Macroinvertebrates	Macroinvertebrates	red
Benthic Phytoplankton	Producer Demersal	Producer	blue
Thalassia	Producer Seagrass	Producer	blue
Halodule	Producer Seagrass	Producer	blue
Syringodium	Producer Seagrass	Producer	blue
Drift Algae	Producer Algae	Producer	blue
Epiphytes	Producer Algae	Producer	blue
Benthic Flagellates	Sediment Organism microfauna	Microfauna	blue
Benthic Ciliates	Sediment Organism microfauna	Microfauna	blue
Meiofauna	Sediment Organism microfauna	Microfauna	blue
Other Cnidaridae	Macroinvertebrates	Macroinvertebrates	blue
Echinoderma	Macroinvertebrates	Macroinvertebrates	blue
Bivalves	Macroinvertebrates	Macroinvertebrates	blue
Detritivorous Gastropods	Macroinvertebrates	Macroinvertebrates	blue
Predatory Gastropods	Macroinvertebrates	Macroinvertebrates	blue
Detritivorous Polychaetes	Macroinvertebrates	Macroinvertebrates	blue
Predatory Polychaetes	Macroinvertebrates	Macroinvertebrates	blue
Suspension Feeding Polych	Macroinvertebrates	Macroinvertebrates	blue
Macrobenthos	Macroinvertebrates	Macroinvertebrates	blue
Benthic Crustaceans	Macroinvertebrates	Macroinvertebrates	blue
Detritivorous Amphipods	Macroinvertebrates	Macroinvertebrates	blue
Herbivorous Amphipods	Macroinvertebrates	Macroinvertebrates	blue
Isopods	Macroinvertebrates	Macroinvertebrates	blue
Predatory Shrimp	Macroinvertebrates	Macroinvertebrates	blue
Pink Shrimp	Macroinvertebrates	Macroinvertebrates	blue
Omnivorous Crabs	Macroinvertebrates	Macroinvertebrates	blue
Catfish	Benthic Fishes	Benthic Fishes	blue
Mullet	Pelagic Fishes	Pelagic Fishes	blue
Benthic POC	Detritus	Detritus	blue
Toadfish	Benthic Fishes	Benthic Fishes	blue
Brotalus	Demersal Fishes	Demersal Fishes	blue
Blennies	Benthic Fishes	Benthic Fishes	blue
Flatfish	Benthic Fishes	Benthic Fishes	blue
Other Demersal Fishes	Demersal Fishes	Demersal Fishes	blue

Table 2.4 – *Evaluation of clustering algorithms in the Florida Bay food web.* We compare the motif-based algorithms against other methods for finding the “ground truth” classifications listed in Table 2.3. Performance is evaluated based on Adjusted Rand Index (ARI), F1 score, Normalized Mutual Information (NMI), and Purity. In all cases, the motif-based methods have the best performance.

	Evaluation	Motif embedding + k-means	Motif recursive bi-partitioning	Edge embedding + k-means	Edge recursive bi-partitioning	Infomap	Louvain
Classification 1	ARI	0.3005	0.2156	0.1564	0.1226	0.1423	0.2207
	F1	0.4437	0.3853	0.3180	0.2888	0.3100	0.4068
	NMI	0.5040	0.4468	0.4112	0.3879	0.4035	0.4220
	Purity	0.5645	0.5323	0.4032	0.4194	0.4194	0.5323
Classification 2	ARI	0.3265	0.2356	0.1814	0.1190	0.1592	0.2207
	F1	0.4802	0.4214	0.3550	0.3035	0.3416	0.4068
	NMI	0.4822	0.4185	0.3533	0.3034	0.3471	0.4220
	Purity	0.6129	0.5806	0.4839	0.4355	0.4677	0.5323

2.3.4 Coherent feedforward loops in the *S. cerevisiae* transcriptional regulation network

The transcription regulation network of the yeast *S. cerevisiae*⁶ we study here describes how genes regulate genetic transcription in one another. In the network, each node is an operon (a group of genes in a mRNA molecule), and a directed edge from operon i to operon j means that i is regulated by a transcriptional factor encoded by j [Alon, 2007].⁷ Edges are directed and signed. A positive sign represents activation and a negative sign represents repression.

For this case study, we examine the coherent feedforward loop motif (Figure 2.9A), which acts as a sign-sensitive delay element in transcriptional regulation networks [Mangan and Alon, 2003; Mangan et al., 2003]. Formally, the coherent feedforward loop is represented by the following simple signed motifs

(2.37)

$$B_1 = \begin{bmatrix} 0 & + & + \\ 0 & 0 & + \\ 0 & 0 & 0 \end{bmatrix}, B_2 = \begin{bmatrix} 0 & - & - \\ 0 & 0 & + \\ 0 & 0 & 0 \end{bmatrix}, B_3 = \begin{bmatrix} 0 & + & - \\ 0 & 0 & - \\ 0 & 0 & 0 \end{bmatrix}, B_4 = \begin{bmatrix} 0 & - & + \\ 0 & 0 & - \\ 0 & 0 & 0 \end{bmatrix}.$$

These motifs have the same edge pattern and only differ in sign. All of the motifs are simple ($\mathcal{A} = \{1, 2, 3\}$). Mangan and Alon [2003] identified the functionality of every coherent feedforward loop instance, so we have ground truth on the role that these motifs play in the network. For our analysis, we consider all coherent feedforward loops that are subgraphs on the induced subgraph of any three nodes. However, there is only one instance where the coherent feedforward loop itself is a subgraph but not an induced subgraph on three nodes (the induced subgraph of DAL80, GAT1, and GLN3 contains a bidirectional edge between DAL80 and GAT1 and unidirectional edges from DAL80 and GAT1 to GLN3).

Again, we analyze the component structure of the motif adjacency matrix as a pre-processing step. The original network consists of 690 nodes and 1082 edges, and its largest weakly connected component consists of 664 nodes and 1066 edges. Every coherent feedforward loop in the network resides in the largest weakly connected component, so we subsequently consider this sub-network in the following analysis. Of the 664 nodes in the network, only 62 participate in a coherent feedforward loop. The motif adjacency matrix has nine connected components—of sizes 18, 9, 9, 6, 6, 5, 3, 3, and 3—as well as some isolated components. Table 2.5 lists the operons in the components of size at least 3.

⁶Fun fact: *S. cerevisiae* is commonly used in brewing and winemaking.

⁷The network data was downloaded from <http://www.weizmann.ac.il/mcb/UriAlon/sites/mcb.UriAlon/files/uploads/NMpaper/yeastdata.mat>

Table 2.5 – Non-trivial connected components of the motif adjacency matrix of the *S. cerevisiae* network for the coherent feedforward loop.

Size	operons
18	ALPHA ₁ , CLN ₁ , CLN ₂ , GAL ₁₁ , HO, MCM ₁ , MFALPHA ₁ , PHO ₅ , SIN ₃ , SPT ₁₆ , STA ₁ , STA ₂ , STE ₃ , STE ₆ , SWI ₁ , SWI ₄ /SWI ₆ , TUP ₁ , SNF ₂ /SWI ₁
9	HXT ₁₁ , HXT ₉ , IPT ₁ , PDR ₁ , PDR ₃ , PDR ₅ , SNQ ₂ , YOR ₁ , YRR ₁
9	GCN ₄ , ILV ₁ , ILV ₂ , ILV ₅ , LEU ₃ , LEU ₄ , MET ₁₆ , MET ₁₇ , MET ₄
6	CHO ₁ , CHO ₂ , INO ₂ , INO ₂ /INO ₄ , OPI ₃ , UME ₆
6	DAL ₈₀ , DAL ₈₀ /GZF ₃ , GAP ₁ , GAT ₁ , GLN ₁ , GLN ₃
5	CYC ₁ , GAL ₁ , GAL ₄ , MIG ₁ , HAP _{2/3/4/5}
3	ADH ₂ , CCR ₄ , SPT ₆
3	CDC ₁₉ , RAP ₁ , REB ₁
3	DIT ₁ , IME ₁ , RIM ₁₀₁

Although the original network is connected, the motif adjacency matrix has several components, and this already reveals much of the structure in the network (Figure 2.9B). Indeed, this shattering of the graph into components for the feedforward loop has previously been observed in transcriptional regulation networks [Dobrin et al., 2004]. We additionally use Algorithm 1 to partition the largest connected component of the motif adjacency matrix (consisting of 18 nodes). This reveals the cluster

$$\{\text{CLN}_2, \text{CLN}_1, \text{SWI}_4/\text{SWI}_6, \text{SPT}_{16}, \text{HO}\},$$

which contains three coherent feedforward loops (Figure 2.9D). All three instances of the motif correspond to the function “cell cycle and mating type switch”. The motifs in this cluster are the only feedforward loops for which the function is described by Mangan and Alon [2003]. Using the same procedure on the undirected version of the induced subgraph of the 18 nodes (i.e., using motif M_{edge}) results in the cluster

$$\{\text{CLN}_1, \text{CLN}_2, \text{SPT}_{16}, \text{SWI}_4/\text{SWI}_6\}.$$

This cluster breaks the coherent feedforward loop formed by HO, SWI₄/SWI₆, and SPT₁₆.

We also evaluate our method based on the motif functionality labels provided by Mangan and Alon [2003].⁸ In total, there are 12 different functionalities and 29 labeled coherent feedforward loop instances. We consider the motif-based

⁸This data was downloaded from http://www.weizmann.ac.il/mcb/UriAlon/sites/mcb.UriAlon/files/uploads/DownloadableData/list_of_ffls.pdf.

clustering of the graph to be the connected components of the motif adjacency matrix with the additional partition of the largest connected component. To form an edge-based clustering, we used the embedding + k-means algorithm on the undirected graph (i.e., motif M_{edge}) with $k = 12$ clusters. We also clustered the graph using Infomap and the Louvain method.

We say that a method “consistently” labels a motif instance if all three nodes are assigned to the same cluster, and we would like our clustering algorithms to consistently label motif instances. Table 2.6 summarizes the results. The motif-based clustering consistently labels all 29 motifs, while the edge-based spectral, Infomap, and Louvain clustering consistently labeled 25, 23, and 23 motif instances, respectively.

We measure the accuracy of each clustering method as the rand index [Manning et al., 2008] on the consistently labeled motifs, multiplied by the fraction of consistently labeled motifs. The motif-based clustering has much highest accuracy (97%) compared to the other methods (68–82%). We conclude that motif-based clustering provides an advantage over edge-based clustering methods in identifying functionalities of coherent feedforward loops in the the *S. cerevisiae* transcriptional regulation network.

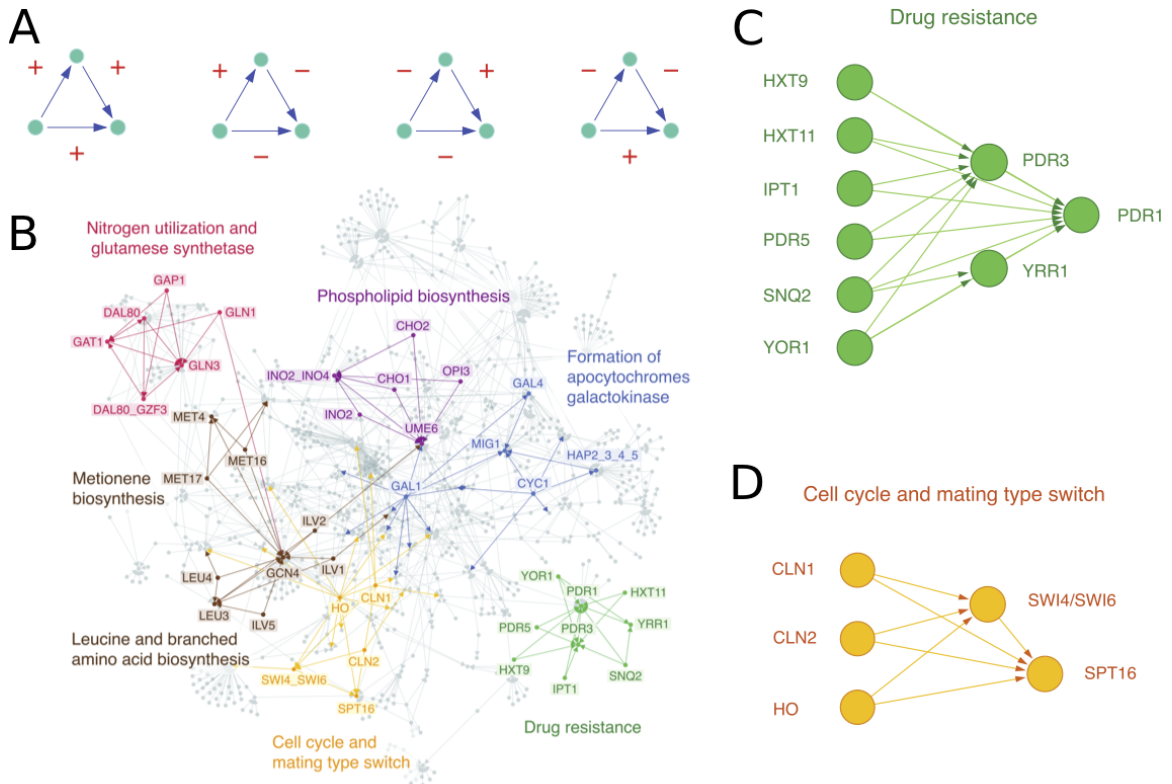


Figure 2.9 – Higher-order organization of the *S. cerevisiae* transcriptional regulation network. **A:** The four higher-order structures used by our higher-order clustering method, which can model signed motifs. These are the coherent feedforward loop motifs, which act as sign-sensitive delay elements in transcriptional regulation networks [Mangan et al., 2003]. The edge signs refer to activation (positive) or suppression (negative). **B:** Six higher-order clusters revealed by the motifs in (A). Clusters show functional modules consisting of several motif instances, which were previously studied individually [Mangan and Alon, 2003]. The higher-order clustering framework identifies the functional modules with higher accuracy (97%) than existing methods (68–82%). **C–D:** Two higher-order clusters from (B). In these clusters, all edges have positive sign. The functionality of the motifs in the modules correspond to drug resistance (C) or cell cycle and mating type switch (D). The clustering suggests that coherent feedforward loops function together as a single processing unit rather than as independent elements. The cluster in (C) is simply revealed by a connected component of the motif adjacency matrix (Table 2.5).

Table 2.6 – Clustering of coherent feedforward loops. We compare the classification performance of motif-based clustering to other methods. In a given motif instance, we say that it is consistently labeled if the nodes comprising the motif are in the same cluster. If a motif is not consistently labeled, a “-1” is listed. The accuracy is the rand index on the labels and motif functionality on consistently labeled motifs, multiplied by the fraction of consistently labeled motifs. Functions of each feedforward loop were identified by Mangano and Alon [2003].

	Motif nodes		Function	Class label					
	Motif-based	Edge-based		Infomap	Louvain	Frac. consistently labeled	Accuracy		
GAL11	ALPHA1	MEALPHA1	pheromone response	1	1	-1	-1	29 / 29	0.97
GCN4	MET4	MET16	Methionine biosynthesis	2	2	1	-1	25 / 29	0.82
GCN4	MET4	MET17	Methionine biosynthesis	2	2	1	-1	23 / 29	0.68
GCN4	LEU3	ILEV1	Leucine and branched amino acid biosynthesis	2	2	1	-1	23 / 29	0.76
GCN4	LEU3	ILEV2	Leucine and branched amino acid biosynthesis	2	2	1	1		
GCN4	LEU3	ILEV5	Leucine and branched amino acid biosynthesis	2	2	1	1		
GCN4	LEU3	LEU4	Leucine and branched amino acid biosynthesis	2	2	1	1		
GCN4	LEU3	GAP1	Nitrogen utilization	3	3	1	2		
GCN4	GAT1	DAL80	Nitrogen utilization	3	3	1	2		
GCN4	GAT1	DAL80/GZF3	Nitrogen utilization	3	3	1	2		
GCN3	GAT1	GLN1	Glutamate synthetase	3	3	1	2		
GCN3	GAT1	CYC1	Glutamate synthetase	3	3	1	2		
GLN3	HAP2/3/4/5	GLN1	formation of apocytochromes	4	4	-1	-1		
MIG1	GAL4	GAL1	Galactokinase	4	4	-1	-1		
MIG1	YRR1	SNQ2	Drug resistance	5	5	2	3		
PDR1	YRR1	YOR1	Drug resistance	5	5	2	3		
PDR1	PDR3	HXT11	Drug resistance	5	5	2	3		
PDR1	PDR3	HXT9	Drug resistance	5	5	2	3		
PDR1	PDR3	PDR5	Drug resistance	5	5	2	3		
PDR1	PDR3	IPT1	Drug resistance	5	5	2	3		
PDR1	PDR3	SNQ2	Drug resistance	5	5	2	3		
PDR1	PDR3	YOR1	Drug resistance	5	5	2	3		
RIM101	IME1	DTI1	sporulation-specific	6	6	3	4		
SPT16	SWI4/SWI6	CLN1	Cell cycle and mating type switch	7	7	4	5		
SPT16	SWI4/SWI6	CLN2	Cell cycle and mating type switch	7	7	-1	-1		
SPT16	SWI4/SWI6	HO	Cell cycle and mating type switch	7	7	-1	-1		
TUP1	ALPHA1	MEALPHA1	Mating factor alpha	1	1	-1	-1		
UME6	INO2/INO4	CHO1	Phospholipid biosynthesis	8	8	6	4		
UME6	INO2/INO4	CHO2	Phospholipid biosynthesis	8	8	6	4		
UME6	INO2/INO4	OP13	Phospholipid biosynthesis	8	8	6	4		

2.3.5 Bi-directed length-2 paths in a transportation reachability network

Our framework also provides new insights into network organization beyond the clustering of nodes into modules. Here we study a transportation reachability network where the nodes are cities in the United States and Canada, and there is an edge from city i to city j if the estimated travel time from i to j is less than some threshold [Frey and Dueck, 2007].⁹ The network is asymmetric.

Here we show results on a transportation reachability network [Frey and Dueck, 2007] that demonstrate how it finds the essential hub interconnection airports (Figure 2.10). These appear as extrema on the primary spectral direction (Figure 2.10C) when two-hop motifs (Figure 2.10A) are used to capture highly connected nodes and non-hubs. The first spectral coordinate of the normalized motif Laplacian embedding is positively correlated with the airport city's metropolitan population with Pearson correlation 99% confidence interval [0.33, 0.53]. The secondary spectral direction identifies the West-East geography in the North American flight network (it is negatively correlated with the airport city's longitude with Pearson correlation 99% confidence interval [-0.66, -0.50]). On the other hand, edge-based methods conflate geography and hub structure. For example, Atlanta, a large hub, is embedded next to Salina, a non-hub, with an edge-based method (Figure 2.10D).

⁹Data was downloaded from <http://www.psi.toronto.edu/index.php?q=affinity%20propagation>.

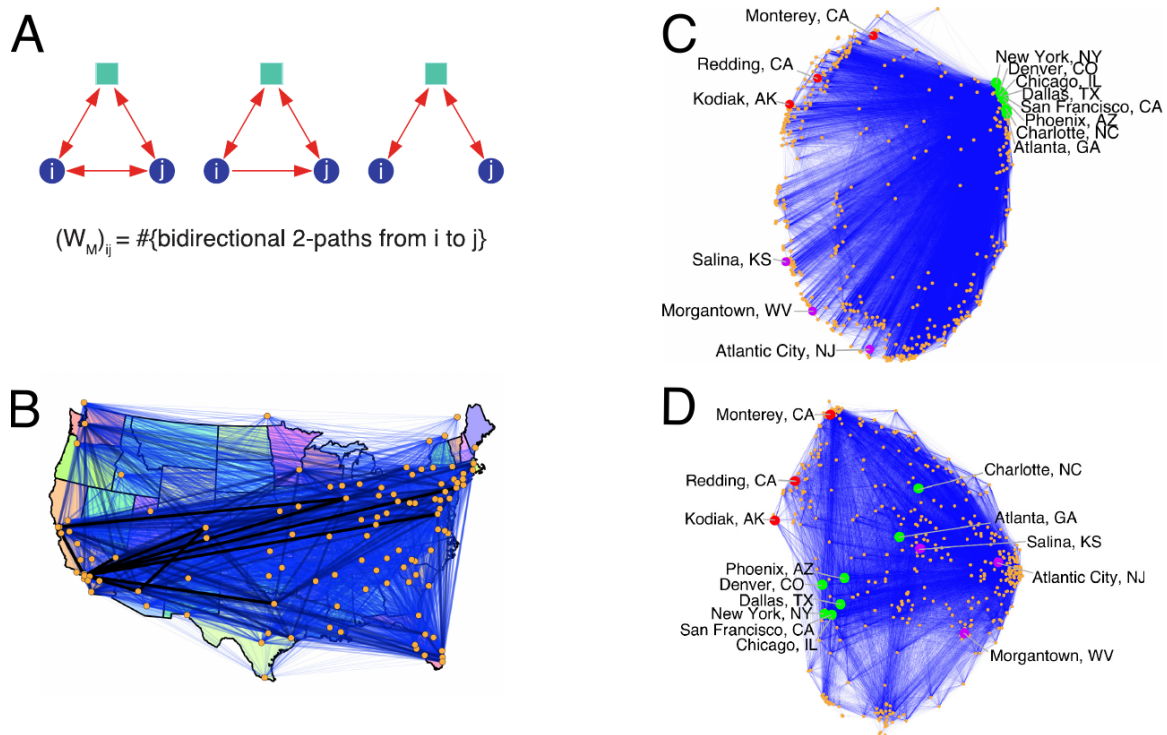


Figure 2.10 – Higher-order spectral analysis of a network of airports in Canada and the United States. A: The three higher-order structures used in our analysis. Each motif is “anchored” by the blue nodes i and j , which means our framework only seeks to cluster together the blue nodes. Specifically, the motif adjacency matrix adds weight to the (i, j) edge based on the number of third intermediary nodes (green squares). The first two motifs correspond to highly-connected cities and the motif on the right connects non-hubs to non-hubs. **B:** The top 50 most populous cities in the United States which correspond to nodes in the network. The edge thickness is proportional to the weight in the motif adjacency matrix W_M . The thick, dark lines indicate that large weights correspond to popular mainline routes. **C:** Embedding of nodes provided by their corresponding components of the first two non-trivial eigenvectors of the normalized motif Laplacian N_M . The marked cities are eight large U.S. hubs (green), three West coast non-hubs (red), and three East coast non-hubs (purple). The primary spectral coordinate (left to right) reveals how much of a hub the city is, and the second spectral coordinate (top to bottom) captures West-East geography. **D:** Embedding of nodes provided by their corresponding components in the first two non-trivial eigenvectors of the standard, edge-based normalized Laplacian. This method does not capture the hub and geography found by the higher-order method. For example, Atlanta, the largest hub, is in the center of the embedding, next to Salina, a non-hub.

To study these results in more detail, we compare the motif-based spectral embedding of the transportation reachability network to spectral embeddings from other connectivity matrices. The two-dimensional spectral embedding for a graph defined by a (weighted) adjacency matrix $W \in \mathbb{R}^{n \times n}$ comes from Algorithm 2:

- i. Form the normalized Laplacian $N = I - D^{-1/2}WD^{-1/2}$, where D is the diagonal degree matrix with $D_{ii} = \sum_j W_{ij}$.
- ii. Compute the first 3 eigenvectors z_1, z_2, z_3 of smallest eigenvalues for N (z_1 has the smallest eigenvalue, which is 0).
- iii. Form the normalized matrix $Y \in \mathbb{R}^{n \times 3}$ by $Y_{ij} = z_{ij} / \sqrt{\sum_{j=1}^3 z_{ij}^2}$.
- iv. Define the primary and secondary spectral coordinates of node i to be Y_{i2} and Y_{i3} , respectively.

We use the following three matrices W for embeddings.

- i. **Motif:** The sum of the motif adjacency matrix for three different anchored motifs:

$$(2.38) \quad B_1 = \begin{bmatrix} 0 & 1 & 1 \\ 1 & 0 & 1 \\ 1 & 1 & 0 \end{bmatrix}, \quad B_2 = \begin{bmatrix} 0 & 1 & 1 \\ 1 & 0 & 1 \\ 0 & 1 & 0 \end{bmatrix}, \quad B_3 = \begin{bmatrix} 0 & 1 & 0 \\ 1 & 0 & 1 \\ 0 & 1 & 0 \end{bmatrix}, \quad \mathcal{A} = \{1, 3\}.$$

If B is the matrix of bidirectional links in the graph ($B = A \circ A^T$), then the motif adjacency matrix for these motifs is $W_M = B^2$. Figure 2.10C shows the resulting embedding. This is equivalent to putting a weight between two nodes as the number of bidirectional length-2 paths between the nodes (Figure 2.10A).

- ii. **Undirected:** The adjacency matrix is formed by ignoring edge direction. In other words, this is the motif adjacency matrix for motif M_{edge} . This is the standard spectral embedding. Figure 2.10D shows the resulting embedding.
- iii. **Undirected complement:** The adjacency matrix is formed by taking the complement of the undirected adjacency matrix. This matrix tends to connect non-hubs to each other.

In all three cases, the network is connected.

We compute 99% confidence intervals for the Pearson correlation of the primary spectral coordinate with the metropolitan population of the city using the Pearson correlation coefficient (Table 2.7). Since eigenvectors are only unique up to sign, we list the interval with the largest positive end point under this symmetry to be consistent across embeddings. The motif-based primary spectral coordinate has the strongest correlation with the city populations. Table 2.7 also lists the correlation between the secondary spectral coordinate and the longitude of the city. Again, the motif-based clustering has the strongest correlation. Furthermore, the lower end of the confidence interval for the motif-based embedding is above the

Table 2.7 – Correlations between principal eigenvectors and city metadata. The table lists the 99% confidence interval for the Pearson correlation coefficients for (i) metropolitan population and the primary spectral coordinate (eigenvector corresponding to the second smallest eigenvalue) and (ii) city longitude and the secondary spectral coordinate (eigenvector corresponding to the third smallest eigenvalue).

	Primary spectral coordinate and metropolitan population	Secondary spectral coordinate and longitude
Embedding	99% confidence interval	99% confidence interval
Motif	0.43 ± 0.09	0.59 ± 0.08
Undir.	0.11 ± 0.12	0.39 ± 0.11
Undir. comp.	0.31 ± 0.11	0.10 ± 0.12

higher end of the confidence interval for the other two embeddings.

In order to visualize these relationships, we compute Loess regressions of city metropolitan population and longitude against the primary and secondary spectral coordinates for each of the embeddings (Figure 2.11). The sign of the eigenvector used in each regression was chosen to match correlation shown in Figures 2.10C and 2.10D.¹⁰ The Loess regressions visualize the stronger correlation of the motif-based spectral coordinates with the metropolitan population and longitude.

¹⁰The primary spectral coordinate positively correlated with population and secondary spectral coordinate negatively correlated with longitude.

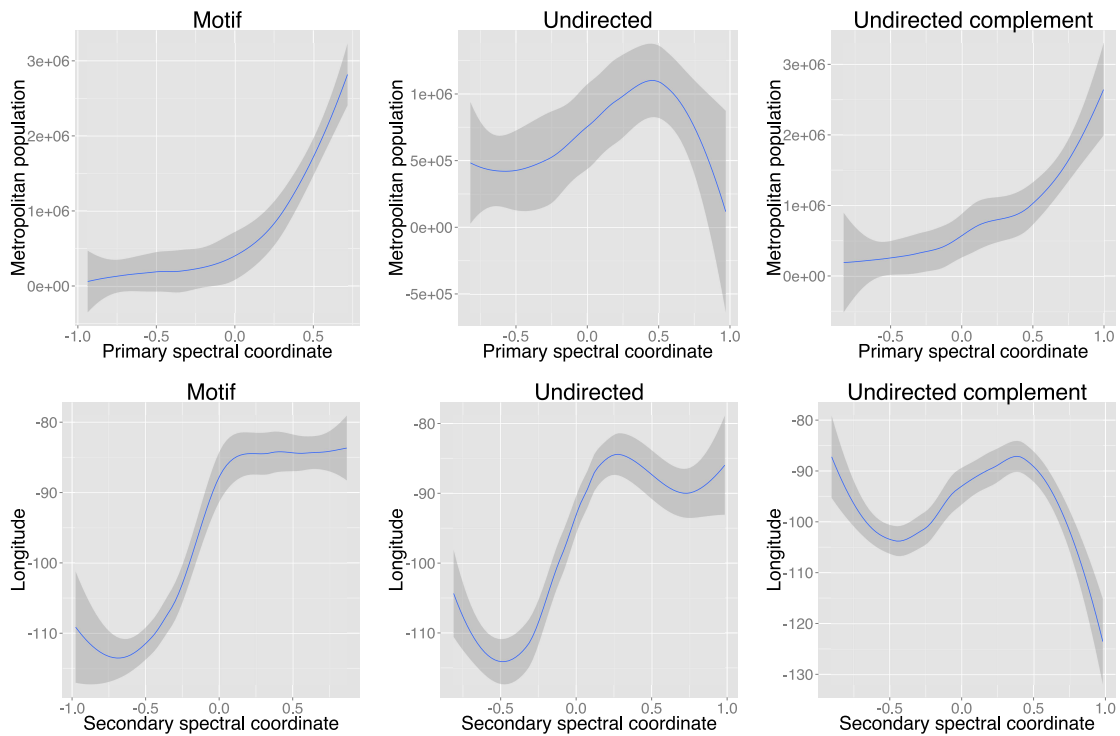


Figure 2.11 – Loess regressions of city metadata against principal eigenvectors. Specifically, the figures show the Loess regressions of city metropolitan population against the primary spectral coordinate (top) and longitude against secondary spectral coordinate (bottom) for the motif (left), undirected (middle), and undirected complement (right) motif adjacency matrices.

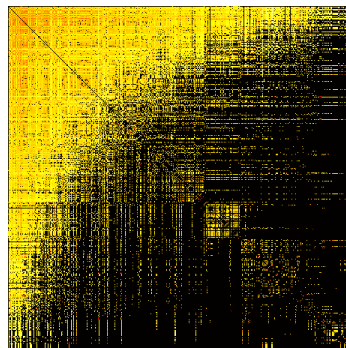


Figure 2.12 – Transportation reachability network matrix. Nodes are ordered according to the spectral ordering of the motif adjacency matrix. A black dot means no edge exists in the network. For the edges in the network, lighter colors correspond longer estimated travel times.

We conclude that the embedding provided by the motif adjacency matrix more strongly captures the hub nature of airports and West-East geography of the network. To gain further insight into the relationship of the primary spectral coordinate’s relationship with the hub airports, we visualize the adjacency matrix in Figure 2.12, where the nodes are ordered by the spectral ordering. We see a clear relationship between the spectral ordering and the connectivity.

2.3.6 The bi-fan motif in the *C. elegans* neuronal network

Next, we apply the higher-order clustering framework to the *C. elegans* neuronal network with the four-node “bi-fan” M_{bifan} (Figure 2.13A), which is known to be over-expressed in neural networks [Milo et al., 2002]. Specifically, the network is of the frontal neurons, where edges represent synapses between the neurons [Kaiser and Hilgetag, 2006].¹¹ The original network is weakly connected with 131 nodes and 764 edges. The largest connected component of the motif adjacency matrix for motif M_{bifan} contains 112 nodes. The remaining 19 nodes are isolated and correspond to the neurons AFDL, AIAR, AINR, ASGL/R, ASIL/R, ASJL/R, ASKL/R, AVL, AWAL, AWCR, RID, RMFL, SIADR, and SIBDL/R.

Using the bi-fan motif and Algorithm 1, we find a cluster of 20 neurons in the frontal section with low bi-fan motif conductance (Figure 2.13B). The cluster shows a plausible way for how nictation is controlled. Within the cluster, ring motor neurons (RMEL/V/R), proposed pioneers of the nerve ring [Riddle et al., 1997], propagate information to IL2 neurons, regulators of nictation [Lee et al., 2012],

¹¹The data was downloaded from <http://www.biological-networks.org/pubs/suppl/celegans131.zip>.

through the neuron RIH and several inner labial sensory neurons (Figure 2.13C). Our framework contextualizes the significance of the bi-fan motif in this control mechanism.

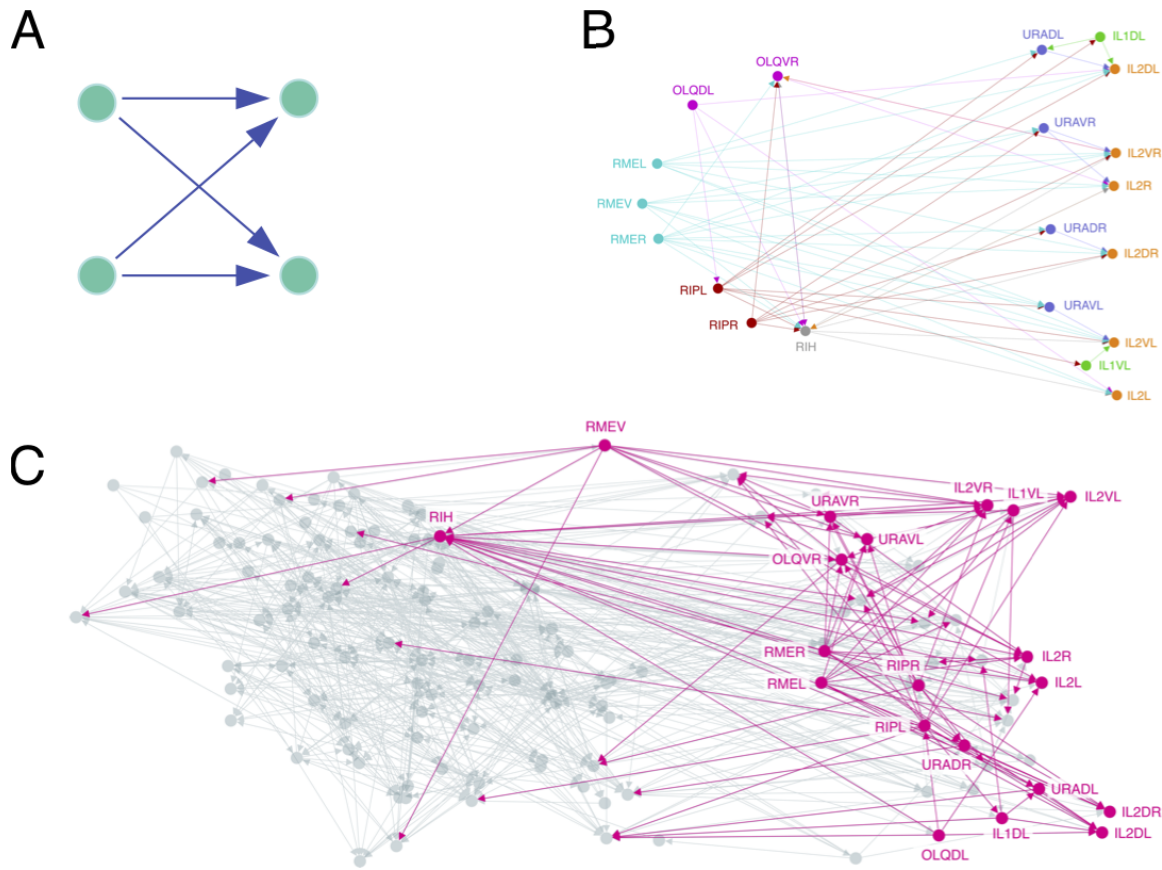


*Figure 2.13 – Higher-order cluster in the *C. elegans* neuronal network. A:* The 4-node “bi-fan” motif, which is over-expressed in neuronal networks [Milo et al., 2002]. Conceptually, this motif describes a cooperative propagation of information from the nodes on the left to the nodes on the right. **B:** The best higher-order cluster in the *C. elegans* frontal neuronal network based on the motif in (A). The cluster contains three ring motor neurons (RMEL/V/R; cyan) with many outgoing connections, serving as the source of information; six inner labial sensory neurons (IL2DL/VR/R/DR/VL; orange) with many incoming connections, serving as the destination of information; and four URA neurons (purple) acting as intermediaries. These RME neurons are pioneers of the nerve ring [Riddle et al., 1997], while the IL2 neurons are known regulators of nictation [Lee et al., 2012], and the higher-order cluster exposes their organization. The cluster also reveals that RIH serves as a critical intermediary of information processing. This neuron has incoming links from all three RME neurons, outgoing connections to five of the six IL2 neurons, and the largest total number of connections of any neuron in the cluster. **C:** Illustration of the higher-order cluster in the context of the entire network. Node locations are the true two-dimensional spatial embedding of the neurons. RME/V/R/L and RIH serve as sources of information to the neurons on the right.

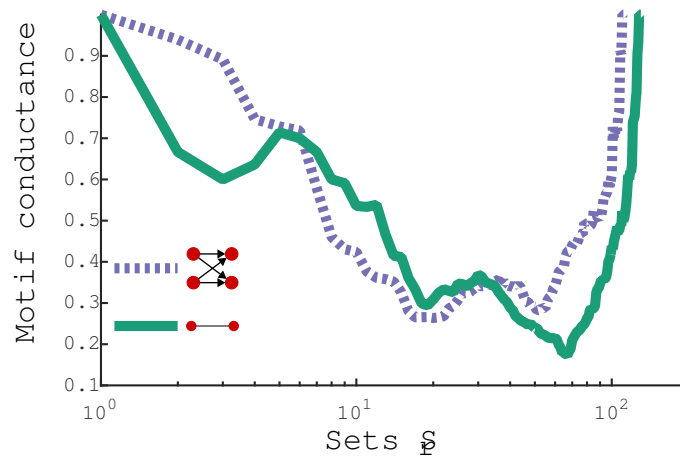


Figure 2.14 – Sweep profile plots for *C. elegans*. The sweep profile plot shows $\phi_M(S)$ as a function of set size from the sweep procedure in Algorithm 1. We show the profiles for M_{bifan} (purple) and M_{edge} (green).

We compare the M_{bifan} -based cluster to the clusters found by edge-based methods. First, Figure 2.14 shows the sweep profile plot from running Algorithm 1 for motifs M_{bifan} and M_{edge} . Both curves have a similar shape with local minima near the same set sizes—however, the cluster found with M_{bifan} is substantially smaller (20 nodes) than for M_{edge} (64 nodes). Figure 2.15 provides a visualization of these two clusters. It turns out that the M_{edge} -based cluster is a superset of the M_{bifan} -based cluster, so we can roughly interpret clustering with M_{bifan} as identifying a more precise cluster than would be found with spectral partitioning based on edges. We also compute clusterings of the network with Infomap and the Louvain method, to see if this trend holds for other edge-based clustering methods. Infomap finds a cluster that overlaps with the M_{bifan} -based cluster by 19 nodes but contains 114 total nodes. The Louvain method finds a cluster that overlaps by 13 nodes and has 27 total nodes. We conclude that common edge-based methods do not capture the same cluster information as our higher-order clustering framework with the bi-fan motif.

We also compute the exact conductance minimizer of the weighted motif adjacency matrix for the bi-fan motif, which is identical to the M_{edge} -based cluster. In other words, the output of Algorithm 1 is not the global minimum for the objective function, even though it contains meaningful structure. The idea that the spectral method can give more meaningful results than the conductance minimizer has been observed in other analyses [Gleich, 2017].

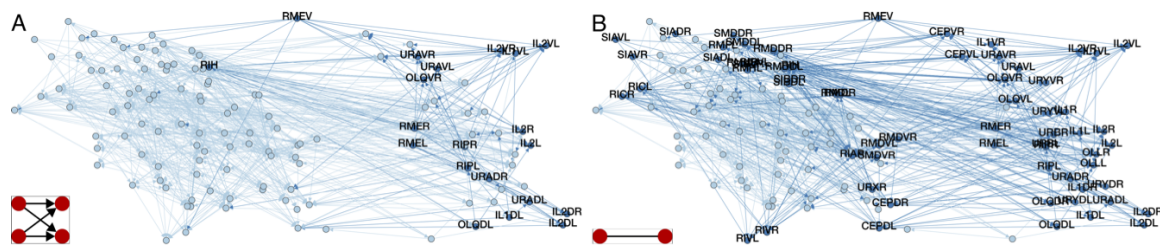


Figure 2.15 – Clusters in *C. elegans*. The nodes are embedded according to a true two-dimensional spatial embedding of the frontal neurons [Kaiser and Hilgetag, 2006]. **A:** The M_{bifan} -based cluster consists of the labeled nodes (same as Figure 2.13B). **B:** The M_{edge} -based cluster consists of the labeled nodes. This cluster is a superset of M_{bifan} -based cluster.

2.3.7 Motif M_6 in the English Wikipedia article network

The English Wikipedia network [Boldi et al., 2004, 2011; Boldi and Vigna, 2004] consists of 4.21 million nodes (representing articles) and 101.31 million edges, where an edge from node i to node j means that there is a hyperlink from the i th article to the j th article.¹² We use Algorithm 1 to find a motif-based cluster for motifs M_6 and M_{edge} (the algorithm was run on the largest connected component of the motif adjacency matrix). Figure 2.16 shows the clusters. The nodes in the motif-based cluster are cities and barangays (small administrative divisions) in the Philippines. The cluster has a set of nodes with many outgoing links that form the source node in motif M_6 . In total, the cluster consists of 22 nodes and 338 edges. The linking pattern appears anomalous and suggests that perhaps the pages uplinking should receive reciprocated links. On the other hand, the edge-based cluster is much larger cluster and does not have too much structure. The cluster consists of several high-degree nodes and their neighbors.

¹²The data was downloaded from <http://law.di.unimi.it/webdata/enwiki-2013/>.

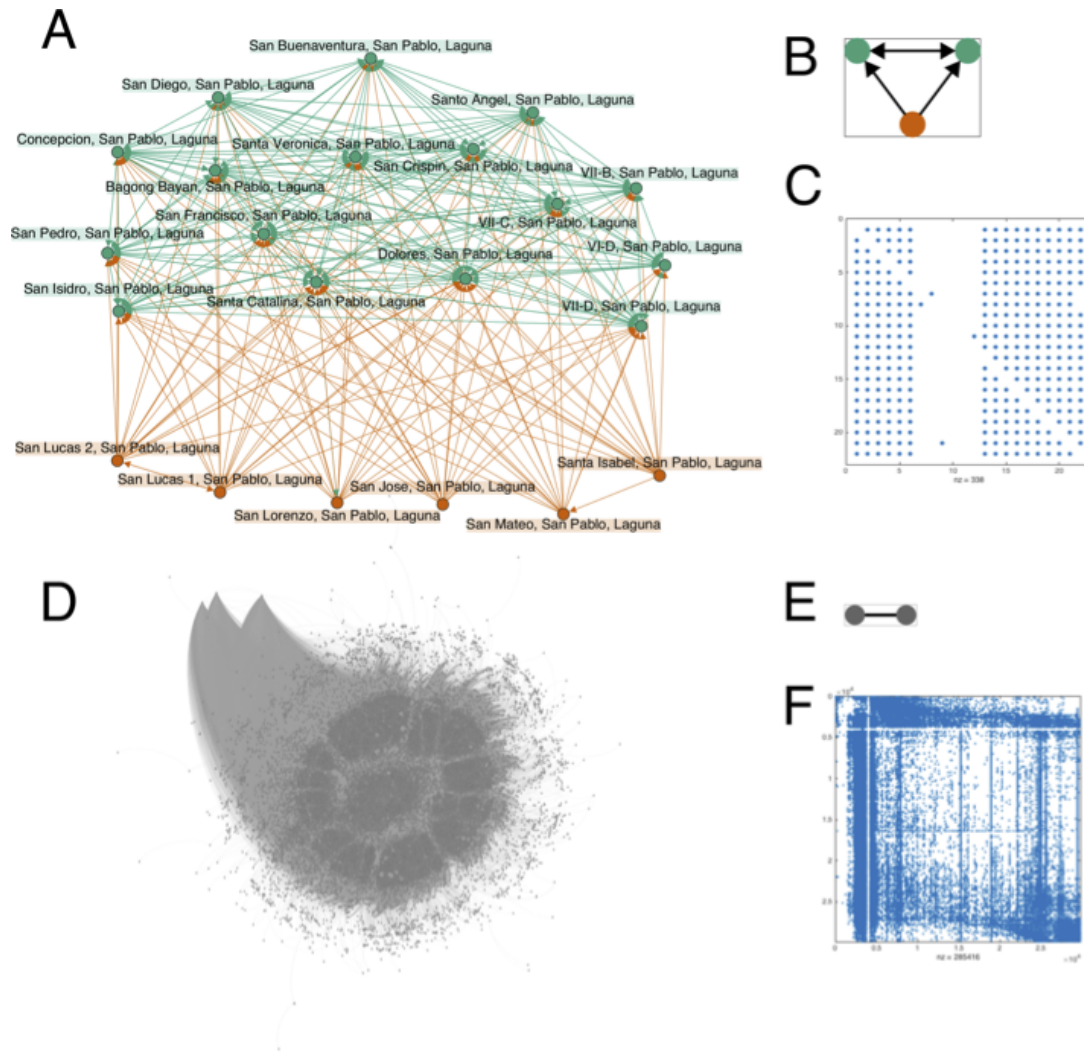


Figure 2.16 – Clusters in the English Wikipedia hyperlink network. A–C: Motif-based cluster (A) for motif M_6 (B). The cluster consists of cities and small administrative divisions in the Philippines. The green nodes have many bidirectional links with each other and many incoming links from orange nodes at the bottom of the figure. The spy plot illustrates this network structure (C). D–F: Cluster (D) for undirected edges (E). The cluster has a few very high-degree nodes, as evidenced by the spy plot (F).

2.3.8 Motif M_6 in the Twitter follower network

We also analyze the complete Twitter follower graph from 2010 [Boldi et al., 2011; Boldi and Vigna, 2004; Kwak et al., 2010]. The graph consists of 41.65 million nodes (users) and 1.47 billion edges, where an edge from node i to node j signifies that user i is followed by user j on the social network.¹³ We use Algorithm 1 to find a motif-based cluster for motif M_6 (the algorithm was run on the largest connected component of the motif adjacency matrix). The cluster contains 151 nodes and consists of two disconnected components. Here, we consider the smaller of the two components, which consists of 38 nodes. We also found an edge-based cluster on the undirected graph (using Algorithm 1 with motif M_{edge}), which consists of 44 nodes.

Figure 2.17 illustrates the motif-based and edge-based clusters. Both clusters capture anomalies in the graph. The motif-based cluster consists of holding accounts for a photography company. The nodes that form bidirectional links have completed profiles (contain a profile picture) while several nodes with incomplete profiles (without a profile picture) are followed by the completed accounts (Figure 2.18). The edge-based cluster is a near clique, where the user screen names all begin with “LC_”. We suspect that the similar usernames are either true social communities, holding accounts, or bots. (For the most part, the tweets of these accounts are protected, so we cannot verify if any of these scenarios are true.) Both M_6 and M_{edge} find anomalous clusters, but their structures are quite different. We conclude that M_6 can lead to the detection of new anomalous clusters in social networks.

¹³The data was downloaded from <http://law.di.unimi.it/webdata/twitter-2010/>.

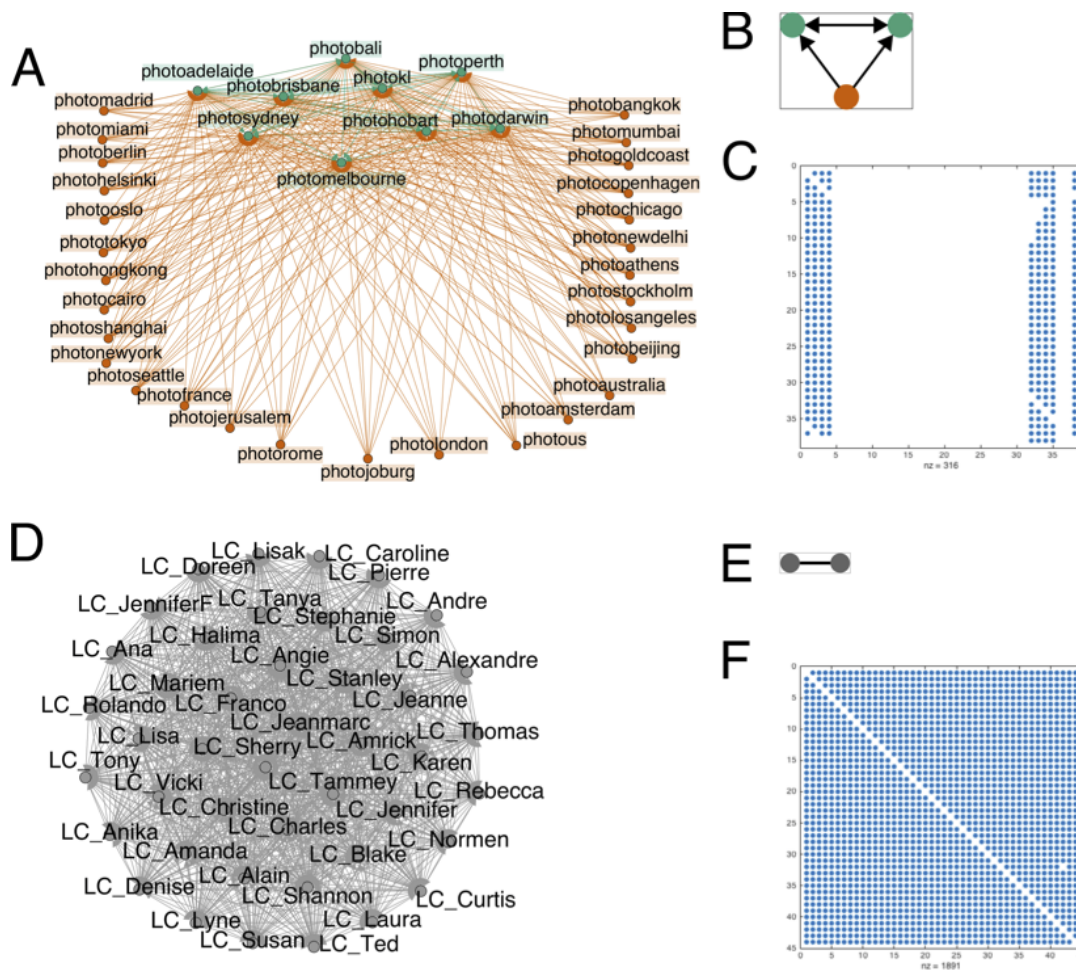


Figure 2.17 – Clusters in the 2010 Twitter follower network. A–C: Motif-based cluster (A) for motif M_6 (B). All accounts are holding accounts for a photography company. The green nodes correspond to accounts that have completed profiles, while the accounts corresponding to the orange nodes have incomplete profiles (see Figure 2.18). The spy plot illustrates how the cluster is formed around this motif (C). D–F: Cluster (D) for edge-based clustering (E). The cluster consists of a near-clique (F) where all users have the prefix “LC_”.

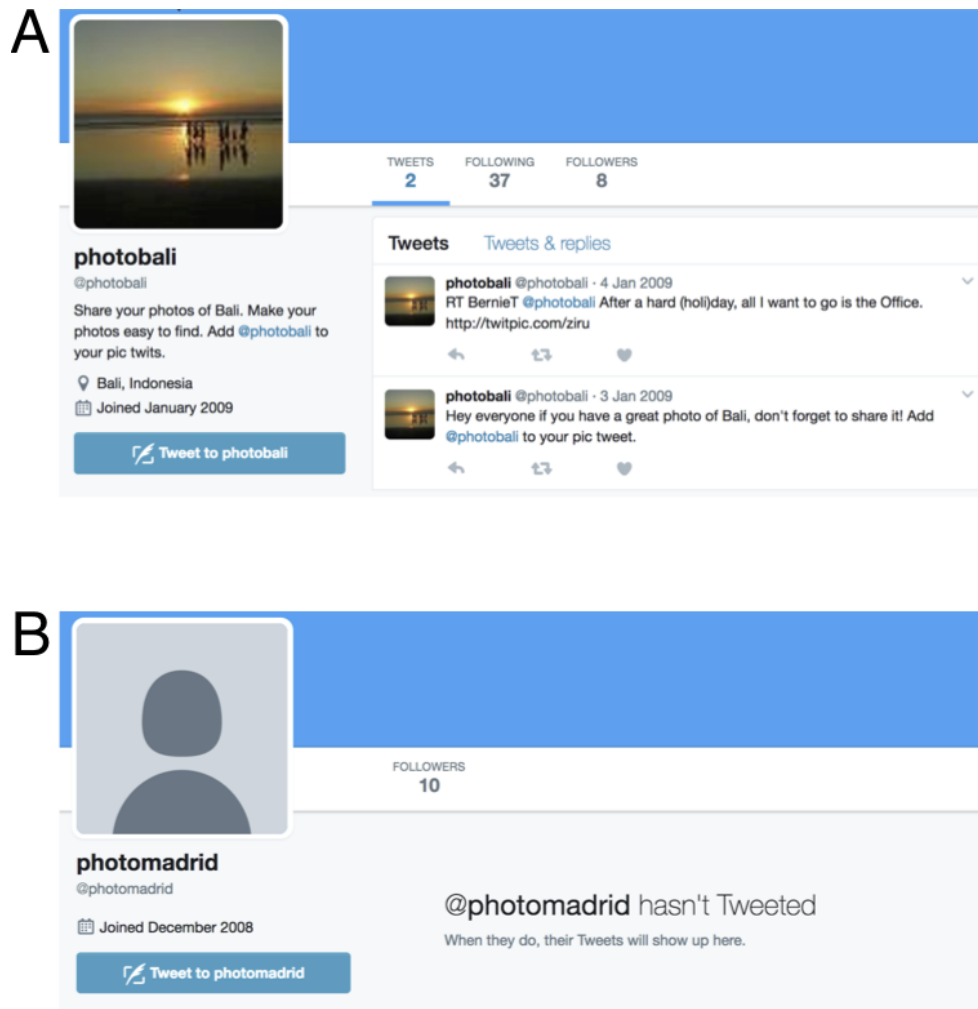


Figure 2.18 – @photobali and @photomadrid Twitter accounts. The motif-based cluster for M_6 (Figure 2.17A) consists of holding accounts for a photography company. The nodes forming bidirectional links in motif M_6 have complete profiles (A) and those forming unidirectional links have incomplete profiles (B).

2.3.9 Motif M_7 in the Stanford web graph

The Stanford web graph consists of 281,903 nodes and 2,312,497 edges, where an edge from node i to node j means that there is a hyperlink from the i th web page to the j th web page [Hirai et al., 2000; Kamvar et al., 2003]. Here, all of the web pages come from the stanford.edu domain.¹⁴ We use Algorithm 1 to find a motif-based cluster for motif M_7 , a motif that is over-expressed in web graphs [Milo et al., 2002]. Figure 2.19 illustrates this cluster and an edge-based cluster (i.e., using Algorithm 1 with M_{edge}). Both clusters exhibit a core-periphery structure, albeit markedly different ones. The motif-based cluster contains several core nodes with large in-degree. Such core nodes serve as the sink node in motif M_7 . On the periphery are several clusters within which are many bidirectional links (as illustrated by the spy plot in Figure 2.19C). The nodes in these clusters then up-link to the core nodes. This type of organizational unit suggests an explanation for why motif M_7 is over-expressed: clusters of similar pages tend to uplink to more central pages. The edge-based cluster also has a few nodes with large in-degree, serving as a small core. On the periphery are the neighbors of these nodes, which themselves tend *not* to be connected (Figure 2.19F).

¹⁴The data was downloaded from <http://snap.stanford.edu/data/web-Stanford.html>.

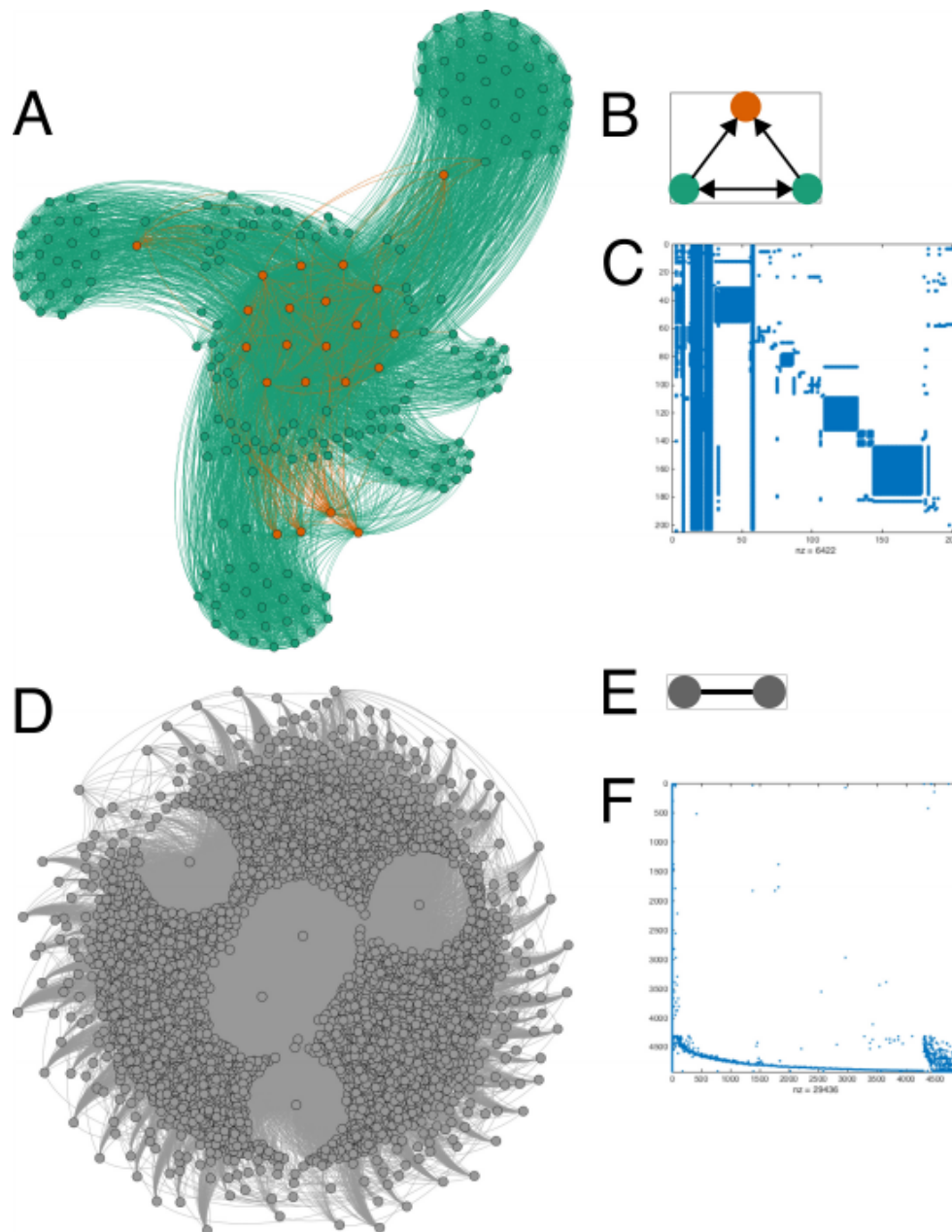


Figure 2.19 – Clusters in the Stanford web graph. **A–C:** Motif-based cluster (A) for motif M_7 (B). The cluster has a core group of nodes with many incoming links (serving as the sink node in M_7 ; shown in orange) and several periphery groups that are tied together (the nodes forming the bidirectional link in M_7 ; shown in green) and also up-link to the core. This is evident from the spy plot (C). **D–F:** Cluster (C) for undirected edges (B). The cluster contains a few high-degree nodes and their neighbors, and the neighbors tend to not be connected (F).

2.3.10 Semi-cliques in collaboration networks

We use Algorithm 1 to identify clusters of the four-node semi-clique motif that has been studied in conjunction with researcher productivity in collaboration networks [Chakraborty et al., 2014]. We found a motif-based cluster in two different collaboration networks (Figures 2.20A and 2.20C). Each network is derived from co-authorship in papers submitted to the arXiv under a certain category—the “High Energy Physics – Theory” (HepTh) and “Condensed Matter Physics” (CondMat) categories [Leskovec et al., 2007b]. The HepTh network has 23,133 nodes and 93,497 edges and the CondMat network has 9,877 nodes and 25,998 edges.¹⁵

Figure 2.20 shows the two clusters for each of the collaboration networks. In both networks, the motif-based cluster consists of a core group of nodes and similarly-sized groups on the periphery. The core group of nodes correspond to the nodes of degree 3 in the motif and the periphery group nodes correspond to the nodes of degree 2. One explanation for this organization is that there is a small group of authors that writes papers with different research groups. Alternatively, the co-authorship could come from a single research group, where senior authors are included on all of the papers and junior authors on a subset of the papers.

On the other hand, the edge-based clusters (i.e., the output of Algorithm 1 for M_{edge}) are a clique in the HepTh network and a clique with a few dangling nodes in the CondMat network. The dense clusters are quite different from the sparser clusters based on the semi-clique. Such dense clusters are not that surprising. For example, a clique could arise from a single paper published by a group of authors.

¹⁵The HepTh network data was downloaded from <http://snap.stanford.edu/data/ca-HepTh.html> and the CondMat network data was downloaded from <http://snap.stanford.edu/data/ca-CondMat.html>.

High Energy Physics – Theory

Condensed Matter Physics

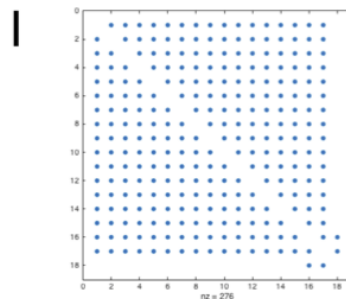
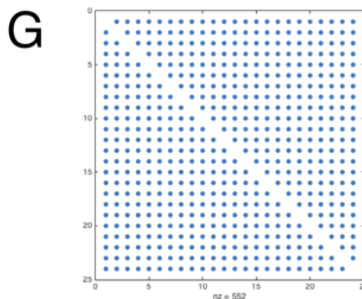
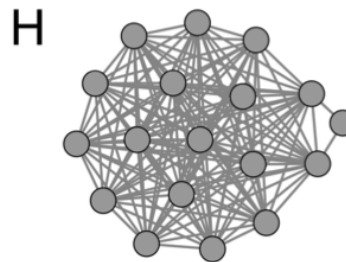
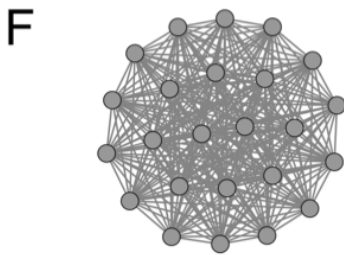
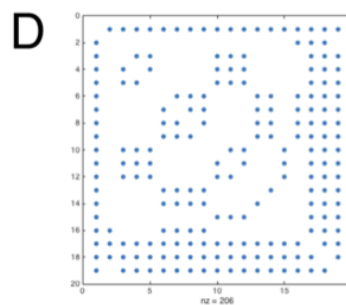
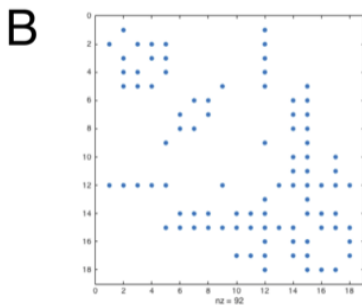
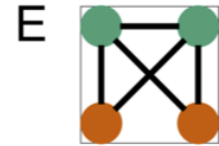
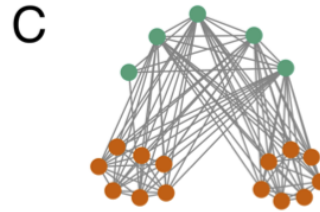
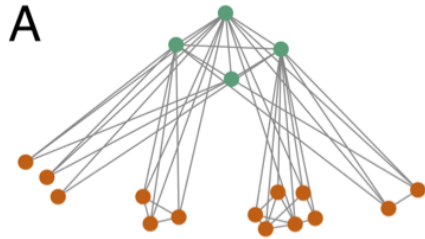


Figure 2.20 – Clusters in co-authorship networks. A–E: Best motif-based cluster for the semi-clique motif (E) in the High Energy Physics–Theory collaboration network (A) and the Condensed Matter Physics collaboration network (C). Corresponding spy plots are shown in (B) and (D). F–I: Best edge-based (I) cluster in the High Energy Physics–Theory collaboration network (F) and the Condensed Matter Physics collaboration network (H). Corresponding spy plots are shown in (G) and (I).

2.4 Scalability experiments

We now empirically analyze the time to find clusters for triangular motifs on a variety of real-world networks, ranging in size from a few hundred thousand edges to nearly two billion edges. Then we show that we can compute the motif adjacency matrix for cliques up to size 9 on a number of real-world networks in a reasonable amount of time.

2.4.1 Triangular motifs

In this section, we demonstrate that our method scales to real-world networks with billions of edges. We tested the scalability of our method on 16 large directed graphs from a variety of real-world applications. These networks range from a couple hundred thousand to two billion edges and from 10 thousand to over 50 million nodes. We briefly describe the networks here and provide some summary statistics in Table 2.8.

- WIKI-RFA represents which users voted for which other users for adminship rights on Wikipedia [West et al., 2014].
- EMAIL-EUALL represents who emailed whom at a European research institution [Leskovec et al., 2005].
- CIT-HEPPH represents citations between papers in the “High Energy Physics – Phenomenology” category on arXiv [Gehrke et al., 2003].
- WEB-NOTREDAME is the hyperlink structure of web pages in the nd.edu domain [Albert et al., 1999].
- AMAZON0601 consists of connections between frequently co-purchased products on Amazon [Leskovec et al., 2007a].
- WIKI-TALK represents which users wrote on which other users’ talk page on Wikipedia [Leskovec et al., 2010b].
- EGO-GPLUS is a collection of egonetworks (1-hop neighborhoods) on the online social network Google+ [Leskovec and Mcauley, 2012].
- UK-2014-TPD is the hyperlink structure of top private domain links in the .uk domain [Boldi et al., 2014, 2011; Boldi and Vigna, 2004].
- SOC-POKEC consists of the friendship relationships on the online social network Pokec [Takac and Zabovskyy, 2012].
- UK-2014-HOST is the hyperlink structure of host links on the .uk domain [Boldi et al., 2014, 2011; Boldi and Vigna, 2004].
- SOC-LIVEJOURNAL1 consists of the friendships on the online social network LiveJournal [Backstrom et al., 2006].
- ENWIKI-2013 is the hyperlink structure of articles on English Wikipedia [Boldi et al., 2004, 2011; Boldi and Vigna, 2004].

- UK-2002 is the hyperlink structure of web pages in the .uk domain [Boldi et al., 2004, 2011; Boldi and Vigna, 2004].
- ARABIC-2005 is the hyperlink structure of arabic-language web pages [Boldi et al., 2004, 2011; Boldi and Vigna, 2004].
- TWITTER-2010 represents the followers of users on the online social network Twitter in 2010 [Boldi et al., 2011; Boldi and Vigna, 2004; Kwak et al., 2010].
- SK-2005 is the hyperlink structure of web pages in the .sk domain [Boldi et al., 2004, 2011; Boldi and Vigna, 2004].

Table 2.8 – Networks for scalability experiments. The total number of edges is the sum of the number of unidirectional edges and twice the number of bidirectional edges.

Dataset	# nodes	# total edges	# unidir. edges	# bidir. edges
WIKI-RFA	10.8K	189K	175K	7.00K
EMAIL-EUALL	265K	419K	310K	54.5K
CIT-HEPPH	34.5K	422K	420K	657
WEB-NOTREDAME	326K	1.47M	711K	380K
AMAZON0601	403K	3.39M	1.50M	944K
WIKI-TALK	2.39M	5.02M	4.30M	362K
EGO-GPLUS	108K	13.7M	10.8M	1.44M
UK-2014-TPD	1.77M	16.9M	13.7M	1.58M
SOC-POKEC	1.63M	30.6M	14.0M	8.32M
UK-2014-HOST	4.77M	46.8M	33.7M	6.55M
SOC-LIVEJOURNAL1	4.85M	68.5M	17.2M	25.6M
ENWIKI-2013	4.21M	101M	82.6M	9.37M
UK-2002	18.5M	292M	231M	30.5M
ARABIC-2005	22.7M	631M	477M	77.3M
TWITTER-2010	41.7M	1.47B	937M	266M
SK-2005	50.6M	1.93B	1.69B	120M

Recall that Algorithm 1 consists of two major computational components:

- i. Form the weighted graph W_M .
- ii. Compute the eigenvector z of second smallest eigenvalue of N_M .

After computing the eigenvector, we sort the vertices and loop over prefix sets to find the lowest motif conductance set. We consider these final steps as part of the eigenvector computation for our performance experiments.

For each network in Table 2.8, we ran the method for all directed triangular motifs (M_1 – M_7). To compute W_M , we used a standard algorithm that meets the $O(m^{3/2})$ bound [Latapy, 2008; Schank and Wagner, 2005] with some additional pre-processing based on the motif. Conceptually, the algorithm is as follows:

- i. Take motif type M and graph G as input.
- ii. (Pre-processing) If M is M_1 or M_5 , ignore all bidirectional edges in G as these motifs only contain unidirectional edges. If M is M_4 , ignore all unidirectional edges in G as this motif only contains bidirectional edges.
- iii. Form the undirected graph G_{undir} by removing the direction of all edges in G .
- iv. Let d_u be the degree of node u in G_{undir} . Order the nodes in G_{undir} by increasing degree, breaking ties arbitrarily. Denote this ordering by ψ .
- v. For every undirected edge $\{u, v\}$ in G_{undir} , if $\psi_u < \psi_v$, add directed edge (u, v) to G_{dir} ; otherwise, add directed edge (v, u) to G_{dir} .
- vi. For every node u in G_{dir} and every pair of directed edges (u, v) and (u, w) , check to see if edge (v, w) or (w, v) is in G_{dir} . If so, check if these three nodes form motif M in G . If they do, increment the weights of edges $(W_M)_{uv}$, $(W_M)_{uw}$, and $(W_M)_{vw}$ by 1.
- vii. Return $W_M + W_M^T$ as the motif weighted adjacency matrix.

The algorithm runs in time $O(m^{3/2})$ time and is also known as an effective heuristic for real-world networks [Berry et al., 2014; Latapy, 2008]. After, we find the largest connected component of the graph corresponding to the motif adjacency matrix W_M , form the motif normalized Laplacian N_M of the largest component, and compute the eigenvector of second smallest eigenvalue of N_M . To compute the eigenvector, we use MATLAB’s `eigs` routine with tolerance $1e-4$ and the “smallest algebraic” option for the eigenvalue type.

Table 2.9 lists the time to compute W_M and the time to compute the eigenvector for each network. We omit the time to read the graph from disk because this time strongly depends on how the graph is compressed. All experiments ran on a 40-core server with four 2.4 GHz Intel Xeon E7-4870 processors. All computations of W_M were in serial and the computations of the eigenvectors were done in parallel (as defaulted to by MATLAB).

Over all networks and all motifs, the longest computation of W_M (including pre-processing time) was for M_2 on sk-2005 and took roughly 52.8 hours. The

longest eigenvector computation was for M_6 on sk-2005 and took about 1.62 hours. We note that W_M only needs to be computed once per network, regardless of the eventual number of clusters that are extracted. Also, the computation of W_M can easily be accelerated by parallel computing (the enumeration of motifs can be done in parallel over nodes, for example) or by more sophisticated algorithms [Berry et al., 2014]. In this work, we perform the computation of W_M in serial in order to better understand the scalability. Our results serve only as a rough baseline.

Table 2.9 – Performance of motif-based clustering. Time to compute the motif adjacency matrix W_M (top) and second eigenvector of the motif normalized Laplacian N_M (bottom) in seconds for each directed triangular motif.

Network	M_1	M_2	M_3	M_4	M_5	M_6	M_7
WIKI-RFA	1.19e+00	2.67e+00	1.71e+00	2.06e-02	1.79e+00	2.42e+00	2.35e+00
EMAIL-EUALL	4.74e-01	8.29e-01	6.26e-01	2.46e-01	5.02e-01	5.40e-01	5.41e-01
CIT-HEP PH	7.65e+00	3.36e+00	2.73e+00	6.22e+00	8.20e+00	3.29e+00	3.35e+00
WEB-NOTRE DAME	9.42e-01	2.39e+01	2.33e+01	2.30e+00	1.17e+00	8.29e+00	8.40e+00
AMAZON0601	2.35e+00	8.66e+00	6.91e+00	1.82e+00	2.94e+00	5.47e+00	5.73e+00
WIKI-TALK	1.07e+01	3.00e+01	2.20e+01	3.11e+00	1.35e+01	2.09e+01	2.10e+01
EGO-GPLUS	8.55e+02	2.42e+03	1.73e+03	2.08e+01	1.63e+03	2.07e+03	2.17e+03
UK-2014-TPD	8.10e+01	5.31e+02	4.07e+02	2.56e+01	1.15e+02	3.04e+02	2.85e+02
SOC-POKEC	4.17e+01	1.34e+02	1.21e+02	3.04e+01	4.88e+01	1.00e+02	1.04e+02
UK-2014-HOST	9.98e+02	4.68e+03	2.76e+03	8.90e+01	1.32e+03	2.89e+03	2.99e+03
SOC-LIVE JOURNAL1	9.08e+01	7.66e+02	6.24e+02	1.24e+02	1.24e+02	4.41e+02	4.49e+02
ENWIKI-2013	8.36e+02	9.62e+02	7.09e+02	3.13e+01	9.77e+02	8.19e+02	8.38e+02
UK-2002	1.47e+03	8.59e+03	5.17e+03	2.45e+02	1.73e+03	4.53e+03	5.29e+03
ARABIC-2005	6.51e+03	7.64e+04	6.05e+04	6.08e+03	8.39e+03	3.59e+04	3.69e+04
TWITTER-2010	1.21e+04	1.38e+05	1.31e+05	3.33e+04	1.99e+04	8.03e+04	7.65e+04
SK-2005	5.52e+04	1.63e+05	1.29e+05	1.55e+04	5.23e+04	9.64e+04	8.42e+04
WIKI-RFA	1.14e-01	2.12e-01	1.22e-01	2.12e-01	2.12e-01	2.94e-01	2.93e-01
EMAIL-EUALL	2.29e-01	1.62e-01	2.43e-01	1.62e-01	1.62e-01	2.35e-01	1.92e-01
CIT-HEP PH	2.11e+00	2.10e+00	2.11e+00	2.10e+00	2.10e+00	2.24e+00	2.30e+00
WEB-NOTRE DAME	1.86e-01	3.62e-01	5.97e-01	3.62e-01	3.62e-01	9.61e-01	2.06e+00
AMAZON0601	1.23e-01	6.96e-01	4.62e+00	6.96e-01	6.96e-01	4.97e+00	4.53e+00
WIKI-TALK	1.28e+00	2.40e+00	2.51e+00	2.40e+00	2.40e+00	2.54e+00	4.52e+00
EGO-GPLUS	4.42e+00	1.68e+01	2.11e+01	1.68e+01	1.68e+01	2.57e+01	4.42e+01
UK-2014-TPD	3.59e+00	9.66e+00	9.92e+00	4.35e+00	9.66e+00	2.10e+01	2.16e+01
SOC-POKEC	1.96e+00	1.75e+01	3.91e+01	1.75e+01	1.75e+01	2.39e+01	2.45e+01
UK-2014-HOST	1.81e+01	4.38e+01	6.80e+01	2.04e+01	4.38e+01	8.28e+01	8.73e+01
SOC-LIVE JOURNAL1	2.32e+00	2.20e+01	1.06e+02	2.20e+01	2.20e+01	4.49e+01	6.13e+01
ENWIKI-2013	2.18e+01	7.58e+01	8.45e+01	7.58e+01	7.58e+01	2.14e+02	1.48e+02
UK-2002	1.66e+01	8.65e+01	2.52e+02	8.65e+01	8.65e+01	7.87e+02	5.32e+02
ARABIC-2005	1.98e+01	1.64e+02	4.80e+02	3.26e+02	1.64e+02	1.95e+03	1.40e+03
TWITTER-2010	2.23e+02	1.23e+03	1.95e+03	1.23e+03	1.23e+03	2.22e+03	2.18e+03
SK-2005	5.73e+01	2.94e+02	7.98e+02	2.94e+02	2.94e+02	5.83e+03	3.81e+03

In theory, the worst-case time for triangle enumeration scales as $m^{1.5}$. We fit a linear regression of the log of the computation time of the last step of the enumeration algorithm to the regressor $\log(m)$ and a constant term:

$$(2.39) \quad \log(\text{time}) \sim a \log(m) + b$$

If the computations truly took $cm^{1.5}$ for some constant c , then the regression coefficient for $\log(m)$ would be 1.5. Because of the pre-processing of the algorithm, the number of edges m depends on the motif. For example, with motifs M_1 and M_5 , we only count the number of unidirectional edges. The pre-processing time, which is linear in the total number of edges, is not included in the time. The regression coefficient for $\log(m)$ (the variable a in Equation (2.39)) is smaller than 1.5 for each motif (Table 2.10). The largest regression coefficient is 1.31 for M_3 (with 95% confidence interval 1.31 ± 0.19). The regression coefficient over the aggregation of data points (the “combined” column in Table 2.10) is 1.17 (with 95% confidence interval 1.17 ± 0.09). We conclude that on real-world datasets, the algorithm for computing W_M performs much better than the worst-case guarantees.

Table 2.10 – Linear models for computation time. The 95% confidence interval for the regression coefficient of the regressor $\log(m)$ in a linear model for predicting the time to compute W_M , based on the computational results for the 16 networks described at the beginning of Section 2.4.1. The algorithm scales as $m^{1.5}$ for the worst-case input. “Combined” refers to the regression coefficient for the union of data points of all motifs.

M_1	M_2	M_3	M_4	M_5	M_6	M_7	combined
1.20 ± 0.19	1.30 ± 0.20	1.31 ± 0.19	0.90 ± 0.31	1.20 ± 0.20	1.27 ± 1.21	1.27 ± 0.21	1.17 ± 0.09

2.4.2 Larger k -clique motifs

On smaller graphs, we can compute larger motifs. To demonstrate this point, we form the motif adjacency matrix W_M based on the k -cliques motif for $k = 4, \dots, 9$ using the algorithm of Chiba and Nishizeki [1985] with the additional pre-processing of computing the $(k - 1)$ -core of the graph. (This pre-processing improves the running time in practice but does not affect the asymptotic complexity.) The motif adjacency matrices for k -cliques are sparser than the adjacency matrix of the original graph, so we do not worry about spatial complexity for these motifs.

We evaluate this procedure on nine real-world networks, ranging from roughly four thousand nodes and 88 thousand edges to over two million nodes and around five million edges. We briefly describe the networks here and list summary statistics in Table 2.11.

- EGO-FACEBOOK is the union of ego networks from the user friendship graph of the online social network Facebook [Leskovec and Mcauley, 2012].
- CA-ASTROPH represents scientists who have co-authored a paper listed on the AstroPhysics category on arXiv [Leskovec et al., 2005].
- SOC-SLASHDOT0811 represents who tagged whom during an event on the online social network Slashdot [Leskovec et al., 2009]. The original network data is directed and signed, and we ignore both of these properties here.
- COM-DBLP represents scientists who have co-authored a paper listed on DBLP [Yang and Leskovec, 2012].
- COM-YOUTUBE consists of friendships on the online social network YouTube [Mislove et al., 2007].

We also use the WIKI-RFA, EMAIL-EUALL, CIT-HEPPH, and WIKI-TALK datasets described earlier, although we now consider the graphs to be undirected.

Each network contains at least one 9-clique and hence at least one k -clique for $k < 9$. All computations ran on the same server as for the triangular motifs and again there was no parallelism. We terminated computations after two hours. For five of the nine networks, it takes less than two hours to compute W_M for any k -clique motif, $k = 4, \dots, 9$ (Table 2.11). Furthermore, on all of these networks, the computation takes less than two hours for $k = 4, 5, 6$. The smallest network (in terms of number of nodes and number of edges) is EGO-FACEBOOK, where it took just under two hours to compute W_M for the 6-clique motif and over two hours for the 7-clique motif. This network has around 80,000 edges. On the other hand, for COM-YOUTUBE, which contains nearly 3 million edges, we can compute W_M for the 9-clique motif in under a minute. We conclude that it is possible to use our framework with motifs much larger than the three-node motifs on which we performed many of our experiments. However, the number of edges is not a good predictor of the running time to compute W_M . This makes sense because the

complexity of the algorithm of Chiba and Nishizeki [1985] is $O(a^{k-2}m)$, where a is the arboricity of the graph. Hence, the dependence on the number of edges is always linear, and the arboricity drives the running time.

Table 2.11 – Time to compute W_M for k -clique motifs. All times are in seconds. Only computations that finished within two hours are listed.

Network	# nodes	# edges	Number of nodes in clique (k)					
			4	5	6	7	8	9
EGO-FACEBOOK	4.04K	88.2K	14	317	6816	–	–	–
WIKI-RFA	10.8K	182K	6	22	63	134	218	286
CA-ASTROPH	18.8K	198K	5	35	285	2164	–	–
EMAIL-EUALL	265K	364K	1	2	4	5	6	6
CIT-HEPPh	34.5K	421K	3	6	11	18	30	36
SOC-SLASHDOT0811	77.4K	469K	3	12	55	282	1018	2836
COM-DBLP	317K	1.05M	9	129	3234	–	–	–
COM-YOUTUBE	1.13M	2.99M	12	17	25	33	35	33
WIKI-TALK	2.39M	4.66M	64	466	2898	–	–	–

2.5 An extension to local higher-order clustering

2.5.1 Overview

Thus far, our algorithms have focused on finding a *global clustering* of the network—we assign every node in the network to a cluster. In contrast, *local* graph clustering methods aim to find a cluster of nodes by exploring a small region of the graph. More specifically, the idea is to identify a single cluster nearby a seed set of nodes without ever exploring the entire graph, which makes the local clustering methods much faster than their global counterparts. Because of its speed and scalability, this approach is frequently used in applications including ranking and community detection on the Web [Epasto et al., 2014; Gargi et al., 2011], social networks [Jeub et al., 2015], and bioinformatics [Jiang et al., 2009]. Furthermore, the seed-based targeting is also critical to many applications. In analysis of protein-protein interaction networks, for instance, local clustering aids in determining additional members of a protein complex [Voevodski et al., 2009]. However, current local graph partitioning methods are also not designed to account for higher-order structures.

A major advantage of the theory we developed for global higher-order clustering is that it can immediately be adapted for other objectives. Specifically, we can re-interpret objective functions based on cuts and volumes of sets (e.g., conductance) to motif cuts and motif volumes of sets (e.g., motif conductance). And in fact, much of the theory and algorithms for local clustering are most well developed when using conductance as the cluster quality measure [Andersen et al., 2006; Zhu et al., 2013]. In this section, we adapt one of these methods—the approximate personalized PageRank (APPR) algorithm [Andersen et al., 2006]—to find local clusters containing a seed node with minimal *motif conductance*. The theory of the approximate personalized PageRank method is based on the graph Laplacian and conductance, so we get new theory and algorithms for motif-based local clusters “for free”.¹⁶ In particular, we get guarantees of fast running time (independent of the size of the graph, assuming we have pre-computed the motif adjacency matrix W) and cluster quality (in terms of motif conductance). For community detection tasks on both synthetic and real-world networks, our new framework outperforms the current edge-based personalized PageRank methodology. From a data mining perspective, the main advantage of local higher-order clustering is to provide new types of heretofore unexplored local information based on higher-order structures.

As stated above, our approach to local higher-order clustering is to generalize the APPR of Andersen et al. [2006] to finding sets of provably small motif conductance (Theorem 12 is the main result). The APPR method is a graph diffusion

¹⁶We need to be a little careful with the analysis, but the core ideas come “for free”.

that “spreads mass” from a seed set to identify the cluster. It has an extremely fast running time, which is roughly proportional to the size of the output cluster. Our generalization just uses a pre-processing step that transforms the original (possibly directed) network into the motif-weighted graph, where the weight on edge (i, j) is the number of times that nodes i and j co-participate in an instance of the motif. We show that running APPR on this weighted network maintains the provably fast running time and has theoretical guarantees on cluster output quality in terms of motif conductance. An additional benefit of our motif-based APPR method is that it naturally handles directed graphs on which graph clustering has been a longstanding challenge. The original APPR method can only be used for undirected graphs, and existing local approaches for APPR on directed graphs are challenging to interpret [Andersen et al., 2008].

We use our motif-based APPR method on a number of community detection tasks and show improvements over the corresponding edge-based methods. We show that using the triangle motif improves the detection of ground truth communities in synthetic networks. In addition, we identify important directed triangle motifs for recovering community structure in directed graphs. We note that there are several methods for finding clusters containing a seed node beyond the personalized PageRank method considered here, including other graph diffusions [Chung and Simpson, 2013; Kloster and Gleich, 2014], local spectral methods [Li et al., 2015; Mahoney et al., 2012], local modularity maximization [Clauset, 2005], and flow-based algorithms [Orecchia and Zhu, 2014]. We focus on generalizing the personalized PageRank method because of the algorithm’s simplicity and scalability. Finally, the local method of Rohe and Qin [2013] is specifically designed around growing a seed set to avoid cutting the triangle motif, which is most similar to our ideas, and their analysis is developed from a stochastic blockmodel point of view.

2.5.2 Motif-based personalized PageRank

We now generalize the classical personalized PageRank method to account for motifs. The essential idea of our approach is to transform the input graph, which is unweighted and possibly directed, into a weighted undirected graph—the motif adjacency matrix defined in Section 2.2.4. We then show that the fast approximate personalized PageRank method on this weighted graph will efficiently find a set with small motif conductance that contains a given seed node. We also explain how previous theoretical results are applicable to this approach, which gives us formal guarantees on running time and cluster output quality in terms of motif conductance.

Background on approximate personalized PageRank (APPR). The personalized PageRank (PPR) vector represents the stationary distribution of a particular random

walk. At each step of the random walk, with a teleportation parameter $\alpha \in (0, 1)$, the random walker will “teleport” back to a specified seed node u ; and with probability $1 - \alpha$, the walker will transition uniformly at random to an adjacent node. The key idea is that the stationary distribution of this process for a seed node u (the PPR vector p_u) will have large values for nodes “close” to u . We can write the stationary distribution as the solution to the following system of equations

$$(2.40) \quad (I - \alpha P)p_u = (1 - \alpha)e_u,$$

where P is the column-stochastic transition matrix representing the standard random walk over the graph and e_u is the indicator vector for node u . Formally, $P = AD^{-1}$, where A is the adjacency matrix, $D = \text{diag}(Ae)$ is the diagonal degree matrix, and e is the vector of all ones.

Andersen et al. [2006] developed a fast algorithm for approximating p_u by a vector \tilde{p}_u where $0 \leq D^{-1}(p_u - \tilde{p}_u) \leq \varepsilon$ component-wise. To obtain a cluster with small conductance from this approximation, we again use the sweep procedure:

- i. sort the nodes by descending value in the vector $D^{-1}\tilde{p}_u$,
- ii. compute the conductance of each prefix in this sorted list, and
- iii. output the prefix set with smallest conductance.

This is the same sweep procedure as in Algorithm 1, but the node values are given by $D^{-1}\tilde{p}_u$ instead of the Fiedler vector. Overall, this algorithm is fast (it runs in time proportional to the size of the output cluster) and is guaranteed to have small conductance provided that node u is in a set with small conductance. We will be more specific with the guarantees in the following section, when we derive the analogous theory for the motif-based approach.

Motif-weighted APPR. We now propose an algorithm that finds a cluster with small motif conductance by finding an approximate PPR vector on a weighted graph based on the motif. The algorithm has three steps:

- i. construct the motif adjacency matrix (Equation (2.21)), where W_{ij} is the number of instances of M containing nodes i and j ,
- ii. compute the approximate PPR vector for this weighted graph,
- iii. use the sweep procedure to output the set with minimal conductance.

Algorithm 3 formally describes this method. Note that step (i) needs to be done only once, whereas steps (ii) and (iii) would be repeated for multiple subsequent runs. This approach is directly motivated by Theorem 6, which says that edge-based conductance of sets in the weighted network is equal to motif-based conductance in the original network.

The APPR method is designed for *unweighted* graphs, whereas we want to use the method for weighted graphs. Mathematically, this corresponds to replacing the column stochastic matrix P in the linear system with the column stochastic matrix

Algorithm 3 – Motif-PageRank-Nibble. This algorithm finds localized clusters with small motif conductance

Input: Unweighted graph $G = (V, E)$, motif M , seed node u , teleportation parameter α , tolerance ε
Output: Motif-based cluster (set $S \subset V$)

- 1 $W_{ij} \leftarrow \#(\text{instances of } M \text{ containing nodes } i \text{ and } j)$
- 2 $\tilde{p} \leftarrow \text{Approximate-Weighted-PPR}(W, u, \alpha, \varepsilon)$ (Algorithm 4)
- 3 $D_W \leftarrow \text{diag}(We)$
- 4 $\sigma_i \leftarrow i\text{th smallest entry of } D_W^{-1}\tilde{p}$
- 5 **return** $S \leftarrow \arg \min_{\ell} \phi_M(S_{\ell})$, where $S_{\ell} = \{\sigma_1, \dots, \sigma_{\ell}\}$

Algorithm 4 – Approximate-Weighted-PPR.

Input: Undirected edge-weighted graph $G_w = (V_w, E_w, W)$, seed node u , teleportation parameter α , tolerance ε
Output: an ε -approximate weighted PPRvector \tilde{p}

- 1 $\tilde{p} \leftarrow 0$
- 2 $r \leftarrow e_u$
- 3 $d_w \leftarrow We$
- 4 **while** $r(v)/d_w(v) \geq \varepsilon$ for some node $v \in V_w$ **do**
- 5 /* push operation */
- 6 $\tilde{p}(v) \leftarrow \tilde{p}(v) + (1 - \alpha)r(u)$
- 7 $r(v) \leftarrow \frac{\alpha}{2}r(v)$
- 8 **for each** x such that $(v, x) \in E_w$:
- 9 $r(x) \leftarrow r(x) + \frac{W_{v,w}}{d_w(v)} \cdot \frac{\alpha}{2}r(v)$
- 10 **return** \tilde{p}

$P_W = WD_W^{-1}$, where $D_W = \text{diag}(We)$ is the diagonal weighted degree matrix. For the purposes of implementation, this modification is simple. We just need to change the algorithm's push method (Line 5 in Algorithm 4) to push residual weights to neighbors proportional to edge weights (instead of evenly). We state the procedure in Algorithm 4.

Theory. For the purposes of theoretical analysis with motifs, it is important that our edge weights are integers so that we can interpret an edge with weight k as k parallel edges. Since all of the analysis of APPR permits parallel edges in the graph, we can combine previous results for theoretical guarantees on Algorithm 3. The following theorem says that our algorithm runs in time proportional to the size of the output set.

Theorem 11. *Algorithm 3, after line 1, runs in $O(\frac{1}{\varepsilon(1-\alpha)})$ time, and the number of nodes with non-zero values in the output approximated PPR vector is at most $\frac{1}{\varepsilon(1-\alpha)}$.*

Proof. This follows from Andersen et al. [2006, Lemma 2], where we translate G_w into a unweighted graph with parallel edges. \square

Although APPR with weighted edges has been used before [Andersen et al., 2008; Gleich and Mahoney, 2015], there was never a runtime bound. This result is the first (albeit straightforward) theoretical bound on the runtime of APPR with weighted edges when they arise from integers.

Our next result is a theoretical guarantee on the quality of the output of Algorithm 3 in terms of motif conductance. The proof of the result follows from combining Theorem 6 and the analysis of Zhu et al. [2013] (an improvement over the analysis of Andersen et al. [2006]). The result says that if there is some set T with small motif conductance, then there are several nodes in T for which Algorithm 3 outputs a set with small motif conductance. For notation, let η be the inverse mixing time of the random walk on the subgraph induced by T .

Theorem 12. *Suppose $T \subset V$ is some unknown targeted community we are trying to retrieve from an unweighted graph using motif M . Then for most seeds $u \in T$, Algorithm 3 with $1 - \alpha = \Theta(\eta)$ and $\varepsilon \in [\frac{1}{10\text{vol}_M(T)}, \frac{1}{5\text{vol}_M(T)}]$ runs in time $O(\text{vol}_M(T) / \phi_M(T))$ and outputs a set S with*

$$\phi_M(S) \leq \tilde{O} \left(\min \left\{ \sqrt{\phi_M(T)}, \phi_M(T) / \sqrt{\eta} \right\} \right).$$

For the computational complexity, the final piece we need to consider is the complexity of forming the motif adjacency matrix (Line 1 of Algorithm 3), which we have analyzed in Section 2.2.9. For the experiments in this section, we will only use triangular motifs, so the $O(am)$ bound from Chiba and Nishizeki [1985] suffices, where a is the arboricity of the graph and m is the number of edges.

Towards purely local methods. The graph weighting procedure can also be done locally by having the push procedure compute W_{vx} “on the fly” for all nodes x adjacent to node v . While this suffices for Algorithm 4, the Nibble method (Algorithm 3) needs to know the total volume of the weighted graph to compute the motif conductance scores. To address this, one might use recent techniques for quickly estimating the total ℓ -clique volume on large graphs [Jain and Seshadhri, 2017]. We leave these optimizations for future work.

Practical considerations. The formal theory underlying the methods (Theorem 12) requires multiple a priori unknowable parameters including the inverse mixing time η of the target community and the volume of the output. As practical guidance,

we suggest using $\alpha = 0.99$, computing the PPR vector for $\varepsilon = 10^{-2}/\bar{d}_M, 10^{-3}/\bar{d}_M, 10^{-4}/\bar{d}_M$, where $\bar{d}_M = \frac{1}{n}\text{vol}_M(G)$ is the average motif-degree of all nodes, and outputting the set of best motif conductance. The reason for scaling by \bar{d}_M is as follows. Theorem 11 bounds the running time by volume as if accessing an edge (i, j) with weight W_{ij} takes $\Theta(W_{ij})$ time (i.e., as if the edges are parallel). However, we merely need to access the value W_{ij} , which takes $O(1)$ time. Scaling ε by \bar{d}_M accounts for the average effect of parallel edges present due to the weights of the motifs and permits the algorithm to do more computation with roughly the same running time guarantees.

Rather than using the global minimum in the sweep procedure in the last step of the Nibble method, we apply the common heuristic of finding the first local minimum [Yang and Leskovec, 2012]. The first local minimum is the smallest set where the PageRank vector suggests a border between the seed and the rest of the graph. It also better models the small size scale of most ground truth communities that we encounter in our experiments.

2.5.3 Experiments on synthetic networks

On a network with ground truth communities or clusters, our evaluation procedure of both edge-based and motif-based APPR method is the following. For each ground truth community, we use every node as a seed in the APPR method to obtain a set and pick the set with the highest F_1 score for recovering the ground truth. Then we take the average of the F_1 scores over all detected communities for the detection accuracy of the method. This measurement captures how well the communities can possibly be recovered (i.e., given the best seed) and has previously been used to compare seeded clustering algorithms [Kloster and Gleich, 2014].

We first evaluate our motif-based APPR method for recovering ground truth in two common synthetic random graph models—the planted partition model and the LFR model. In both cases, we find that using the triangle motif increases the range of parameters in which APPR is able to recover the ground truth communities.

Planted partition model. The planted partition model generates random, undirected, unweighted graphs with kn_1 nodes. Nodes are partitioned into k built-in communities, each of size n_1 . Between any pair of nodes from the same community, an edge exists with probability p and between any pair of nodes from different communities, an edge exists with probability q . Each edge exists independently of all other edges.

In our experiment, we examine the behavior of the edge-based and motif-based APPR methods by fixing parameters $n_1 = 50, k = 10, p = 0.5$, and taking different values of q such that the community mixing level $\mu = [(k - 1)q] / [p + (k - 1)q]$,

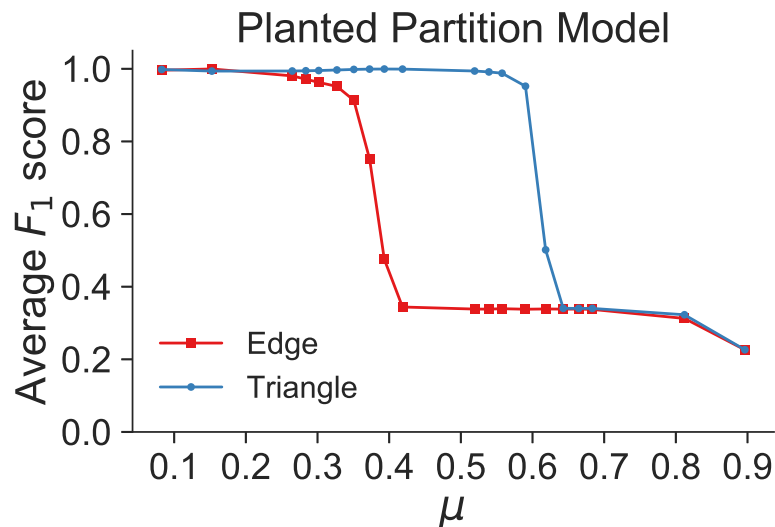


Figure 2.21 – Recovery in the planted partition model. The plot shows the average F_1 score of detected clusters in the model as a function of the mixing parameter μ that specifies the fraction of neighbors of a node that cross cluster boundaries (μ varies as the intra-cluster edge probability p is fixed). We use edge-based and triangle-based approximate personalized PageRank to recover ground truth clusters. There is a large parameter regime where the triangle-based approach significantly out-performs the edge-based approach.

which measures the fraction of expected neighbors of a node that cross cluster boundary, varies from 0.1 to 0.9. For each value of μ , we computed the average of the “mean best” F_1 score described above over 20 random instances of the graph. For the motif-based APPR method, we used the triangle motif. We are motivated in part by recent theoretical results of Tsourakakis et al. [2017] showing that with high probability, the triangle conductance of a true community in the planted partition model is smaller than the edge conductance. Here we take an empirical approach and study recovery instead of conductance.

Figure 2.21 illustrates the results. The triangle-based APPR significantly out-performs the edge-based APPR method when $\mu \in [0.4, 0.6]$. In this regime, for any given node, the expected number of intra-community edges and inter-community edges is roughly the same. Thus, the edge-based method degrades in performance. However, the number of intra-community triangles remains greater than the number of inter-community triangles, so the triangle-based method is able to recover the planted partition.

LFR model. The LFR model also generates random graphs with planted communities, but the model is designed to capture several properties of real-world networks with community structure such as skew in the degree and community size distributions and overlap in community membership for nodes [Lancichinetti and Fortunato, 2009; Lancichinetti et al., 2008]. For our purposes, the most important model parameter is the mixing parameter μ , which is the fraction of a node’s edges that connect to a node in another community. We fix the other parameters as follows: $n = 1000$ is the number of nodes, where 500 nodes belong to 1 community and 500 belong to 2; the number of communities is randomly chosen between 43 and 50; the average degree is 20; and the community sizes range from 20 to 50.

We again used the edge-based and triangle-based APPR methods, and Figure 2.22 shows the results. The performance of the edge-based method decays as we increase the mixing parameter μ from 0.1 to 0.4, while the triangle-based method maintains an F_1 score of approximately 0.9 in this regime. For mixing parameters as large as 0.6, the F_1 score for the triangle-based method is still three times larger than that of the edge-based method, and throughout nearly the entire parameter space, using triangles improves performance.

To summarize, incorporating triangles into personalized PageRank dramatically improves the recovery of ground truth community structure in synthetic models. In the next section, we run experiments on both undirected and directed real-world networks.

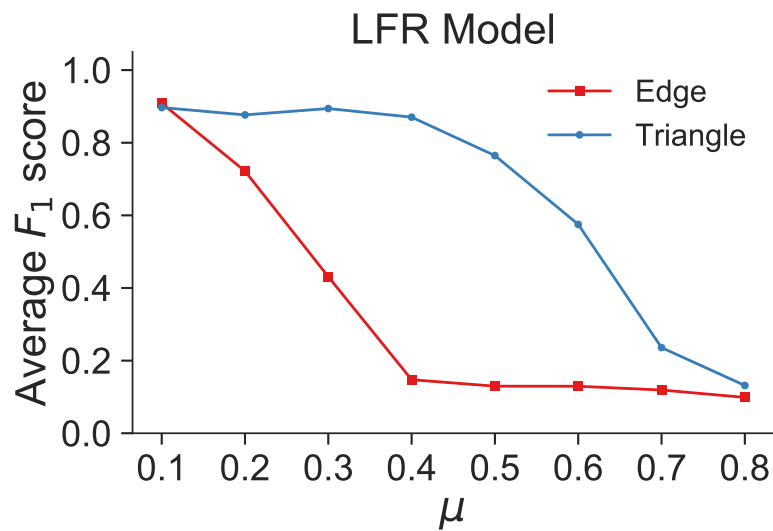


Figure 2.22 – Recovery in the LFR model. The plot shows the average F_1 score of detected clusters in the model as a function of the mixing parameter μ that specifies the fraction of neighbors of a node that cross cluster boundaries. We use edge-based and triangle-based approximate personalized PageRank to recover ground truth clusters. As was the case for the planted partition model (Figure 2.21), there is a large parameter regime where the triangle-based approach significantly out-performs the edge-based approach.

2.5.4 Experiments on real-world networks

We now compare the edge- and motif-based APPR methods on real-world networks with ground truth communities. Although these graphs have as many as 1.8 billion edges, the APPR method takes at most a few seconds per seed once the graph is in memory and the motif weighted adjacency matrix has been computed.

Undirected graphs. We analyze several well-known networks with ground truth community structure constructed from Web data:

- COM-AMAZON represents frequent co-purchasing of items on the online retailer Amazon. The communities are the connected components of the subgraph induced by nodes in a product category [Yang and Leskovec, 2012].
- COM-DBLP represents co-authorship on DBLP. The communities are the connected components of the subgraph induced by individuals who have published at a particular conference or in a particular journal [Yang and Leskovec, 2012].
- COM-YOUTUBE represents friendships between users on the online social network YouTube. The communities are connected components of user-defined groups [Mislove et al., 2007].
- COM-LIVEJOURNAL represents friendships between users on the online social network LiveJournal. The communities are connected components of user-defined groups [Mislove et al., 2007].
- COM-ORKUT represents friendships between users on the online social network Orkut. The communities are connected components of user-defined groups [Mislove et al., 2007].
- COM-FRIENDSTER represents friendships between users on the online social network Friendster. The communities are connected components of user-defined groups [Yang and Leskovec, 2012].

For each network, we examine 100 communities whose sizes ranged between 10 and 200 nodes. We use both edge-based and motif-based APPR for the triangle motif to recover the known communities. Summary statistics of the datasets and our experiment are in Table 2.12. In 5 out of 6 networks, motif-based APPR achieves a higher F_1 score than edge-based APPR. In 3 of the 5 networks, the F_1 score provides a relative improvement of over 5%. In all 6 networks, the average precision of the recovered clusters is larger, and in 4 of these networks, the change is greater than 5%. We suspect this arises from triangles encouraging more tight-knit clusters. For example, dangling nodes connected by one edge to a cluster are ignored by the triangle-based method, whereas such a node would increase the edge-based conductance of the set. In 4 of the 6 networks, recall in the triangle-based method provides relative improvements of at least 5%.

Table 2.12 – Recovery of ground truth community structure in undirected graphs. We use edge-based and motif-based APPR for the triangle motif. Bold numbers denote better recovery or smaller conductance with 5+% relative difference. F_1 score, precision, and recall are all averages over the 100 ground truth communities.

	COM-AMAZON	COM-DBLP	COM-YOUTUBE	COM-LIVEJOURNAL	COM-ORKUT	COM-FRIENDSTER
# nodes	335K	317K	1.13M	4.00M	3.07M	65.6M
# edges	926K	1.05M	2.99M	34.7M	117M	1.81B
# comms.	100	100	100	100	100	100
comm. sizes	10–178	10–36	10–200	10–10	10–200	10–191
F_1 score						
edge	0.620	0.264	0.140	0.255	0.063	0.095
triangle	0.556	0.269	0.165	0.274	0.078	0.114
Precision						
edge	0.634	0.342	0.233	0.216	0.072	0.103
triangle	0.660	0.366	0.390	0.280	0.117	0.158
Recall						
edge	0.704	0.310	0.147	0.606	0.212	0.204
triangle	0.567	0.329	0.188	0.672	0.166	0.234
Conductance						
edge	0.163	0.393	0.536	0.498	0.702	0.747
triangle	0.065	0.384	0.739	0.409	0.510	0.622

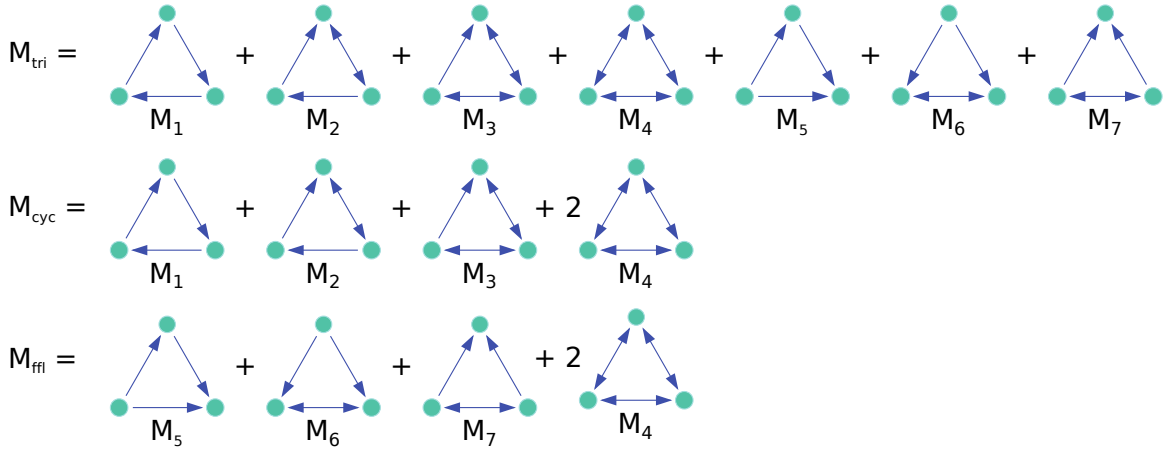


Figure 2.23 – Three directed motif groups. We use these three directed triangle motif groups in our experiments: a triangle with any edge directions (M_{tri}), the number of directed 3-cycles between three nodes (M_{cyc}), and the number of feed-forward loops between three nodes (M_{ffl}).

Directed graphs. A major advantage of our motif-based APPR method is that it is straightforward to analyze directed graphs—we simply need to specify the directed motifs for our motif-based APPR algorithm. Here, we use the three different directed triangle motifs in Figure 2.23: M_{tri} , the undirected triangle; M_{cyc} , the cycle; and M_{ffl} , the feed-forward loop. We form our motif weighted matrix W with respect to subgraphs and *not* induced subgraphs. Thus, a triangle with all six directed edges contains 1 instance of motif M_{tri} , 2 instances of motif M_{cyc} , and 2 instances of motif M_{ffl} . The equivalent weighting scheme for simultaneously analyzing several motifs is in Figure 2.23.

We analyze two directed networks:

- EMAIL-EU-CORE is an e-mail network between members of a European research institution. Department membership of researchers determines the ground truth communities.
- WIKI-CATS is the hyperlink network of English Wikipedia. The article categories are the ground truth communities (we only consider 100 categories for our analysis) [Klymko et al., 2014].

The datasets and recovery results are summarized in Table 2.13. For both networks, using motif M_{tri} provides an improvement in F_1 score over the edge-based method. The improvement is drastic in EMAIL-EU-CORE (25% relative improvement). In fact, all three motifs lead to substantial improvements in this network. We also see that in both networks, the motifs provide additional precision but sacrifice recall. These tighter clusters are expected for the same reasons as for the undirected networks.

Table 2.13 – Recovery of ground truth communities in directed graphs. We use edge-based and motif-based APPR for the three triangular motifs in Figure 2.23. Bold numbers denote (i) cases where a motif-based method’s score is a 5+% relative improvement over the edge-based method and (ii) cases where the edge-based method out-performs all 3 motif-based methods by 5+%.

	EMAIL-EU-CORE	WIKI-CATS
# nodes	1.00K	1.79M
# edges	25.6K	28.5M
# comms.	28	100
comm. sizes	10–109	21–192
<hr/>		
F_1 score		
edge	0.396	0.237
M_{tri}	0.496	0.245
M_{cyc}	0.447	0.233
M_{ffl}	0.472	0.231
<hr/>		
Precision		
edge	0.478	0.322
M_{tri}	0.584	0.349
M_{cyc}	0.616	0.376
M_{ffl}	0.630	0.333
<hr/>		
Recall		
edge	0.779	0.380
M_{tri}	0.690	0.327
M_{cyc}	0.577	0.227
M_{ffl}	0.607	0.344

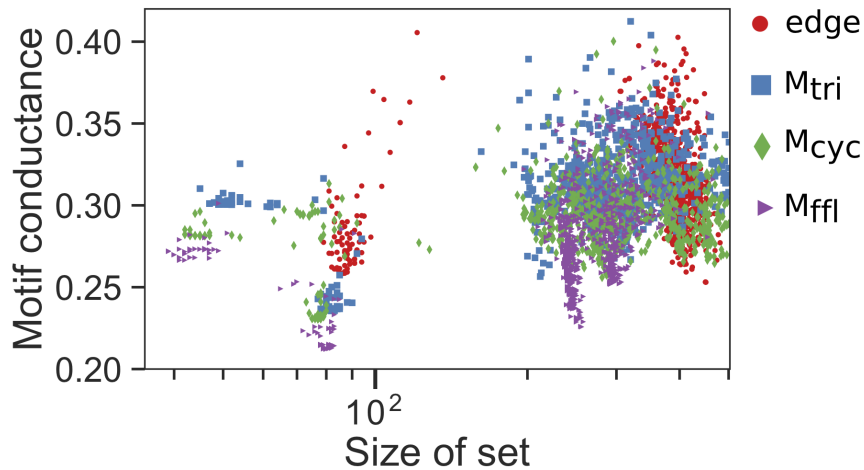


Figure 2.24 – Distribution of set size and conductance for seeded APPR in EMAIL-EU-CORE. We use each node in the graph as a seed for the edge-based and motif-based APPR methods. There is a bifurcation into small clusters and large clusters. Small edge-based cluster concentrate in sizes of 70–100, a regime in which there are also many motif-based clusters with smaller conductance. Of the larger clusters, edge-based clusters tend to be even larger than motif-based clusters.

We investigate the results of the EMAIL-EU-CORE network in more detail, as the use of motifs dramatically improves the recovery of ground truth clusters with respect to F_1 score. First, we use every node in the network as a seed for the APPR method with edges and the three motifs (Figure 2.24). The clusters bifurcate into small (< 100 nodes) and large (> 200 nodes) groups. For the small clusters, the edge-based ones concentrate in sizes of 70–100. In this range, there are several clusters with much smaller motif-based conductance for all three motifs. This provides evidence that the 3 motifs are better models for the community structure in the network. We also see that, of the large clusters, the edge-based ones tend to be the largest. Since these sets are larger than the sizes of the communities in the network, this observation provides evidence for why precision is better with motif-based APPR.

Next, we examine the sweep profile for a single seed node in the EMAIL-EU-CORE network (Figure 2.25). The sweep profile highlights key differences between the output of the motif-based and edge-based algorithm. Although the general shape of the sweep profile is the same across the 3 motifs and edges, the minimum of the curves occurs for a smaller set and at a smaller conductance value for the motifs. A plausible explanation is that the edge-based and motif-based APPR methods

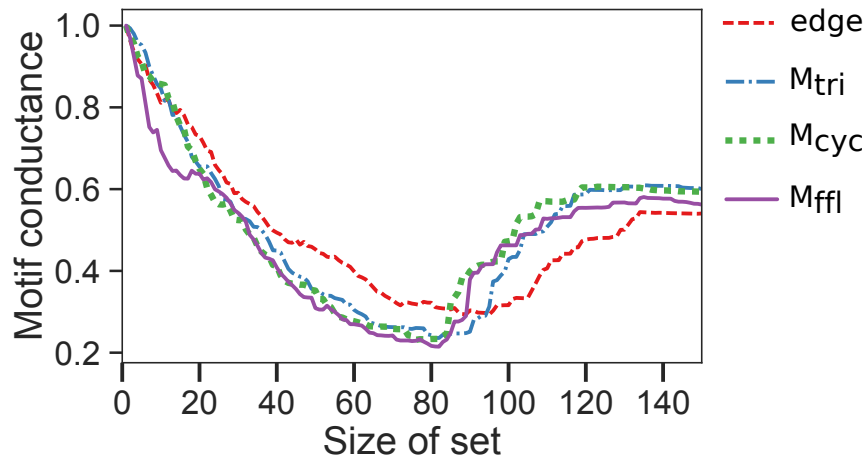


Figure 2.25 – Sweep profile for a single seed in EMAIL-EU-CORE. The shape of the curves is similar, but the minimum for the 3 motif-based curves occur for a smaller set size and have a smaller conductance compared to the curve for edges.

are capturing roughly the same set, but the constraint of triangle participation excludes some nodes. The smaller motif conductance values indicate that these motifs are better models for the cluster structure in the network.

2.6 Related work and discussion

The work in this chapter fits into the saga of network clustering, community detection, and graph partitioning, where the goal is to assign the nodes in a graph into clusters, communities, or partition components. The literature in this space is vast, but there are a few surveys providing an overview of the topic [Fortunato, 2010; Fortunato and Hric, 2016; Malliaros and Vazirgiannis, 2013; Schaeffer, 2007]. In particular, the recent survey by Fortunato and Hric [2016] discusses our motif-based clustering methodology within a broader context.

We now discuss existing methods for global graph clustering that consider motifs or higher-order structures. In my own work, we clustered networks based on metrics similar to motif conductance using generalizations of spectral methods to tensor data [Benson et al., 2015]. Klymko et al. [2014] add weights to the edges of directed graphs based on the participation of edges in cyclic motifs 3-node triangle motifs (M_4 , M_5 , M_6 , and M_7) before plugging the weighted graph into an existing clustering algorithm. In this method, the weight does not depend on the number of instances of the motif—it only matters whether an edge participates in at least

one instance. [Gupta et al. \[2016\]](#) provide an algorithm to decompose triangle-dense graphs into an “approximate union of cliques”; more specifically, most of the nodes can be partitioned into edge- and triangle-dense subgraphs with radius at most 2. This approach has been extended to also provide estimates of clique counts in real-world networks [[Comandur et al., 2014](#)]. [Michoel et al. \[2011\]](#) and [Michoel and Nachtergaele \[2012\]](#) use a max-cut-like objective to decompose graphs based on triangular motifs. More specifically, they aim to find sets of nodes X_1 , X_2 , and X_3 , such that in many instances of a given triangular motif, the three nodes in the instance are in the three different sets. Eigenvectors of the non-backtracking operator, which looks at 3-node length-2 paths as higher-order structures, have been used to get better recovery results in the stochastic block model [[Krzakala et al., 2013](#)]. Finally, there are studies of the hierarchical composition of complex networks based on self-similarity and higher-order structures [[Angulo et al., 2015](#); [Derényi et al., 2005](#); [Itzkovitz et al., 2005](#)] as well as generalizations of k -core decompositions [[Sariyuce et al., 2015](#); [Zhang and Parthasarathy, 2012](#)].

[Arenas et al. \[2008\]](#) proposed a “motif modularity” that measures how many more motifs are contained within cluster in a given partition compared to a random configuration. A few years later, [Serrouer et al. \[2011\]](#) showed that the classical spectral algorithm for modularity maximization [[Newman, 2006](#)] can be adapted for the case of triangular motifs and this definition of motif modularity. The approach simply uses the same spectral algorithm on the modularity matrix coming from the weighted motif adjacency matrix we proposed in this chapter. In fact, this idea is a simple corollary of our cut and volume equivalence results (Lemmas 3 and 5) and the fact that modularity can be written in terms of cuts and volumes [[Gleich and Mahoney, 2016](#)].

In addition to the motif modularity ideas above, Lemmas 3 and 5 make our theoretical results much more general than the extension of the Cheeger inequality introduced in this chapter. Any objective function based on cuts, volumes, and set sizes are immediately translated, in addition to any algorithms based on conductance. This was the case for the localized methods developed in Section 2.5. We can use the same motif Laplacian for motif normalized cut or motif ratio cut objectives [[Von Luxburg, 2007](#)] as well as for Laplacian-based methods for non-exhaustive and overlapping clustering [[Whang et al., 2015](#)]. We can also generalize more theoretical algorithms for sparsest cut [[Arora et al., 2009](#)]. However, we focused on the simpler Cheeger bounds because they are easy to use in practice and actually scale to large datasets. The central challenge to these generalizations is that we now have to deal with weighted graphs and often the theory assumes an unweighted graph.

The work of [Serrouer et al. \[2011\]](#) is not the only place where our proposed weighting scheme has shown up. [Rohe and Qin \[2013\]](#) use the same motif adjacency

matrix weights (specifically for the triangle motif) for single linkage clustering—the resulting dendrogram is cut at some threshold level and the connected components are returned as clusters. Tsourakakis et al. [2017] use the same Laplacian (and independently arrived at some of our same results), but their experiments analyze undirected graphs. The motif Laplacian was originally studied by Rodríguez [2002], who related eigenvalues of this Laplacian to bounds on hypergraph generalizations of partition quantities like bisection, max-cut, and the isoperimetric number. This same Laplacian was used for hypergraph-based semi-supervised learning tasks [Zhou et al., 2006]. In this case, hyperedges are constructed from data points that share a feature (e.g., the nodes are animals and a hyperedge is constructed between all animals that have a tail).

The general problem of partitioning a graph based on relationships between more than two nodes has been studied in hypergraph partitioning [Karypis et al., 1999]. We can interpret motifs as hyperedges in a hypergraph. The key difference of our methods is that *we are constructing a hypergraph from patterns in a standard graph rather than receiving the hyperedges a priori*. The way in which we construct the hyperedges leads to different information about the underlying dataset. One goal with our analysis of the Florida Bay food web, for example, was to find which hyperedge constructs (induced by different motifs) provide a good clustering of the network (see Section 2.3.3).

Our motif-based spectral clustering methodology falls into the area of encoding a hypergraph partitioning problem by a graph partitioning problem [Agarwal et al., 2006]. The motif Cheeger inequality we proved (Theorem 7) explains why previous methods (such as clustering based on the Laplacian proposed by Rodríguez [2002]) are appropriate for 3-regular hypergraphs. Specifically, it respects the standard cut and volume metrics for graph partitioning. There are also a couple spectral clustering approaches designed directly for hypergraphs. For example, Angelini et al. [2015] use a non-backtracking walk approach for recovering planted clusters in a hypergraph stochastic block model. In the theory community, Louis and Makarychev [2014] introduced an *edge expansion* metric for vertex sets in hypergraphs and a diffusion process whose second eigenvalue leads to a Cheeger-like bound.

Lastly, it is worth mentioning that our framework is also a principled approach for clustering directed graphs, a longstanding problem in network analysis. Some existing principled generalizations of undirected graph partitioning to directed graph partitioning proceed from graph circulations [Chung, 2005] or random walks [Boley et al., 2011] and are difficult to interpret. Yoshida [2016] uses a nonlinear Laplacian to derive a Cheeger-like inequality where the “cut” measures the number of outgoing edges from a set (in this case, the cut is asymmetric, so the measure is actually the minimum over the set S and the complement set \bar{S}).

Our motif-based clustering framework provides a simple, rigorous framework for directed graph partitioning—the algorithm user simply needs to specify which motif he or she wants to use.

We can also interpret common heuristics for directed graph clustering in terms of motifs. For example, consider the simple approach of clustering the symmetrized graph $W = A + A^T$, where A is the (directed) adjacency matrix [Malliaros and Vazirgiannis, 2013]. Following Theorem 6, conductance-minimizing methods for partitioning W are actually trying to minimize a weighted sum of motif-based conductances for the directed edge motif and the bidirectional edge motif:

$$B_1 = \begin{bmatrix} 0 & 1 \\ 0 & 0 \end{bmatrix}, \quad B_2 = \begin{bmatrix} 0 & 1 \\ 1 & 0 \end{bmatrix},$$

where both motifs are simple ($\mathcal{A} = \{1, 2\}$). If W_{B_1} and W_{B_2} are the motif adjacency matrices for motifs B_1 and B_2 , then $A + A^T = W_M = W_{B_1} + 2W_{B_2}$. This weighting scheme gives a weight of two to bidirectional edges in the original graph and a weight of one to unidirectional edges. An alternative method for clustering a directed graph is to simply remove the direction on all edges, treating bidirectional and unidirectional edges the same. This is equivalent to using the motif M_{edge} discussed earlier in this chapter. The resulting adjacency matrix is equivalent to the motif adjacency matrix for the bidirectional and unidirectional edges (without any weighting), i.e., $W = W_{B_1} + W_{B_2}$.

We conclude this chapter with an executive summary of our contributions.

- i. We are the first to really demonstrate how clustering based on motifs leads to new discoveries in network data from several domains. Moreover, we show how “first-order” methods that only consider edge relationships do not make the same discoveries. This should encourage practitioners analyzing network data to think about higher-order structures.
- ii. Our methods come with a theoretical guarantees on cluster quality by generalizing steadfast ideas in spectral graph theory. The theory explains why certain hypergraph partitioning methods work for 3-regular hypergraphs. The theory also makes the idea of higher-order clustering easily extendible, which we demonstrate with with the localized methods in Section 2.5.
- iii. Our methods provide a simple, easy-to-understand, and principled approach to clustering directed graphs.

Chapter 3

Higher-order clustering coefficients

3.1 The clustering coefficient and closure probabilities

As we have discussed, networks are a fundamental tool for understanding and modeling complex physical, social, informational, and biological systems. Although such networks are typically sparse, a recurring trait of networks throughout all of these domains is the tendency of edges to appear in small clusters or cliques [Watts and Strogatz, 1998]. In many cases, such clustering can be explained by local evolutionary processes. For example, in social networks, clusters appear due to the formation of triangles where two individuals who share a common friend are more likely to become friends themselves. This process is known as *triadic closure* [Granovetter, 1973; Rapoport, 1953; Simmel, 1908]. Similar triadic closures occur in other information networks. For example, in citation networks, two references appearing in the same publication are more likely to be on the same topic and hence more likely to cite each other [Wu and Holme, 2009]. And in co-authorship networks, scientists with a mutual collaborator are more likely to collaborate in the future [Jin et al., 2001]. In other cases, local clustering arises from highly connected functional units operating within a larger system, e.g., metabolic networks are organized by densely connected modules [Ravasz and Barabási, 2003].

The *clustering coefficient* quantifies the extent to which edges of a network cluster. The clustering coefficient is defined as the fraction of length-2 paths, or *wedges*, that are closed with a triangle [Barrat and Weigt, 2000; Watts and Strogatz, 1998] (Figure 3.1, C_2). In other words, the clustering coefficient measures the probability of triadic closure in the network. However, the clustering coefficient is inherently restrictive as it measures the closure pattern of just one simple structure—the triangle. Higher-order structures such as larger cliques are crucial

to the structure and function of complex networks [Benson et al., 2016; Yaveroğlu et al., 2014]. For example, 4-cliques reveal community structure in word association and protein-protein interaction networks [Palla et al., 2005] and maximal cliques of size 5–7 appear more than expected in many real-world networks compared to a configuration model [Slater et al., 2014]. However, the extent of clustering of such higher-order structures has not been well understood nor quantified.

Here we introduce higher-order clustering coefficients that measure the closure probability of higher-order network structures (specifically, larger cliques) and provide a more comprehensive view of how the edges of complex networks cluster. Our higher-order clustering coefficients are a natural generalization of the classical clustering coefficient.

Below, we derive several properties about higher-order clustering coefficients and analyze them under common random graph models. We then use higher-order clustering coefficients to gain new insights into the structure of real-world networks from several domains. For example, we show that the *C. elegans* neural network exhibits clustering in the traditional sense (i.e., in terms of triadic closure) but not in the higher-order sense. On the other hand, co-authorship and social networks exhibit both traditional and higher-order clustering. Finally, we make a connection between higher-order clustering coefficients and motif conductance for clique motifs. More specifically, we show that if the graph has a large higher-order clustering coefficient, then there is a 1-hop neighborhood of same node u with small motif conductance for a clique motif.

3.2 Definitions of higher-order clustering coefficients

We first give an alternative interpretation of the clustering coefficient that will later allow us to generalize it and quantify clustering of higher-order network structures. First consider a 2-clique K in a graph G (that is, a single edge K). Now, “expand” the clique K by considering any edge e adjacent to K (i.e., e and K share exactly one node). In our parlance, this expanded subgraph is a *wedge* (length-2 path). The global clustering coefficient C of G [Barrat and Weigt, 2000; Luce and Perry, 1949] can then be defined as the fraction of wedges that are *closed*, meaning that the 2-clique and adjacent edge induce a $(2 + 1)$ -clique, or a triangle (Figure 3.1, C_2). Formally,

$$(3.1) \quad C = \frac{6|K_3|}{|W|},$$

where K_3 is the set of 3-cliques (triangles), W is the set of wedges, and the coefficient 6 comes from the fact that each 3-clique closes 6 wedges (the 6 ordered pairs of

edges in the triangle).¹

Our novel interpretation of the global clustering coefficient as a measurement of 2-cliques expanding to 3-cliques through closure of an adjacent edge naturally carries over to the local clustering coefficient [Watts and Strogatz, 1998]. Each wedge consists of a 2-clique and adjacent edge (Figure 3.1), and we call the unique node in the intersection of the 2-clique and adjacent edge the *center* of the wedge. Under this view, the *local clustering clustering coefficient* of a node u can be defined as the fraction of wedges centered at u that are closed:

$$(3.2) \quad C(u) = \frac{2|K_3(u)|}{|W(u)|},$$

where $K_3(u)$ is the set of 3-cliques containing u and $W(u)$ is the set of wedges with center u (if $|W(u)| = 0$, we say that $C(u)$ is undefined). The *average clustering coefficient* \bar{C} is the mean of the local clustering coefficients,

$$(3.3) \quad \bar{C} = \frac{1}{|\tilde{V}|} \sum_{u \in \tilde{V}} C(u),$$

where \tilde{V} is the set of nodes in the network where the local clustering coefficient is defined [Watts and Strogatz, 1998].

Our alternative interpretation of the clustering coefficient, described above as a form of clique expansion, leads to a natural generalization to higher-order structures. Instead of expanding 2-cliques to 3-cliques, we expand ℓ -cliques to $(\ell + 1)$ -cliques (Figure 3.1, C_3 and C_4). Formally, we define an ℓ -wedge to consist of an ℓ -clique and an adjacent edge. Then we define the global ℓ th-order clustering coefficient C_ℓ as the fraction of ℓ -wedges that are closed, meaning that they induce an $(\ell + 1)$ -clique in the network. We can write this as

$$(3.4) \quad C_\ell = \frac{\binom{\ell+1}{\ell} \binom{\ell}{1} |K_{\ell+1}|}{|W_\ell|},$$

where $K_{\ell+1}$ is the set of $(\ell + 1)$ -cliques, W_ℓ is the set of ℓ -wedges, and the coefficient $\binom{\ell+1}{\ell} \binom{\ell}{1}$ comes from the fact that each $(\ell + 1)$ -clique closes that many wedges.

We also define higher-order local clustering coefficients:

$$(3.5) \quad C_\ell(u) = \frac{\binom{\ell}{\ell-1} |K_{\ell+1}(u)|}{|W_\ell(u)|},$$

¹We use an ordered pair of edges in order to make the constants in our formulas consistent with the higher-order generalization.

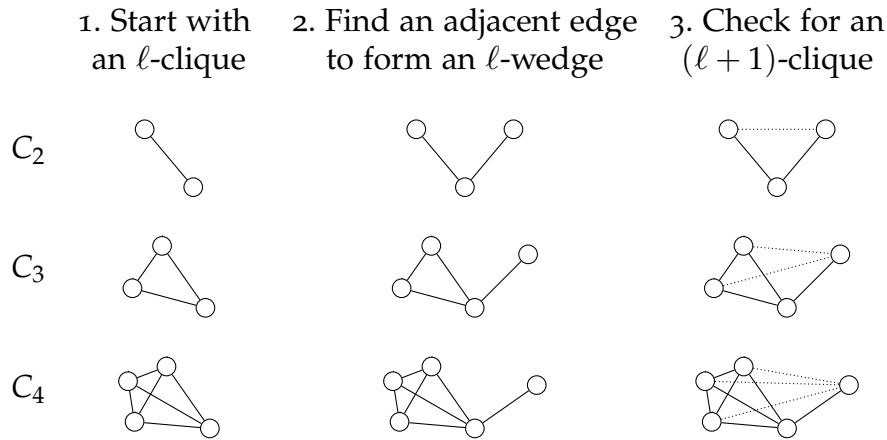


Figure 3.1 – Overview of higher-order clustering coefficients as clique expansion probabilities. The ℓ th-order clustering coefficient C_ℓ measures the probability that an ℓ -clique and an adjacent edge, i.e., an ℓ -wedge, is closed, meaning that the $\ell - 1$ possible edges between the ℓ -clique and the outside node in the adjacent edge exist to form an $(\ell + 1)$ -clique. The case of $\ell = 2$ is the traditional (global) clustering coefficient—the fraction of length-2 paths that induce a triangle. We also define the local higher-order clustering coefficients for a node u to be the same probability over all ℓ -wedges where u is at the “center,” meaning that u is the unique node intersecting the ℓ -clique and the adjacent edge.

where $K_{\ell+1}(u)$ is the set of $(\ell + 1)$ -cliques containing u , $W_\ell(u)$ is the set of ℓ -wedges with center u , and the coefficient $\binom{\ell}{\ell-1}$ comes from the fact that each $(\ell + 1)$ -clique containing u closes that many ℓ -wedges in $W_\ell(u)$.

The ℓ th-order clustering coefficient of a node is defined for any node that is the center of at least one ℓ -wedge, and the average ℓ th-order clustering coefficient is the mean of the local clustering coefficients:

$$(3.6) \quad \bar{C}_\ell = \frac{1}{|\tilde{V}_\ell|} \sum_{u \in \tilde{V}_\ell} C_\ell(u),$$

where \tilde{V}_ℓ is the set of nodes that are the centers of at least one ℓ -wedge.

We have considered the average (higher-order) clustering coefficient to be the mean over only nodes at the center of at least one ℓ -wedge. This makes some of the theoretical analysis easier. We could also consider the clustering at node u to be 0 if u does not participate in any ℓ -wedge. There is not a consensus definition in the literature, and this issue is usually not even discussed (see Kaiser [2008] for a discussion on how this seemingly small difference in definition can affect

network analyses). At the very least, we should report what fraction of nodes in the network participate in at least one ℓ -wedge. We do this in our experiments later and also report the value of \bar{C}_ℓ for both definitions.

3.3 Theoretical Analysis

3.3.1 A method to compute higher-order clustering coefficients

We first discuss how to compute higher-order clustering coefficients. Substituting the identity

$$(3.7) \quad |W_\ell(u)| = |K_\ell(u)| \cdot (d_u - \ell + 1),$$

into Equation (3.5) gives

$$(3.8) \quad C_\ell(u) = \frac{\ell \cdot |K_{\ell+1}(u)|}{(d_u - \ell + 1) \cdot |K_\ell(u)|}.$$

From Equation (3.8), it is easy to see that we can compute all local ℓ th-order clustering coefficients, by enumerating all $(\ell + 1)$ -cliques and ℓ -cliques in the graph. The computational complexity of the algorithm is thus bounded by the time to enumerate $(\ell + 1)$ -cliques and ℓ -cliques. Using the Chiba and Nishizeki algorithm (discussed in Section 2.2.9), the complexity is $O(\ell a^{\ell-2} m)$, where a is the arboricity of the graph, and m is the number of edges. We note that the arboricity a may be as large as \sqrt{m} , so this algorithm is only guaranteed to take polynomial time if ℓ is a constant. In general, determining if there exists a single clique with at least ℓ nodes is NP-complete [Karp, 1972].

For the global clustering coefficient, note that

$$(3.9) \quad |W_\ell| = \sum_{u \in V} |W_\ell(u)|.$$

Thus, it suffices to enumerate ℓ -cliques (to compute $|W_\ell|$ through Equation (3.7)) and to count the total number of ℓ -cliques. In practice, we use the Chiba and Nishizeki to enumerate cliques and simultaneously compute C_ℓ and $C_\ell(u)$ for all nodes u .

3.3.2 Probabilistic interpretations

To facilitate understanding of higher-order clustering coefficients, we now present two probabilistic interpretations of the measurements. First, we can interpret $C_\ell(u)$

as the probability that a wedge w chosen uniformly at random from all wedges centered at u is closed:

$$(3.10) \quad C_\ell(u) = \mathbb{P}[w \in K_{\ell+1}(u)].$$

We will use this interpretation in Section 3.5 when relating higher-order clustering coefficients to motif conductance.

For the next interpretation, it is useful to analyze the structure of the 1-hop neighborhood graph N_u of a given node u (not containing node u) in a graph $G = (V, E)$, $u \in V$. The vertex set of N_u is the set of all nodes adjacent to u , and the edge set consists of all edges between neighbors of u , i.e., $\{(v, w) \mid (u, v), (u, w), (v, w) \in E\}$.

Any ℓ -clique in G containing node u corresponds to a unique $(\ell - 1)$ -clique in N_u , and specifically for $\ell = 2$, any edge (u, v) corresponds to a node v in N_u . Therefore, each ℓ -wedge centered at u corresponds to an $(\ell - 1)$ -clique K and one of the $d_u - \ell + 1$ nodes outside K (i.e., in $N_u \setminus K$). Thus, Equation (3.8) can be re-written as

$$(3.11) \quad \frac{\ell \cdot |K_\ell(N_u)|}{(d_u - \ell + 1) \cdot |K_{\ell-1}(N_u)|}.$$

If we uniformly at random select an $(\ell - 1)$ -clique K from N_u and then also uniformly at random select a node v from N_u outside of this clique, then $C_\ell(u)$ is the probability that these ℓ nodes form an ℓ -clique:

$$(3.12) \quad C_\ell(u) = \mathbb{P}[K \cup \{v\} \in K_\ell(N_u)].$$

Moreover, if we condition on observing an ℓ -clique from this sampling procedure, then the ℓ -clique itself is selected uniformly at random from all ℓ -cliques in N_u . Therefore, $C_{\ell-1}(u) \cdot C_\ell(u)$ is the probability that an $(\ell - 1)$ -clique and two nodes selected uniformly at random from N_u form an $(\ell + 1)$ -clique. Applying this recursively gives

$$(3.13) \quad \prod_{j=2}^{\ell} C_j(u) = \frac{|K_\ell(N_u)|}{\binom{d_u}{\ell}}.$$

In other words, the product of the higher-order local clustering coefficients of node u up to order ℓ is the ℓ -clique density amongst u 's neighbors.

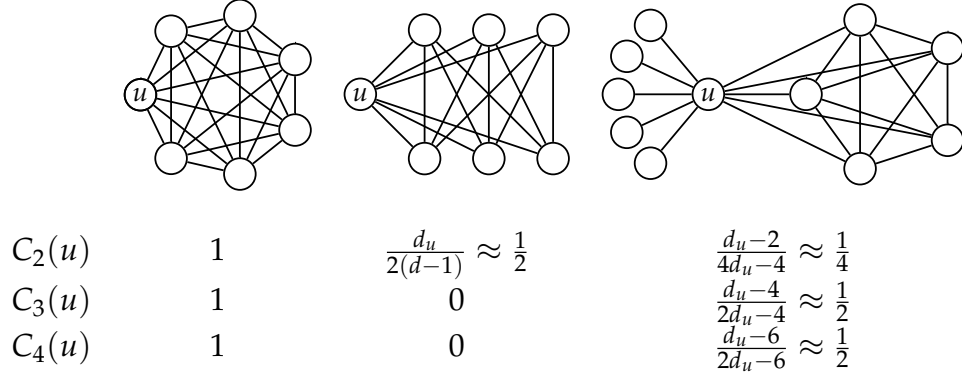


Figure 3.2 – Families of 1-hop neighborhoods of a node u with degree d_u . These families illustrate the difference between higher-order clustering coefficients of different orders. Left: For cliques, $C_\ell(u) = 1$ for all ℓ . Middle: If node u 's neighbors form a complete bipartite graph, then $C_2(u)$ is constant while $C_\ell(u) = 0$ for $\ell \geq 3$. Right: If half of node u 's neighbors form a star and the other half form a clique with u , then $C_\ell(u) = \sqrt{C_2(u)}$, reaching the upper bound of Equation (3.14).

3.3.3 Bounds on higher-order clustering coefficients

Next we analyze relationships between local higher-order clustering coefficients of different orders. Our technical result is Proposition 13, which provides tight lower and upper bounds for higher-order local clustering coefficients in terms of the traditional local clustering coefficient. The main ideas of the proof are illustrated in Figure 3.2.

Proposition 13. For any fixed $\ell \geq 3$,

$$(3.14) \quad 0 \leq C_\ell(u) \leq \sqrt{C_2(u)}.$$

Moreover,

- i. There exists a finite graph G with node u such that the lower bound is tight for any prescribed value of $C_2(u) \in [0, 1]$.
- ii. There exists a sequence of growing graphs $\{G_i\}_{i=1}^\infty$, each with node u , such that the upper bound is tight in the limit for any prescribed limiting value of $C_2(u) \in [0, 1]$.

Proof. Clearly, $0 \leq C_\ell(u)$ if the local clustering coefficient is well defined. This bound is tight, even if $C_2(u)$ is constant, when N_u is $(\ell - 1)$ -partite (see Figure 3.2, middle).

To derive the upper bound, consider the 1-hop neighborhood N_u , and let $\delta_\ell(N_u) = |K_\ell(N_u)| / \binom{d_u}{\ell}$ denote the ℓ -clique density of N_u . The Kruskal-Katona

theorem [Katz, 1966; Kruskal, 1963] implies that $\delta_\ell(N_u) \leq [\delta_{\ell-1}(N_u)]^{\frac{\ell}{\ell-1}}$ and $\delta_{\ell-1}(N_u) \leq [\delta_2(N_u)]^{\frac{\ell-1}{2}}$. Combining this with Equation (3.8) gives

$$(3.15) \quad C_\ell(u) \leq [\delta_{\ell-1}(N_u)]^{\frac{1}{\ell-1}} \leq \sqrt{\delta_2(N_u)} = \sqrt{C_2(u)},$$

where the last equality uses the fact that $C_2(u)$ is the edge density of N_u .

The upper bound is tight if N_u consists of a clique and isolated nodes (Figure 3.2, right) and we take $d_u \rightarrow \infty$. Specifically, let N_u consist of a clique of size c and b isolated nodes. When $\ell = 2$,

$$C_\ell(u) = \frac{\binom{c}{2}}{\binom{c+b}{2}} = \frac{(c-1)c}{(b+c-1)(b+c)} \rightarrow \left(\frac{c}{c+b}\right)^2$$

and by Equation (3.11), when $3 \leq \ell \leq c$,

$$C_\ell(u) = \frac{\ell \cdot \binom{c}{\ell}}{(c+b-\ell+1) \cdot \binom{c}{\ell-1}} = \frac{c-\ell+1}{c+b-\ell+1} \rightarrow \frac{c}{c+b}$$

By adjusting the ratio $c/(b+c)$ in N_u , we can construct a family of graphs such that $C_2(u)$ may take any value in $[0, 1]$ as $d_u \rightarrow \infty$ and $C_\ell(u) = \sqrt{C_2(u)}$ as $d_u \rightarrow \infty$. \square

Again, we have an asymptotic result. However, in Section 3.4, we will see that in some real-world data, there are nodes u for which $C_3(u)$ is close to $\sqrt{C_2(u)}$.

3.3.4 Analysis for the $G_{n,p}$ model

Next, we analyze higher-order clustering coefficients in the classical Erdős-Rényi model with edge probability p , i.e., the $G_{n,p}$ model [Erdős and Rényi, 1959]. We implicitly assume that ℓ is small in the following analysis so that there should be at least one ℓ -wedge in the graph (with high probability and n large, there is no clique of size greater than $(2 + \epsilon) \log n / \log(1/p)$ for any $\epsilon > 0$ [Bollobás and Erdős, 1976]). Our results are summarized in the following proposition.

Proposition 14. *Let G be a random graph drawn from the $G_{n,p}$ model.*

- i. $\mathbb{E}_G [C_\ell] = p^{\ell-1}$,
- ii. $\mathbb{E}_G [C_\ell(u) \mid W_\ell(u) > 0] = p^{\ell-1}$ for any node u ,
- iii. $\mathbb{E}_G [\bar{C}_\ell] = p^{\ell-1}$, and

iv. For constant ℓ ,

$$\mathbb{E}_G [C_\ell(u) \mid C_2(u), W_\ell(u) > 0] = \left[C_2(u) - (1 - C_2(u)) \cdot O(1/d_u^2) \right]^{\ell-1} \approx (C_2(u))^{\ell-1}.$$

Proof. For Item i:

$$\begin{aligned} \mathbb{E} [C_\ell] &= \mathbb{E}_G \left[\mathbb{E}_{W_\ell} [C_\ell \mid W_\ell] \right] \\ &= \mathbb{E}_G \left[\mathbb{E}_{W_\ell} \left[\frac{1}{|W_\ell|} \sum_{w \in W_\ell} \mathbb{P} [w \text{ is closed}] \right] \right] \\ &= \mathbb{E}_G \left[\mathbb{E}_{W_\ell} \left[\frac{1}{|W_\ell|} \sum_{w \in W_\ell} p^{\ell-1} \right] \right] \\ &= \mathbb{E}_G [p^{\ell-1}] \\ &= p^{\ell-1}. \end{aligned}$$

The second equality is well defined (with high probability) for small ℓ . The third equality comes from the fact that any ℓ -wedge is closed if and only if the $\ell - 1$ possible edges between the ℓ -clique and the outside node in the adjacent edge exist to form an $(\ell + 1)$ -clique.

The proof of Item ii is similar.

$$\begin{aligned} \mathbb{E} [C_\ell(u) \mid W_\ell(u) > 0] &= \mathbb{E}_G \left[\mathbb{E}_{W_\ell(u) > 0} [C_\ell(u) \mid W_\ell(u)] \right] \\ &= \mathbb{E}_G \left[\mathbb{E}_{W_\ell(u) > 0} \left[\frac{1}{|W_\ell(u)|} \sum_{w \in W_\ell(u)} \mathbb{P} [w \text{ is closed}] \right] \right] \\ &= \mathbb{E}_G \left[\mathbb{E}_{W_\ell(u) > 0} \left[\frac{1}{|W_\ell(u)|} \sum_{w \in W_\ell(u)} p^{\ell-1} \right] \right] \\ &= \mathbb{E}_G [p^{\ell-1}] \\ &= p^{\ell-1}. \end{aligned}$$

For Item [iii](#):

$$\begin{aligned}
\mathbb{E}_G [\bar{C}_\ell] &= \mathbb{E}_G \left[\mathbb{E}_{\tilde{V}} \left[\bar{C}_\ell \mid \tilde{V} \right] \right] \\
&= \mathbb{E}_G \left[\mathbb{E}_{\tilde{V}} \left[\frac{1}{|\tilde{V}|} \sum_{u \in \tilde{V}} \mathbb{E} [C_\ell(u)] \right] \right] \\
&= \mathbb{E}_G \left[\mathbb{E}_{\tilde{V}} \left[\frac{1}{|\tilde{V}|} \sum_{u \in \tilde{V}} p^{\ell-1} \right] \right] \\
&= \mathbb{E}_G \left[p^{\ell-1} \right] \\
&= p^{\ell-1}.
\end{aligned}$$

In the second line, \tilde{V} is nonempty with high probability for ℓ small, so $1/|\tilde{V}|$ is well defined. The third equality comes from Item [ii](#).

For Item [iv](#), first consider

$$\begin{aligned}
&\mathbb{E}_G [C_\ell(u) \mid C_2(u), W_\ell(u) > 0] \\
&= \mathbb{E}_G \left[\mathbb{E}_{W_\ell(u) > 0} [C_\ell(u) \mid C_2(u), W_\ell(u)] \right] \\
&= \mathbb{E}_G \left[\mathbb{E}_{W_\ell(u) > 0} \left[\frac{1}{|W_\ell(u)|} \sum_{w \in W_\ell(u)} \mathbb{P} [w \text{ is closed} \mid C_2(u)] \right] \right].
\end{aligned}$$

Now, note that N_u has $m = C_2(u) \cdot \binom{d_u}{2}$ edges. Knowing that $w \in W_\ell(u)$ accounts for $\binom{\ell-1}{2}$ of these edges. By symmetry, the other $q = m - \binom{\ell-1}{2}$ edges appear in any of the remaining $r = \binom{d_u}{2} - \binom{\ell-1}{2}$ edges uniformly at random. There are $\binom{r}{q}$ ways to place these edges, of which $\binom{r-\ell+1}{q-\ell+1}$ would close the wedge w . Thus,

$$(3.16) \quad \mathbb{P} [w \text{ is closed} \mid C_2(u)] = \frac{\binom{r-\ell+1}{q-\ell+1}}{\binom{r}{q}}$$

$$(3.17) \quad = \frac{(r-\ell+1)!q!}{(q-\ell+1)!r!}$$

$$(3.18) \quad = \frac{(q-\ell+2)(q-\ell+3) \cdots q}{(r-\ell+2)(r-\ell+3) \cdots r}$$

Now, for any small nonnegative integer k ,

$$\begin{aligned} \frac{q - k}{r - k} &= \frac{C_2(u) \cdot \binom{d_u}{2} - \binom{\ell-1}{2} - k}{\binom{d_u}{2} - \binom{\ell-1}{2} - k} \\ &= C_2(u) - (1 - C_2(u)) \left[\frac{\binom{\ell-1}{2} + k}{\binom{d_u}{2} - \binom{\ell-1}{2} - k} \right] \\ &= C_2(u) - (1 - C_2(u)) \cdot O(1/d_u^2) \end{aligned}$$

We are able to use the big-O notation because ℓ is a constant by assumption. Thus, the expression in Equation (3.18) approaches $(C_2(u))^{\ell-1}$ as $C_2(u) \rightarrow 1$ and as $d_u \rightarrow \infty$. \square

Item iv of Proposition 14 says that even if the second-order local clustering coefficient is large, the ℓ th-order clustering coefficient will still decay exponentially in ℓ , at least in the limit as d_u grows. We will use this as a reference point in our analysis of real-world networks in Section 3.4.

3.3.5 Analysis for the small-world model

We also study higher-order clustering in the small-world random graph model [Watts and Strogatz, 1998]. The model begins with a ring network where each node connects to its $2k$ nearest neighbors. Then, for each node u and each of the k edges (u, v) with v following u “clockwise” in the ring, the edge is “rewired” to (u, w) with probability p , where w is chosen uniformly at random.²

With no rewiring ($p = 0$) and $k \ll n$, $\bar{C}_2 \approx 3/4$ [Watts and Strogatz, 1998]. As p increases, the average clustering coefficient \bar{C}_2 slightly decreases until a phase transition near $p = 0.1$, where \bar{C}_2 decays to 0 [Watts and Strogatz, 1998] (also see Figure 3.3). We generalize these results for higher-order clustering coefficients. Specifically, when $p = 0$, we can analytically show that

$$(3.19) \quad \bar{C}_\ell \approx (\ell + 1)/(2\ell)$$

for any $\ell \geq 2$. Thus, \bar{C}_ℓ decreases as ℓ increases. Furthermore, via simulation, we observe the same behavior as for \bar{C}_2 when adjusting the rewiring probability p (Figure 3.3). Regardless of ℓ , the phase transition happens near $p = 0.1$ and this is partly due to the fact that $C_\ell(u) \rightarrow 0$ as $C_2(u) \rightarrow 0$ (Proposition 13).

²Bret Victor has a wonderful visual explanation of the small-world model at <http://worrydream.com/ScientificCommunicationAsSequentialArt/>.

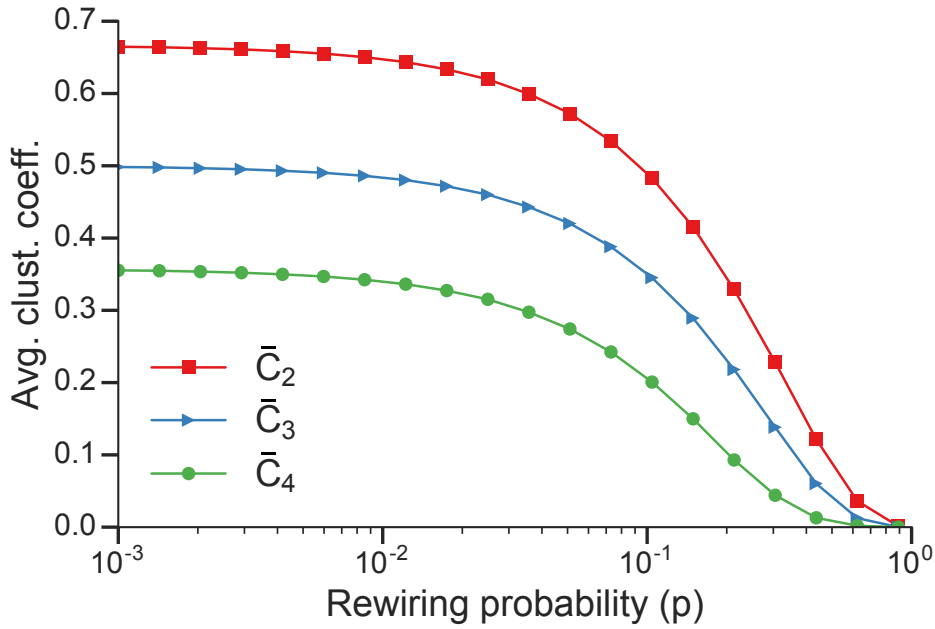


Figure 3.3 – Higher-order clustering in the small-world model. The plot shows the average higher-order clustering coefficient \bar{C}_ℓ as a function of rewiring probability p in small-world networks for $\ell = 2, 3, 4$. Each data point is the average over 20 small-world random graph instances with 20,000 nodes where each node connects to its 10 nearest neighbors before rewiring.

The following proposition gives an argument for Equation (3.19). We will not be precise in the proof.

Proposition 15. *In the small world model with no rewiring ($p = 0$) and $2k < n$, for any node u , $C_\ell(u) \approx \frac{\ell+1}{2^\ell}$ for large k .*

Proof. To derive Equation (3.19), we first label the $2k$ neighbors of u as $1, 2, \dots, 2k$ by their clockwise ordering in the ring. Since $2k < n$, these nodes are unique. Next, define the *span* of any ℓ -clique containing u as the difference between the largest and smallest label of the $\ell - 1$ nodes in the clique other than u . The span s of any ℓ -clique satisfies $s \leq k - 1$ since any node is directly connected with a node of label difference no greater than $k - 1$. Also, $s \geq \ell - 2$ since there are $\ell - 1$ nodes in an ℓ -clique other than u . For each span s , we can find $2k - 1 - s$ pairs of (i, j) such that $1 \leq i, j \leq 2k$ and $j - i = s$. Finally, for every such pair (i, j) , there are $\binom{s-1}{\ell-3}$ choices of $\ell - 3$ nodes between i and j which will form an ℓ -clique together

with nodes u , i , and j . Therefore,

$$\begin{aligned}
|K_\ell(u)| &= \sum_{s=\ell-2}^{k-1} (2k-1-s) \cdot \binom{s-1}{\ell-3} \\
&= \sum_{s=\ell-2}^{k-1} (2k-1-s) \cdot \frac{(s-1)(s-2)\cdots(s-\ell+3)}{(\ell-3)!} \\
&= \sum_{t=1}^{k-\ell+2} (2k+2-t-\ell) \cdot \frac{t(t+1)\cdots(t+\ell-4)}{(\ell-3)!} \\
&\approx \sum_{t=1}^k \frac{(2k-t)t^{\ell-3}}{(\ell-3)!} \quad (\text{ignoring lower-order terms of } t) \\
&= \frac{1}{(\ell-3)!} \sum_{t=1}^k 2kt^{\ell-3} - t^{\ell-2} \\
&= \frac{1}{(\ell-3)!} \left[2k \cdot \left(\frac{k^{\ell-2}}{\ell-2} + O(k^{\ell-3}) \right) - \frac{k^{\ell-1}}{\ell-1} + O(k^{\ell-2}) \right] \\
&= \frac{1}{(\ell-3)!} \left[\frac{2k^{\ell-1}}{\ell-2} - \frac{k^{\ell-1}}{\ell-1} \right] \quad (\text{ignoring lower-order terms of } k) \\
&= \frac{k^{\ell-1}}{(\ell-3)!} \left[\frac{2}{\ell-2} - \frac{1}{\ell-1} \right] \\
&= \frac{\ell k^{\ell-1}}{(\ell-1)!}
\end{aligned}$$

Then, following Equation (3.8),

$$\begin{aligned}
C_\ell(u) &= \frac{\ell \cdot |K_{\ell+1}(u)|}{(d_u - \ell + 1) \cdot |K_\ell(u)|} \\
&\approx \frac{\ell \cdot \frac{(\ell+1)k^\ell}{\ell!}}{(2k - \ell + 1) \cdot \frac{\ell k^{\ell-1}}{(\ell-1)!}} \\
&= \frac{(\ell+1)k}{(2k - \ell + 1) \cdot \ell} \rightarrow \frac{\ell+1}{2\ell} \text{ as } k \rightarrow \infty.
\end{aligned}$$

□

Proposition 15 is an imprecise and asymptotic result, but Figure 3.3 at least captures the trend that the clustering decreases with ℓ .

3.4 Empirical Analysis

We now measure and analyze higher-order clustering in five networks:

- i. an Erdős-Rényi graph with $n = 1,000$ nodes and edge probability $p = 0.2$;
- ii. a small-world network with $n = 20,000$ nodes, $k = 10$ edges per node, and rewiring probability $p = 0.1$;
- iii. the neural network of the nematode worm *C. elegans* [Watts and Strogatz, 1998], where we take the edges in this network to be undirected;
- iv. the friendships between Stanford students on Facebook from September 2005 [Traud et al., 2012] (denoted FB-STANFORD3); and
- v. a co-authorship network constructed from papers posted to the Astrophysics category on arXiv [Leskovec et al., 2007b] (denoted CA-ASTROPH).

Table 3.1 lists the higher-order clustering coefficients for $\ell = 2, 3$, and 4. Proposition 14 and Figure 3.3 say that the average clustering coefficient should decrease as the order increases for the Erdős-Rényi and small-world models, and indeed, this is the case. We see that $\bar{C}_4 < \bar{C}_3 < \bar{C}_2$ also holds for the three real-world networks. (This does not necessarily have to hold—the right column of Figure 3.2 shows an example where $\bar{C}_3 > \bar{C}_2$.) Thus, when averaging over nodes, higher-order cliques are less likely to close in both the synthetic and real-world networks. However, the same trends do not hold for the higher-order global clustering coefficient, which can decrease with ℓ (*C. elegans*), increase with ℓ (CA-ASTROPH), or non-monotonic with ℓ (FB-STANFORD3).

For the three real-world networks, we also measure the higher-order clustering coefficients with respect to two null models (Table 3.1). First, we use the Configuration Model (CM) that samples uniformly at random from simple graphs with the same degree distribution [Bollobás, 1980; Milo et al., 2003]. In the real-world networks, \bar{C}_2 is much larger than expected with respect to the CM null model (Table 3.1); this behavior was observed by Watts and Strogatz [Watts and Strogatz, 1998]. Unsurprisingly, we find that the same result holds for \bar{C}_3 and \bar{C}_4 .

Second, we use a null model that samples graphs that preserve both the degree distribution and \bar{C}_2 . Specifically, these are samples from an ensemble of exponential graphs where the Hamiltonian measures the absolute value of the difference in \bar{C}_2 between the original network and the sampled network [Park and Newman, 2004]. Such samples are referred to as Maximally Random Clustered Networks (MRCN) and are sampled with a simulated annealing procedure [Colomer-de Simón et al., 2013]. Comparing \bar{C}_3 between the real-world and the null network, we observe different behavior in higher-order clustering. The *C. elegans* neural network has less than expected higher-order clustering in terms of \bar{C}_3 with respect to the MRCN null model (Table 3.1). On the other hand, the Facebook friendship and co-authorship networks exhibit higher than expected \bar{C}_3 (although only slightly

higher for CA-ASTROPH). Thus, while all three of the real-world networks exhibit clustering in the classical sense of triadic closure, only the friendship and (and to some extent) the co-authorship networks exhibit higher-order clustering.

The lack of higher-order clustering in the *C. elegans* network³ agrees with previous results that 4-cliques are under-expressed in parts of *C. elegans*, while open 3-wedges related with cooperative information propagation are over-expressed [Benson et al., 2016; Milo et al., 2002; Varshney et al., 2011]. This also provides credence for the “3-layer” model of *C. elegans* [Varshney et al., 2011]. The observed clustering in the friendship network is consistent with prior work showing the relative infrequency of open ℓ -wedges in many Facebook network subgraphs with respect to a null model accounting for triadic closure [Ugander et al., 2013]. Co-authorship networks are known to have large clustering in the traditional sense, which is partially attributed to papers with multiple authors that form cliques [Newman, 2001]. It is natural that these cliques contribute to higher-order clustering as well.

³Here, we mean the lack of clustering with respect to the higher-order clustering coefficient defined in this chapter. In Chapter 2, we found a meaningful *higher-order cluster* in *C. elegans* in terms of the bi-fan motif. These results are compatible and exemplify the different dimensions of higher-order network analysis in this thesis.

E-R	S-W	<i>C. elegans</i>			FB-STANFORD3			CA-ASTROPH			
		orig.	CM	MRCN	orig.	CM	MRCN	orig.	CM	MRCN	
$ V $	1K	20K	297	297	297	11.6K	11.6K	11.6K	18.8K	18.8K	18.8K
$ E $	99.8K	100K	2.15K	2.15K	2.15K	568K	568K	568K	198K	198K	198K
\bar{C}_2	0.20	0.49	0.31	0.15 [0.13, 0.16]	0.31 [0.31, 0.31]	0.25	0.03 [0.03, 0.03]	0.25 [0.25, 0.25]	0.68	0.01 [0.01, 0.01]	0.68 [0.68, 0.68]
\bar{C}_3	0.04	0.35	0.14	0.04 [0.02, 0.05]	0.17 [0.15, 0.17]	0.18	0.00 [0.00, 0.00]	0.14 [0.14, 0.14]	0.61	0.00 [0.00, 0.00]	0.60 [0.60, 0.60]
\bar{C}_4	0.01	0.20	0.06	0.01 [0.00, 0.01]	0.09 [0.07, 0.11]	0.16	0.00 [0.00, 0.00]	0.09 [0.09, 0.09]	0.56	0.00 [0.00, 0.00]	0.52 [0.52, 0.53]
$\frac{ V_2 }{ V }$	1.00	1.00	0.95	0.95 [0.95, 0.95]	0.95 [0.95, 0.95]	0.95	0.95 [0.95, 0.95]	0.95 [0.95, 0.95]	0.93	0.93 [0.93, 0.93]	0.93 [0.93, 0.93]
$\frac{ V_3 }{ V }$	1.00	1.00	0.93	0.89 [0.86, 0.91]	0.94 [0.93, 0.94]	0.92	0.85 [0.85, 0.86]	0.93 [0.93, 0.93]	0.84	0.46 [0.45, 0.46]	0.84 [0.84, 0.84]
$\frac{ V_4 }{ V }$	1.00	1.00	0.81	0.54 [0.48, 0.60]	0.83 [0.79, 0.87]	0.88	0.63 [0.63, 0.64]	0.91 [0.91, 0.91]	0.74	0.04 [0.03, 0.04]	0.75 [0.75, 0.75]
\bar{C}'_2	0.20	0.49	0.29	0.14 [0.13, 0.15]	0.29 [0.29, 0.29]	0.24	0.03 [0.03, 0.03]	0.24 [0.24, 0.24]	0.63	0.01 [0.01, 0.01]	0.63 [0.63, 0.63]
\bar{C}'_3	0.04	0.35	0.13	0.03 [0.02, 0.04]	0.16 [0.14, 0.16]	0.17	0.00 [0.00, 0.00]	0.13 [0.13, 0.13]	0.51	0.00 [0.00, 0.00]	0.50 [0.50, 0.50]
\bar{C}'_4	0.01	0.20	0.05	0.00 [0.00, 0.01]	0.08 [0.06, 0.09]	0.14	0.00 [0.00, 0.00]	0.08 [0.08, 0.08]	0.42	0.00 [0.00, 0.00]	0.40 [0.39, 0.40]
C_2	0.20	0.48	0.18	0.10 [0.10, 0.11]	0.14 [0.14, 0.15]	0.16	0.03 [0.03, 0.03]	0.05 [0.05, 0.05]	0.32	0.01 [0.01, 0.01]	0.14 [0.13, 0.14]
C_3	0.04	0.36	0.08	0.02 [0.02, 0.03]	0.04 [0.04, 0.05]	0.11	0.00 [0.00, 0.00]	0.02 [0.02, 0.02]	0.33	0.00 [0.00, 0.00]	0.10 [0.10, 0.10]
C_4	0.01	0.23	0.06	0.01 [0.00, 0.01]	0.02 [0.01, 0.03]	0.12	0.00 [0.00, 0.00]	0.02 [0.02, 0.02]	0.36	0.00 [0.00, 0.00]	0.09 [0.09, 0.09]

Table 3.1 – Higher-order clustering coefficients for several networks. We measure higher-order clustering in the Erdős-Rényi (E-R) and small-world (S-W) random graph models as well as three real-world networks. For the real-world networks, we also measure the clustering coefficients with respect to two null models: a Configuration Model (CM) that produces random graphs with the same degree distribution as in the real graph [Bollobás, 1980; Milo et al., 2003] and Maximally Random Clustered Networks (MRCN) that preserve the degree distribution as well as \bar{C}_2 [Colomer-de Simón et al., 2013; Park and Newman, 2004]. For the random networks, we report the sample mean and the minimum and maximum values (in brackets) over 100 samples. Under a CM null model, there is more clustering than expected for all orders of the clustering coefficient. Under the MRCN null model, the *C. elegans* neural network does not exhibit higher-order clustering, while FB-STANFORD3 and CA-ASTROPH do exhibit higher-order clustering (although CA-ASTROPH has only slightly larger higher-order clustering than expected under the null model). We measure the higher-order average clustering coefficient (\bar{C}_ℓ), the fraction of nodes that are the center of at least one ℓ -wedge ($|\tilde{V}_\ell|/|V|$), the alternative higher-order average clustering coefficient that considers the clustering of a node not at the center of at least one ℓ -wedge to be 0, and the higher-order global clustering coefficient (C_ℓ).

Figure 3.4 plots the joint distribution of $C_2(u)$ and $C_3(u)$. The lower trend line represents random behavior (i.e., the asymptotic behavior of Erdős-Rényi networks in expectation; see Proposition 14) and the upper trend line denotes the maximum possible value of $C_3(u)$ given $C_2(u)$ (Equation (3.14)). For many nodes in the *C. elegans* network, local clustering is nearly random, resembling the Erdős-Rényi joint distribution. This provides further evidence that the *C. elegans* neural network lacks higher-order clustering. In the co-authorship network, there are many nodes u with a large value of $C_2(u)$ that have an even larger value of $C_3(u)$ near the upper bound of Equation (3.14) (see the inset). Thus, our upper bound is nearly tight in practice. We emphasize that this does not imply that these nodes are simply members of large cliques—if the 1-hop neighborhood of u is a clique, then $C_2(u) = C_3(u) = 1$. Instead, some nodes likely appear in both cliques and as the center of star-like patterns, as in Figure 3.2 (right). This pattern would appear, for example, with an advisor writing several 2-author papers with students and a multi-author paper with other collaborators.

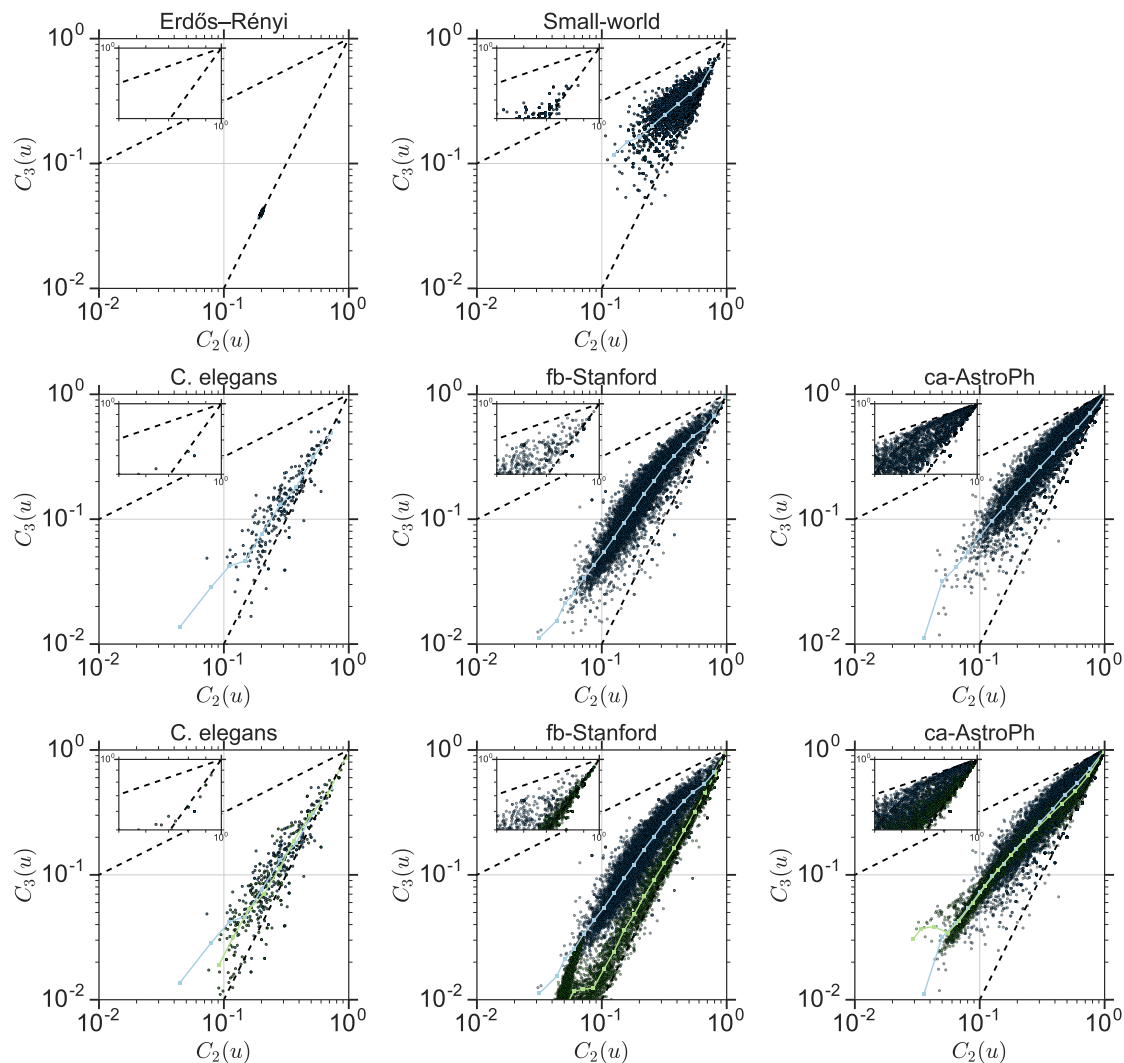


Figure 3.4 – Joint distributions of $(C_2(u), C_3(u))$. Each blue dot corresponds to a node in the original network, and the light blue curve tracks the average over logarithmic bins. The upper trend line is the upper bound in Equation (3.14), and the lower trend line follows the Erdős-Rényi model where edges appear randomly (Proposition 14). The inset enlarges the portion of the plot where $C_2(u)$ and $C_3(u)$ are greater than 0.5. In the bottom row, each green dot corresponds to a node in one of the MRCN random samples, and the light green line tracks the average over logarithmic bins.

We also compute the higher-order clustering coefficient as a function of node degree (Figure 3.5). In the Erdős-Rényi, small-world, and *C. elegans* networks, there is a distinct gap between the average higher-order clustering coefficients for nodes of all degrees. Thus, the observed decrease in clustering as the order increases is independent of degree. In the Facebook friendship network, $C_2(u)$ is larger than $C_3(u)$ and $C_4(u)$ on average for nodes of all degrees, but $C_3(u)$ and $C_4(u)$ are roughly the same for nodes of all degrees, which means that 4-cliques and 5-cliques close at roughly the same rate, independent of degree, albeit at a smaller rate than traditional triadic closure. In the co-authorship network, nodes u have roughly the same $C_\ell(u)$ for $\ell = 2, 3, 4$, which means that ℓ -cliques close at about the same rate, independent of ℓ . We note that the global clustering coefficient C_ℓ slightly increases with ℓ in this network (Table 3.1), which probably means there are nodes participating in a *large* clique and also serving as the center of a star-like pattern (Figure 3.2, right), which causes the global clustering coefficient to increase with the order.

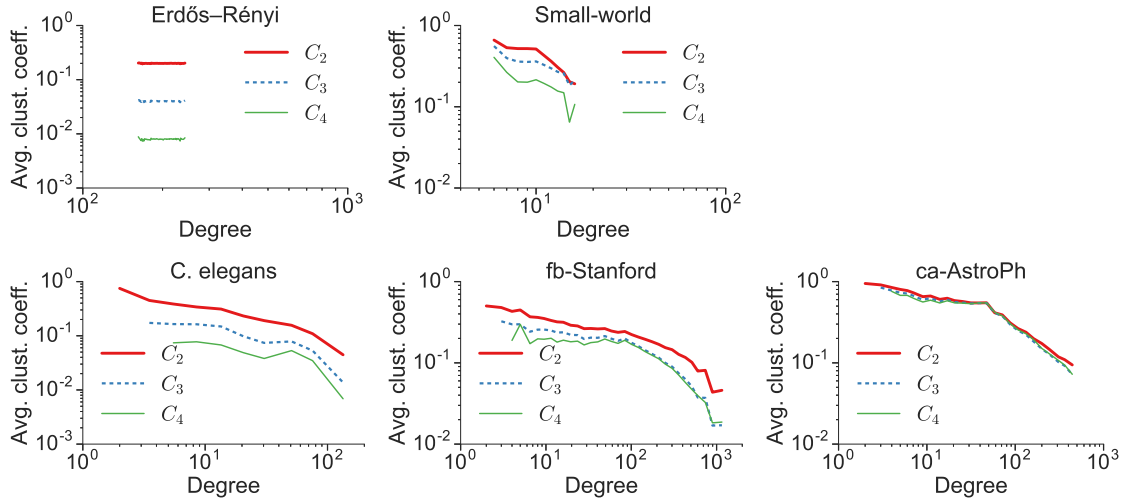


Figure 3.5 – Average higher-order clustering coefficients as a function of degree.

3.5 Relating higher-order clustering coefficients to motif conductance through 1-hop neighborhoods

In this section, we relate our higher-order clustering coefficients to motif conductance, which was introduced in Chapter 2 as a measure of how good of a cluster a subset of nodes is, in terms of some motif. Here we will look at motif conductance for clique motifs. Our main technical result (Theorem 16) says that if a graph has a large ℓ th-order global clustering coefficient, then there is a node whose 1-hop neighborhood has small motif conductance for the ℓ -clique motif. This is a generalization of similar results from Gleich and Seshadhri [2012] for edge conductance. In fact, these generalizations are what led to us to our definitions for higher-order clustering coefficients.

3.5.1 A formal relationship between 1-hop neighborhoods and motif conductance

We first state our main technical result of this section, which says that if the network exhibits higher-order clustering, i.e., C_ℓ is large, then there is a 1-hop neighborhood with small ℓ -clique conductance. For notation, let N'_u denote the nodes in the 1-hop neighborhood graph of node u (including u):

$$(3.20) \quad N'_u = \{v \in V \mid (u, v) \in E\} \cup \{u\}.$$

Above, we used the notation N_u to denote the graph induced by the neighborhoods of u . Here, N'_u includes node u and represents a set of vertices— u and its neighbors. Also, let K_ℓ denote the ℓ -clique motif.

Theorem 16. *Let $G = (V, E)$ with global ℓ th-order clustering coefficient C_ℓ . Suppose that $\text{vol}_{K_\ell}(N'_u) \leq \text{vol}_{K_\ell}(V)/2$ for each node u . Then there exists a node u such that*

$$(3.21) \quad \phi_{K_\ell}(N'_u) \leq \frac{1 - C_\ell}{1 - C_\ell + [C_\ell / (1 + \sqrt{1 - C_\ell})]^2}$$

$$(3.22) \quad \leq \min\{2(1 - C_\ell), 1\}.$$

The bound in Equation (3.21) is monotonically decreasing, approaches 0 as C_ℓ approaches 1, and is bounded above by 1. The result is a generalization of a similar statement for edge conductance by [Gleich and Seshadhri \[2012\]](#), but prior results contain only the case of $\ell = 2$, and only use the weaker bound of Equation (3.22).

We now prove this result via several technical results relating higher-order clustering coefficients and motif conductance, where the motif is a clique. We note that many of the results are generalizations of previous theory developed by [Gleich and Seshadhri \[2012\]](#).

First, we show the extreme-case result that when $C_\ell = 1$, each connected component of the graph is a clique.

Proposition 17. *If a graph has global high-order clustering coefficient $C_\ell = 1$, then each connected component of this graph is either complete or ℓ -clique free.*

Proof. We prove this by contradiction. Suppose a connected component contains an ℓ -clique and that the maximum clique of this connected component is of size $j \geq \ell$. If this connected component is not a complete graph, there must be a node connecting to the maximum clique but not forming a bigger clique, giving an open ℓ -wedge. \square

Corollary 18. *If $C_\ell = 1$ and there are two ℓ -cliques, then there exists a node u with $\phi_{K_\ell}(N'_u) = 0$.*

Corollary 18 provides some intuition for the main idea. If there is perfect clustering, then there is a perfect cut. Theorem 16 is a relaxation of this observation. We now prove a series of technical lemmas that will be used to prove Theorem 16. To begin, the following lemma relates the higher-order clustering coefficient with neighborhood cuts.

Lemma 19. *The sum of the clique-motif cuts of all 1-hop neighborhoods is bounded above by a $(1 - C_\ell)$ fraction of the total ℓ -wedges:*

$$(3.23) \quad \sum_{v \in V} \text{cut}_{K_\ell}(N'_v) \leq (1 - C_\ell) \cdot |W_\ell|.$$

Proof. If an ℓ -clique (u_1, \dots, u_ℓ) gets cut by the partition induced by N'_v , then v must directly connect with one of u_1, \dots, u_ℓ , say u_1 . Note that the clique (u_1, \dots, u_ℓ) and adjacent edge (u_1, v) form an open $(\ell + 1)$ -wedge since v cannot connect to all of u_1, \dots, u_ℓ (otherwise, the clique is not cut). Therefore, we have an injective map from any cut clique on the left-hand side of the inequality to an open ℓ -wedge. Thus, $\sum_{v \in V} \text{cut}_{K_\ell}(N'_v)$ is no greater than the number of open ℓ -wedges, which is exactly $(1 - C_\ell) \cdot |W_\ell|$. \square

Next, we define a probability distribution on the nodes,

$$(3.24) \quad p_\ell(u) = |W_\ell(u)| / |W_\ell|.$$

The following lemma creates a random variable with the probability distribution in Equation (3.24) whose expectation is bounded by $1 - C_\ell$, which we use in the proof of Theorem 16.

Lemma 20. *Let X be a random variable that takes value $\frac{\text{cut}_{K_\ell}(N'_u)}{|W_\ell(u)|}$ with probability $p_\ell(u)$. Then $\mathbb{E}[X] \leq 1 - C_\ell$.*

Proof.

$$\begin{aligned} \mathbb{E}[X] &= \sum_{u \in V} p_\ell(u) \frac{\text{cut}_{K_\ell}(N'_u)}{|W_\ell(u)|} \\ &= \frac{1}{|W_\ell|} \sum_{u \in V} \text{cut}_{K_\ell}(N'_u) \\ &\leq \frac{1}{|W_\ell|} (1 - C_\ell) \cdot |W_\ell| \quad (\text{by Lemma 19}) \\ &= 1 - C_\ell. \end{aligned}$$

\square

Lemma 21. *There exists some node u such that*

$$(3.25) \quad \text{cut}_{K_\ell}(N'_u) \leq a(1 - C_\ell) \cdot |W_\ell(u)| \text{ and } C_\ell(u) \geq b$$

Proof. Consider the random variable X defined in Lemma 20 with $\mathbb{E}[X] \leq 1 - C_\ell$. For any constant $a > 1$, by Markov's inequality, we have that

$$(3.26) \quad \mathbb{P}[X > a(1 - C_\ell)] \leq 1/a.$$

Let $b = (aC_\ell - 1)/(a - 1) \leq 1$, and $p = \mathbb{P}[C_\ell(u) < b]$. Now,

$$\begin{aligned}
C_\ell &= \frac{\ell}{|W_\ell|} \cdot (\ell + 1) |K_{\ell+1}| \\
&= \frac{\ell}{|W_\ell|} \cdot \sum_{u \in V} |K_{\ell+1}(u)| \\
&= \sum_{u \in V} \frac{|W_\ell(u)|}{|W_\ell|} \cdot \frac{\ell \cdot |K_{\ell+1}(u)|}{|W_\ell(u)|} \\
&= \sum_{u \in V} p_\ell(u) C_\ell(u) \\
&= \sum_{C_\ell(u) < b} p_\ell(u) C_\ell(u) + \sum_{C_\ell(u) \geq b} p_\ell(u) C_\ell(u) \\
&< b \sum_{C_\ell(u) < b} p_\ell(u) + \sum_{C_\ell(u) \geq b} p_\ell(u) \\
&= bp + (1 - p).
\end{aligned}$$

Thus,

$$(3.27) \quad \mathbb{P}[C_\ell(u) < b] = p < (1 - C_\ell)/(1 - b) = 1 - 1/a.$$

By the union bound with the results in Equations (3.26) and (3.27),

$$1 - \mathbb{P} \left[\frac{\text{cut}_{K_\ell}(N'_u)}{|W_\ell(u)|} > a(1 - C_\ell) \text{ or } C_\ell(u) < b \right] > 0.$$

The result holds by the probabilistic method. \square

We now prove a final lemma, from which Theorem 16 will be a corollary.

Lemma 22. *For any node u satisfying the bounds in Equation (3.25),*

$$\frac{\text{cut}_{K_\ell}(N'_u)}{\text{vol}_{K_\ell}(N'_u)} \leq \frac{1 - C_\ell}{1 - C_\ell + (aC_\ell - 1)/(a - 1)}.$$

Proof. We first provide a lower bound for $\text{vol}_{K_\ell}(N'_u)$. First, each ℓ -clique cut by the partition induced by N'_u contributes at least one to $\text{vol}_{K_\ell}(N'_u)$. Second, each $(\ell + 1)$ -clique in $K_{\ell+1}(u)$ uniquely corresponds to an ℓ -clique in N'_u which is induced by the ℓ nodes in the $(\ell + 1)$ -clique other than u , thus will contribute ℓ into $\text{vol}_{K_\ell}(N'_u)$. Note that each $(\ell + 1)$ -clique in $K_{\ell+1}(u)$ closes ℓ different ℓ -wedges in $W_\ell(u)$, and

there are $C_\ell(u)|W_\ell(u)|$ closed ℓ -wedges. Combining these observations,

$$\begin{aligned} \text{vol}_{K_\ell}(N'_u) &\geq \text{cut}_{K_\ell}(N'_u) + \ell \cdot C_\ell(u)|W_\ell(u)|/\ell \\ &\geq \text{cut}_{K_\ell}(N'_u) + b|W_\ell(u)| \quad (\text{by Equation (3.25)}). \end{aligned}$$

Now,

$$\begin{aligned} \frac{\text{cut}_{K_\ell}(N'_u)}{\text{vol}_{K_\ell}(N'_u)} &\leq \frac{\text{cut}_{K_\ell}(N'_u)}{\text{cut}_{K_\ell}(N'_u) + b|W_\ell(u)|} \\ &\leq \frac{a(1 - C_\ell) \cdot |W_\ell(u)|}{a(1 - C_\ell)|W_\ell(u)| + b|W_\ell(u)|} \quad (\text{by Equation (3.25)}) \\ &= \frac{1 - C_\ell}{1 - C_\ell + \frac{aC_\ell - 1}{a(a-1)}}. \end{aligned}$$

□

Finally, Theorem 16 follows from Lemmas 21 and 22, setting

$$a = (1 + \sqrt{1 - C_\ell})/C_\ell,$$

and the fact that $\text{vol}_{K_\ell}(N'_u) \leq \text{vol}_{K_\ell}(V)/2$ implies that

$$\phi_{K_\ell}(N'_u) = \frac{\text{cut}_{K_\ell}(N'_u)}{\text{vol}_{K_\ell}(N'_u)}.$$

The theory in this section holds for cliques of any size, and the results do not use the approximation to motif conductance in Section 2.2.8 needed by our motif-based spectral clustering method for motifs with four or more nodes. Thus, our definitions of motif conductance are still meaningful for motifs with at least 4 nodes.

3.5.2 Experiments

The goals of our experiments are

- i. to demonstrate that there are 1-hop neighborhood clusters of small motif conductance as a test of how well Theorem 16 holds in practice; and
- ii. to use this idea to quickly find many clusters with small motif conductance by running targeted cluster expansion around a subset of the 1-hop neighborhood clusters.

Regarding Item i, we find that real-world networks exhibit much better results than predicted by the theory and the 1-hop neighborhood with minimal motif

Table 3.2 – Summary statistics of datasets. The EMAIL-ENRON and WEB-GOOGLE networks are treated as undirected, even though the original datasets are directed.

Dataset	$ V $	$ E $	C_2	C_3	C_4
CA-CONDMAT	14,788	187,278	0.33	0.33	0.36
EMAIL-ENRON	18,561	156,139	0.11	0.06	0.05
FB-HARVARD1	13,319	793,410	0.14	0.07	0.07
WEB-GOOGLE	393,582	2,905,337	0.07	0.06	0.07

conductance is competitive with spectral graph theory approaches. Regarding Item ii, we show that a subset of 1-hop neighborhoods called locally minimal neighborhoods are better seeds than random nodes. We use this insight to find the global structure of clique conductance clusters more quickly than exhaustive enumeration.

We evaluate 1-hop neighborhood cluster quality in terms of motif conductance for 2-clique (edge), 3-clique (triangle), and 4-clique motifs using four networks where we can exhaustively sample targeted clusters easily: CA-CONDMAT, a co-authorship network constructed from papers posted to the condensed matter category on arXiv [Leskovec et al., 2007b]; FB-HARVARD1, a snapshot of the friendships network between Harvard students on Facebook in September 2005 [Traud et al., 2012]; EMAIL-ENRON, an e-mail communication network of the employees of Enron Corporation and their contacts [Klimt and Yang, 2004]; and WEB-GOOGLE, a Web graph released by Google for a programming contest [Leskovec et al., 2009]. Summary statistics for the networks are in Table 3.2.

There are 1-hop neighborhoods of low motif conductance. Plugging the higher-order clustering coefficients from Table 3.2 into the bound from Theorem 16 yields weak, albeit non-trivial bounds on the smallest neighborhood conductance (all bounds are ≥ 0.9 for the networks we consider). However, the spirit of the theorem rather than the bound itself motivates our experiments: with large higher-order clustering, there should be a neighborhood with small motif conductance for clique motifs. We indeed find this to be true in our results.

Table 3.3 compares the neighborhood with smallest motif conductance for the 2-clique, 3-clique, and 4-clique motifs with the Fiedler cluster described in Algorithm 1 in Chapter 2. (For 4-cliques, we actually use the quadratic approximation from Equation (2.27) because it is easier to compute.) Here, the Fiedler cluster represents a method that uses the global structure of the network to compare against the purely local neighborhood clusters. In all cases, the best neighborhood cluster has motif conductance far below the upper bound of Theorem 16. For all clique orders, the best neighborhood cluster always has conductance within a factor of

3.5 of the Fiedler cluster in `CA-CONDMAT`, `EMAIL-ENRON`, and `FB-HARVARD1`. With `WEB-GOOGLE`, the conductances are much smaller but the best neighborhood still has conductance within an order of magnitude of the Fiedler set. We conclude that the best neighborhood cluster in terms of motif conductance, which comes from purely local constructs, is competitive with the Fiedler vector that takes into account the global graph structure. This motivates our next set of experiments that uses nodes that induce small neighborhood conductance as seeds for the APPR method developed in Section 2.5.

Table 3.3 – Fiedler and 1-hop neighborhood clusters. We compare the cluster found by the spectral sweep cut algorithm (Algorithm 1; Fiedler) to the 1-hop neighborhood with smallest motif conductance. A star (*) denotes when 1-hop neighborhood clusters are the same across different clique sizes, a dagger (†) denotes when Fiedler clusters are the same, and a bullet (•) denotes when the neighborhood and Fiedler clusters are the same. In CA-CONDMAT, EMAIL-ENRON, and FB-HARVARD1, the best neighborhood cluster always has conductance within a factor of 3.5 of the Fiedler cluster.

(*) We report the quadratic form approximation to motif conductance for 4-cliques (Equation (2.27)) because it is easier to compute.

	CA-CONDMAT	EMAIL-ENRON	FB-HARVARD1	WEB-GOOGLE
<hr/> <i>M = 2-cliques</i> <hr/>				
Neighborhood				
# nodes	23 [•]	21 [*]	4	203
motif cond.	$1.1 \cdot 10^{-2}$	$2.4 \cdot 10^{-2}$	$2.0 \cdot 10^{-1}$	$1.5 \cdot 10^{-3}$
Fiedler				
# nodes	23 [•]	25 [†]	1,470	5,335
motif cond.	$1.1 \cdot 10^{-2}$	$1.7 \cdot 10^{-2}$	$1.1 \cdot 10^{-1}$	$9.2 \cdot 10^{-5}$
<hr/>				
<i>M = 3-cliques</i> <hr/>				
Neighborhood				
# nodes	17 [*]	21 [*]	5 [*]	62 [*]
motif cond.	$2.0 \cdot 10^{-3}$	$1.3 \cdot 10^{-2}$	$1.4 \cdot 10^{-1}$	$1.8 \cdot 10^{-4}$
Fiedler				
# nodes	18 [†]	25 [†]	1,429	10,803
motif cond.	$1.5 \cdot 10^{-3}$	$6.7 \cdot 10^{-3}$	$4.9 \cdot 10^{-2}$	$5.9 \cdot 10^{-5}$
<hr/>				
<i>M = 4-cliques</i> <hr/>				
Neighborhood				
# nodes	17 [*]	8	5 [*]	62 [*]
motif cond.*	$1.4 \cdot 10^{-4}$	$3.6 \cdot 10^{-3}$	$7.7 \cdot 10^{-2}$	$1.1 \cdot 10^{-5}$
Fiedler				
# nodes	18 [†]	25 [†]	1,299	8,001
motif cond.*	$1.1 \cdot 10^{-4}$	$1.6 \cdot 10^{-3}$	$2.2 \cdot 10^{-2}$	$2.2 \cdot 10^{-6}$

Table 3.4 – Testing neighborhood centers as seeds. We report the p -values from Mann-Whitney U tests of the null hypothesis that the motif conductances of sets from APPR seeded with local minima are *not less than* the motif conductances of sets from APPR seeded with non-local minima. In all but CA-CONDMAT with the standard edge motif, we reject the null at a significance level < 0.003 .

motif	CA-CONDMAT	EMAIL-ENRON	FB-HARVARD1	WEB-GOOGLE
edge	0.87	$< 1 \cdot 10^{-16}$	$8.17 \cdot 10^{-05}$	$< 1 \cdot 10^{-16}$
triangle	$2.07 \cdot 10^{-03}$	$< 1 \cdot 10^{-16}$	$4.32 \cdot 10^{-04}$	$< 1 \cdot 10^{-16}$
4-clique	$7.20 \cdot 10^{-10}$	$< 1 \cdot 10^{-16}$	$1.55 \cdot 10^{-05}$	$< 1 \cdot 10^{-16}$

Finding good seeds. So far, we have used our theory to find a single node whose 1-hop neighborhood has small motif conductance for clique motifs. We examine this further by using nodes whose neighborhoods induce good cuts as seeds for the motif-based APPR method. Following the terminology of [Gleich and Seshadhri \[2012\]](#), we say that a node u is a *local minimum* if $\phi_M(N'_u) \leq \phi_M(N'_v)$ for all neighbors v of u . To test whether local minima are good seeds for APPR, we first exhaustively compute APPR clusters using every node in each of our networks as a seed. Next, we used a one-sided Mann Whitney U test to test the null hypothesis that the local minima yield APPR clusters with motif conductances that are *not less than* motif conductances from using non-local minima as seeds (Table 3.4). The p -values from these tests say that we can safely reject the null hypothesis at significance level < 0.003 for all cliques and networks considered except for 2-cliques in CA-CONDMAT. In other words, local minima are better seeds than non-local minima.

Finally, we use these local minimum seeds to construct network community profile (NCP) plots for different motifs. NCP plots are defined as the optimal conductance over all sets of a fixed size k as a function of k [[Leskovec et al., 2009](#)]. The shapes of the curves reveal the cluster structure of the networks. In practice, these plots are generated by exhaustively using every node in the network as a seed for the APPR method [[Leskovec et al., 2009](#)]. Here, we compare this approach to two simpler ones: (i) using the neighborhood sizes and conductances and (ii) using only local minima as seeds for APPR. In the latter case, between 1% and 15% of nodes are local minima, depending on the network, so this serves as an economical alternative to the typical exhaustive approach.

Figure 3.6 shows the NCP plots for CA-CONDMAT and FB-HARVARD1 with the triangle and 4-clique motifs. Seeding with local minima is sufficient for capturing the major trends of the NCP plot. In general, the curves constructed from neighborhood information capture the first downward spike in the plot, but

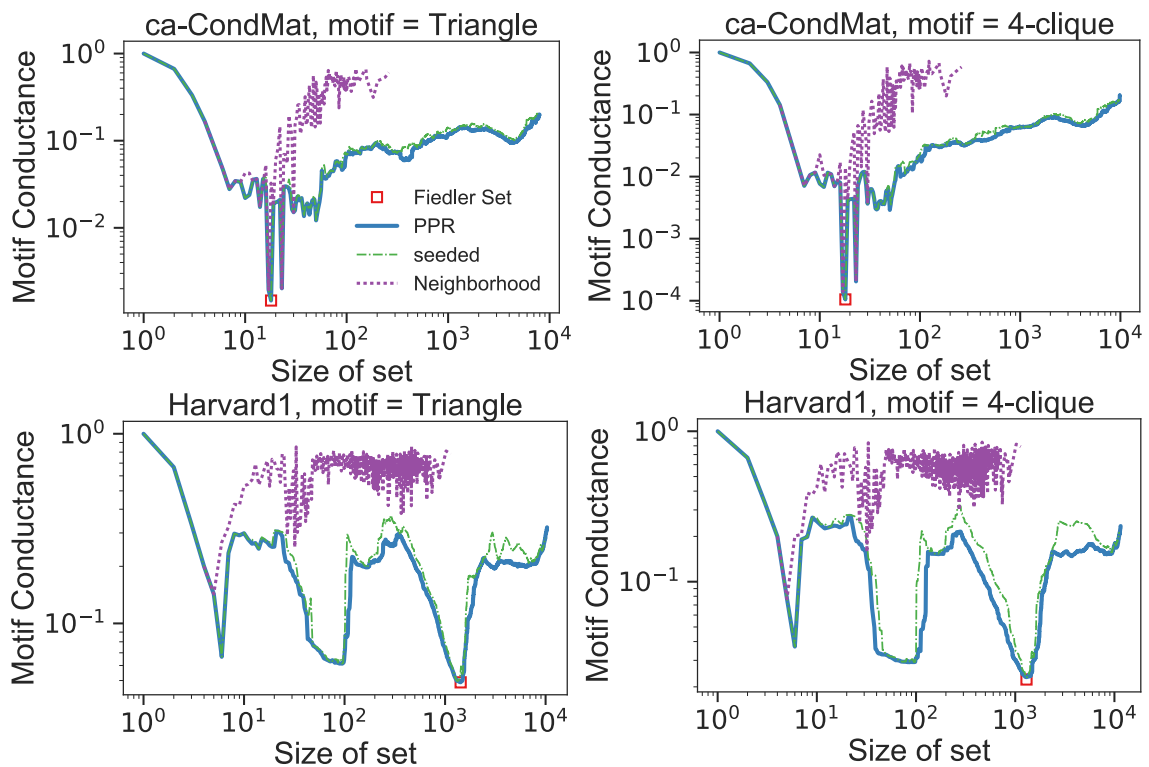


Figure 3.6 – NCP plots for two networks with two different clique sizes. Curves are constructed from APPR with all nodes as seeds (blue), APPR with just local minima as seeds (“seeded”, green), and all 1-hop neighborhoods (“Neighborhood”, purple). Using local minima as seeds captures the trends of exhaustive PPR using only a fraction of the seeds. A local minima seed also captures the Fiedler set (marked by \square).

do not capture larger sets with small conductance. Finally, the triangle and 4-clique NCP plots are quite similar for both networks. Thus, we suspect that local minima for lower-order cliques could also be used as good seeds when looking for sets based on higher-order cliques.

3.6 Related work and discussion

We have proposed a methodology for higher-order clustering coefficients to study higher-order closure patterns in networks, which generalizes the widely used clustering coefficient that measures triadic closure. Our methodology gives new insights into the clustering behavior of both real-world networks and random graph models, and our theoretical analysis provides intuition for the way in which higher-order clustering coefficients describe local clustering in graphs.

There have been a few prior efforts along these lines. [Fronczak et al. \[2002\]](#) define an ℓ th-order local clustering coefficient at node u to be the fraction of neighbors of u that have shortest path distance ℓ in the 1-hop neighborhood graph of u with u removed (i.e., in N_u). In this definition, $\ell = 1$ corresponds to the traditional local clustering coefficient. We note that this generalization does not have a natural global clustering coefficient. [Andrade et al. \[2006\]](#) also look at shortest paths of length ℓ in an effort to generalize graph measures and mention the clustering coefficient, although they do not actually compute it. [Caldarelli et al. \[2004\]](#) define the *grid coefficient* at node u as the number of 4-cycles containing u divided by the total possible number of 4-cycles u could participate in, given the degrees of u and its neighbors. This is a generalization of the classical clustering coefficient, which measures the number of 3-cycles containing u divided by the total possible number of 3-cycles u could participate in, given the degree of u . [Jiang and Claramunt \[2004\]](#) define an ℓ th-order local clustering coefficient of node u as the edge density in the ℓ -hop neighborhood of node u with u removed. In this case, $\ell = 1$ is the classical clustering coefficient.

None of the prior work captures the closure patterns of higher-order cliques, which fits with the notion of triadic closure in sociology. The prior generalizations also do not discuss algorithms for the computations of the proposed measurements. For example, finding shortest paths in all neighborhood graphs N_u could be expensive. A nice property of our generalization is that we only have to enumerate ℓ -cliques and $(\ell - 1)$ -cliques.

There are also a few other approaches to finding higher-order structure through generalizations or relaxations of some notion of density. These include the k -clique densest subgraph problem [[Tsourakakis, 2015](#)], triangle cores [[Rossi et al., 2013](#); [Zhang and Parthasarathy, 2012](#)], trusses (relaxations of cliques) [[Cohen, 2008](#)], other generalizations of cores and trusses [[Sariyuce et al., 2015](#)], and the k -plex [[Seidman and Foster, 1978](#)]. We view these analyses as complimentary to our own. In contrast to other work, our analysis in Section 3.4, shows how *combining* existing tools (the classical clustering coefficient) with new higher-order tools (the higher-order clustering coefficient) can provide new analysis (e.g., Figure 3.4). We hope that this guides future research in the area.

Chapter 4

Motifs in temporal networks

4.1 Analyzing network data with timestamped edges

Thus far, we have used networks to describe static relationships between things (nodes) and connections between things (edges). However, many systems are not static as the links between objects dynamically change over time [Holme and Saramäki, 2012]. Such *temporal networks* can be represented by a series of timestamped edges, or *temporal edges*. For example, a network of email or instant message communication can be represented as a sequence of timestamped directed edges, one for every message that is sent from one person to another. Similar representations can be used to model computer networks, phone calls, financial transactions, and biological signaling networks. The goal of this chapter is to bring higher-order analysis to this type of data—in particular, to develop motifs as a tools for studying temporal network data.

Data in these systems often have two important properties:

- i. There are often many temporal edges between the same set of nodes. For example, two individuals may text back and forth several times.
- ii. The time resolution of the edges is small compared to the time span encompassed by the entire dataset. In the EMAIL-EU dataset studied later, we know the exact second that an e-mail is sent, and we have e-mails sent over more than 2 years apart.

While temporal networks are ubiquitous, there are few tools for modeling and characterizing the underlying structure of such datasets. Current analytic methods of temporal network data can be characterized by a few broad categories. First, there are methods and models that study networks as if they are strictly growing over time, where a pair of nodes connect once and stay connected forever [Barabási and Albert, 1999; Jacobs et al., 2015; Lattanzi and Sivakumar, 2009; Leskovec et al., 2008, 2007b]. Such methods fail to address Item i. The second approach is to

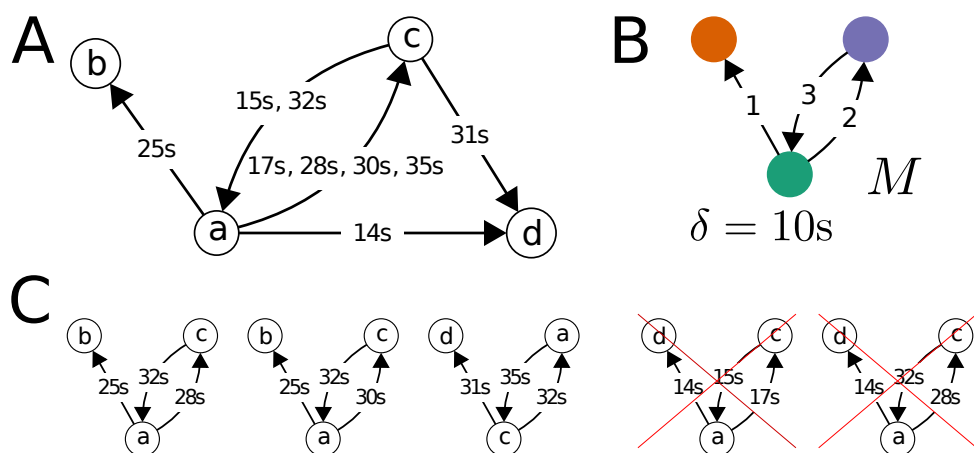


Figure 4.1 – Temporal graphs and δ -temporal motifs. A: A temporal graph with nine temporal edges. Each edge has a timestamp (listed here in seconds). B: Example 3-node, 3-edge, δ -temporal motif M . The edge labels correspond to the ordering of the edges. The time duration of the motif is $\delta = 10$ seconds. C: Instances of the δ -temporal motif M . The crossed-out patterns are not instances of M because either the edge sequence is out of order or the edges do not all occur within the time window δ .

aggregate the temporal network into a sequence of static snapshots [Araujo et al., 2014; Dunlavy et al., 2011; Tantipathananandh et al., 2007]. These approaches throw away much of the rich, fine-grained temporal information in the data (Item ii). Third, there are models and analysis that treat time as continuous. Examples include studies on macroscopic characteristics of the data, such as the distribution of the inter-event times between a pair of nodes or of an individual in a network [Barabasi, 2005; Malmgren et al., 2009], and models for information diffusion [Du et al., 2015; Farajtabar et al., 2015]. Work in this area has not focused on measuring the interaction of time and structure in temporal networks, although such joint analysis has been considered with, e.g., temporal strong components [Bhadra and Ferreira, 2003; Nicosia et al., 2012; Rossi et al., 2015].

Our goal in this chapter to develop motifs as a tool for jointly analyzing time and structure in temporal networks. We extend static motifs to temporal networks and define δ -temporal motifs, where all the edges in a given motif M have to occur inside the time period of δ time units. These δ -temporal motifs simultaneously account for ordering of edges and a temporal window in which edges can occur. For example, Figure 4.1B shows a motif on three nodes and three edges, where the edge label denotes the order in which the edges appear. While we focus on directed edges with a single timestamp in this work, our methodology seamlessly

generalizes to common variations on this model. For example, our methods can incorporate timestamps with durations (common in telephone call networks), colored edges that identify different types of connections, and temporal networks with undirected edges.

We then consider the problem of counting how many times does each δ -temporal motif occur in a given temporal network. We develop a general algorithm for counting temporal network motifs defined by any number of nodes and edges that avoids enumeration over subsets of temporal edges and whose complexity depends on the structure of the static graph induced by the temporal motif. For motifs defined by a constant number of temporal edges between 2 nodes, this general algorithm is optimal up to constant factors—it runs in $O(m)$ time, where m is the number of temporal edges.

Furthermore, we design fast variations of the algorithm that allow for counting certain classes of δ -temporal motifs including star and triangle patterns. These algorithms are based on a common framework for managing summary counts in specified time windows. For star motifs with 3 nodes and 3 temporal edges, we again achieve a running time linear in the input, i.e., $O(m)$ time. Given a temporal graph with n nodes and τ induced triangles in its induced static graph, our fast algorithm counts temporal triangle motifs with 3 temporal edges in $O(\min(m\tau^{1/2}, mn))$ worst-case time, after the τ triangles have been identified. In contrast, any algorithm that processes triangles individually takes $O(\min(m\tau, mn))$ worst-case time. In practice, our fast temporal triangle counting algorithm is up to 56 times faster than a competitive baseline and runs in just a couple of hours on a network with over two billion temporal edges.

Our algorithmic framework enables us to study the structure of several complex systems. For example, we explore the differences in human communication patterns by analyzing motif frequencies in text message, Facebook wall post, email and private online message network datasets. Temporal network motif counts reveal that text messaging and Facebook wall posting are dominated by one-to-one communication, where a user only engages with one other user at a time, whereas email is mostly characterized by one-to-many or broadcast patterns as individuals send out several emails in a row.

Temporal network motifs can also be used to measure the frequency of patterns at different time scales. For example, the difference in δ -temporal motif counts for $\delta = 60$ minutes and $\delta = 30$ minutes counts only the motifs that take at least 30 minutes and at most 60 minutes to form. With this type of analysis, we find that certain question-and-answer patterns on Stack Overflow need at least 30 minutes to develop. We also see that in online private messaging, star patterns constructed by outgoing messages sent by one user tend to increase in frequency from time scales of 1 to 20 minutes before peaking and then declining in frequency.

In summary, our work defines a flexible notion of motifs in temporal networks and provides efficient algorithms for counting them. It enables new analyses in a variety of scientific domains and paves a new way for modeling dynamic complex systems.

4.2 Definitions of temporal networks and temporal motifs

We now provide formal definitions of temporal graphs and δ -temporal motifs. In Section 4.3, we provide algorithms for counting the number of δ -temporal motifs in a given temporal graph.

We define a *temporal edge* to be a timestamped directed edge between an ordered pair of nodes. We call a collection of temporal edges a *temporal graph* (Figure 4.1A), as formalized in the following definition.

Definition 23. A temporal graph T on a node set V is a collection of tuples (u_i, v_i, t_i) , $i = 1, \dots, m$, where each u_i and v_i are elements of V and each t_i is a timestamp in \mathbb{R} . A tuple (u_i, v_i, t_i) in T is a temporal edge.

Note that there can be many temporal edges directed from u to v . We assume that the timestamps t_i are unique so that the tuples may be strictly ordered. This assumption makes the presentation of the definitions and algorithms clearer, but our methods can be adapted to the case when timestamps are not unique. When it is clear from context, we refer to a temporal edge as simply an *edge*. Finally, by ignoring timestamps and duplicate edges, the temporal graph induces a standard (static) directed graph.

Definition 24. The static graph G of a temporal graph T on node set V is a graph with edge set $E = \{(u, v) \mid \exists t : (u, v, t) \in T\}$. An edge in E is called a static edge of T .

Sometimes, it will be useful to think about all temporal edges (u, v, t) associated with a specified static edge (u, v) . We will sometimes refer to these as the timestamps of these temporal edges as the *timestamps along the static edge* (u, v) . For example, there are 4 timestamps along the edge (a, c) in Figure 4.1A.

We now formalize δ -temporal motifs.

Definition 25. A k -node, l -edge, δ -temporal motif $M = (K, \sigma, \delta)$ consists of a multi-graph $K = (V, E)$ with k nodes and l edges, an ordering σ on the edges of E , and a time span $\delta \in \mathbb{R}_+$. We typically represent (K, σ) by a sequence $(u_1, v_1), (u_2, v_2) \dots, (u_l, v_l)$, $u_i, v_i \in V$, $i = 1, \dots, l$.

We often just refer to a motif M by just the multigraph K and the ordering σ , considering δ to be arbitrary. Figure 4.1B illustrates a particular 3-node, 3-edge δ -temporal motif with δ specified to be a 10 second duration.

Definition 25 provides a template for a particular pattern, and we are interested in how many times a given pattern occurs in a given temporal network. Intuitively, a collection of edges in a given temporal graph is an *instance* of a δ -temporal motif M if it matches the same edge pattern of the multigraph, the temporal edges occur in the specified order, and all of the temporal edges occur with a δ time window (Figure 4.1C).

Definition 26. *In a temporal graph T , a time-ordered sequence of $S = (w_1, x_1, t_1), \dots, (w_l, x_l, t_l)$ of l unique edges in T ($t_1 < t_2 < \dots < t_l$) is an instance of the temporal motif $M = (K, \sigma, \delta)$ with $(K, \sigma) = (u_1, v_1), \dots, (u_l, v_l)$ if*

- i. *There exists a bijection f on the vertices such that $f(w_i) = u_i$ and $f(x_i) = v_i$, $i = 1, \dots, l$, and*
- ii. *the edges all occur within δ time, i.e., $t_l - t_1 \leq \delta$*

The central algorithmic goal of this chapter is to count the number of ordered subsets of edges from a temporal graph T that are instances of a particular motif. In other words, given a k -node, l -edge δ -temporal motif, we seek to find how many of the $l! \binom{m}{l}$ ordered length- l sequences of edges in the temporal graph T are instances of the motif. A naive approach to this problem would be to simply enumerate all ordered subsets and then check if it is an instance of the motif. In modern datasets, the number of edges m is typically quite large (we analyze a dataset in Section 4.4 with over $m > 2$ billion), and this approach is impractical even for $l = 2$. In the following section, we discuss several faster algorithms for counting the number of instances of δ -temporal motifs in a temporal graph.

In contrast to Chapter 2, here we define motifs by just the existence of edges (a general subgraph) and not the non-existence of edges (an induced subgraph). This is crucial for our development of fast counting algorithms.

Table 4.1 summarizes the notation introduced in this section and the next.

Table 4.1 – Notation for Chapter 4.

T	temporal network
$e = ((u, v), t)$	temporal edge
m	number of temporal edges in a temporal network
n	number of nodes in a temporal network
K	multigraph component of a temporal motif
σ	ordering on the multigraph edges of a temporal motif
δ	time span of a temporal motif
$M = (K, \sigma, \delta)$	temporal motif
$M_{i,j}$ for $1 \leq i, j, \leq 6$	one of the motifs illustrated in Figure 4.2
k	number of nodes in a temporal motif (number of nodes in the multigraph)
ℓ	number of edges in a temporal motif (number of edges in the multigraph)
S	ordered sequence of temporal edges
G	static graph induced by a temporal network
τ	number of triangles in a static graph
H	motif pattern in a static graph
H'	instance of a static motif in a static graph

4.3 Counting algorithms

We now present several algorithms for counting the exact number of instances of temporal motifs in a temporal graph. We first present a general counting algorithm in Section 4.3.1, which can count instances of any k -node, l -edge temporal motif faster than simply enumerating over all size- l ordered subsets of edges. The computational complexity depends on the multigraph structure of the motif, but the algorithm is optimal for counting 2-node, l -edge temporal motifs (for constant l) in the sense that it is linear in the number of edges in the temporal graph. In Section 4.3.2, we provide faster, specialized algorithms for counting specific types of 3-node, 3-edge temporal motifs (Figure 4.2). The computational complexities of all of our algorithms are independent of δ .

4.3.1 General counting framework

We begin with a general framework for counting the number of instances of a of a temporal motif $M = (K, \sigma, \delta)$. To start, consider H to be the static directed graph induced by K (i.e., H consists of all unique edges in K). A sequence of temporal edges is an instance of M if and only if

- i. the static subgraph induced by the edges in the sequence is isomorphic to H
- ii. the ordering of the edges in the sequence matches σ ,
- iii. all the edges in the sequence span a time window of at most δ time units.

This leads to the following general algorithm for counting instances of M in a temporal graph T :

- i. Identify all instances H' of the static motif H within the static graph G induced by the temporal graph T . For example, there are three instances of H induced in Figure 4.1 ($\{(a, b), (a, c), (c, a)\}$, $\{(a, d), (a, c), (c, a)\}$, and $\{(c, d), (c, a), (a, c)\}$).
- ii. For each static motif instance H' , gather all temporal edges between pairs of nodes forming an edge in H' into an ordered sequence $S = (u_1, v_1, t_1), \dots, (u_L, v_L, t_L)$.
- iii. Count the number of (potentially non-contiguous) subsequences of edges in S occurring within δ time units that match (K, σ) .

The first step can use known algorithms for enumerating motifs in static graphs such as those by [Wernicke and Rasche \[2006\]](#), and the second step is a simple matter of fetching the appropriate temporal edges. To perform the third step efficiently, we develop a dynamic programming approach for counting the number of subsequences (instances of motif M) that match a particular pattern within a larger sequence (S). The key idea is that, as we stream through an input sequence of edges, the count of a given length- l pattern (i.e., motif) with a given final edge

Algorithm 5 – General counting method for temporal motifs. This routine counts the number of instances of all possible l -edge δ -temporal motifs. The input is an ordered sequence of temporal edges. We assume the keys of `counts[·]` are accessed in order of length.

Input: Sequence S of edges $(e_1 = (u_1, v_1), t_1), \dots, (e_L, t_L)$ with $t_1 < \dots < t_L$, time window δ

Output: Number of instances of each l -edge δ -temporal motif M contained in the sequence

```

1 start  $\leftarrow$  1, counts  $\leftarrow$  Counter(default = 0)
2 for end = 1, ..., L :
3   /* Remove edges out of  $\delta$  window */
4   while  $t_{\text{start}} + \delta < t_{\text{end}}$  do
5     | DecrementCounts( $e_{\text{start}}$ ), start += 1
6   /* Update counts with edge ( $e_{\text{end}}, t_{\text{end}}$ ) */
7   | IncrementCounts( $e_{\text{end}}$ )
8 return counts
9
10 Procedure DecrementCounts( $e$ )
11 | counts[ $e$ ] -= 1
12 | for suffix in counts.keys of length  $< l - 1$  :
13 | | counts[concat( $e$ , suffix)] -= counts[suffix]
14 Procedure IncrementCounts( $e$ )
15 | for prefix in counts.keys.reverse() of length  $< l$  :
16 | | counts[concat(prefix,  $e$ )] += counts[prefix]
17 | counts[ $e$ ] += 1

```

is computed from the current count of the length- $(l - 1)$ prefix of the pattern. Inductively, we maintain auxiliary counters of all of the prefixes of the pattern (motif). Second, we also require that all edges in the motif be at most δ time apart. Thus, we use the notion of a moving time window such that any two edges in the time window are at most δ time apart. The auxiliary counters now keep track of only the subsequences occurring within the current time window. Last, it is important to note that the algorithm only *counts* the number of instances of motifs rather than *enumerating* them. This is critical to making the algorithm fast.

For simplicity of presentation, Algorithm 5 counts *all* possible l -edge motifs that occur in a given sequence of edges. The data structure `counts[·]` maintains auxiliary counts of all (ordered) patterns of length at most l . Specifically, `counts[$e_1 \dots e_r$]` is

	15s (c, a)	17s (a, c)	25s (a, b)	28s (a, c)	30s (a, c)	32s (c, a)	35s (a, c)
counts[(a, b)]	0	0	1	1	1	1	1
counts[(a, c)]	0	1	1	1	2	2	3
counts[(c, a)]	1	1	1	0	0	1	1
counts[(a, b)(a, c)]	0	0	0	1	2	2	3
counts[(a, b)(a, c)(c, a)]	0	0	0	0	0	2	2
start	1	1	1	3	3	3	3
end	1	2	3	4	5	6	7

Table 4.2 – Example execution of Algorithm 5 for counting instances of the δ -temporal motif M and network in Figure 4.1. Each column shows the value of counters at the end of the for loop that processes temporal edges (after Line 7 in Algorithm 5). Color indicates change in the variable: incremented (blue), decremented (red), incremented and decremented (purple), or no change (black). At the end of execution, $\text{counts}[(a, b)(a, c)(c, a)] = 2$ for the two instances of the temporal motif M with center node a . Here we only show the counters needed to count M , whereas Algorithm 5 as presented would count all 3-edge patterns in the sequence (maintaining 39 total counters). However, for any particular l -edge temporal network motif, Algorithm 5 only needs to maintain $O(l^2)$ counters.

the number of times the subsequence $[e_1 \cdots e_r]$ occurs in the current time window (if $r < l$) or the number of times the subsequence has occurred within all time windows of length δ (if $r = l$). Crucially, we also assume the keys of $\text{counts}[\cdot]$ are accessed in order of length. Moving the time window forward by adding a new edge into the window, all edges ($e = (u, v), t$) farther than δ time from the new edge are removed from the window and the appropriate counts are decremented (the *DecrementCounts()* method)—first, the single edge counts ($[e]$) are updated. Based on these updates, length-2 subsequences formed with e as its first edge are updated and so on, up through length- $(l - 1)$ subsequences. On the other hand, when an edge e is added to the window, similar updates take place, but in reverse order, from longest to shortest subsequences, in order to increment counts in subsequences where e is the last edge (the *IncrementCounts()* method). Importantly, length- l subsequence counts are incremented in this step but never decremented. As the time window moves from the beginning to the end of the sequence of edges, the algorithm accumulates counts of all length- l subsequences in all possible time windows of length δ .

While Algorithm 5 maintains counts for all l -edge motifs, we could simply maintain the $\text{counts}[\cdot]$ data structure for the contiguous prefixes of the motif M . As

an example, Table 4.2 shows the execution of Algorithm 5 for a particular sequence of edges and a particular motif, where counts of only the necessary contiguous subsequences of the motif are maintained. In general, there are $O(l^2)$ contiguous subsequences of an l -edge motif M , and there are $O(|H|^l)$ total keys in $\text{counts}[\cdot]$, where $|H|$ is the number of edges in the static subgraph H induced by M , in order to count all l -edge motifs in the sequence (i.e., not just motif M).

We now analyze the complexity of the overall 3-step algorithm. We assume that the temporal graph T has edges sorted by timestamps, which is reasonable if edges are logged in their order of occurrence, and we also assume that we have pre-processed T so that we can access the sorted list of all edges between u and v in $O(1)$ time. Given an instance H' of H , constructing the time-sorted sequence S in step 2 of the algorithm then takes $O(\log(|H|)|S|)$ time (by merging sorted lists). Each edge inputted to Algorithm 5 is processed exactly twice: once to increment counts when it enters the time window and once to decrement counts when it exits the time window. As presented in Algorithm 5, each update changes $O(|H|^l)$ counters resulting in an overall complexity of $O(|H|^l|S|)$. However, one could modify Algorithm 5 to only update counts for contiguous subsequences of the sequence M , which would change $O(l^2)$ counters and have overall complexity $O(l^2|S|)$. We are typically only interested in small constant values of $|H|$ and l (for our experiments in Section 4.4, $|H| \leq 3$ and $l = 3$), in which case the running time of Algorithm 5 is linear in the size of the input to the algorithm, i.e., $O(|S|)$. What remains is to identify all instances H' of H . Of course, this depends on the structure of H . For example, if H is an edge, this can be done in linear time. If H is a triangle, this can be done in $O(a|G|)$ time, where $|G|$ is the number of edges in the static graph G induced by T and a is the arboricity of G [Chiba and Nishizeki, 1985].

In the remainder of this section we analyze our 3-step algorithm with respect to different types of motifs (2-node, stars, and triangles) and argue benefits and deficiencies of the proposed framework. We show that for 2-node motifs, our general counting framework takes time linear in the total number of edges m . Since all the input data needs to be examined for computing exact counts, this means the algorithm is optimal for 2-node motifs. However, we also show that for star and triangle motifs the algorithm is not optimal, which then motivates us to design faster algorithms in Section 4.3.2.

General algorithm for 2-node motifs. We first show how to map 2-node motifs to the framework described above. Any induced graph H of a 2-node δ -temporal motif is either a single or a bidirectional edge. In either case, it is straightforward to enumerate over all instances of H in the induced static graph. This leads to the following procedure. For each pair of nodes u and v for which there is at least one edge, gather and sort the edges in either direction between u and v and call

Algorithm 5 with these edges. To obtain the total motif count, we simply need to sum the results from each call to Algorithm 5.

We only need to input each edge to Algorithm 5 once, and under the assumption that we can access the sorted directed edges from one node to another in $O(1)$ time, the merging of edges into sorted order takes linear time (merging 2 sorted lists). Therefore, the total running time is $O(l^2m)$, where l is the number of edges in the motif, which is linear in the number of temporal edges m . We are mostly interested in small patterns, i.e., cases when l is a small constant. Thus, this methodology is optimal (linear in the input size, m) for counting 2-node δ -temporal motif instances.

General algorithm for star motifs. Next, we consider k -node, l -edge star motifs M , whose induced static graph H consists of a center node and $k - 1$ neighbors, where edges may occur in either direction between the center node and a neighbor node. For example, in the top left corner of Figure 4.2, $M_{1,1}$ is a star motif with all edges pointing toward the center node (the orange node). In such motifs, the induced static graph H contains at most $2(k - 1) = 2k - 2$ static edges—one incoming and outgoing edge from the center node to each neighbor node. We have the following method for counting the number of instances of k -node, l -edge star motifs. For each node u in the static graph and for each unique set of $k - 1$ neighbors, gather and sort the edges in either direction between u and the neighbors. Then, count the number of instances of M using Algorithm 5. The counts from each call to Algorithm 5 are summed over all center nodes and sets of $k - 1$ neighbors.

The major drawback of this approach is that we have to loop over each size- $(k - 1)$ neighbor set. This can be prohibitively expensive even when $k = 3$ if the center node has large degree. In Section 4.3.2, we will design an algorithm that avoids this issue for the case when the star motif has $k = 3$ nodes and $l = 3$ edges.

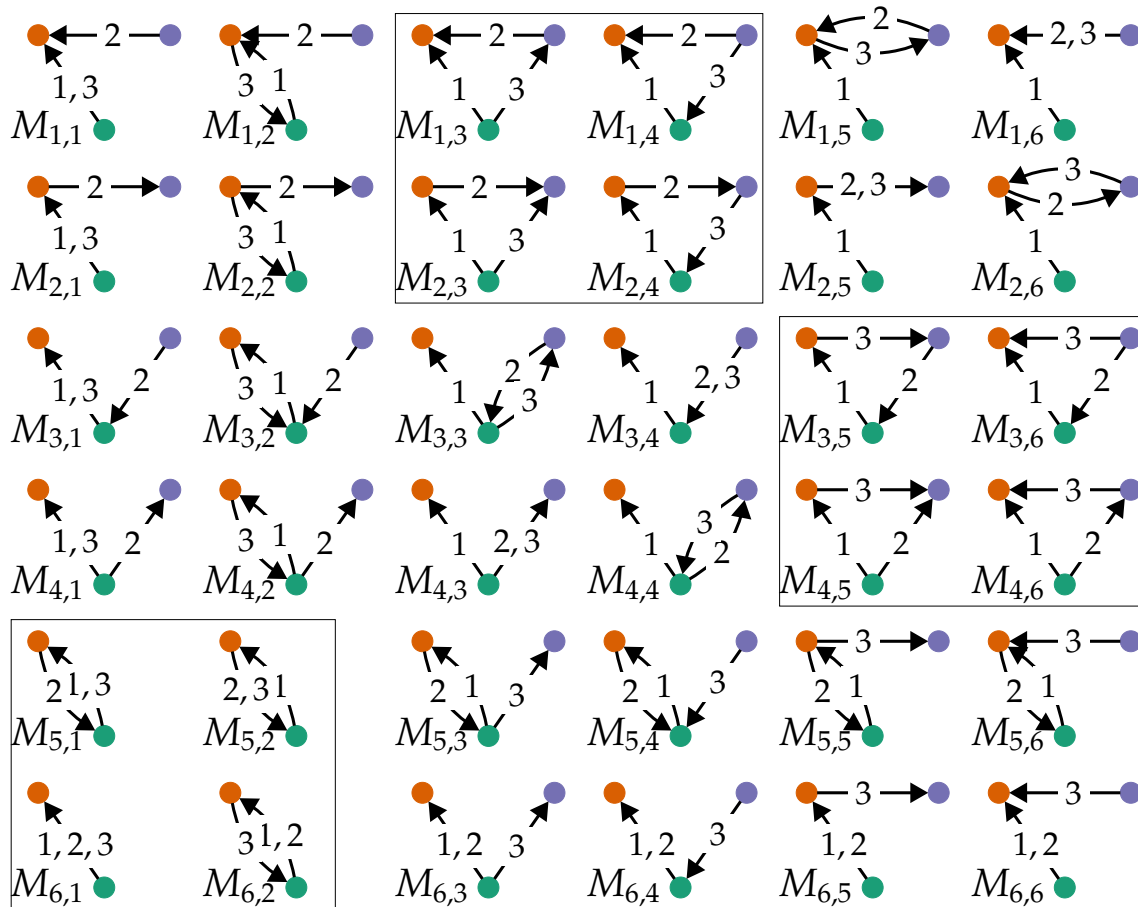


Figure 4.2 – All 2-node and 3-node, 3-edge δ -temporal motifs. The box in the bottom left contains the four 2-node motifs, and the two boxes in the top right contain the eight triangles. The 24 other motifs are stars. We index the 36 motifs $M_{i,j}$ by 6 rows and 6 columns. The first edge in each motif is from the green node to the orange node. The second edge is the same along each row, and the third edge is the same along each column. We develop fast algorithms for counting the number of instances of each of these motifs.

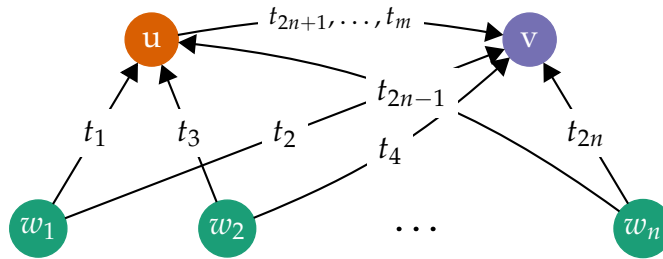


Figure 4.3 – Worst-case example for counting triangular motifs with Algorithm 5. When using the general algorithm (Algorithm 5) to count instances of motif $M_{4,5}$ (Figure 4.2) with $\delta = \infty$, we would need to analyze the edges t_{2n+1}, \dots, t_m for each of the n nodes w_1, \dots, w_n forming a triangle with nodes u and v .

General algorithm for triangle motifs. With triangle motifs, the induced graph H consists of 3 nodes and at least one directed edge between any pair of nodes (see Figure 4.2 for all eight of the 3-edge triangle motifs). The induced static graph H of M contains at least three and at most six static edges. A straightforward algorithm for counting l -edge triangle motifs in a temporal graph T is:

- i. Use a fast static graph triangle enumeration algorithm to find all triangles in the static graph G induced by T (using, e.g., one of the methods analyzed by Latapy [2008]).
- ii. For each triangle, merge all temporal edges from each pair of nodes to get a time-sorted list of edges. Use Algorithm 5 to count the number of instances of M .

This approach is problematic as the edges between a pair of nodes may participate in many triangles. Figure 4.3 shows a worst-case example for the motif $M = (w, u), (w, v), (u, v)$ with $\delta = \infty$. In the figure, the timestamps are ordered by their index. There are $m - 2n$ edges between u and v , and each of these edges forms an instance of M with every w_i . Thus, the overall worst-case running time of the algorithm is $O(\Delta_{\text{enum}} + \min(m\tau, mn))$, where Δ_{enum} is the time to enumerate the number of triangles τ in the static graph. (The mn running time comes from the case that each edge can participate in at most n triangles). In the following section, we devise an algorithm that significantly reduces the dependency on τ from linear to sub-linear (specifically, to $O(\Delta_{\text{enum}} + \min(m\sqrt{\tau}, mn))$) when there are $l = 3$ edges.

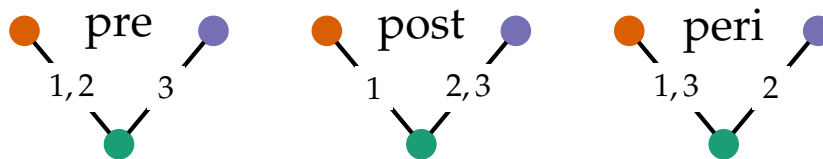


Figure 4.4 – The three classes of 3-node, 3-edge star temporal motifs. Each of the 3-edges in each class can be directed outward from or inward towards the center node. Thus, each class consists of 8 motifs, and there are 24 total 3-node, 3-edge star temporal motifs (see Figure 4.2 for illustrations of all of them).

4.3.2 Faster algorithms

The general counting algorithm from the previous section counts the number of instances of any k -node, l -edge δ -temporal motif, and is also optimal for 2-node motifs. However, the computational cost may be expensive for other motifs such as stars and triangles. We now develop specialized algorithms that count certain motif classes faster. Specifically, we design faster algorithms for counting all 3-node, 3-edge star and 3-node, 3-edge triangle motifs (Figure 4.2 illustrates these motifs). Our algorithm for stars is linear in the input size, so it is optimal up to constant factors.

Fast algorithm for 3-node, 3-edge stars. With 3-node, 3-edge star motifs, the drawback of the previous algorithmic approach is the need to loop over all pairs of neighbors given a center node. Instead, we will count all instances of star motifs for a given center node in just a single pass over the edges adjacent to the center node.

We use a dynamic programming approach for counting star motifs. First, note that every temporal edge in a star with center u is defined by

- i. a neighbor node,
- ii. a direction of the edge (outward from or inward toward u), and
- iii. the timestamp.

With this characterization, there are 3 classes of star motifs with 3 nodes and 3 edges (illustrated in Figure 4.4).

- i. “pre” – the first two edges contain node u and neighbor v , and the third edge contains node u and a different neighbor w .
- ii. “post” – the last two edges contain node u and neighbor w , and the first edge contains node u and a different neighbor v .
- iii. “peri” – the first and third edges contain node u and neighbor v , and the second edge contains node u and a different neighbor w .

Each class consists of $2^3 = 8$ motifs corresponding to the different combinations of the direction of the edges from u to the neighbors (see Figure 4.2, which shows all

of the $3 \cdot 8 = 24$ 3-node, 3-edge stars).

Now, suppose we process the time-ordered sequence of all edges containing the center node u . We maintain the following counters when processing an edge with timestamp t_j :

- $\text{pre_sum}[\text{dir1}, \text{dir2}]$ is the number of sequentially ordered pairs of edges in $[t_j - \delta, t_j)$ where the first edge points in direction dir1 and the second edge points in direction dir2 . We can think of a direction as being outward from u or inward toward u .
- $\text{post_sum}[\text{dir1}, \text{dir2}]$ is the number of sequentially ordered pairs of edges in $(t_j, t_j + \delta]$ where the first edge points in direction dir1 and the second edge points in direction dir2 .
- $\text{peri_sum}[\text{dir1}, \text{dir2}]$ is the number of pairs of edges where the first edge is in direction dir1 and occurred at time $t < t_j$, the second edge is in direction dir2 and occurred at time $t' > t_j$, and $t' - t \leq \delta$.

If we are currently processing an edge, the “pre” class gets $\text{pre_sum}[\text{dir1}, \text{dir2}]$ new motif instances for any choice of directions dir1 and dir2 (specifying the first two edge directions) and the current edge serves as the third edge in the motif (hence specifying the third edge direction). Similar updates are made with the $\text{post_sum}[\cdot, \cdot]$ and $\text{peri_sum}[\cdot, \cdot]$ counters, where the current edge serves as the first or second edge in the motif, respectively.

In order for our algorithm to be fast, we must be able to efficiently update these counters when processing edges. To aid in this, we introduce two additional counters:

- $\text{pre_nodes}[\text{dir}, v_i]$ is the number of times node v_i has appeared in an edge with u with direction dir in the time window $[t_j - \delta, t_j)$. We can think of the direction as being outward from u to v_i or inward from v_i toward u .
- $\text{post_nodes}[\text{dir}, v_i]$ is the number of times node v_i has appeared in an edge with u with direction dir in the time window $(t_j, t_j + \delta]$.

Following the ideas of Algorithm 5, it is easy to update these counters when we process a new edge. Consequently, $\text{pre_sum}[\cdot, \cdot]$, $\text{post_sum}[\cdot, \cdot]$, and $\text{peri_sum}[\cdot, \cdot]$ can be maintained when processing an edge with just a few simple primitives:

- $\text{Push}()$ and $\text{Pop}()$ update the counts for $\text{pre_nodes}[\cdot, \cdot]$, $\text{post_nodes}[\cdot, \cdot]$, $\text{pre_sum}[\cdot, \cdot]$ and $\text{post_sum}[\cdot, \cdot]$ when edges enter and leave the time windows $[t_j - \delta, t_j)$ and $(t_j, t_j + \delta]$.
- $\text{ProcessCurrent}()$ updates motif counts involving the current edge and updates the counter $\text{peri_sum}[\cdot, \cdot]$.

We describe the general procedure in Algorithm 6, which calls the subroutines $\text{Push}()$, $\text{Pop}()$, and $\text{ProcessCurrent}()$, and Algorithm 7 implements these subroutines. The $\text{pre_count}[\cdot, \cdot, \cdot]$, $\text{post_count}[\cdot, \cdot, \cdot]$, and $\text{peri_count}[\cdot, \cdot, \cdot]$ counters in Algorithm 7 maintain the counts of the three different classes of stars described

above. The edges input to each call of Algorithm 7 assumes that an edge consists of the following two pieces of information:

- i. the neighbor node nbr of u and
- ii. the direction dir of the edge.

The timestamps are all handled in Algorithm 6.

We have intentionally separated the logic of the *Push()*, *Pop()*, and *ProcessCurrent()* from Algorithm 6. The reason for this is that our fast 3-node, 3-edge triangle counting procedure follows the same logic of Algorithm 6, only with different implementations of these subroutines. We will get to this idea shortly.

Finally, we note that our counting scheme incorrectly includes instances of 2-node motifs such as $M = (u, v_i), (u, v_i), (u, v_i)$, but we can use our fast 2-node motif counting algorithm to account for this. Putting everything together, we have the following procedure:

- i. For each node u in the temporal graph T , get a time-ordered list of all edges containing u .
- ii. Use Algorithms 6 and 7 to count star motif instances.
- iii. For each neighbor v of a star center u , subtract the 2-node motif counts using Algorithm 5.

If the m temporal edges of T are time-sorted, the first step takes linear time. The second and third steps also run in linear time in the input size. Each edge is used in steps (ii) and (iii) exactly twice: once for each end point as the center node. Thus, the overall complexity of the algorithm is $O(m)$. This is optimal (linear in the size of the dataset). We also need $O(n)$ memory (in addition to storing the graph) to maintain the counters in Algorithm 6.

Algorithm 6 – Framework for fast counting of 3-node, 3-edge star and triangle temporal motifs. The fast star counting method (Algorithm 7) and triangle counting method (Algorithm 8) implement different versions of the *Push()*, *Pop()*, and *ProcessCurrent()* subroutines.

Input: Sequence of edges $(e_1 = (u_1, v_1), t_1), \dots, (e_L, t_L)$ with $t_1 < \dots < t_L$, time window δ

- 1 Initialize counters pre_nodes, post_nodes, peri_sum, pre_sum, post_sum
- 2 start \leftarrow 1, end \leftarrow 1
- 3 **for** $j = 1, \dots, L$:
- 4 */* Adjust counts in time window $[t_j - \delta, t_j]$ */*
- 5 **while** $t_{\text{start}} + \delta < t_j$ **do**
- 6 *Pop*(pre_nodes, pre_sum, e_{start})
- 7 start += 1
- 8 */* Adjust counts in time window $(t_j, t_j + \delta]$ */*
- 9 **while** $t_{\text{end}} \leq t_j + \delta$ **do**
- 10 *Push*(post_nodes, post_sum, e_{end})
- 11 end += 1
- 12 */* Handle current edge */*
- 13 *Pop*(post_nodes, post_sum, e_j)
- 14 *ProcessCurrent*(e_j)
- 15 *Push*(pre_nodes, pre_sum, e_j)

Algorithm 7 – Fast counting of 3-node, 3-edge temporal star motifs. These are implementations of the subroutines *Push()*, *Pop()*, and *ProcessCurrent()* used in Algorithm 6. Temporal edges are specified by a neighbor *nbr* (the neighbor of some given node *u*) and a direction *dir* (incoming to *u* or outgoing from *u*). The “:” notation represents a selection of all indices in an array.

```

1 Initialize counters pre_count, post_count, peri_count
2 Procedure Push(node_count, sum, e = (nbr, dir))
3   | sum[:, dir] += node_count[:, nbr]
4   | node_count[dir, nbr] += 1
5 Procedure Pop(node_count, sum, e = (nbr, dir))
6   | node_count[dir, nbr] -= 1
7   | sum[dir, :] -= node_count[:, nbr]
8 Procedure ProcessCurrent(e = (nbr, dir))
9   | peri_sum[:, dir] -= pre_nodes[:, nbr]
10  | pre_count[:, :, dir] += pre_sum[:, :]
11  | post_count[dir, :, :] += post_sum[:, :]
12  | peri_count[:, dir, :] += peri_sum[:, :]
13  | peri_sum[dir, :] += post_nodes[:, nbr]
14 return pre_count, post_count, peri_count

```

Fast algorithm for 3-edge triangle motifs. While our fast 3-node, 3-edge star counting routine relied on counting motif instances for all edges adjacent to a given *node*, our fast triangle algorithm is based on counting instances for all edges adjacent to a given *pair of nodes*. Specifically, given a pair of nodes u and v and a list of common neighbors w_1, \dots, w_d , we count the number of motif instances for triangles (w_i, u, v) , $i = 1, \dots, d$. Given all of the temporal edges in these d static triangles, the counting procedures are nearly identical to the case of stars. We use the same general counting method (Algorithm 6), but the behavior of the subroutines *Push()*, *Pop()*, and *ProcessCurrent()* depends on whether or not the edge is between u and v .

These methods are implemented in Algorithm 8. The input is a list of edges adjacent to a given pair of neighbors u and v , where each edge consists of three pieces of information:

- i. a neighbor node *nbr*,
- ii. an indicator of whether or not the node *nbr* connects to node u or node v ,
and
- iii. the direction *dir* of the edge.

The node counters (`pre_nodes[·, ·, ·]` and `post_nodes[·, ·, ·]`) in Algorithm 8 have an extra dimension compared to Algorithm 7 to indicate whether the counts correspond to edges containing node u or node v (denoted by “*u_or_v*”). For example, `pre_nodes[u, dir, w_i]` is the number of times node w_i has appeared in an edge with u with directed *dir* (incoming to u or outgoing from u) in the time window $[t_j - \delta, t_j)$. Similarly, the sum counters (`pre_sum[·, ·, ·]`, `peri_sum[·, ·, ·]` and `post_sum[·, ·, ·]`) have an extra dimension to denote if the first edge is incident on node u or node v . For example, `pre_sum[u, dir1, dir2]` is the number of sequentially ordered pairs of edges containing some node w_i in the time window $[t_j - \delta, t_j)$, where the first edge is adjacent to u in direction *dir1* and the second edge is adjacent to v in direction *dir2*.

Algorithm 8 – Fast temporal triangle motif counting subroutine. These are implementations of the subroutines *Push()*, *Pop()*, and *ProcessCurrent()* in Algorithm 6 for counting 3-edge triangle motifs containing a specified pair of nodes u and v . Temporal edges are specified by a neighbor nbr , a direction dir (incoming or outgoing), an indicator “ u_or_v ” denoting if the edge connects to u or v . The “ $:$ ” notation represents a selection of all indices in an array.

```

1 Initialize counter count
2 Procedure Push(node_count, sum,  $e = (nbr, dir, u\_or\_v)$ )
3   if  $nbr \in \{u, v\}$  then return
4   sum[1-u_or_v, :, dir] += node_count[1-u_or_v, :, nbr]
5   node_count[u_or_v, dir, nbr] += 1
6 Procedure Pop(node_count, sum,  $e = (nbr, dir, u\_or\_v)$ )
7   if  $nbr \in \{u, v\}$  then return
8   node_count[u_or_v, dir, nbr] -= 1
9   sum[u_or_v, dir, :] -= node_count[1-u_or_v, :, nbr]
10 Procedure ProcessCurrent( $e = (nbr, dir, u\_or\_v)$ )
11   if  $nbr \notin \{u, v\}$  then
12     peri_sum[1-u_or_v, :, dir] -= pre_nodes[1-u_or_v, :, nbr]
13     peri_sum[u_or_v, dir, :] += post_nodes[1-u_or_v, :, nbr]
14   else
15     u_to_v = (nbr == u) XOR dir
16     for  $0 \leq i, j, k \leq 1$  :
17       count[i, j, k] += peri_sum[j XOR u_to_v, i, k]
18                       + post_sum[i XOR u_to_v, j, 1 - k]
19                       + pre_sum[k XOR u_to_v, 1 - i, 1 - j]
20 /* count key map to Figure 4.2: */
21 /* [0,0,0]  $\mapsto M_{1,3}$ , [0,0,1]  $\mapsto M_{1,4}$ , [0,1,0]  $\mapsto M_{2,3}$ , [0,1,1]  $\mapsto M_{2,4}$  */
22 /* [1,0,0]  $\mapsto M_{3,5}$ , [1,0,1]  $\mapsto M_{3,6}$ , [1,1,0]  $\mapsto M_{4,5}$ , [1,1,1]  $\mapsto M_{4,6}$  */
23 return count

```

Algorithm 9 – Fast temporal triangle motif counting. This is a sketch of the fast algorithm for counting the number of 3-edge δ -temporal triangle motifs in a temporal graph T .

```

1 Enumerate all triangles in the undirected static graph  $G$  of  $T$ 
2  $\rho \leftarrow$  number of temporal edges on each static edge  $e$  in  $G$ 
3 foreach static triangle  $\Delta = (e_1, e_2, e_3)$  in  $G$  do
4    $e_{\max} = \arg \max_{e \in \Delta} \{\rho_e\}$ 
5   foreach  $e$  in  $\Delta$  do
6     /*  $e' \in \ell_e$  if  $e \in \Delta$  and  $\Delta$  assigned to  $e'$  */
7     Append  $e_{\max}$  to edge list  $\ell_e$ 
8 foreach temporal edge  $(e = (u, v), t)$  in time-sorted  $T$  do
9   foreach  $e'$  in  $\ell_e$  do
10    /*  $a_{e'}$  contains  $(e, t)$  if  $e$  belongs to a static triangle assigned to  $e'$  */
11    Append  $(e, t)$  to temporal-edge list  $a_{e'}$ 
12 foreach undirected edge  $e$  in  $G$  do
13   Update counts using Algorithm 8 with input  $a_e$ 

```

Recall that the problem with counting triangle motifs by the general framework in Algorithm 5 is that a pair of nodes with many edges might have to be counted for many triangles in the graph. However, with Algorithm 8, we can simultaneously count all triangles adjacent to a given pair of nodes. What remains is that we must assign each triangle in the static graph to a pair of nodes. Here, we propose to assign each triangle to the pair of nodes in that triangle containing the largest number of edges (this is sketched in Algorithm 9). The core idea of this assignment procedure is that we should simultaneously process as many triangles as possible for pairs of nodes with many edges. The following theorem says that this is faster than simply counting for each triangle (described in Section 4.3.1). Specifically, we reduce $O(\Delta_{\text{enum}} + \min(m\tau, mn))$ complexity to $O(\Delta_{\text{enum}} + \min(m\sqrt{\tau}, mn))$, where τ is the number of triangles in the graph.

Theorem 27. *In the worse case, Algorithm 9 runs in time $O(\Delta_{\text{enum}} + \min(m\sqrt{\tau}, mn))$ where Δ_{enum} is the time to enumerate all triangles in the static graph G , m is the total number of temporal edges, n is the number of nodes, and τ is the number of static triangles in G .*

Proof. Let ρ_e be the number of temporal edges along the static edge e , and let $z_e \geq 1$ be the number of times that timestamps along this static edge are used in a call to Algorithm 8 by Algorithm 9. Since Algorithm 8 runs in linear time in the number of edges in its input, the total running time is on the order of $\sum_e \rho_e z_e$. Each static edge appears in at most n triangles and has at most m temporal edges, so $\sum_e \rho_e z_e \leq mn$. We now consider the case when $\sqrt{\tau} \leq n$.

The ρ_e are fixed, and we wish to find the values of z_e that maximize the summation. Without loss of generality, write $\{\rho_e\}$ by $\rho_1 \geq \rho_2 \geq \dots \geq \rho_r$, where r is the number of static edges in the static graph induced by the temporal graph. Consequently, $z_i \leq i$, $i = 1, \dots, r$. There are τ static triangles, so Algorithm 8 will look at the timestamps along 3τ static edges. Thus, $\sum_i z_i \leq 3\tau$. The summation $\sum_{i=1}^r \rho_i z_i$ is maximized when $z_1 = 1, z_2 = 2$, and so on up to some index $J = O(\sqrt{\tau})$ for which $\sum_{i=1}^J z_i = \sum_{i=1}^J i = 3\tau$. Now given that the z_i are fixed and the ρ_i are ordered, the summation is maximized when $\rho_1 = \rho_2 = \dots = \rho_j = m/j$. In this case,

$$\sum_i \rho_i z_i = \sum_{i=1}^J \frac{m}{J} \cdot i = \frac{m}{J} \sum_{i=1}^J i = O\left(\frac{m}{J} \cdot J^2\right) = O(m\sqrt{\tau}).$$

□

We now show a worst-case example for the algorithm, which is illustrated in Figure 4.5. The graph consists of $k + 1$ nodes u, v_1, \dots, v_k , and the static edges are (v_i, v_j) , $1 \leq i < j \leq k$, and (v_r, u) , $1 \leq r \leq k$. Each edge (v_i, v_j) has a single temporal timestamp, and each edge (v_i, u) has an equal number of timestamps.

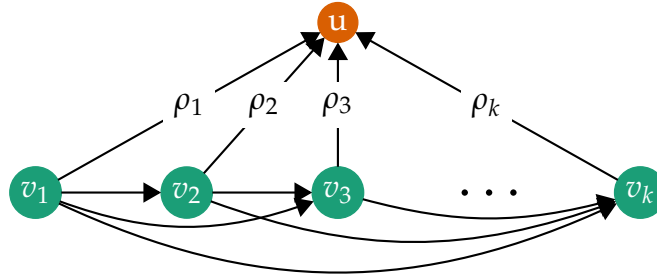


Figure 4.5 – Graph structure of worst-case instance for Algorithm 9. There is one temporal edge along each static edge (v_i, v_j) . Each static edge (v_i, u) contains an equal number of temporal edges, and the number of such temporal edges is strictly greater than 1. The ρ_i denote the ordering of edges in the proof of Theorem 27.

Without loss of generality, the first k edges in the ordering of the static edges is $\rho_1 = (v_1, u)$, $\rho_2 = (v_2, u)$, \dots , $\rho_k = (v_k, u)$ (the remainder of the ordering is arbitrary). Finally, suppose that we are counting the motif $M = (a, b), (a, c), (b, c)$.

In this case, the call to the Algorithm 8 subroutine for edge (v_r, u) ($1 \leq r \leq k$) in Algorithm 9 processes temporal edges along $(v_r, v_2), \dots, (v_r, v_k)$ and $(v_r, u), \dots, (v_k, u)$. Each temporal edge along (v_i, v_j) is processed only once, and the temporal edges along (v_r, u) are processed r times. Thus, the total number of temporal edges processed is

$$\binom{k}{2} + \sum_{r=1}^k r \frac{m - \binom{k}{2}}{k} = O(k^2) + O(mk) = O(\tau + m\sqrt{\tau}).$$

In this case, Algorithm 5 has the same asymptotic running time. Each of the $O(k^2)$ static triangles contains $O(m/k)$ temporal edges.

Finally, we emphasize that, if we ignore the pre-processing time in Algorithm 8, the amount of computation in Algorithm 8 is always less than the computation done by Algorithm 5 for counting triangles. Thus, regardless of the asymptotics, Algorithm 8 is still a strict improvement over the general algorithm.

4.4 Experiments

Next, we use our algorithms to reveal patterns in a variety of temporal network datasets. We find that the number of instances of various δ -temporal motifs reveal basic mechanisms of the networks.

Table 4.3 – Summary statistics of temporal network datasets. The time span is the time between latest and earliest timestamp available in the data. All timestamps are recorded at one second resolution.

dataset	# nodes	# static edges	# edges	time span (days)
EMAIL-EU	986	2.49K	332K	803
PHONECALL-EU	1.05M	2.74M	8.55M	7
SMS-A	44.1K	67.2K	545K	338
COLLEGEMSG	1.90K	20.3K	59.8K	193
STACKOVERFLOW	2.58M	34.9M	47.9M	2774
BITCOIN	24.6M	88.9M	123M	1811
FBWALL	45.8K	264K	856K	1560
WIKITALK	1.09M	3.13M	6.10M	2277
PHONECALL-ME	18.7M	360M	2.04B	364
SMS-ME	6.94M	51.5M	800M	89

4.4.1 Data

We gathered a variety of datasets in order to study the patterns of δ -temporal motifs in several domains. The datasets are described below and summary statistics are in Table 4.3. The time resolution of the edges in all datasets is one second.

- EMAIL-EU¹ is a collection of emails between members of a European research institution [Leskovec et al., 2007b]. An edge (u, v, t) signifies that person u sent person v an email at time t .
- PHONECALL-EU was constructed from telephone call records for a major European service provider. An edge (u, v, t) signifies that person u called person v starting at time t .
- SMS-A is a collection of short messaging service (SMS) texting records from a company charging account [Wu et al., 2010]. In this dataset, an edge (u, v, t) means that person u sent an SMS message to person v at time t .
- COLLEGEMSG is comprised of private messages sent on an online social network at the University of California, Irvine [Panzarasa et al., 2009]. Users could search the network for others and then initiate conversation based on profile information. An edge (u, v, t) means that user u sent a private message to user v at time t .
- STACKOVERFLOW is constructed from communication on Stack Overflow. On stack exchange web sites, users post questions and receive answers from

¹This is the same network as EMAIL-EU-CORE in Section 2.5.4, but we are now using the temporal information.

other users, and users may comment on both questions and answers. We derive a temporal network by creating an edge (u, v, t) if, at time t , user u : (1) posts an answer to user v 's question, (2) comments on user v 's question, or (3) comments on user v 's answer. We formed the temporal network from the entirety of Stack Overflow's history up to March 6, 2016.

- **BITCOIN** consists of all payments made with the decentralized digital currency and payment system Bitcoin up to October 19, 2014 [Kondor et al., 2014]. Nodes in the network correspond to Bitcoin addresses, and an individual may have several addresses. An edge (u, v, t) signifies that bitcoin was transferred from address u to address v at time t .
- **FBWALL** consists of wall posts between users on the social network Facebook located in the New Orleans region [Viswanath et al., 2009]. Any friend of a given user can see all posts on that user's wall, so communication is public among friends. An edge (u, v, t) means that user u posted on user v 's wall at time t .
- **WIKITALK** represents edits on user talk pages on Wikipedia [Leskovec et al., 2010b]. An edge (u, v, t) means that user u edited user v 's talk page at time t .
- **PHONECALL-ME** is constructed from phone call records of a large telecommunications service provider in the Middle East. An edge (u, v, t) means that user u initiated a call to user v at time t .
- **SMS-ME** is constructed from SMS texting records from the same telecommunications service provider in the Middle East. An edge (u, v, t) means that user u sent an SMS message to user v at time t .

4.4.2 Empirical observations of motif counts

We first examine the distribution of 2- and 3-node, 3-edge motif instance counts from 8 of the datasets described in Section 4.4.1 with $\delta = 1$ hour (Figure 4.6). We choose 1 hour for the time window as this is close to the median time for a node to take part in three edges in most of our datasets. We make a few empirical observations uniquely available due to temporal motifs and provide possible explanations for these observations.

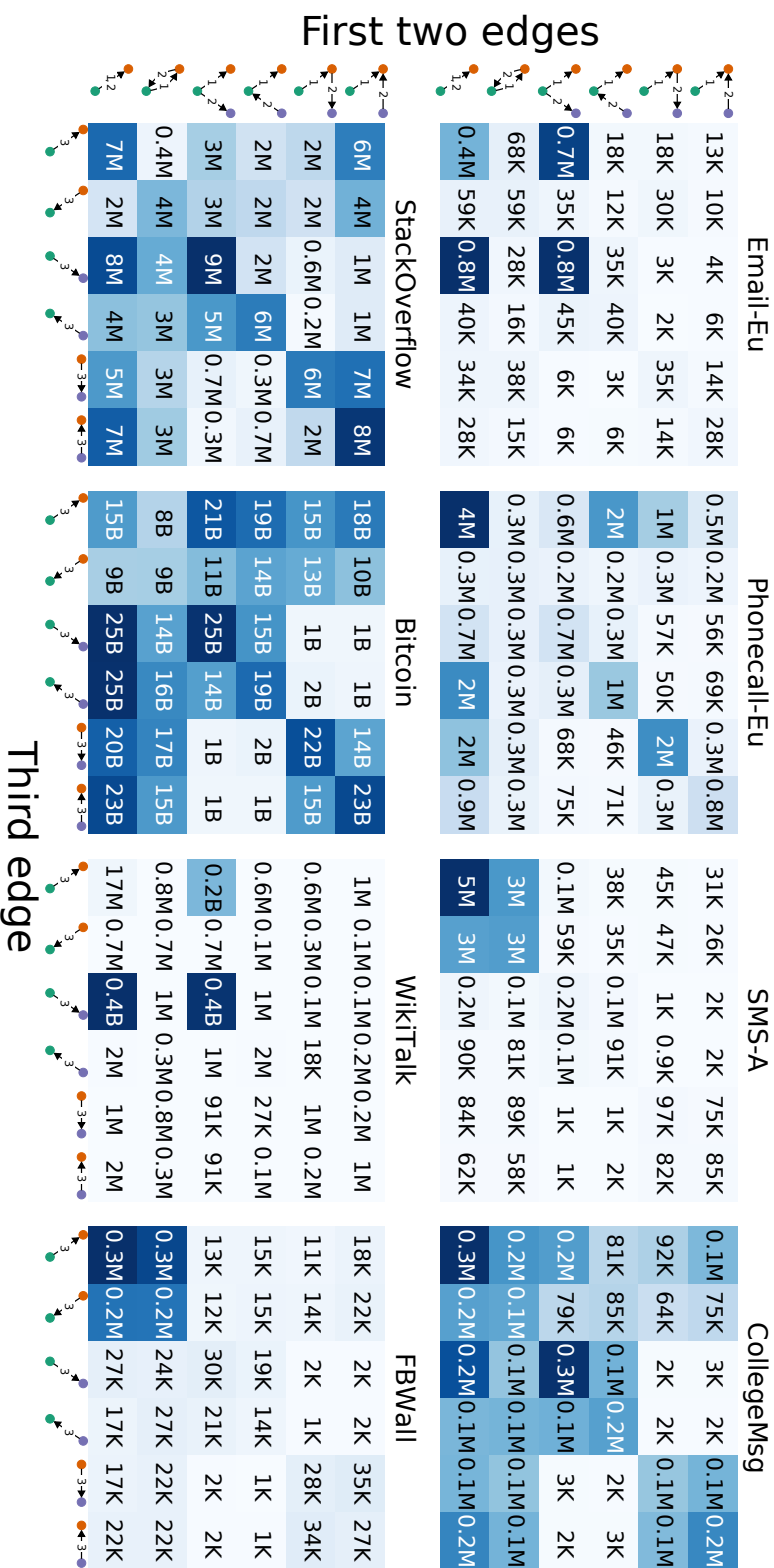


Figure 4.6 – Counts of instances of all 2- and 3-node, 3-edge δ -temporal motifs with $\delta = 1$ hour. For each dataset, counts in the i th row and j th column is the number of instances of motif $M_{i,j}$ (see Figure 4.2); this motif is the union of the two edges in the row label and the edge in the column label. For example, there are 0.7 million instances of motif $M_{4,1}$ in the Email-Eu dataset. The color for the count of motif $M_{i,j}$ indicates the fraction over all $M_{i,j}$ on a linear scale—darker blue means a higher count.

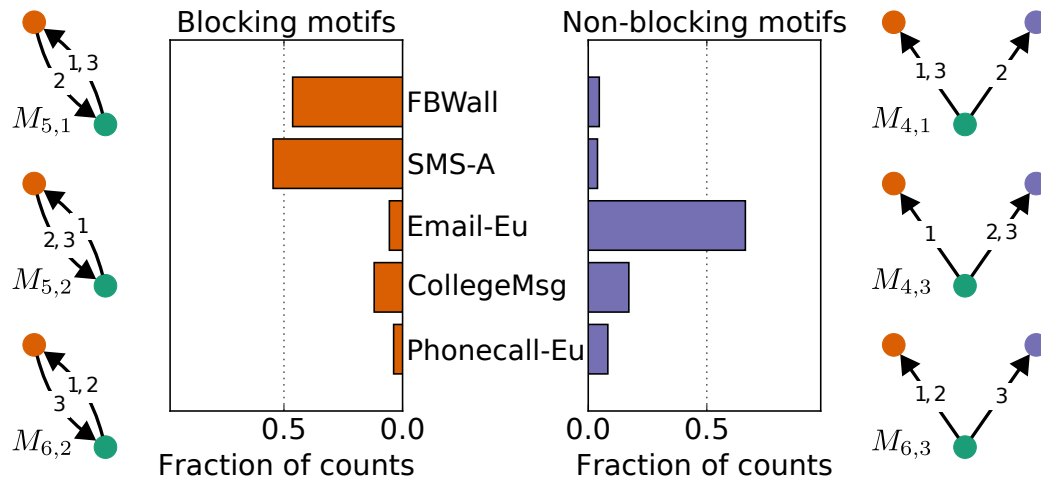


Figure 4.7 – *Blocking and non-blocking behavior.* Fraction of the 2- and 3-node, 3-edge δ -temporal motif instance counts that correspond to two groups of motifs ($\delta = 1$ hour). Motifs on the left capture “blocking” behavior, common in SMS-A and FBWALL posting, where most communication is one-to-one at this time scale. Motifs on the right exhibit “non-blocking” behavior, common in EMAIL-EU, where broadcast patterns are common. COLLEGE MSG contains a mixture of the two behaviors at this time scale.

Blocking communication. If an individual typically waits for a reply from one individual before proceeding to communicate with another individual, we consider it a *blocking* form of communication. A typical conversation between two individuals characterized by fast exchanges happening back and forth is blocking as it requires complete attention of both individuals. We capture this behavior in the “blocking motifs” $M_{5,1}$, $M_{5,2}$ and $M_{6,2}$, which contain 3 edges between two nodes with at least one edge in either direction (Figure 4.7, left). However, if the reply doesn’t arrive soon, we might expect the individual to communicate with others without waiting for a reply from the first individual. This is a non-blocking form of communication and is captured by the “non-blocking motifs” $M_{4,1}$, $M_{4,3}$ and $M_{6,3}$ having edges originating from the same source but directed to different destinations (Figure 4.7, right)

The fractions of counts corresponding to the blocking and non-blocking motifs out of the counts for all 36 motifs in Figure 4.2 uncover several interesting characteristics in communication networks ($\delta = 1$ hour; see Figure 4.7). In FBWALL and SMS-A, blocking communication is vastly more common, while in EMAIL-EU non-blocking communication is prevalent. Email is not a dynamic method of communication and replies within an hour are rare. Thus, we would expect non-blocking behavior. Interestingly, the COLLEGE MSG dataset shows both behaviors as

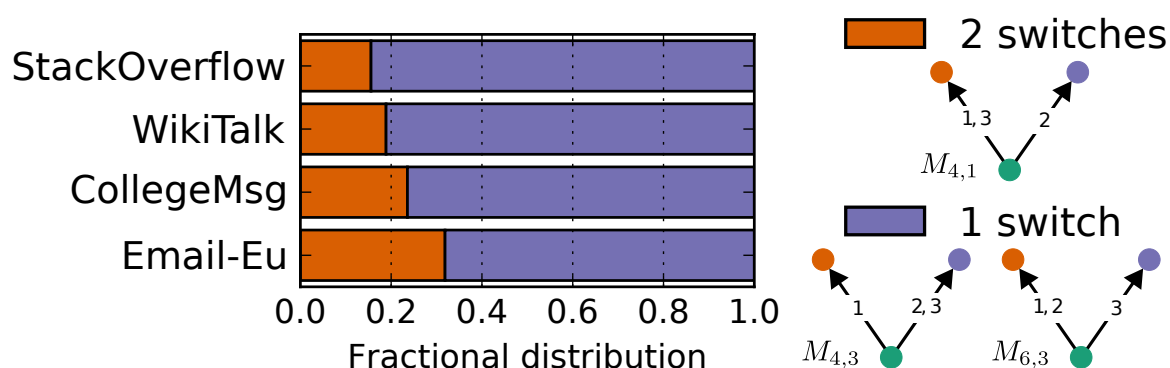


Figure 4.8 – Switching behavior in non-blocking motifs. A “switch” occurs with two temporal edges (u, v, t_1) and (u, w, t_2) , $t_1 < t_2$, where node u switches an outgoing neighbor. Switching is least common on Stack Overflow and most common in email. We also see differences in switching behavior as we vary time scales in the COLLEGMMSG dataset (see Figure 4.11).

we might expect individuals to engage in multiple conversations simultaneously. In complete contrast, the PHONECALL-EU dataset shows neither behavior. A simple explanation is that a single edge (a phone call) captures an entire conversation and hence blocking behavior does not emerge.

Cost of switching. Amongst the non-blocking motifs discussed above, $M_{4,1}$ captures two consecutive “switches” between pairs of nodes whereas $M_{4,3}$ and $M_{6,3}$ each have a single switch (Figure 4.8, right). In communication networks, a switch corresponds to a change in message destination for a node u . Prevalence of $M_{4,1}$ indicates a lower cost of switching targets, whereas prevalence of the other two motifs are indicative of a higher cost. We observe in Figure 4.8 that the ratio of 2-switch to 1-switch motif counts is the least in STACKOVERFLOW, followed by WIKITALK, COLLEGMMSG and then EMAIL-EU. On Stack Overflow and Wikipedia talk pages, there is a high cost to switch targets because of peer engagement and depth of discussion. On the other hand, in the COLLEGMMSG dataset there is less cost to switch because it lacks depth of discussion within the time frame of $\delta = 1$ hour. In EMAIL-EU, there is almost no peer engagement, and cost of switching is negligible.

Cycles in Bitcoin. Of the eight 3-edge triangle motifs, $M_{2,4}$ and $M_{3,5}$ are cyclic, i.e., the target of each edge serves as the source of another edge.² We observe in Figure 4.9 that the fraction of triangles that are cyclic is much higher in BITCOIN compared to any other dataset. This can be attributed to the transactional nature

²By “cyclic” we do not mean that the temporal edges must form a cycle. Rather, the multigraph K in the formal motif definition is a cycle.

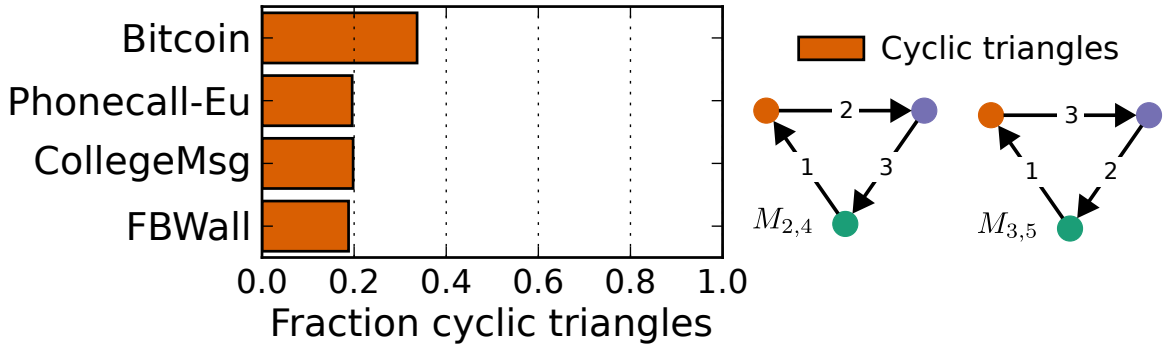


Figure 4.9 – Cyclic temporal triangles. Fraction of 3-edge δ -temporal triangle motif counts ($\delta = 1$ hour) corresponding to cyclic triangles (right) in the four datasets for which this fraction is the largest. BITCOIN has a much higher fraction compared to all other datasets.

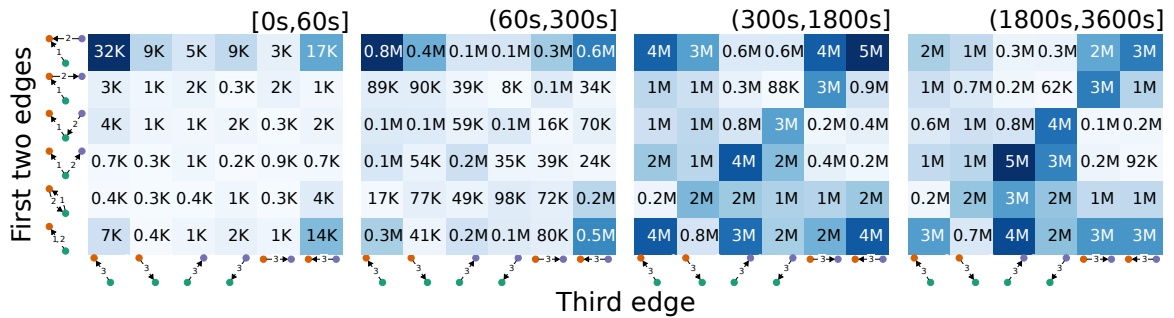


Figure 4.10 – Counts for all 2- and 3-node, 3-edge δ -temporal motifs in four time intervals for the STACKOVERFLOW dataset. For each interval, the count in the i th row and j th column is the number of instances of motif $M_{i,j}$ (see Figure 4.2).

of BITCOIN where the total amount of bitcoin is limited. Since remittance (outgoing edges) is typically associated with earnings (incoming edges), we should expect cyclic behavior.

Motif counts at varying time scales. We now explore how motif counts change at different time scales. For the STACKOVERFLOW dataset we counted the number of instances of 2- and 3-node, 3-edge δ -temporal motifs for $\delta = 60, 300, 1800,$ and 3600 seconds (Figure 4.10). These counts determine the number of motifs that completed in the intervals $[0, 60], (60, 300], (300, 1800s],$ and $(1800, 3600]$ seconds (e.g., subtracting 60 second counts from 300 second counts gives the interval $(60, 300]$). Observations at smaller timescales reveal phenomenon which start to get eclipsed at larger timescales. For instance, on short time scales, motif $M_{1,1}$ (Figure 4.10, top-left corner) is quite common. We suspect this arises from

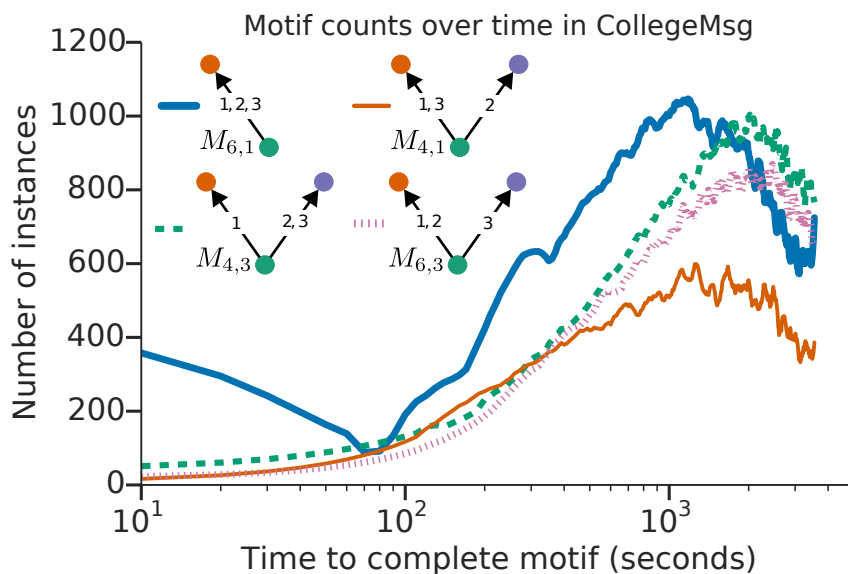


Figure 4.11 – Motif counts over various time scales in the COLLEGEMSG dataset. The four motifs correspond to all motifs where a node sends 3 outgoing messages to 1 or 2 neighbors. At early time scales, one-to-one communication is the most common ($M_{1,1}$, blue curve). At later time scales, the motif with two switches ($M_{4,1}$, orange curve) is less common than the motifs with one or two switches.

multiple, quick comments on the original question, so the original poster receives many incoming edges. At larger time scales, this behavior is still frequent but relatively less so. Now let us compare counts for $M_{1,5}$, $M_{1,6}$, $M_{2,5}$, $M_{2,6}$ (the four in the top right corner) with counts for $M_{3,3}$, $M_{3,4}$, $M_{4,3}$, $M_{4,4}$ (the four in the center). The former counts likely correspond to conversations with the original poster while the latter are constructed by the same user interacting with multiple questions. Between 300 and 1800 seconds (5 to 30 minutes), the former counts are relatively more common while the latter counts only become more common after 1800 seconds. A possible explanation is that the typical length of discussions on a post is about 30 minutes, and later on, users answer other questions.

Next, we examine messaging behavior in the COLLEGEMSG dataset at fine-grained time intervals. We counted the number of motifs consisting of a single node sending three outgoing messages to one or two neighbors (motifs $M_{6,1}$, $M_{6,3}$, $M_{4,1}$, and $M_{4,3}$) in the time bins $[10(i-1), 10i)$ seconds, $i = 1, \dots, 500$ (Figure 4.11). We first notice that at small time scales, the motif consisting of three edges to a single neighbor ($M_{6,1}$) occurs frequently. This pattern could emerge from a succession of quick introductory messages. Overall, motif counts increase from roughly 1 minute to 20 minutes and then decline. After 5 minutes, counts for

Table 4.4 – Time to count the eight 3-edge δ -temporal triangle motifs. We compare the time of our general counting method (Algorithm 5) and our fast counting method (Algorithm 9). The fast algorithm provides significant speedups for all datasets. In these experiments, $\delta = 3600$, but this does not significantly affect the running times. All times are listed in seconds.

dataset	# static triangles	Algorithm 5	Algorithm 9	speedup
WIKITALK	8.11M	51.1	26.6	1.92x
BITCOIN	73.1M	27.3K	483	56.5x
SMS-ME	78.0M	2.54K	1.11K	2.28x
STACKOVERFLOW	114M	783	606	1.29x
PHONECALL-ME	667M	12.2K	8.59K	1.42x

the three motifs with one switch in the target ($M_{6,1}$, $M_{6,3}$, and $M_{4,3}$) grow at a faster rate than the counts for the motif with two switches ($M_{4,1}$). As mentioned above, this pattern could emerge from a tendency to send several messages in one conversation before switching to a conversation with another friend.

4.4.3 Algorithm scalability

Finally, we performed scalability experiments of our algorithms. All algorithms were implemented in C++, and all experiments ran using a single thread of a 2.4GHz Intel Xeon E7-4870 processor. We did not measure the time to load datasets into memory, but our timings include all pre-processing time needed by the algorithms (e.g., the triangle counting algorithms first find triangles in the static graph). We emphasize that our implementation is single threaded, and there is ample room for parallelism in our algorithms.

First, we used both the general counting method (Algorithm 5) and the fast counting method (Algorithm 9) to count the number of all eight 3-edge δ -temporal triangle motifs in our datasets ($\delta = 1$ hour). Table 4.4 reports the running times of the algorithms for all datasets with at least one million triangles in the static graph. For all of these datasets, our fast temporal triangle counting algorithm provides significant performance gains over the general counting method, ranging between a 1.29x and a 56.5x speedup. The gains of the fast algorithm are the largest for BITCOIN, which is due to some pairs of nodes having many edges between them and also participating in many triangles.

Second, we measured the time to count various 3-edge δ -temporal motifs in our largest dataset, PHONECALL-ME. Specifically, we measured the time to compute (1) 2-node motifs, (2) 3-node stars, and (3) triangles on the first k million edges in the

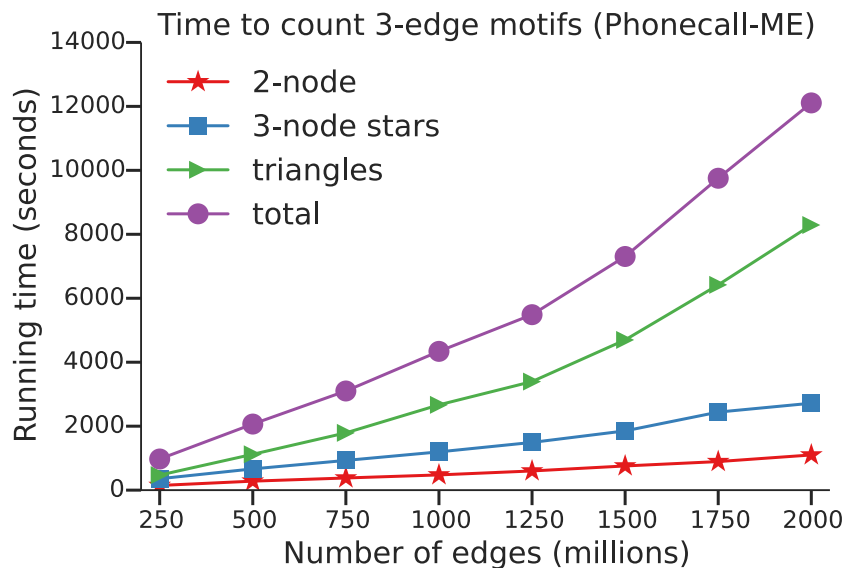


Figure 4.12 – Scalability of temporal motif counting in. The plot reports the time to count 3-edge motifs on the first k temporal million edges in PHONECALL-ME as a function of k . The time to count star and edge patterns scales linearly with the number of edges in correspondence with our computational complexity analysis.

dataset for $k = 250, 500, \dots, 2000$ (Figure 4.12). The time to compute the 2-node, 3-edge motifs and the 3-node, 3-edge stars scales linearly, as expected from our complexity analysis. The time to count triangle motifs grows superlinearly and becomes the dominant cost when there is a large number of edges. For practical purposes, the running times are quite modest. With two billion edges, our methods take less than 3.5 hours to complete (executing sequentially).

4.5 Prior definitions of temporal motifs and other related work

There are several studies on pattern formation in growing networks where one only considers the addition of edges to a static graph over time. In this context, motif-like patterns have been used to create evolution rules that govern the ways that networks develop [Berlingerio et al., 2009; Ugander et al., 2013]. The way we consider ordering of temporal edges in our definition of δ -temporal motifs is similar in spirit. There are also several analyses on the formation of triangles in a variety of social networks [Huang et al., 2014; Kossinets and Watts, 2006;

Leskovec et al., 2010a; Zignani et al., 2014]. In contrast, in the temporal graphs we study here, three nodes may form a triangle several times. On the algorithmic side, a large amount of research has been devoted simply to exact counting and enumeration of triangles in undirected static graphs (see, e.g., [Latapy, 2008]) and to approximating the total number of triangles in static graphs [Ahmed et al., 2015; De Stefani et al., 2016; Seshadhri et al., 2014].

There are some definitions of temporal motifs for sequences of snapshot graphs [Jin et al., 2007; Lahiri and Berger-Wolf, 2007; Zhang et al., 2014b], but we focus our discussion here on alternative definitions that target temporal graphs in the way that we defined them in Definition 23. To understand prior definitions of temporal motifs, we need one more definition. We say that two temporal edges (u, v, t_1) and (w, x, t_2) are ω -adjacent if $|t_2 - t_1| \leq \omega$ and (u, v) and (w, x) share at least one node (i.e., $|\{u, v, w, x\}| < 4$). With this connectivity, we can partition the temporal edges of a temporal graph into ω -connected components where every edge in a component is able to reach every other by following ω -adjacent connections.

Zhao et al. [2010] induce static graphs from ω -connected components and then use the standard static graph motifs that we used in Chapter 2. This definition is used to analyze the structure of communication data. Gurukar et al. [2015]; Hulovatyy et al. [2015] both propose additional equivalent definitions of temporal motifs, and the definition is similar to ours. The motifs consist of ordered directed multigraphs and a time span ω . An instance of the motif is a subset of events that match the ordered multigraph, where every sequential edge in the ordering is ω -connected. While the definition is similar, Gurukar et al. [2015] do not have theoretical guarantees on running time and Hulovatyy et al. [2015] have running times that are as expensive as temporal motif enumeration.

Kovanen et al. [2011] use the same notion of ω -adjacency of events with an ordered multigraph but further restrict motif instances to cases where the events are consecutive for the nodes. In other words, in the time spanned by the motif instance, there can be no other temporal edge adjacent to one of the nodes. While this is a severe restriction, a major benefit of this definition is that it permits fast count algorithms. For example, triangle motifs may be enumerated in linear time. This motif definition has been used to analyze phone call records [Kovanen et al., 2013] and Wikipedia edits [Jurgens and Lu, 2012]. While Kovanen et al. [2011] present their work for directed temporal graphs, the ideas have been extended to undirected temporal networks and applied to the analysis of proximity and contact networks [Zhang et al., 2015].

Our definition of temporal motifs is a bit simpler by throwing out any requirements for ω -adjacency of edges. The time duration is modeled at the level of the motif, rather than at the level of individual edges. This keeps with the spirit of

higher-order modeling and analysis.

We also note that Viard et al. [2016] developed algorithms for counting what they call maximal Δ -cliques. Their definition requires that all pairs of nodes in a clique interact at least once in sub-intervals of size Δ .

4.6 Discussion

We have developed δ -temporal network motifs as a tool for analyzing temporal networks. We introduced a general framework for counting instances of any temporal motif as well as faster algorithms for certain classes of motifs and found that motif counts reveal key structural patterns in a variety of temporal network datasets. Our fast algorithms are designed for 3-node, 3-edge star and triangle motifs. We expect that the same general techniques can be used to count more complex temporal motifs. There is also a host of theoretical questions in this area for lower bounds on temporal motif counting.

Our fast algorithms only *count* the number of instances of motifs rather than *enumerate* the instances, and this was crucial to the design of the algorithms. Temporal motif enumeration algorithms provide an additional algorithmic design challenge. The concept of avoiding enumeration has also been used to accelerate static motif counting [Pinar et al., 2017]. A general disadvantage of counting algorithms is that such statistics cannot immediately be used to equip nodes or edges with features, on which subsequent analysis can be performed. However, there are still many features that we can use from the fast algorithms developed here. When using the general algorithm, we can still count how often a node u participates in a given position in a given motif. For example, we can easily count in how many motif instances of motif $M_{5,1}$, $M_{5,2}$, $M_{6,1}$, and $M_{6,2}$ node u serves as the source node (the green node in Figure 4.2). With our fast 3-node, 3-edge star counting algorithms, we can compute in how many motif instances a given node u serves as the center for all 24 of these motifs. Our fast 3-edge triangle counting algorithm are not amenable to per-node statistics. However, one could use the general algorithm for this purpose.

Although we did not run parallel performance experiments, there is ample room for parallelism in these algorithms:

- The general algorithm parallelizes over all instances of the induced static motif.
- The fast star counting algorithm parallelizes over all center nodes u .
- The fast triangle counting algorithm parallelizes over all edges (u, v) that are assigned at least one triangle.

Motif counts can also be measured with respect to a null model [Kovanen

et al., 2011; Milo et al., 2002] and such analysis may yield additional discoveries. Importantly, our algorithms will speed up such computations, which use motif counts from many random instances of a generative null model.

Finally, our definition of a temporal network motif and the associated counting algorithms only rely on an *ordering* on the edges in the temporal graph and some way of measuring the *distance* between edges in the ordering. While temporal network data is natural, our data does not necessarily have to come from time. We can count motifs for any collection of edges when each edge is equipped with a (unique) element from an ordered field. This could lead to new applications in future work.

Bibliography

- [Aberger et al., 2016] C. R. ABERGER, S. TU, K. OLUKOTUN, and C. RÉ. *Emptyheaded: A relational engine for graph processing*. In *Proceedings of the International Conference on Management of Data*, pp. 431–446. 2016.
- [Agarwal et al., 2006] S. AGARWAL, K. BRANSON, and S. BELONGIE. *Higher order learning with graphs*. In *Proceedings of the International Conference on Machine Learning*, pp. 17–24. 2006.
- [Ahmed et al., 2015] N. K. AHMED, J. NEVILLE, R. A. ROSSI, and N. DUFFIELD. *Efficient graphlet counting for large networks*. In *IEEE International Conference on Data Mining*, pp. 1–10. 2015.
- [Albert et al., 1999] R. ALBERT, H. JEONG, and A.-L. BARABÁSI. *Internet: Diameter of the world-wide web*. *Nature*, 401 (6749), pp. 130–131, 1999.
- [Alon, 1986] N. ALON. *Eigenvalues and expanders*. *Combinatorica*, 6 (2), pp. 83–96, 1986.
- [Alon and Milman, 1985] N. ALON and V. D. MILMAN. λ_1 , *isoperimetric inequalities for graphs, and superconcentrators*. *Journal of Combinatorial Theory, Series B*, 38 (1), pp. 73–88, 1985.
- [Alon, 2007] U. ALON. *Network motifs: theory and experimental approaches*. *Nature Reviews Genetics*, 8 (6), pp. 450–461, 2007.
- [Andersen et al., 2006] R. ANDERSEN, F. CHUNG, and K. LANG. *Local graph partitioning using pagerank vectors*. In *Proceedings of the IEEE Symposium on Foundations of Computer Science*, pp. 475–486. 2006.
- [Andersen et al., 2008] ———. *Local partitioning for directed graphs using pagerank*. *Internet Mathematics*, 5 (1-2), pp. 3–22, 2008.
- [Andrade et al., 2006] R. F. ANDRADE, J. G. MIRANDA, and T. P. LOBÃO. *Neighborhood properties of complex networks*. *Physical Review E*, 73 (4), p. 046101, 2006.
- [Angelini et al., 2015] M. C. ANGELINI, F. CALTAGIRONE, F. KRZAKALA, and L. ZDEBOROVÁ. *Spectral detection on sparse hypergraphs*. In *Proceedings of the Allerton Conference on Communication, Control, and Computing*, pp. 66–73. 2015.
- [Angulo et al., 2015] M. T. ANGULO, Y.-Y. LIU, and J.-J. SLOTINE. *Network motifs emerge from interconnections that favour stability*. *Nature Physics*, 11 (10), pp. 848–852, 2015.
- [Araujo et al., 2014] M. ARAUJO, S. PAPANIMITRIOU, S. GÜNNEMANN, C. FALOUTSOS, P. BASU, A. SWAMI, E. E. PAPALEXAKIS, and D. KOUTRA. *Com2: fast automatic discovery of temporal ('coment') communities*. In *Proceedings of the Pacific-Asia Conference on Knowledge Discovery and Data Mining*, pp. 271–283. 2014.
- [Arenas et al., 2008] A. ARENAS, A. FERNANDEZ, S. FORTUNATO, and S. GÓMEZ. *Motif-based communities in complex networks*. *Journal of Physics A: Mathematical and Theoretical*, 41 (22), p. 224001, 2008.
- [Arora et al., 2009] S. ARORA, S. RAO, and U. VAZIRANI. *Expander flows, geometric embeddings and graph partitioning*. *Journal of the ACM*, 56 (2), p. 5, 2009.

- [Azad et al., 2015] A. AZAD, A. BULUÇ, and J. R. GILBERT. *Parallel triangle counting and enumeration using matrix algebra*. In *Proceedings of the IPDPSW Workshop on Graph Algorithm Building Blocks*, pp. 804–811. 2015.
- [Backstrom et al., 2006] L. BACKSTROM, D. HUTTENLOCHER, J. KLEINBERG, and X. LAN. *Group formation in large social networks: membership, growth, and evolution*. In *Proceedings of the ACM SIGKDD International Conference on Knowledge Discovery and Data Mining*, pp. 44–54. 2006.
- [Barabasi, 2005] A.-L. BARABASI. *The origin of bursts and heavy tails in human dynamics*. *Nature*, 435 (7039), pp. 207–211, 2005.
- [Barabási and Albert, 1999] A.-L. BARABÁSI and R. ALBERT. *Emergence of scaling in random networks*. *Science*, 286 (5439), pp. 509–512, 1999.
- [Barrat and Weigt, 2000] A. BARRAT and M. WEIGT. *On the properties of small-world network models*. *The European Physical Journal B: Condensed Matter and Complex Systems*, 13 (3), pp. 547–560, 2000.
- [Bascompte, 2009] J. BASCOMPTE. *Disentangling the web of life*. *Science*, 325 (5939), pp. 416–419, 2009.
- [Bascompte et al., 2005] J. BASCOMPTE, C. J. MELIÁN, and E. SALA. *Interaction strength combinations and the overfishing of a marine food web*. *Proceedings of the National Academy of Sciences*, 102 (15), pp. 5443–5447, 2005.
- [Bavelas, 1950] A. BAVELAS. *Communication patterns in task-oriented groups*. *The Journal of the Acoustical Society of America*, 22 (6), pp. 725–730, 1950.
- [Benson et al., 2015] A. R. BENSON, D. F. GLEICH, and J. LESKOVEC. *Tensor spectral clustering for partitioning higher-order network structures*. In *Proceedings of the SIAM International Conference on Data Mining*, pp. 118–126. 2015.
- [Benson et al., 2016] ———. *Higher-order organization of complex networks*. *Science*, 353 (6295), pp. 163–166, 2016.
- [Benson et al., 2017] A. R. BENSON, D. F. GLEICH, and L.-H. LIM. *The spacey random walk: A stochastic process for higher-order data*. *SIAM Review*, 59 (2), pp. 321–345, 2017.
- [Benson et al., 2014] A. R. BENSON, C. RIQUELME, and S. SCHMIT. *Learning multifractal structure in large networks*. In *Proceedings of the ACM SIGKDD International Conference on Knowledge Discovery and Data Mining*, pp. 1326–1335. 2014.
- [Berlingerio et al., 2009] M. BERLINGERIO, F. BONCHI, B. BRINGMANN, and A. GIONIS. *Mining graph evolution rules*. *Machine Learning and Knowledge Discovery in Databases*, pp. 115–130, 2009.
- [Berry et al., 2014] J. W. BERRY, L. K. FOSTVEDT, D. J. NORDMAN, C. A. PHILLIPS, C. SESHADHRI, and A. G. WILSON. *Why do simple algorithms for triangle enumeration work in the real world?* In *Proceedings of the Conference on Innovations in Theoretical Computer Science*, pp. 225–234. 2014.
- [Bhadra and Ferreira, 2003] S. BHADRA and A. FERREIRA. *Complexity of connected components in evolving graphs and the computation of multicast trees in dynamic networks*. In *Proceedings of the International Conference on Ad-Hoc Networks and Wireless*, pp. 259–270. 2003.
- [Bickel et al., 2011] P. J. BICKEL, A. CHEN, E. LEVINA, ET AL. *The method of moments and degree distributions for network models*. *The Annals of Statistics*, 39 (5), pp. 2280–2301, 2011.
- [Blondel et al., 2008] V. D. BLONDEL, J.-L. GUILLAUME, R. LAMBIOTTE, and E. LEFEBVRE. *Fast unfolding of communities in large networks*. *Journal of Statistical Mechanics: Theory and Experiment*, 2008 (10), p. P10008, 2008.
- [Boldi et al., 2004] P. BOLDI, B. CODENOTTI, M. SANTINI, and S. VIGNA. *Ubicrawler: A scalable fully distributed web crawler*. *Software: Practice and Experience*, 34 (8), pp. 711–726, 2004.

- [Boldi et al., 2014] P. BOLDI, A. MARINO, M. SANTINI, and S. VIGNA. *Bubing: Massive crawling for the masses*. In *Proceedings of the International Conference on World Wide Web*, pp. 227–228. 2014.
- [Boldi et al., 2011] P. BOLDI, M. ROSA, M. SANTINI, and S. VIGNA. *Layered label propagation: A multiresolution coordinate-free ordering for compressing social networks*. In *Proceedings of the International Conference on World Wide Web*, pp. 587–596. 2011.
- [Boldi and Vigna, 2004] P. BOLDI and S. VIGNA. *The WebGraph framework I: Compression techniques*. In *Proceedings of the International Conference on World Wide Web*, pp. 595–602. 2004.
- [Boley, 1998] D. BOLEY. *Principal direction divisive partitioning*. *Data Mining and Knowledge Discovery*, 2 (4), pp. 325–344. 1998.
- [Boley et al., 2011] D. BOLEY, G. RANJAN, and Z.-L. ZHANG. *Commuter times for a directed graph using an asymmetric Laplacian*. *Linear Algebra and its Applications*, 435 (2), pp. 224–242. 2011.
- [Bollobás, 1980] B. BOLLOBÁS. *A probabilistic proof of an asymptotic formula for the number of labelled regular graphs*. *European Journal of Combinatorics*, 1 (4), pp. 311–316. 1980.
- [Bollobás and Erdős, 1976] B. BOLLOBÁS and P. ERDÖS. *Cliques in random graphs*. In *Mathematical Proceedings of the Cambridge Philosophical Society*, pp. 419–427. 1976.
- [Bonato et al., 2014] A. BONATO, D. F. GLEICH, M. KIM, D. MITSCHKE, P. PRAËT, Y. TIAN, and S. J. YOUNG. *Dimensionality of social networks using motifs and eigenvalues*. *PLOS ONE*, 9 (9), p. e106052. 2014.
- [Bressan et al., 2017] M. BRESSAN, F. CHIERICHETTI, R. KUMAR, S. LEUCCI, and A. PANCONESI. *Counting graphlets: Space vs time*. In *Proceedings of the ACM International Conference on Web Search and Data Mining*, pp. 557–566. 2017.
- [Caldarelli et al., 2004] G. CALDARELLI, R. PASTOR-SATORRAS, and A. VESPIGNANI. *Structure of cycles and local ordering in complex networks*. *The European Physical Journal B: Condensed Matter and Complex Systems*, 38 (2), pp. 183–186. 2004.
- [Camacho et al., 2007] J. CAMACHO, D. STOUFFER, and L. AMARAL. *Quantitative analysis of the local structure of food webs*. *Journal of Theoretical Biology*, 246 (2), pp. 260–268. 2007.
- [Chakraborty et al., 2014] T. CHAKRABORTY, N. GANGULY, and A. MUKHERJEE. *Automatic classification of scientific groups as productive: An approach based on motif analysis*. In *Proceedings of the IEEE/ACM International Conference on Advances in Social Networks Analysis and Mining*, pp. 130–137. 2014.
- [Cheeger, 1970] J. CHEEGER. *A lower bound for the smallest eigenvalue of the Laplacian*. *Problems in analysis*, pp. 195–199. 1970.
- [Chiba and Nishizeki, 1985] N. CHIBA and T. NISHIZEKI. *Arboricity and subgraph listing algorithms*. *SIAM Journal on Computing*, 14 (1), pp. 210–223. 1985.
- [Chierichetti et al., 2012] F. CHIERICHETTI, R. KUMAR, P. RAGHAVAN, and T. SARLOS. *Are web users really Markovian?* In *Proceedings of the International Conference on World Wide Web*, pp. 609–618. 2012.
- [Chung, 2005] F. CHUNG. *Laplacians and the Cheeger inequality for directed graphs*. *Annals of Combinatorics*, 9 (1), pp. 1–19. 2005.
- [Chung and Simpson, 2013] F. CHUNG and O. SIMPSON. *Solving linear systems with boundary conditions using heat kernel pagerank*. In *International Workshop on Algorithms and Models for the Web-Graph*, pp. 203–219. 2013.
- [Chung, 2007] F. R. CHUNG. *Four proofs for the cheeger inequality and graph partition algorithms*. In *Proceedings of the International Congress of Chinese Mathematicians*, p. 378. 2007.
- [Clauset, 2005] A. CLAUSET. *Finding local community structure in networks*. *Physical Review E*, 72 (2),

- p. 026132, 2005.
- [Cohen, 2008] J. COHEN. *Trusses: Cohesive subgraphs for social network analysis*. National Security Agency Technical Report, p. 16, 2008.
- [Cohen, 2009] ———. *Graph twiddling in a MapReduce world*. *Computing in Science & Engineering*, 11 (4), pp. 29–41, 2009.
- [Colomer-de Simón et al., 2013] P. COLOMER-DE SIMÓN, M. Á. SERRANO, M. G. BEIRÓ, J. I. ALVAREZ-HAMELIN, and M. BOGUÑA. *Deciphering the global organization of clustering in real complex networks*. *Scientific Reports*, 3, p. 2517, 2013.
- [Comandur et al., 2014] S. COMANDUR, R. GUPTA, T. ROUGHGARDEN, ET AL. *Counting small cliques in social networks via triangle-preserving decompositions*. Technical report, Sandia National Laboratories (SNL-CA), Livermore, CA (United States), 2014.
- [Davis and Leinhardt, 1971] J. A. DAVIS and S. LEINHARDT. *The structure of positive interpersonal relations in small groups*. In *Sociological Theories in Progress, Vol. 2*. Houghton-Mifflin, 1971.
- [De Stefani et al., 2016] L. DE STEFANI, A. EPASTO, M. RIONDATO, and E. UPFAL. *TRIÈST: Counting local and global triangles in fully-dynamic streams with fixed memory size*. In *Proceedings of the ACM SIGKDD International Conference on Knowledge Discovery and Data Mining*, pp. 825–834. 2016.
- [Demeyer et al., 2013] S. DEMEYER, T. MICHOEL, J. FOSTIER, P. AUDENAERT, M. PICKAVET, and P. DEMEESTER. *The index-based subgraph matching algorithm (ISMA): fast subgraph enumeration in large networks using optimized search trees*. *PLOS ONE*, 8 (4), p. e61183, 2013.
- [Derényi et al., 2005] I. DERÉNYI, G. PALLA, and T. VICSEK. *Clique percolation in random networks*. *Physical Review Letters*, 94 (16), p. 160202, 2005.
- [D’haeseleer, 2006] P. D’HAESELEER. *What are DNA sequence motifs?* *Nature biotechnology*, 24 (4), pp. 423–425, 2006.
- [Dobrin et al., 2004] R. DOBRIN, Q. K. BEG, A.-L. BARABÁSI, and Z. N. OLTVAI. *Aggregation of topological motifs in the escherichia coli transcriptional regulatory network*. *BMC bioinformatics*, 5 (1), p. 10, 2004.
- [Du et al., 2015] N. DU, Y. WANG, N. HE, J. SUN, and L. SONG. *Time-sensitive recommendation from recurrent user activities*. In *Advances in Neural Information Processing Systems*, pp. 3492–3500. 2015.
- [Dunlavy et al., 2011] D. M. DUNLAVY, T. G. KOLDA, and E. ACAR. *Temporal link prediction using matrix and tensor factorizations*. *ACM Transactions on Knowledge Discovery from Data*, 5 (2), p. 10, 2011.
- [Epasto et al., 2014] A. EPASTO, J. FELDMAN, S. LATTANZI, S. LEONARDI, and V. MIRROKNI. *Reduce and aggregate: similarity ranking in multi-categorical bipartite graphs*. In *Proceedings of the International Conference on World Wide Web*, pp. 349–360. 2014.
- [Erdős and Rényi, 1959] P. ERDÖS and A. RÉNYI. *On random graphs, I*. *Publicationes Mathematicae (Debrecen)*, 6, pp. 290–297, 1959.
- [Farajtabar et al., 2015] M. FARAJTABAR, Y. WANG, M. G. RODRIGUEZ, S. LI, H. ZHA, and L. SONG. *Coevolve: A joint point process model for information diffusion and network co-evolution*. In *Advances in Neural Information Processing Systems*, pp. 1954–1962. 2015.
- [Fiedler, 1973] M. FIEDLER. *Algebraic connectivity of graphs*. *Czechoslovak Mathematical Journal*, 23 (2), pp. 298–305, 1973.
- [Fortunato, 2010] S. FORTUNATO. *Community detection in graphs*. *Physics Reports*, 486 (3), pp. 75–174, 2010.
- [Fortunato and Hric, 2016] S. FORTUNATO and D. HRIC. *Community detection in networks: A user*

- guide*. Physics Reports, 659, pp. 1–44, 2016.
- [Frey and Dueck, 2007] B. J. FREY and D. DUECK. *Clustering by passing messages between data points*. Science, 315 (5814), pp. 972–976, 2007.
- [Fronczak et al., 2002] A. FRONCZAK, J. A. HOLYST, M. JEDYNAK, and J. SIENKIEWICZ. *Higher order clustering coefficients in Barabási–Albert networks*. Physica A: Statistical Mechanics and its Applications, 316 (1), pp. 688–694, 2002.
- [Gargi et al., 2011] U. GARGI, W. LU, V. S. MIRROKNI, and S. YOON. *Large-scale community detection on YouTube for topic discovery and exploration*. In *Proceedings of the International Conference on Web and Social Media*. 2011.
- [Gehrke et al., 2003] J. GEHRKE, P. GINSPARG, and J. KLEINBERG. *Overview of the 2003 KDD Cup*. ACM SIGKDD Explorations Newsletter, 5 (2), pp. 149–151, 2003.
- [Gleich, 2017] D. F. GLEICH. Personal communication, 2017.
- [Gleich and Mahoney, 2015] D. F. GLEICH and M. W. MAHONEY. *Using local spectral methods to robustify graph-based learning algorithms*. In *Proceedings of the ACM SIGKDD International Conference on Knowledge Discovery and Data Mining*, pp. 359–368. 2015.
- [Gleich and Mahoney, 2016] ———. *Mining large graphs*. In *Handbook of Big Data*, pp. 191–220. CRC Press, 2016.
- [Gleich and Owen, 2012] D. F. GLEICH and A. B. OWEN. *Moment-based estimation of stochastic kronecker graph parameters*. Internet Mathematics, 8 (3), pp. 232–256, 2012.
- [Gleich and Seshadhri, 2012] D. F. GLEICH and C. SESHADHRI. *Vertex neighborhoods, low conductance cuts, and good seeds for local community methods*. In *Proceedings of the ACM SIGKDD International Conference on Knowledge Discovery and Data Mining*, pp. 597–605. 2012.
- [Granovetter, 1973] M. S. GRANOVETTER. *The strength of weak ties*. American Journal of Sociology, 78 (6), pp. 1360–1380, 1973.
- [Gupta et al., 2016] R. GUPTA, T. ROUGHGARDEN, and C. SESHADHRI. *Decompositions of triangle-dense graphs*. SIAM Journal on Computing, 45 (2), pp. 197–215, 2016.
- [Gurukar et al., 2015] S. GURUKAR, S. RANU, and B. RAVINDRAN. *COMMIT: A Scalable Approach to Mining Communication Motifs from Dynamic Networks*. In *Proceedings of the ACM SIGMOD International Conference on Management of Data*, pp. 475–489. 2015.
- [Henderson et al., 2012] K. HENDERSON, B. GALLAGHER, T. ELIASSI-RAD, H. TONG, S. BASU, L. AKOGLU, D. KOUTRA, C. FALOUTSOS, and L. LI. *RolX: structural role extraction & mining in large graphs*. In *Proceedings of the ACM SIGKDD International Conference on Knowledge Discovery and Data Mining*, pp. 1231–1239. 2012.
- [Hirai et al., 2000] J. HIRAI, S. RAGHAVAN, H. GARCIA-MOLINA, and A. PAEPCKE. *WebBase: A repository of web pages*. Computer Networks, 33 (1), pp. 277–293, 2000.
- [Holland and Leinhardt, 1970] P. W. HOLLAND and S. LEINHARDT. *A method for detecting structure in sociometric data*. American Journal of Sociology, pp. 492–513, 1970.
- [Holme and Saramäki, 2012] P. HOLME and J. SARAMÄKI. *Temporal networks*. Physics Reports, 519 (3), pp. 97–125, 2012.
- [Homans, 1950] G. C. HOMANS. *The human group*, Harcourt Brace & World, 1950.
- [Honey et al., 2007] C. J. HONEY, R. KÖTTER, M. BREAKSPEAR, and O. SPORNS. *Network structure of cerebral cortex shapes functional connectivity on multiple time scales*. Proceedings of the National Academy of Sciences, 104 (24), pp. 10240–10245, 2007.
- [Houbraken et al., 2014] M. HOUBRAKEN, S. DEMEYER, T. MICHOEL, P. AUDENAERT, D. COLLE, and

- M. PICKAVET. *The Index-Based Subgraph Matching Algorithm with General Symmetries (ISMAGS): Exploiting Symmetry for Faster Subgraph Enumeration*. PLOS ONE, 9 (5), p. e97896, 2014.
- [Huang et al., 2014] H. HUANG, J. TANG, S. WU, L. LIU, ET AL. *Mining triadic closure patterns in social networks*. In *Proceedings of the International Conference on World Wide Web*, pp. 499–504. 2014.
- [Hulovatyy et al., 2015] Y. HULO VATYY, H. CHEN, and T. MILENKOVIĆ. *Exploring the structure and function of temporal networks with dynamic graphlets*. Bioinformatics, 31 (12), pp. i171–i180, 2015.
- [Ihler et al., 1993] E. IHLER, D. WAGNER, and F. WAGNER. *Modeling hypergraphs by graphs with the same mincut properties*. Information Processing Letters, 45 (4), pp. 171–175, 1993.
- [Inokuchi et al., 2000] A. INOKUCHI, T. WASHIO, and H. MOTODA. *An apriori-based algorithm for mining frequent substructures from graph data*. In *Principles of Data Mining and Knowledge Discovery*, pp. 13–23. Springer, 2000.
- [Itzkovitz et al., 2005] S. ITZKOVITZ, R. LEVITT, N. KASHTAN, R. MILO, M. ITZKOVITZ, and U. ALON. *Coarse-graining and self-dissimilarity of complex networks*. Physical Review E, 71 (1), p. 016127, 2005.
- [Jacobs et al., 2015] A. Z. JACOBS, S. F. WAY, J. UGANDER, and A. CLAUSET. *Assembling thefacebook: Using heterogeneity to understand online social network assembly*. In *Proceedings of the ACM Web Science Conference*, p. 18. 2015.
- [Jain and Seshadhri, 2017] S. JAIN and C. SESHADHRI. *A fast and provable method for estimating clique counts using turán’s theorem*. In *Proceedings of the International Conference on World Wide Web*, pp. 441–449. 2017.
- [Jeub et al., 2015] L. G. JEUB, P. BALACHANDRAN, M. A. PORTER, P. J. MUCHA, and M. W. MAHONEY. *Think locally, act locally: Detection of small, medium-sized, and large communities in large networks*. Physical Review E, 91 (1), p. 012821, 2015.
- [Jha et al., 2015] M. JHA, C. SESHADHRI, and A. PINAR. *Path sampling: A fast and provable method for estimating 4-vertex subgraph counts*. In *Proceedings of the International Conference on World Wide Web*, pp. 495–505. 2015.
- [Jiang and Claramunt, 2004] B. JIANG and C. CLARAMUNT. *Topological analysis of urban street networks*. Environment and Planning B: Planning and Design, 31 (1), pp. 151–162, 2004.
- [Jiang et al., 2009] B.-B. JIANG, J.-G. WANG, Y. WANG, and J. XIAO. *Gene prioritization for type 2 diabetes in tissue-specific protein interaction networks*. Systems Biology, 10801131, pp. 319–28, 2009.
- [Jin et al., 2001] E. M. JIN, M. GIRVAN, and M. E. J. NEWMAN. *Structure of growing social networks*. Physical Review E, 64 (4), p. 046132, 2001.
- [Jin et al., 2007] R. JIN, S. MCCALLEN, and E. ALMAAS. *Trend motif: A graph mining approach for analysis of dynamic complex networks*. In *Proceedings of the IEEE International Conference on Data Mining*, pp. 541–546. 2007.
- [Jurgens and Lu, 2012] D. JURGENS and T.-C. LU. *Temporal motifs reveal the dynamics of editor interactions in wikipedia*. In *Proceedings of the International Conference on Web and Social Media*. 2012.
- [Kaiser, 2008] M. KAISER. *Mean clustering coefficients: the role of isolated nodes and leaves on clustering measures for small-world networks*. New Journal of Physics, 10 (8), p. 083042, 2008.
- [Kaiser and Hilgetag, 2006] M. KAISER and C. C. HILGETAG. *Nonoptimal component placement, but short processing paths, due to long-distance projections in neural systems*. PLOS Computational Biology, 2 (7), p. e95, 2006.
- [Kamvar et al., 2003] S. D. KAMVAR, T. H. HAVELIWALA, C. D. MANNING, and G. H. GOLUB. *Extrapolation methods for accelerating pagerank computations*. In *Proceedings of the International Conference on World Wide Web*, pp. 261–270. 2003.

- [Kannan et al., 2004] R. KANNAN, S. VEMPALA, and A. VETTA. *On clusterings: Good, bad and spectral*. Journal of the ACM, 51 (3), pp. 497–515, 2004.
- [Karp, 1972] R. M. KARP. *Reducibility among combinatorial problems*. In *Complexity of computer computations*, pp. 85–103. Springer, 1972.
- [Karypis et al., 1999] G. KARYPIS, R. AGGARWAL, V. KUMAR, and S. SHEKHAR. *Multilevel hypergraph partitioning: applications in VLSI domain*. IEEE Transactions on Very Large Scale Integration Systems, 7 (1), pp. 69–79, 1999.
- [Katona, 1966] G. KATONA. *A theorem of finite sets*. In *Theory of Graphs: Proceedings of the Colloquium held at Tihany, Hungary*, pp. 187–207. 1966.
- [Kelner et al., 2013] J. A. KELNER, L. ORECCHIA, A. SIDFORD, and Z. A. ZHU. *A simple, combinatorial algorithm for solving sdd systems in nearly-linear time*. In *Proceedings of the ACM Symposium on Theory of Computing*, pp. 911–920. 2013.
- [Klimt and Yang, 2004] B. KLIMT and Y. YANG. *Introducing the Enron Corpus*. In CEAS. 2004.
- [Kloster and Gleich, 2014] K. KLOSTER and D. F. GLEICH. *Heat kernel based community detection*. In *Proceedings of the ACM SIGKDD International Conference on Knowledge Discovery and Data Mining*, pp. 1386–1395. 2014.
- [Klymko et al., 2014] C. KLYMKO, D. F. GLEICH, and T. G. KOLDA. *Using triangles to improve community detection in directed networks*. In *Proceedings of the ASE BigData Conference*. 2014.
- [Kondor et al., 2014] D. KONDOR, M. PÓSFAL, I. CSABAI, and G. VATTAY. *Do the rich get richer? an empirical analysis of the Bitcoin transaction network*. PLOS ONE, 9 (2), p. e86197, 2014.
- [Kossinets and Watts, 2006] G. KOSSINETTS and D. J. WATTS. *Empirical analysis of an evolving social network*. Science, 311 (5757), pp. 88–90, 2006.
- [Koutis et al., 2011] I. KOUTIS, G. L. MILLER, and R. PENG. *A nearly- $m \log n$ time solver for sdd linear systems*. In *Proceedings of the IEEE Symposium on Foundations of Computer Science*, pp. 590–598. 2011.
- [Kovanen et al., 2011] L. KOVANEN, M. KARSAI, K. KASKI, J. KERTÉSZ, and J. SARAMÄKI. *Temporal motifs in time-dependent networks*. Journal of Statistical Mechanics: Theory and Experiment, 2011 (11), p. P11005, 2011.
- [Kovanen et al., 2013] L. KOVANEN, K. KASKI, J. KERTÉSZ, and J. SARAMÄKI. *Temporal motifs reveal homophily, gender-specific patterns, and group talk in call sequences*. Proceedings of the National Academy of Sciences, 110 (45), pp. 18070–18075, 2013.
- [Kruskal, 1963] J. B. KRUSKAL. *The number of simplices in a complex*. Mathematical Optimization Techniques, 10, pp. 251–278, 1963.
- [Krzakala et al., 2013] F. KRZAKALA, C. MOORE, E. MOSSEL, J. NEEMAN, A. SLY, L. ZDEBOROVÁ, and P. ZHANG. *Spectral redemption in clustering sparse networks*. Proceedings of the National Academy of Sciences, 110 (52), pp. 20935–20940, 2013.
- [Kwak et al., 2010] H. KWAK, C. LEE, H. PARK, and S. MOON. *What is Twitter, a social network or a news media?* In *Proceedings of the International Conference on World Wide Web*, pp. 591–600. 2010.
- [Kyng and Sachdeva, 2016] R. KYNG and S. SACHDEVA. *Approximate gaussian elimination for laplacians-fast, sparse, and simple*. In *Proceedings of the Symposium on Foundations of Computer Science*, pp. 573–582. 2016.
- [Lahiri and Berger-Wolf, 2007] M. LAHIRI and T. Y. BERGER-WOLF. *Structure prediction in temporal networks using frequent subgraphs*. In *Proceedings of the IEEE Symposium on Computational Intelligence and Data Mining*, pp. 35–42. 2007.

- [Lancichinetti and Fortunato, 2009] A. LANCICHINETTI and S. FORTUNATO. *Benchmarks for testing community detection algorithms on directed and weighted graphs with overlapping communities*. *Physical Review E*, 80 (1), p. 016118, 2009.
- [Lancichinetti et al., 2008] A. LANCICHINETTI, S. FORTUNATO, and F. RADICCHI. *Benchmark graphs for testing community detection algorithms*. *Physical Review E*, 78 (4), p. 046110, 2008.
- [Latapy, 2008] M. LATAPY. *Main-memory triangle computations for very large (sparse (power-law)) graphs*. *Theoretical Computer Science*, 407 (1), pp. 458–473, 2008.
- [Lattanzi and Sivakumar, 2009] S. LATTANZI and D. SIVAKUMAR. *Affiliation networks*. In *Proceedings of the ACM Symposium on Theory of Computing*, pp. 427–434. 2009.
- [Lee et al., 2012] H. LEE, M.-k. CHOI, D. LEE, H.-s. KIM, H. HWANG, H. KIM, S. PARK, Y.-k. PAIK, and J. LEE. *Nictation, a dispersal behavior of the nematode *Caenorhabditis elegans*, is regulated by IL2 neurons*. *Nature Neuroscience*, 15 (1), pp. 107–112, 2012.
- [Lee et al., 2014] J. R. LEE, S. O. GHARAN, and L. TREVISAN. *Multisway spectral partitioning and higher-order cheeger inequalities*. *Journal of the ACM*, 61 (6), p. 37, 2014.
- [Leskovec et al., 2007a] J. LESKOVEC, L. A. ADAMIC, and B. A. HUBERMAN. *The dynamics of viral marketing*. *ACM Transactions on the Web*, 1 (1), p. 5, 2007a.
- [Leskovec et al., 2008] J. LESKOVEC, L. BACKSTROM, R. KUMAR, and A. TOMKINS. *Microscopic evolution of social networks*. In *Proceedings of the ACM SIGKDD International Conference on Knowledge Discovery and Data Mining*, pp. 462–470. 2008.
- [Leskovec et al., 2010a] J. LESKOVEC, D. HUTTENLOCHER, and J. KLEINBERG. *Signed networks in social media*. In *Proceedings of the SIGCHI Conference on Human Factors in Computing Systems*, pp. 1361–1370. 2010a.
- [Leskovec et al., 2010b] J. LESKOVEC, D. P. HUTTENLOCHER, and J. M. KLEINBERG. *Governance in social media: A case study of the wikipedia promotion process*. In *Proceedings of the International Conference on Web and Social Media*. 2010b.
- [Leskovec et al., 2005] J. LESKOVEC, J. KLEINBERG, and C. FALOUTSOS. *Graphs over time: densification laws, shrinking diameters and possible explanations*. In *Proceedings of the ACM SIGKDD International Conference on Knowledge Discovery in Data Mining*, pp. 177–187. 2005.
- [Leskovec et al., 2007b] ———. *Graph evolution: Densification and shrinking diameters*. *ACM Transactions on Knowledge Discovery from Data*, 1 (1), p. 2, 2007b.
- [Leskovec et al., 2009] J. LESKOVEC, K. J. LANG, A. DASGUPTA, and M. W. MAHONEY. *Community structure in large networks: Natural cluster sizes and the absence of large well-defined clusters*. *Internet Mathematics*, 6 (1), pp. 29–123, 2009.
- [Leskovec and McAuley, 2012] J. LESKOVEC and J. J. MCAULEY. *Learning to discover social circles in ego networks*. In *Advances in Neural Information Processing Systems*, pp. 539–547. 2012.
- [Li et al., 2015] Y. LI, K. HE, D. BINDEL, and J. E. HOPCROFT. *Uncovering the small community structure in large networks: A local spectral approach*. In *Proceedings of the International Conference on World Wide Web*, pp. 658–668. 2015.
- [Lim and Kang, 2015] Y. LIM and U. KANG. *Mascot: Memory-efficient and accurate sampling for counting local triangles in graph streams*. In *Proceedings of the ACM SIGKDD International Conference on Knowledge Discovery and Data Mining*, pp. 685–694. 2015.
- [Louis and Makarychev, 2014] A. LOUIS and Y. MAKARYCHEV. *Approximation algorithms for hypergraph small set expansion and small set vertex expansion*. arXiv:1404.4575, 2014.
- [Luce and Perry, 1949] R. D. LUCE and A. D. PERRY. *A method of matrix analysis of group structure*.

- Psychometrika, 14 (2), pp. 95–116, 1949.
- [Mahoney et al., 2012] M. W. MAHONEY, L. ORECCHIA, and N. K. VISHNOI. *A local spectral method for graphs: With applications to improving graph partitions and exploring data graphs locally*. Journal of Machine Learning Research, 13, pp. 2339–2365, 2012.
- [Malliaros and Vazirgiannis, 2013] F. D. MALLIAROS and M. VAZIRGIANNIS. *Clustering and community detection in directed networks: A survey*. Physics Reports, 533 (4), pp. 95–142, 2013.
- [Malmgren et al., 2009] R. D. MALMGREN, D. B. STOFFER, A. S. CAMPANHARO, and L. A. N. AMARAL. *On universality in human correspondence activity*. Science, 325 (5948), pp. 1696–1700, 2009.
- [Mangan and Alon, 2003] S. MANGAN and U. ALON. *Structure and function of the feed-forward loop network motif*. Proceedings of the National Academy of Sciences, 100 (21), pp. 11980–11985, 2003.
- [Mangan et al., 2003] S. MANGAN, A. ZASLAVER, and U. ALON. *The coherent feedforward loop serves as a sign-sensitive delay element in transcription networks*. Journal of Molecular Biology, 334 (2), pp. 197–204, 2003.
- [Manning et al., 2008] C. D. MANNING, P. RAGHAVAN, H. SCHÜTZE, ET AL. *Introduction to Information Retrieval*, Cambridge University Press, 2008.
- [Marcus and Shavitt, 2010] D. MARCUS and Y. SHAVITT. *Efficient counting of network motifs*. In *Proceedings of the IEEE International Conference on Distributed Computing Systems Workshops*, pp. 92–98. 2010.
- [Maschhoff and Sorensen, 1996] K. J. MASCHHOFF and D. C. SORENSEN. *P_ARPACK: An efficient portable large scale eigenvalue package for distributed memory parallel architectures*. In *Applied Parallel Computing Industrial Computation and Optimization*, pp. 478–486. Springer, 1996.
- [Meier et al., 2016] J. MEIER, M. MÄRTENS, A. HILLEBRAND, P. TEWARIE, and P. VAN MIEGHEM. *Motif-based analysis of effective connectivity in brain networks*. In *International Workshop on Complex Networks and their Applications*, pp. 685–696. 2016.
- [Meila and Shi, 2001] M. MEILA and J. SHI. *A random walks view of spectral segmentation*. In *Proceedings of the International Conference on Artificial Intelligence and Statistics*. 2001.
- [Michoel et al., 2011] T. MICHUEL, A. JOSHI, B. NACHTERGAELE, and Y. VAN DE PEER. *Enrichment and aggregation of topological motifs are independent organizational principles of integrated interaction networks*. Molecular BioSystems, 7 (10), pp. 2769–2778, 2011.
- [Michoel and Nachtergaele, 2012] T. MICHUEL and B. NACHTERGAELE. *Alignment and integration of complex networks by hypergraph-based spectral clustering*. Physical Review E, 86 (5), p. 056111, 2012.
- [Mihail, 1989] M. MIHAIL. *Conductance and convergence of Markov chains—a combinatorial treatment of expanders*. In *Proceedings of the Symposium on Foundations of Computer Science*, pp. 526–531. 1989.
- [Milenkovic et al., 2010] T. MILENKOVIC, W. L. NG, W. HAYES, and N. PRZULJ. *Optimal network alignment with graphlet degree vectors*. Cancer Informatics, 9, p. 121, 2010.
- [Milenkovic and Przulj, 2008] T. MILENKOVIC and N. PRZULJ. *Uncovering biological network function via graphlet degree signatures*. Cancer Informatics, 6, 2008.
- [Milo et al., 2004] R. MILO, S. ITZKOVITZ, N. KASHTAN, R. LEVITT, S. SHEN-ORR, I. AYZENSHTAT, M. SHEFFER, and U. ALON. *Superfamilies of evolved and designed networks*. Science, 303 (5663), pp. 1538–1542, 2004.
- [Milo et al., 2003] R. MILO, N. KASHTAN, S. ITZKOVITZ, M. E. J. NEWMAN, and U. ALON. *On the uniform generation of random graphs with prescribed degree sequences*. arXiv:0312028, 2003.
- [Milo et al., 2002] R. MILO, S. SHEN-ORR, S. ITZKOVITZ, N. KASHTAN, D. CHKLOVSKII, and U. ALON. *Network motifs: simple building blocks of complex networks*. Science, 298 (5594), pp. 824–827, 2002.

- [Mislove et al., 2007] A. MISLOVE, M. MARCON, K. P. GUMMADI, P. DRUSCHEL, and B. BHATTACHARJEE. *Measurement and analysis of online social networks*. In *Proceedings of the ACM SIGCOMM conference on Internet measurement*, pp. 29–42. 2007.
- [Mohammadi et al., 2016] S. MOHAMMADI, D. F. GLEICH, T. G. KOLDA, and A. GRAMA. *Triangular alignment (TAME): A tensor-based approach for higher-order network alignment*. *IEEE/ACM Transactions on Computational Biology and Bioinformatics*, 2016.
- [Newman, 2006] M. E. NEWMAN. *Modularity and community structure in networks*. *Proceedings of the National Academy of Sciences*, 103 (23), pp. 8577–8582, 2006.
- [Newman and Girvan, 2004] M. E. NEWMAN and M. GIRVAN. *Finding and evaluating community structure in networks*. *Physical review E*, 69 (2), p. 026113, 2004.
- [Newman, 2001] M. E. J. NEWMAN. *Scientific collaboration networks. I. Network construction and fundamental results*. *Physical review E*, 64 (1), p. 016131, 2001.
- [Ng et al., 2001] A. Y. NG, M. I. JORDAN, Y. WEISS, ET AL. *On spectral clustering: Analysis and an algorithm*. In *Advances in Neural Information Processing Systems*, pp. 849–856. 2001.
- [Nicosia et al., 2012] V. NICOSIA, J. TANG, M. MUSOLESI, G. RUSSO, C. MASCOLO, and V. LATORA. *Components in time-varying graphs*. *Chaos*, 22 (2), p. 023101, 2012.
- [Opsahl and Panzarasa, 2009] T. OPSAHL and P. PANZARASA. *Clustering in weighted networks*. *Social Networks*, 31 (2), pp. 155–163, 2009.
- [Orecchia and Zhu, 2014] L. ORECCHIA and Z. A. ZHU. *Flow-based algorithms for local graph clustering*. In *Proceedings of the ACM-SIAM Symposium on Discrete Algorithms*, pp. 1267–1286. 2014.
- [Palla et al., 2005] G. PALLA, I. DERÉNYI, I. FARKAS, and T. VICSEK. *Uncovering the overlapping community structure of complex networks in nature and society*. *Nature*, 435 (7043), pp. 814–818, 2005.
- [Panzarasa et al., 2009] P. PANZARASA, T. OPSAHL, and K. M. CARLEY. *Patterns and dynamics of users' behavior and interaction: Network analysis of an online community*. *Journal of the American Society for Information Science and Technology*, 60 (5), pp. 911–932, 2009.
- [Paranjape et al., 2017] A. PARANJAPE, A. R. BENSON, and J. LESKOVEC. *Motifs in temporal networks*. In *Proceedings of the ACM International Conference on Web Search and Data Mining*, pp. 601–610. 2017.
- [Park and Newman, 2004] J. PARK and M. E. J. NEWMAN. *Statistical mechanics of networks*. *Physical Review E*, 70 (6), p. 066117, 2004.
- [Pinar et al., 2017] A. PINAR, C. SESHADHRI, and V. VISHAL. *ESCAPE: efficiently counting all 5-vertex subgraphs*. In *Proceedings of the International Conference on World Wide Web*, pp. 1431–1440. 2017.
- [Pržulj et al., 2004] N. PRŽULJ, D. G. CORNEIL, and I. JURISICA. *Modeling interactome: scale-free or geometric?* *Bioinformatics*, 20 (18), pp. 3508–3515, 2004.
- [Pržulj and Malod-Dognin, 2016] N. PRŽULJ and N. MALOD-DOGNIN. *Network analytics in the age of big data*. *Science*, 353 (6295), pp. 123–124, 2016.
- [Rapoport, 1953] A. RAPOPORT. *Spread of information through a population with socio-structural bias: I. Assumption of transitivity*. *Bulletin of Mathematical Biology*, 15 (4), pp. 523–533, 1953.
- [Ravasz and Barabási, 2003] E. RAVASZ and A.-L. BARABÁSI. *Hierarchical organization in complex networks*. *Physical Review E*, 67 (2), p. 026112, 2003.
- [Riddle et al., 1997] D. L. RIDDLE, T. BLUMENTHAL, B. J. MEYER, ET AL., editors. *C. elegans II*, Cold Spring Harbor Laboratory Press, 2 edition, 1997.
- [Rodríguez, 2002] J. RODRÍGUEZ. *On the Laplacian eigenvalues and metric parameters of hypergraphs*. *Linear and Multilinear Algebra*, 50 (1), pp. 1–14, 2002.

- [Rohe and Qin, 2013] K. ROHE and T. QIN. *The blessing of transitivity in sparse and stochastic networks*. arXiv:1307.2302, 2013.
- [Rossi et al., 2013] R. A. ROSSI, D. F. GLEICH, and A. H. GEBREMEDHIN. *Triangle core decomposition and maximum cliques*. In *SIAM Network Science Workshop*, pp. 1–2. 2013.
- [Rossi et al., 2015] ———. *Parallel maximum clique algorithms with applications to network analysis*. *SIAM Journal on Scientific Computing*, 37 (5), pp. C589–C616, 2015.
- [Rosvall and Bergstrom, 2008] M. ROSVALL and C. T. BERGSTROM. *Maps of random walks on complex networks reveal community structure*. *Proceedings of the National Academy of Sciences*, 105 (4), pp. 1118–1123, 2008.
- [Rosvall et al., 2014] M. ROSVALL, A. V. ESQUIVEL, A. LANCICHINETTI, J. D. WEST, and R. LAMBIOTTE. *Memory in network flows and its effects on spreading dynamics and community detection*. *Nature Communications*, 5, 2014.
- [Sariyuce et al., 2015] A. E. SARIYUCE, C. SESHADHRI, A. PINAR, and U. V. CATALYUREK. *Finding the hierarchy of dense subgraphs using nucleus decompositions*. In *Proceedings of the International Conference on World Wide Web*, pp. 927–937. 2015.
- [Schaeffer, 2007] S. E. SCHAEFFER. *Graph clustering*. *Computer Science Review*, 1 (1), pp. 27–64, 2007.
- [Schank and Wagner, 2005] T. SCHANK and D. WAGNER. *Finding, counting and listing all triangles in large graphs, an experimental study*. In *Experimental and Efficient Algorithms*, pp. 606–609. Springer, 2005.
- [Scholtes, 2017] I. SCHOLTES. *When is a network a network? multi-order graphical model selection in pathways and temporal networks*. arXiv:1702.05499, 2017.
- [Scholtes et al., 2016] I. SCHOLTES, N. WIDER, and A. GARAS. *Higher-order aggregate networks in the analysis of temporal networks: path structures and centralities*. *The European Physical Journal B*, 89 (3), p. 61, 2016.
- [Scholtes et al., 2014] I. SCHOLTES, N. WIDER, R. PFITZNER, A. GARAS, C. J. TESSONE, and F. SCHWEITZER. *Causality-driven slow-down and speed-up of diffusion in non-Markovian temporal networks*. *Nature Communications*, 5, p. 5024, 2014.
- [Seidman and Foster, 1978] S. B. SEIDMAN and B. L. FOSTER. *A graph-theoretic generalization of the clique concept*. *Journal of Mathematical Sociology*, 6 (1), pp. 139–154, 1978.
- [Serrouer et al., 2011] B. SERROUR, A. ARENAS, and S. GÓMEZ. *Detecting communities of triangles in complex networks using spectral optimization*. *Computer Communications*, 34 (5), pp. 629–634, 2011.
- [Seshadhri et al., 2014] C. SESHADHRI, A. PINAR, and T. G. KOLDA. *Wedge sampling for computing clustering coefficients and triangle counts on large graphs*. *Statistical Analysis and Data Mining: The ASA Data Science Journal*, 7 (4), pp. 294–307, 2014.
- [Shen-Orr et al., 2002] S. S. SHEN-ORR, R. MILO, S. MANGAN, and U. ALON. *Network motifs in the transcriptional regulation network of Escherichia coli*. *Nature Genetics*, 31 (1), pp. 64–68, 2002.
- [Simmel, 1908] G. SIMMEL. *Sociology: investigations on the forms of sociation*. Duncker & Humblot, Berlin Germany, 1908.
- [Slater et al., 2014] N. SLATER, R. ITZCHACK, and Y. LOUZOUN. *Mid size cliques are more common in real world networks than triangles*. *Network Science*, 2 (03), pp. 387–402, 2014.
- [Slota and Madduri, 2013] G. M. SLOTA and K. MADDURI. *Fast approximate subgraph counting and enumeration*. In *International Conference on Parallel Processing*, pp. 210–219. 2013.
- [Spielman and Teng, 2004] D. A. SPIELMAN and S.-H. TENG. *Nearly-linear time algorithms for graph partitioning, graph sparsification, and solving linear systems*. In *Proceedings of the ACM Symposium on*

- Theory of Computing*, pp. 81–90. 2004.
- [Sporns and Kötter, 2004] O. SPORNS and R. KÖTTER. *Motifs in brain networks*. *PLOS Biology*, 2 (11), p. e369, 2004.
- [Stouffer et al., 2007] D. B. STOFFER, J. CAMACHO, W. JIANG, and L. A. N. AMARAL. *Evidence for the existence of a robust pattern of prey selection in food webs*. *Proceedings of the Royal Society of London B: Biological Sciences*, 274 (1621), pp. 1931–1940, 2007.
- [Sun et al., 2011] Y. SUN, J. HAN, X. YAN, P. S. YU, and T. WU. *PathSim: Meta path-based top-k similarity search in heterogeneous information networks*. *Proceedings of the VLDB Endowment*, 4 (11), pp. 992–1003, 2011.
- [Takac and Zabovsky, 2012] L. TAKAC and M. ZABOVSKY. *Data analysis in public social networks*. In *International Scientific Conference and International Workshop Present Day Trends of Innovations*, pp. 1–6. 2012.
- [Tantipathanandh et al., 2007] C. TANTIPATHANANANDH, T. BERGER-WOLF, and D. KEMPE. *A framework for community identification in dynamic social networks*. In *Proceedings of the ACM SIGKDD International Conference on Knowledge Discovery and Data Mining*, pp. 717–726. 2007.
- [Traud et al., 2012] A. L. TRAUD, P. J. MUCHA, and M. A. PORTER. *Social structure of Facebook networks*. *Physica A: Statistical Mechanics and its Applications*, 391 (16), pp. 4165–4180, 2012.
- [Tsourakakis, 2015] C. TSOURAKAKIS. *The k-clique densest subgraph problem*. In *Proceedings of the International Conference on World Wide Web*, pp. 1122–1132. 2015.
- [Tsourakakis et al., 2017] C. TSOURAKAKIS, J. PACHOCKI, and M. MITZENMACHER. *Scalable motif-aware graph clustering*. In *Proceedings of the International Conference on World Wide Web*. 2017.
- [Tsourakakis et al., 2009] C. E. TSOURAKAKIS, U. KANG, G. L. MILLER, and C. FALOUTSOS. *Doulion: counting triangles in massive graphs with a coin*. In *Proceedings of the ACM SIGKDD International Conference on Knowledge Discovery and Data Mining*, pp. 837–846. 2009.
- [Ugander et al., 2013] J. UGANDER, L. BACKSTROM, and J. KLEINBERG. *Subgraph frequencies: Mapping the empirical and extremal geography of large graph collections*. In *Proceedings of the International Conference on World Wide Web*, pp. 1307–1318. 2013.
- [Ulanowicz et al., 1998] R. E. ULANOWICZ, C. BONDAVALLI, and M. S. EGNOTOVICH. *Trophic Dynamics in South Florida Ecosystem, FY 97: The Florida Bay Ecosystem*. Technical Report CBL 98-123, Chesapeake Biological Laboratory, Solomons, MD, 1998.
- [Varshney et al., 2011] L. R. VARSHNEY, B. L. CHEN, E. PANIAGUA, D. H. HALL, and D. B. CHKLOVSKII. *Structural properties of the Caenorhabditis elegans neuronal network*. *PLOS Computational Biology*, 7 (2), p. e1001066, 2011.
- [Viard et al., 2016] T. VIARD, M. LATAPY, and C. MAGNIEN. *Computing maximal cliques in link streams*. *Theoretical Computer Science*, 609, pp. 245–252, 2016.
- [Viswanath et al., 2009] B. VISWANATH, A. MISLOVE, M. CHA, and K. P. GUMMADI. *On the evolution of user interaction in Facebook*. In *Proceedings of the ACM Workshop on Online Social Networks*, pp. 37–42. 2009.
- [Voevodski et al., 2009] K. VOEVODSKI, S.-H. TENG, and Y. XIA. *Spectral affinity in protein networks*. *BMC Systems Biology*, 3 (1), p. 112, 2009.
- [Von Luxburg, 2007] U. VON LUXBURG. *A tutorial on spectral clustering*. *Statistics and Computing*, 17 (4), pp. 395–416, 2007.
- [Wagner and Wagner, 1993] D. WAGNER and F. WAGNER. *Between min cut and graph bisection*. In *Proceedings of the International Symposium on Mathematical Foundations of Computer Science*, pp.

- 744–750. 1993.
- [Wang et al., 2014] P. WANG, J. LUI, B. RIBEIRO, D. TOWSLEY, J. ZHAO, and X. GUAN. *Efficiently estimating motif statistics of large networks*. *ACM Transactions on Knowledge Discovery from Data*, 9 (2), p. 8, 2014.
- [Wasserman and Pattison, 1996] S. WASSERMAN and P. PATTISON. *Logit models and logistic regressions for social networks: I. an introduction to markov graphs and p^** . *Psychometrika*, 61 (3), pp. 401–425, 1996.
- [Watts and Strogatz, 1998] D. J. WATTS and S. H. STROGATZ. *Collective dynamics of “small-world” networks*. *Nature*, 393 (6684), pp. 440–442, 1998.
- [Wernicke, 2006] S. WERNICKE. *Efficient detection of network motifs*. *IEEE/ACM Transactions on Computational Biology and Bioinformatics*, 3 (4), pp. 347–359, 2006.
- [Wernicke and Rasche, 2006] S. WERNICKE and F. RASCHE. *FANMOD: a tool for fast network motif detection*. *Bioinformatics*, 22 (9), pp. 1152–1153, 2006.
- [West et al., 2014] R. WEST, H. S. PASKOV, J. LESKOVEC, and C. POTTS. *Exploiting social network structure for person-to-person sentiment analysis*. *Transactions of the Association for Computational Linguistics*, 2, pp. 297–310, 2014.
- [Whang et al., 2015] J. J. WHANG, I. S. DHILLON, and D. F. GLEICH. *Non-exhaustive, overlapping k-means*. In *Proceedings of the SIAM International Conference on Data Mining*, pp. 936–944. 2015.
- [Wu et al., 2016] T. WU, A. R. BENSON, and D. F. GLEICH. *General tensor spectral co-clustering for higher-order data*. In *Advances in Neural Information Processing Systems*, pp. 2559–2567. 2016.
- [Wu et al., 2010] Y. WU, C. ZHOU, J. XIAO, J. KURTHS, and H. J. SCHELLNHUBER. *Evidence for a bimodal distribution in human communication*. *Proceedings of the National Academy of Sciences*, 107 (44), pp. 18803–18808, 2010.
- [Wu and Holme, 2009] Z.-X. WU and P. HOLME. *Modeling scientific-citation patterns and other triangle-rich acyclic networks*. *Physical Review E*, 80 (3), p. 037101, 2009.
- [Wuchty et al., 2003] S. WUCHTY, Z. N. OLTVAI, and A.-L. BARABÁSI. *Evolutionary conservation of motif constituents in the yeast protein interaction network*. *Nature Genetics*, 35 (2), pp. 176–179, 2003.
- [Yang and Leskovec, 2012] J. YANG and J. LESKOVEC. *Defining and evaluating network communities based on ground-truth*. In *Proceedings of the International Conference on Data Mining*, pp. 745–754. 2012.
- [Yang and Leskovec, 2014] ———. *Overlapping communities explain core-periphery organization of networks*. *Proceedings of the IEEE*, 102 (12), pp. 1892–1902, 2014.
- [Yaveroğlu et al., 2014] Ö. N. YAVEROĞLU, N. MALOD-DOGNIN, D. DAVIS, Z. LEVNAJIC, V. JANJIC, R. KARAPANDZA, A. STOJMIROVIC, and N. PRŽULJ. *Revealing the hidden language of complex networks*. *Scientific Reports*, 4, 2014.
- [Yin et al., 2017a] H. YIN, A. R. BENSON, and J. LESKOVEC. *Higher-order clustering in networks*. arXiv:1704.03913, 2017a.
- [Yin et al., 2017b] H. YIN, A. R. BENSON, J. LESKOVEC, and D. F. GLEICH. *Local higher-order graph clustering*. In *Proceedings of the ACM SIGKDD International Conference on Knowledge Discovery and Data Mining (to appear)*. 2017b.
- [Yoshida, 2016] Y. YOSHIDA. *Nonlinear Laplacian for digraphs and its applications to network analysis*. In *Proceedings of the ACM International Conference on Web Search and Data Mining*, pp. 483–492. 2016.
- [Zhang et al., 2014a] J. ZHANG, P. S. YU, and Z.-H. ZHOU. *Meta-path based multi-network collective link prediction*. In *Proceedings of the 20th ACM SIGKDD International Conference on Knowledge Discovery*

- and Data Mining*, pp. 1286–1295. 2014a.
- [Zhang et al., 2014b] X. ZHANG, S. SHAO, H. E. STANLEY, and S. HAVLIN. *Dynamic motifs in socio-economic networks*. *Europhysics Letters*, 108 (5), p. 58001, 2014b.
- [Zhang and Parthasarathy, 2012] Y. ZHANG and S. PARTHASARATHY. *Extracting analyzing and visualizing triangle k-core motifs within networks*. In *Proceedings of the IEEE International Conference on Data Engineering*, pp. 1049–1060. 2012.
- [Zhang et al., 2015] Y.-Q. ZHANG, X. LI, J. XU, and A. V. VASILAKOS. *Human interactive patterns in temporal networks*. *IEEE Transactions on Systems, Man, and Cybernetics: Systems*, 45 (2), pp. 214–222, 2015.
- [Zhao et al., 2010] Q. ZHAO, Y. TIAN, Q. HE, N. OLIVER, R. JIN, and W.-C. LEE. *Communication motifs: a tool to characterize social communications*. In *Proceedings of the ACM International Conference on Information and Knowledge Management*, pp. 1645–1648. 2010.
- [Zhou et al., 2006] D. ZHOU, J. HUANG, and B. SCHÖLKOPF. *Learning with hypergraphs: Clustering, classification, and embedding*. In *Advances in Neural Information Processing Systems*, pp. 1633–1640. 2006.
- [Zhu et al., 2013] Z. A. ZHU, S. LATTANZI, and V. S. MIRROKNI. *A local algorithm for finding well-connected clusters*. In *Proceedings of the International Conference on Machine Learning*, pp. 396–404. 2013.
- [Zignani et al., 2014] M. ZIGNANI, S. GAITO, G. P. ROSSI, X. ZHAO, H. ZHENG, and B. Y. ZHAO. *Link and triadic closure delay: Temporal metrics for social network dynamics*. In *Proceedings of the International Conference on Web and Social Media*. 2014.